

School of Chemistry

Cardiff University



**PHthalOCYANINE-BASED MOLECULES
AND POLYMERS OF INTRINSIC
MICROPOROSITY**

Thesis submitted for the degree of Doctor of Philosophy by:

Sabeeha Sarwat Mughal

2014

Declaration

This work has not previously been accepted in substance for any degree and is not concurrently submitted in candidature for any degree.

Signed..... (candidate)

Date.....

STATEMENT 1

This thesis is being submitted in partial fulfilment of the requirements for the degree of Doctor of Philosophy.

Signed..... (candidate)

Date.....

STATEMENT 2

This thesis is the result of my own independent work/investigation, except where otherwise stated. Other sources are acknowledged by explicit references.

Signed..... (candidate)

Date.....

STATEMENT 3

I hereby give consent for my thesis, if accepted, to be available for photocopying and for interlibrary loan, and for the title and summary to be made available to outside organisations.

Signed..... (candidate)

Date.....

Acknowledgements

I'm grateful to my supervisor Professor Neil McKeown for giving me an opportunity to work with him and to carry out an interesting research project and for all the guidance during the course of my PhD. Many thanks goes to Grazia, Kadhum, Lino, Yulia, Rupert, Matt, Richard, Mike, Ian, Rhodri, Sadiq, Ali, Luke and Ben for providing a friendly environment to work in and all the useful discussions and help whenever needed. I'm also grateful to Dr. Simon Pope for his general supervision and his research group for assistance with luminescence measurements. Many thanks to the technical staff in the school for their guidance and expertise whenever needed. I'm also grateful to Dr. Benson Kariuki for solving all the crystal structures presented in this thesis. Finally, I would like to thank all my friends at Cardiff and my family without whom I would not have been able to accomplish this.

Abstract

Syntheses, spectroscopic and microporosity analysis of novel phthalocyanines and porphyrin containing molecules and polymers were carried out. For this purpose, various bulky substituents were introduced on to the aromatic core in order to provide an awkward shape and hence avoid co-facial aggregation and efficient packing.

Firstly, novel phthalocyanines containing dioxy-di-*tert*-butyl-dimethyltritycene substituents were synthesised. UV-vis absorption spectra of these Pcs showed band broadening depending on concentration and solvent suggesting aggregation; although this aggregation was not found to be as significant as that of various phthalocyanines reported in the literature. Apparent BET surface areas of these materials were found to be in the range of 400 to 500 m² g⁻¹.

For comparison, the spectroscopic behaviour of the related, literature based octa-*tert*-butyltetra-2,3-tritycenotetraazaporphyrins were examined which form discrete co-facial dimers in pentane solution. It was found that this high specific dimerisation can be prevented by introducing methyl substituents onto the bridgehead positions of the triptycene subunits.

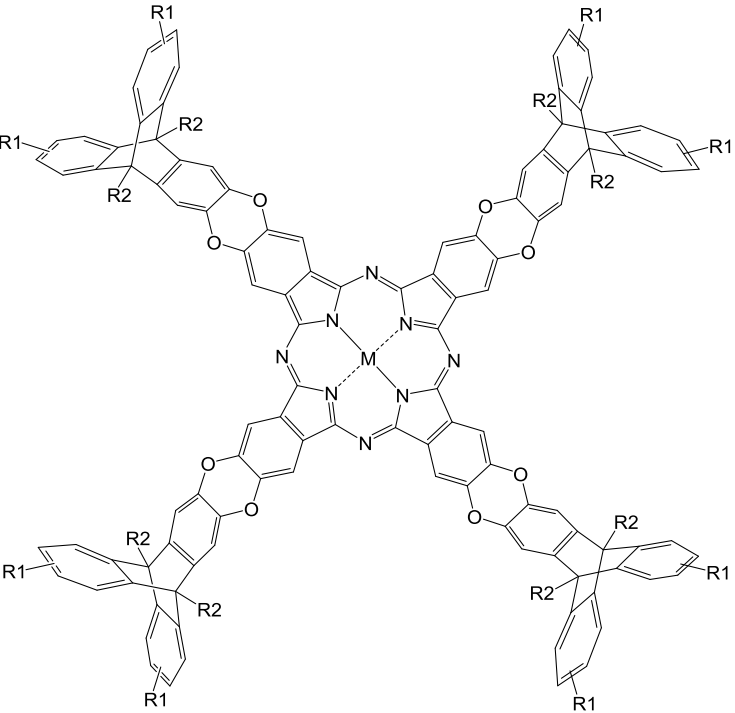
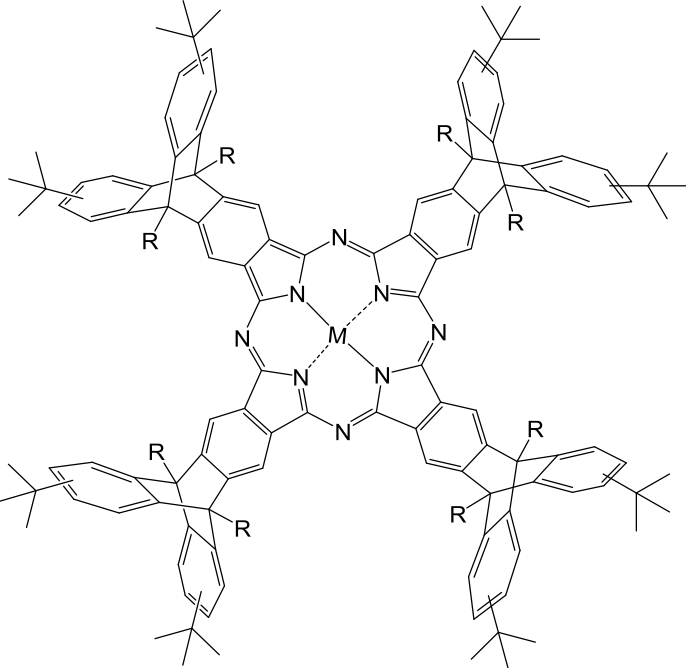
A third category of compounds, tetratriptycenoporphyrins were synthesised using the commercially available tetrakis(pentafluorophenyl)porphyrin precursor and dihydroxy-di-*tert*-butyl-dimethyltritycene. UV-vis absorption and luminescence measurements showed these complexes to be non-aggregating and were found to be microporous with BET surface areas ranging from 450 to 600 m² g⁻¹.

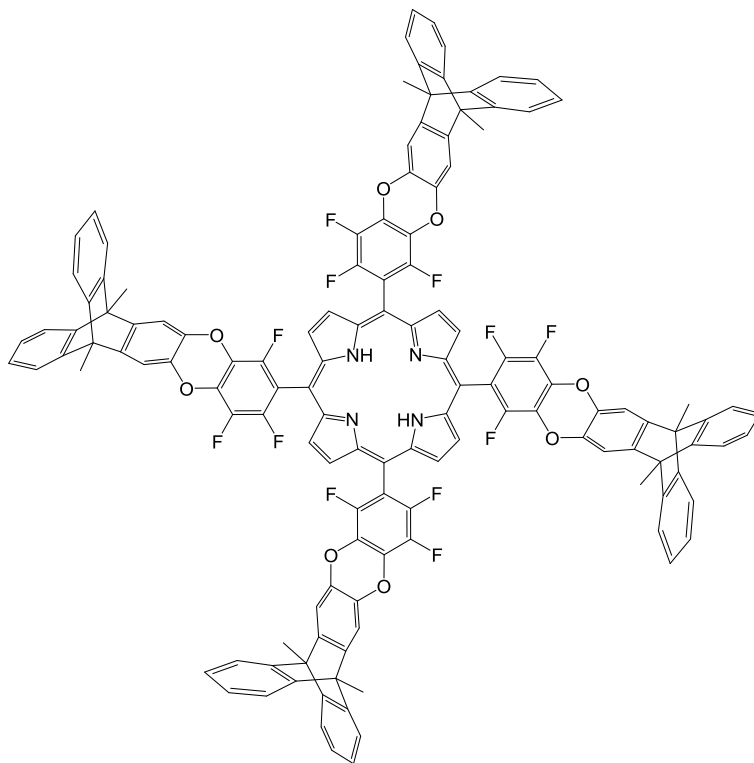
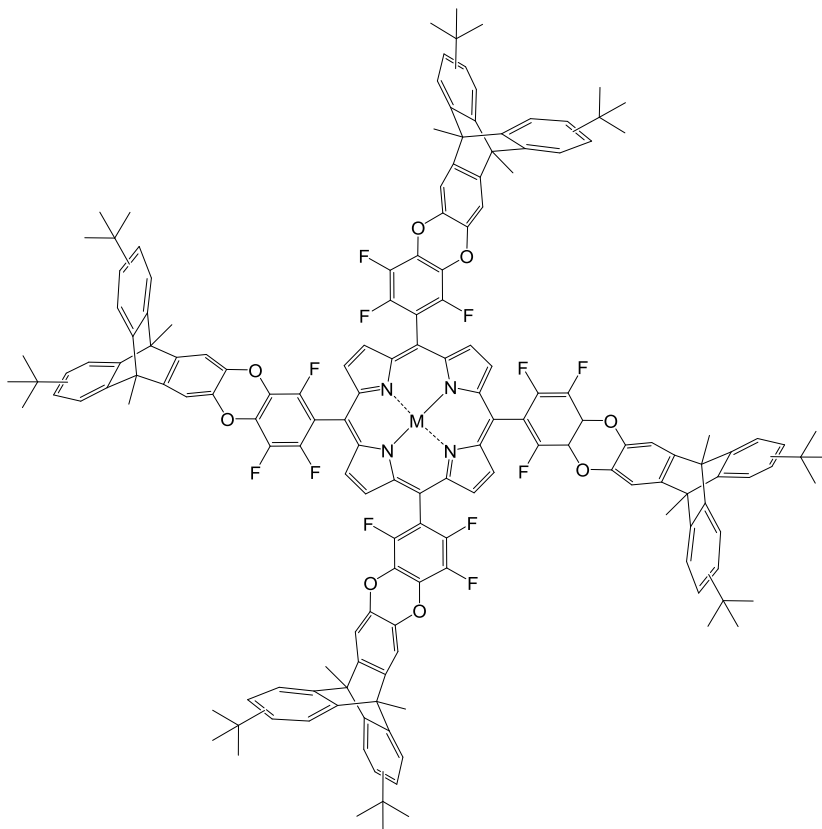
The synthesis and analysis of novel phthalocyanine and porphyrin based network polymers prepared via cyclotetramerisation of bis or tris phthalonitrile containing substituents of contortion (spirobisindane, ethanoanthracene and triptycene) or via nucleophilic aromatic substitution reaction starting from a preformed phthalocyanine or porphyrin precursor, was performed. UV-vis absorption measurements of these polymers proved difficult due to solubility issues, however nitrogen adsorption analysis revealed BET surface areas ranging from 300 to 1000 m² g⁻¹.

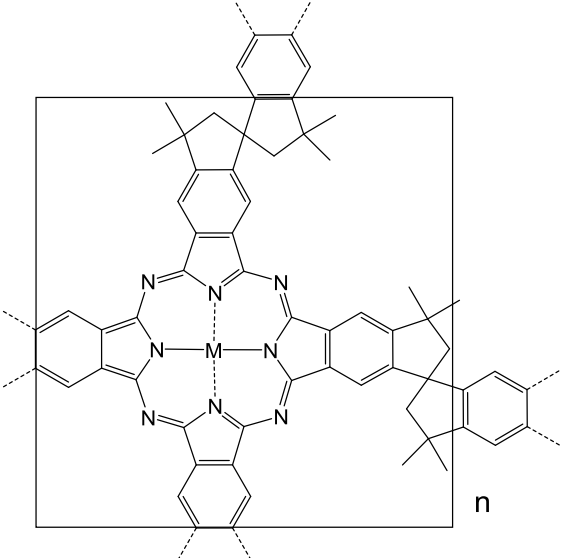
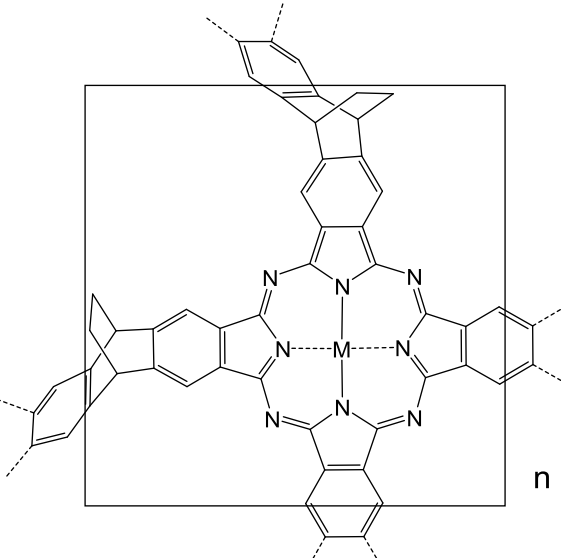
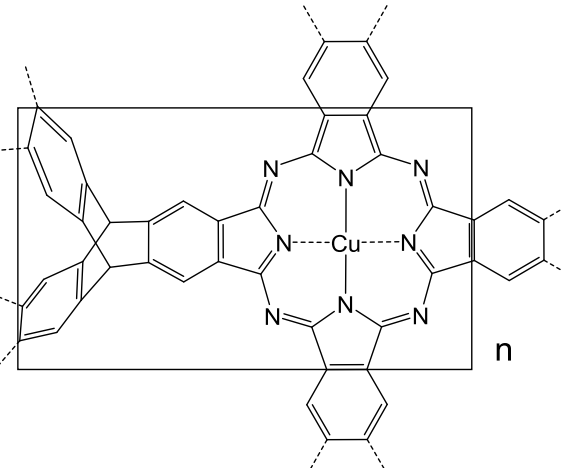
Abbreviations

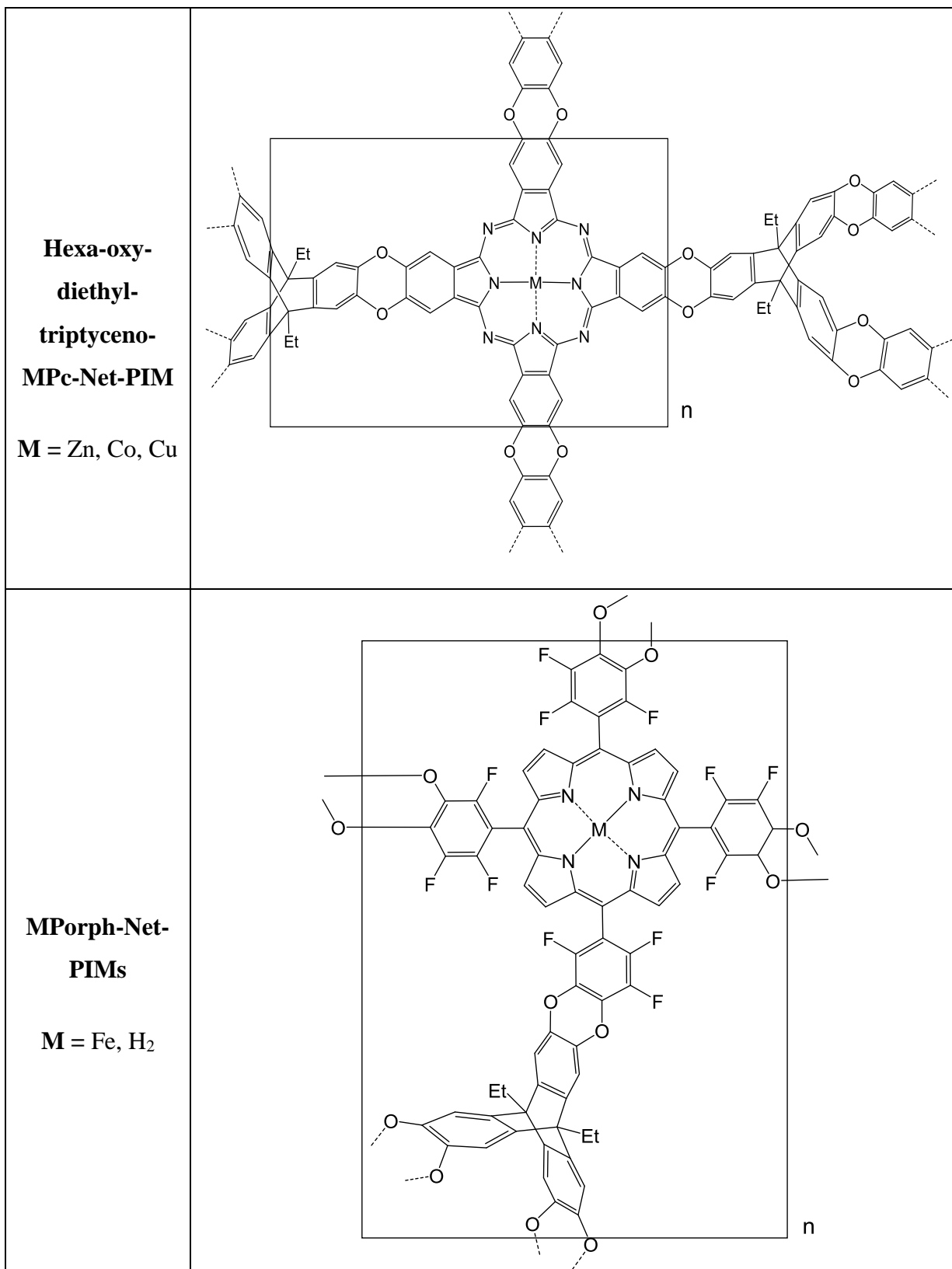
BET	Brunauer, Emmett and Teller
DCM	Dichloromethane
h	hours
MALDI-MS	Matrix Assisted Laser Desorption Ionisation-Mass Spectrometry
NMP	N-methyl-2-pyrrolidinone
OMIM	Organic Molecule of Intrinsic Microporosity
PIM	Polymer of Intrinsic Microporosity
Pc	Phthalocyanine
Pn	Phthalonitrile
Porph	Porphyrin
Pz	Porphyrazine
RT	Room temperature
Subst.	Substituted
THF	Tetrahydrofuran
TLC	Thin Layer Chromatography
XRD	X-ray Diffraction

Appendix 1: Structure abbreviations for Pc and porphyrin molecules and polymers

<p>ZnPc 1 – 4</p> <p>ZnPc1: R1, R2 = H</p> <p>ZnPc2: R1 = <i>t</i>-Bu, R2 = H</p> <p>ZnPc3: R1 = H, R2 = Me</p> <p>MPc4: R1 = <i>t</i>-Bu, R2 = Me</p> <p>M = Zn, Co, H₂, Cu</p>	
<p>MPz</p> <p>MPz1: R = H</p> <p>M = Zn, Co, Cu, H₂</p> <p>MPz2: R = Me</p> <p>M = Zn, Cu</p>	

H₂Porph1**MPorph2****M = Zn, Co, Fe, H₂**

<p>SBI-MPc-NetPIM</p> <p>M = Zn, Co, Cu</p>	 <p>The diagram shows a central metal atom (M) coordinated to four nitrogen atoms of a porphyrin ring. The porphyrin ring is substituted with four phenyl groups. Two of these phenyl groups are further substituted with a side chain consisting of a benzene ring, a methylene group, and a cyclopentane ring. The cyclopentane ring is substituted with two methyl groups. The entire structure is enclosed in a rectangular box with dashed lines extending from the corners, and a small 'n' is located at the bottom right corner of the box.</p>
<p>EA-MPc-NetPIM</p> <p>M = Zn, Co</p>	 <p>The diagram shows a central metal atom (M) coordinated to four nitrogen atoms of a porphyrin ring. The porphyrin ring is substituted with four phenyl groups. Two of these phenyl groups are further substituted with a side chain consisting of a benzene ring, a methylene group, and a cyclopentane ring. The cyclopentane ring is substituted with two methyl groups. The entire structure is enclosed in a rectangular box with dashed lines extending from the corners, and a small 'n' is located at the bottom right corner of the box.</p>
<p>Triptyceno-CuPc-Net-PIM</p>	 <p>The diagram shows a central copper atom (Cu) coordinated to four nitrogen atoms of a porphyrin ring. The porphyrin ring is substituted with four phenyl groups. Two of these phenyl groups are further substituted with a side chain consisting of a benzene ring, a methylene group, and a cyclopentane ring. The cyclopentane ring is substituted with two methyl groups. The entire structure is enclosed in a rectangular box with dashed lines extending from the corners, and a small 'n' is located at the bottom right corner of the box.</p>



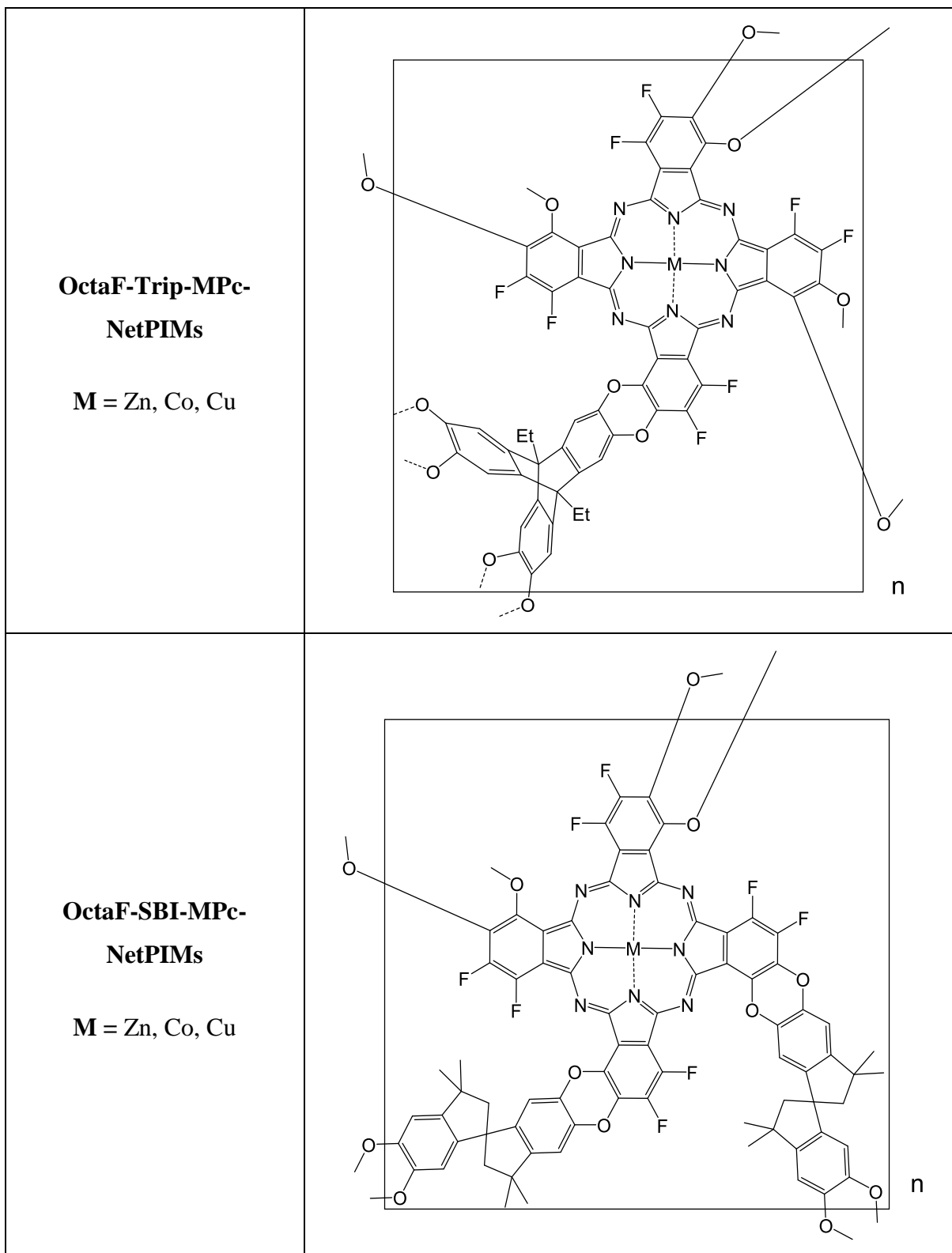


Table of Contents

Declaration	2
Abstract	4
Abbreviations	5
Appendix 1: Structure abbreviations for Pc and porphyrin molecules and polymers	6
1. Introduction	13
1.1 Discovery of phthalocyanines	13
1.2 Some general synthetic routes to Pc	14
1.3 Applications of Pcs as functional materials	16
1.4 Porosity	18
1.5 Surface area measurement	19
1.6 Microporous materials	21
1.7 Polymers of Intrinsic Microporosity (PIMs)	21
1.7.1 Network PIMs	22
1.7.2 Ladder PIMs	28
1.8 MOFs and COFs	30
1.9 Microporous Molecular Crystals	35
1.9.1 Pc based molecular crystals	35
1.9.2 Porous organic cage crystals	37
1.10 Oligomeric Molecules of IM (OMIMs)	40
1.10.1 Triptycene based OMIMs	40
1.10.2 Pc and porphyrin based oligomers	43
2. Aims and objectives	46
3. Phthalocyanine containing Molecules of Intrinsic Microporosity	47
3.1 Introduction	47
3.2 Attempts to make Pc OMIMs from unsymmetrical Pcs	48
3.3 Pcs from dioxin-phthalonitrile-triptycenes (ZnPc 1 – 4)	52
3.3.1 Synthesis of MPc4 complexes	63
3.3.2 An assessment of aggregation via UV-vis absorption spectroscopy and BET 64	
3.4 Triptycenoporphyrazines	69
3.4.1 UV-vis absorption spectra and Molecular Modelling	72
3.4.2 Luminescence Spectroscopy	75

3.4.3	EPR spectra of CuPz1 complex	76
3.5	Triptycene-substituted porphyrins	79
3.5.1	Attempts to make octa-triptycene substituted porphyrin	82
3.5.2	UV-vis absorption and luminescence spectroscopy	84
3.5.3	Nitrogen adsorption analysis	88
3.6	Molecules from hexadecafluoroMPcs	90
3.6.1	Reaction to make tetra substituted Pc	90
3.6.2	Reaction to make an octa substituted Pc	93
3.7	Attempts to make Pc-dimer and trimer molecules of intrinsic microporosity	97
3.7.1	Synthesis of cores	97
3.7.2	Reactions to make Pc-based OMIMs	103
4	Pc and porphyrin containing network-PIMs	106
4.1	Introduction	106
4.2	Network PIMs from cyclotetramerisation reactions	106
4.3	Network PIMs from nucleophilic substitution reactions	110
4.3.1	From tetrakis(pentafluorophenyl)porphyrin	110
4.3.2	Pc polymers from hexadecafluoroMPcs	114
4.4	Conclusion	116
5.	Future Work	117
6.	Experimental	119
6.1	General Remarks	119
6.2	Some general procedures	122
6.3	Synthesis of precursors	125
6.4	Synthesis of Pc and porphyrin molecules	152
6.5	Synthesis of Pc and porphyrin based network polymers	171
Appendix 2: Solid state crystal structure parameters and packing diagrams		
184		
Bibliography		198

1. Introduction

1.1 Discovery of phthalocyanines

Phthalocyanine (Pc) is a highly symmetric 18 π aromatic macrocycle composed of four iminoisoindole units. ^[1] Its structure is closely related to the naturally occurring porphyrin ring system which has four modified pyrrole subunits interconnected by methine bridges at α carbon atoms (**Figure 1.1**).

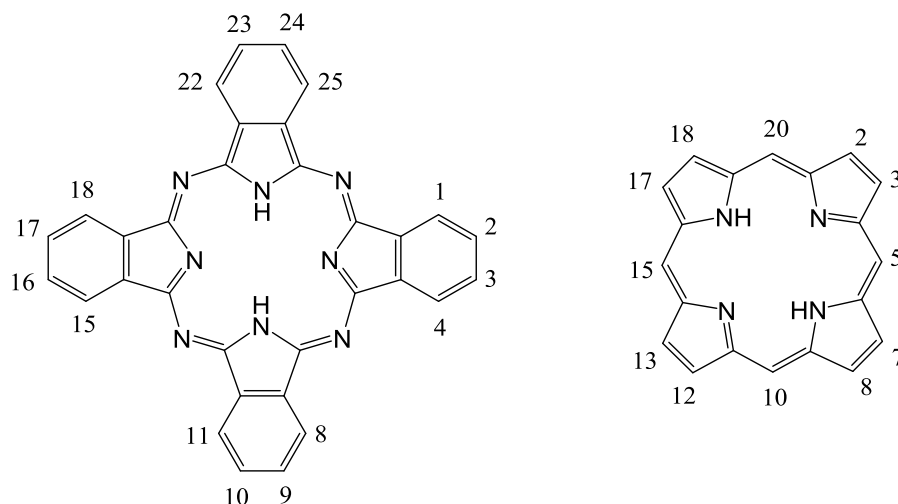


Figure 1.1: The structure of Pc (left) and porphine (right). The numbering scheme for the two systems is also shown.

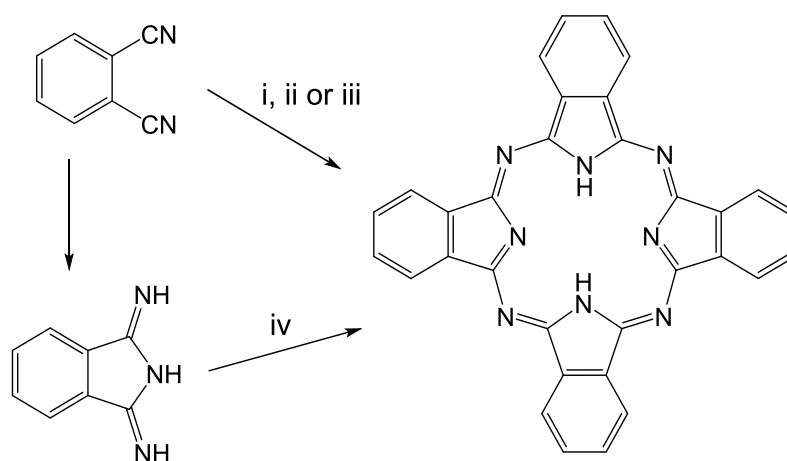
Pc was firstly observed by researchers in 1907 and 1927 as a highly coloured by-product in the chemical conversion of some ortho-(1,2)-substituted benzene derivatives.^[2,3] However, the process of obtaining a full elucidation of its structure began in 1928 at the Grangemouth plant of Scottish Dyes Ltd. during the industrial preparation of phthalimide from phthalic anhydride.^[4,5] The glass-lined reaction vessel cracked exposing the outer steel casing to the reaction which resulted in the formation of an insoluble and highly stable, iron containing blue impurity. Imperial Chemical Industries (ICI), which acquired Scottish Dyes in 1928, was eager to understand this coloured impurity and so a sample was sent to Prof. J. F. Thorpe at Imperial College London who in turn gave it to another lecturer R. P. Linstead. After a series of investigations, this collaboration between ICI and Linstead lead to the publication of six papers in 1934 in the Journal of the Chemical Society which described the structure of Pc and the

synthesis of some of its metal analogues. [6-11] Linstead came up with the name *phthalocyanine*; *phthal* to emphasise the various phthalic acid derived precursors for making Pc and *cyanine* meaning blue.

1.2 Some general synthetic routes to Pc

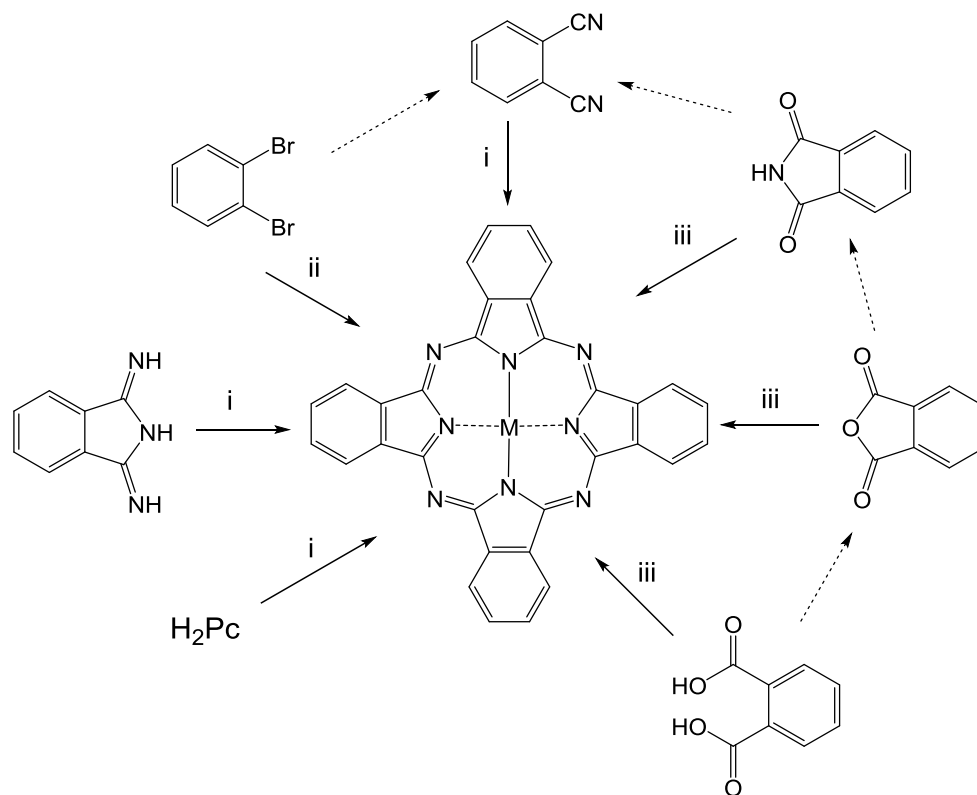
Metal free Pc (H_2Pc) can be synthesized starting with phthalonitrile (1,2-dicyanobenzene or more conveniently 'Pn') or diiminoisoindoline, both of which can undergo cyclotetramerisation under suitable conditions to give Pc (**Scheme 1.1**).

Pn cyclotetramerisation can be achieved by simply heating it with a base e.g. NH_3 , DBU (1,8-diazabicyclo[5.4.0]undec-7-ene) or DBN (1,5-diazabicyclo[4.3.0]non-5-ene) in a solvent such as *n*-pentan-1-ol [12] or heating in a basic solvent such as DMAE (*N,N*-dimethylaminoethanol). [13] A common procedure for making H_2Pc is the "Linstead method" in which lithium, sodium or magnesium alkoxides, most often formed in situ by the addition of the metal to a primary alcohol (e.g. *n*-pentan-1-ol) are used for the cyclotetramerisation of Pn. Upon complexation, the metal ions are removed via an acidic or aqueous work-up to give H_2Pc . [14] Pn cyclotetramerisation can also be achieved in the presence of a reducing agent such as hydroquinone at a temperature > 180 °C above which the Pn melts. [15] Pn can also be firstly converted to diiminoisoindoline via bubbling NH_3 into a refluxing solution of methanol using sodium methoxide [16] which can then be condensed to form H_2Pc . [17]



Scheme 1.1: Synthesis of H_2Pc . *Reagents and conditions:* (i) Heat with NH_3 , DBU or DBN with *n*-pentan-1-ol or heat in DMAE; (ii) Labile metal ion, usually Li, pentan-1-ol, reflux, then acidic workup; (iii) Hydroquinone, Δ ; (iv) Reflux in high boiling point alcohol e.g. DMAE.

Metal phthalocyanines (MPcs) can generally be prepared using a metal salt which acts as a template for cyclotetramerisation (**Scheme 1.2**). For example, a suitable metal salt added to the cyclotetramerisation reaction of diiminoisoindoline can give MPcs. ^[16,18,19] Similarly, Pn cyclotetramerisation using suitable metal compounds in high boiling point solvents e.g. quinoline, NMP (*N*-methyl-2-pyrrolidone), DMF (dimethylformamide), DMAE and 1-chloronaphthalene can give MPcs. ^[20,21] 1,2-Dibromobenzene, a starting material for preparing Pn in the Rosenmund von Braun reaction, ^[22,23] which involves heating the dibromide with CuCN in DMF, can also result in CuPc formation especially under forcing conditions. ^[24] Moreover, phthalic acid, phthalic anhydride and phthalimide can all act as precursors to MPcs ^[25-27] (as well as being precursors to Pn; see **Scheme 3.2**) and most commercial processes are based upon these compounds rather than the more expensive Pn. For these *phthal* precursors, urea is necessary as a source of nitrogen in addition to metal salts and ammonium molybdate as a catalyst to form Pc. The coordination of a preformed H₂Pc with metal ions is another very clean, efficient and high yielding reaction for making MPcs. ^[14]



Scheme 1.2: Synthesis of MPc. *Reagents and conditions:* (i) Heat in a high boiling point solvent with metal salt; (ii) CuCN, DMF, reflux; (iii) Heat in a high boiling point solvent with metal salt and urea. Note: Dotted arrow shows synthetic connectivity between precursors.

1.3 Applications of Pcs as functional materials

Pcs and their derivatives are of interest due to their outstanding optical and electronic properties which arise from electronic delocalization. They find extensive usage as dark green-blue colorants, ^[6] as a consequence of their absorption spectra showing an intense Q-band in the visible region centered usually at 620 – 700 nm. Pcs are thermally and chemically stable, ^[6] the central cavity of the Pc ring is capable of accommodating around seventy different elements ^[1] and various substituents can be incorporated onto the periphery of the macrocycle ^[28] as well as at the axial sites. ^[29,30] The structure of the Pc ring can be modified in a variety of ways giving a range of derivatives with new specific properties; for example, via the replacement of carbons within the benzo units of the Pc with nitrogens to give octaazaphthalocyanines (AzaPcs) ^[31-33] or by extending the π system of the Pc ring in both planar and sandwich type complexes ^[34] or by changing the number of isoindole units to give SubPcs and SuperPcs. ^[35,36] Hence, Pcs are exceptional candidates in the field of materials science due to their versatility and find applications in several areas e.g. optical data storage, ^[37,38] hole and electron transport materials in organic electronic devices, ^[39-41] solar energy conversion, ^[42-44] photodynamic therapy (PDT) of cancer, ^[45,46] as active components of gas sensors ^[47,48] and in catalysis. ^[49,50] Their planar shape, four fold symmetry and synthetic diversity also make them an excellent building blocks for use in supramolecular chemistry ^[51-53] and polymer chemistry. ^[54,55]

The extended planar shape of the Pc unit also results in a strong tendency to form densely packed cofacial aggregates due to π - π stacking interaction. Consequently, their physical, optical, magnetic and electronic properties are also influenced by their packing arrangement and the relative orientation of Pc molecules in solid state and in solution. ^[56-60] For example, in the field of organic light emitting diodes (OLEDs), ^[61] organic solar cells (OSCs) ^[62] and photodetectors, ^[63] vertically standing π - π stacked chromophores are highly desired as active layers for their charge transport properties. As well as having perpendicular carrier transports, these applications also require ultra-dense, large scale and highly arrayed π stacks. To overcome this challenge, ^[64] Lu *et. al.* ^[65] selected a zinc Pc (ZnPc) molecule with four terminal carboxylic functions armed through four amide bonds (**Figure 1.2**), where the carboxylic groups act as bonding sites for anchoring the Pc molecule onto the indium tin oxide (ITO) substrate, ^[66] forming a single molecular layer. The hydrophobic π - π stacking interactions between the faces of ZnPc and strong

hydrogen bonds between amide-to-amide and carboxylic acid-to-carboxylic acid groups induce the formation of coherent perpendicular π stacks on the single molecular layer. The terminal carboxylic acid-to-carboxylic acid hydrogen bonds also provide sticking forces between the vertically standing ZnPc π - π stacks. This supramolecular self-assembly shows a high conductivity and hole mobility and acts as hole-transporting layer on the ITO electrode in organic solar cells, with potential applications in the fabrication of high performance organic electronic devices through solution deposition method. The electronic and charge transporting properties of Pc molecules along with their intense self-assembling ability are therefore highly desirable for the fabrication of organic electronic devices.

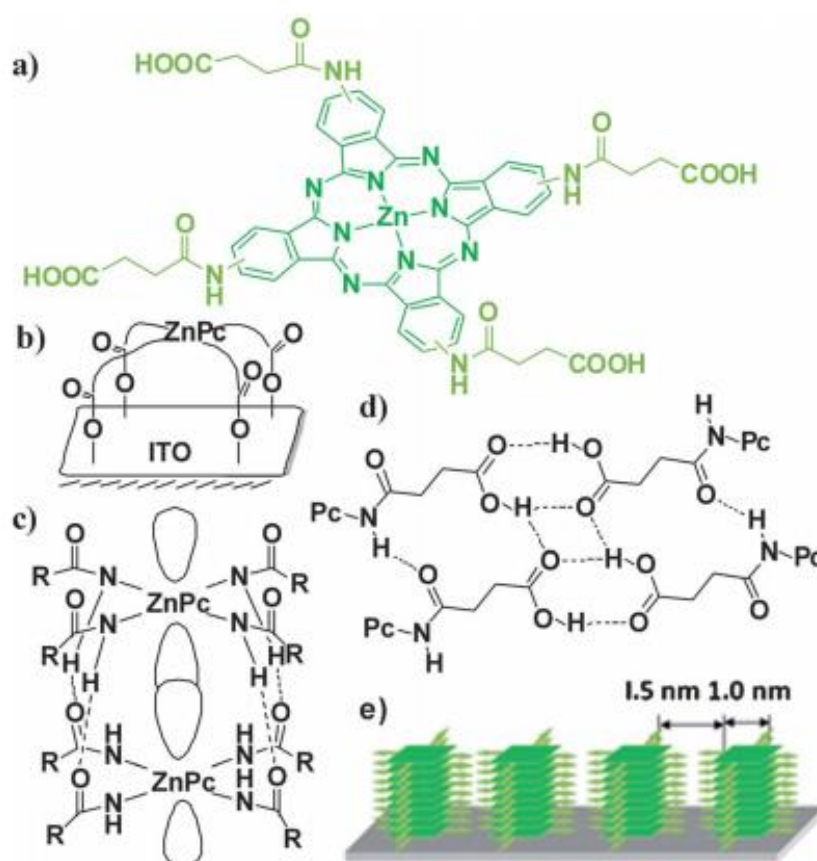


Figure 1.2: (a) Molecular structure of a ZnPc derivative; (b) Illustration of ZnPc molecule bound to ITO surface, (c) and (d) Illustrations of supramolecular self-assembly in face to face mode via π - π stacks of ZnPc and hydrogen bonds of imide and carboxylic acid groups; (d) and (e) Sticking forces of intercolumn hydrogen bonds and π - π stacks perpendicular to ITO surface to form a highly dense, large scale, vertically standing ZnPc stacks. (Figure reproduced from Ref. ^[65]).

1.4 Porosity

A porous solid can be defined as a material with pores (empty voids, channels, cavities or interstices) which are deeper than they are wide. ^[67] According to the definition of IUPAC (International Union of Pure and Applied Chemistry), pores can be classified into three categories depending on their size ^[68]:

- i. Macropores – pores of widths greater than 50 nm.
- ii. Mesopores – pores of widths between 2 nm and 50 nm.
- iii. Micropores – pores of widths smaller than 2 nm.

Pores can further be classified as ‘open’ and ‘closed’ according to their availability to an external fluid (**Figure 1.3**). ^[67] For example, pores which are completely isolated from their neighbours (*a*) are described as ‘closed’ pores. These pores influence only the macroscopic properties and are inactive in gas adsorption and fluid flow. In contrast, ‘open’ pores (*b*, *c*, *d*, *e* and *f*) have a continuous channel of communication with the external surface of the material and play an active role in gas adsorption or porosity. These pores can further be defined according to their shape e.g. *c* and *f* are cylindrical, *b* is ink-bottle shaped and *d* is funnel shaped. Also, some pores are open only at one end e.g. *b* and *f* while others are ‘through’ pores (open at both ends) e.g. *e*. Thus all of these properties can have an influence on the function of the porous materials. Also different from porosity is the roughness of the external surface of the material represented by *g* which cannot be considered porous as the irregularity is not deeper than it is wide.

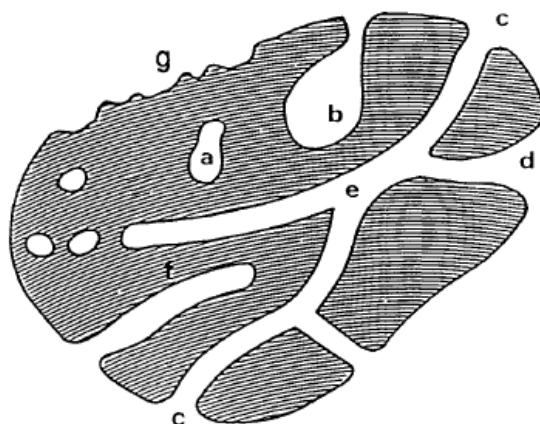


Figure 1.3: Schematic cross section of a porous solid. (Figure reproduced from Ref. ^[67]).

1.5 Surface area measurement

The most widely used method for characterising porous solids is gas adsorption which involves physisorption of free gas molecules on to the surface of a porous solid. Since free gas and adsorbed gas are in dynamic equilibrium, the fractional coverage of the surface depends on the pressure of the overlying gas. The variation of the coverage with pressure at a specific temperature thus gives an adsorption isotherm from which surface area can be determined.

In 1916, Langmuir firstly proposed a model for the analysis of the physisorption isotherm data. [69] This model was based on three main assumptions: firstly, that the adsorption of gas onto a solid cannot proceed beyond monolayer coverage; secondly, all sites are equivalent and the surface is uniform and finally that each molecule adsorbs onto a surface site independent of the occupation of neighbouring sites. Due to the likelihood of these basic assumptions being flawed when applied to real systems, the Langmuir model is now replaced by the most widely accepted BET (Brunauer, Emmett and Teller) method [70] which takes into account multilayer adsorption and is based on the following derived equation (in the form of $y = c + mx$):

$$\frac{P}{V(P - P_o)} = \frac{1}{cV_{mon}} + \frac{(c - 1) P}{cV_{mon} P_o}$$

Where P is adsorption pressure, P_o is saturation vapour pressure, V is the volume of adsorbed gas, V_{mon} is volume corresponding to monolayer coverage and c is a BET constant. Hence, a plot of $P/V(P - P_o)$ against relative pressure P/P_o gives a linear relationship from which the values of V_{mon} and c can be obtained from the slope and the intercept. Using these values and by knowing the mass of the sample and the area occupied by each gaseous molecule (0.16 nm^2 for N_2), the specific surface area in $\text{m}^2 \text{ g}^{-1}$ can be calculated which is a useful parameter for indicating the relative amount of intrinsic microporosity in one material compared to another:

$$S.A. (BET) = V_{mon} N_A \sigma$$

where N_A is Avogadro's constant and σ is the area occupied by an adsorbate molecule.

In practice, BET analysis is carried out at 77 K using an inert gas such as nitrogen. A precisely weighed and degassed sample is subjected to continuous dose of nitrogen. The adsorption isotherm is usually constructed point by point by the admission and withdrawal of known amount of gas with adequate time to allow for equilibration at each point.

The majority of the adsorption isotherms can be grouped into six types. ^[68] At the lowest relative pressures, the very small pores accessible to nitrogen are filled and increasing the pressure causes larger pores to be progressively filled. Hence, of the isotherms shown in **Figure 1.4**, ^[71] Type-I is characteristic of a microporous material, indicated by a high nitrogen uptake at low relative pressure. Type-II and -III demonstrate adsorption on non-porous or macroporous materials, Type-IV and -V represent mesoporosity with hysteresis loop closing at a relative pressure of ≥ 0.4 and Type-VI represents stepped isotherm and non-porosity.

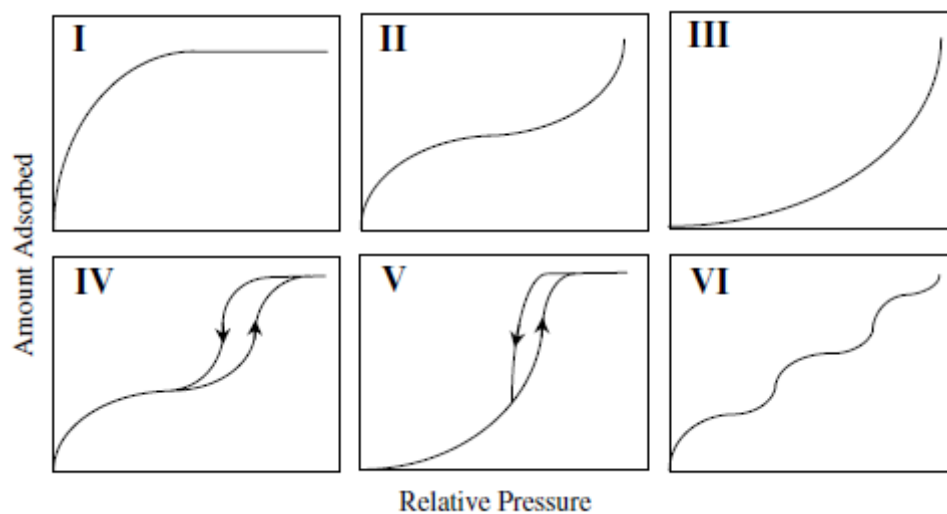


Figure 1.4: Types of isotherm as defined by IUPAC. (Figure reproduced from Ref. ^[68]).

1.6 Microporous materials

Microporous materials that can be defined as solids containing interconnected pores of widths less than 2 nm are of interest for heterogeneous catalysis, molecular separations and gas storage. Generally, these materials can be divided into two categories: (i) Crystalline materials possessing long range order such as zeolites, metal-organic and covalent-organic frameworks (MOFs and COFs) and molecular clathrate crystals and; (ii) Amorphous materials of random packing arrangement with little or no long range order such as activated carbons and Polymers and Oligomers of Intrinsic Microporosity (PIMs and OMIMs). Some relevant examples (**Figure 1.5**) will be reviewed below.

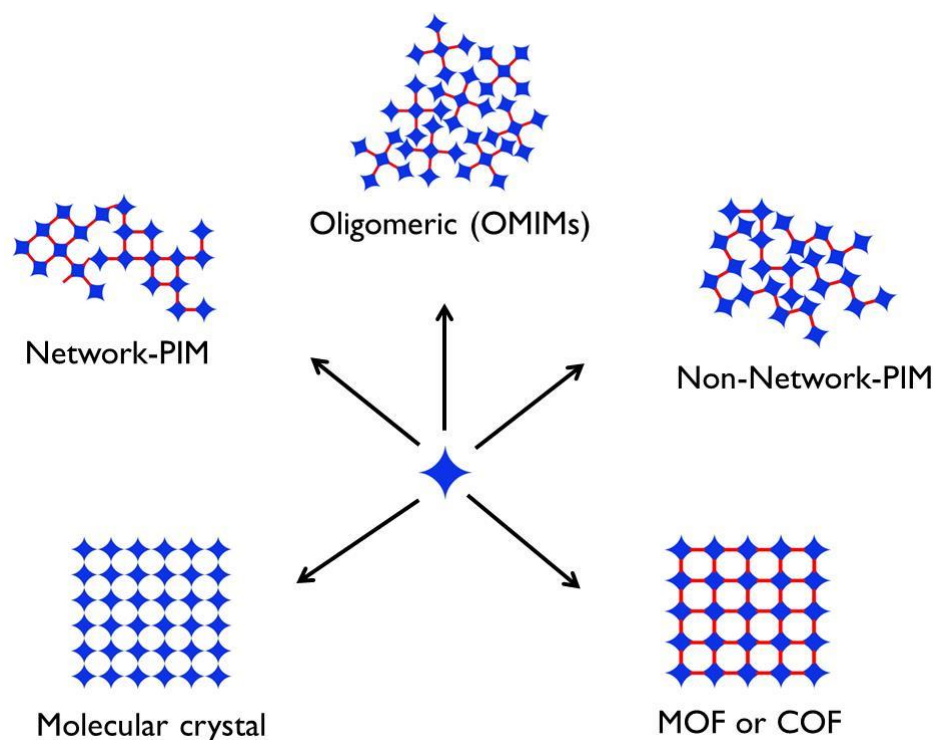


Figure 1.5: 2-D representation of possible solid state packing arrangements of a concave molecular unit.

1.7 Polymers of Intrinsic Microporosity (PIMs)

Figure 1.5 represents solid state packing arrangements of a typical concave molecular unit. Mathematical modelling suggests that random packing of geometric shapes with strongly

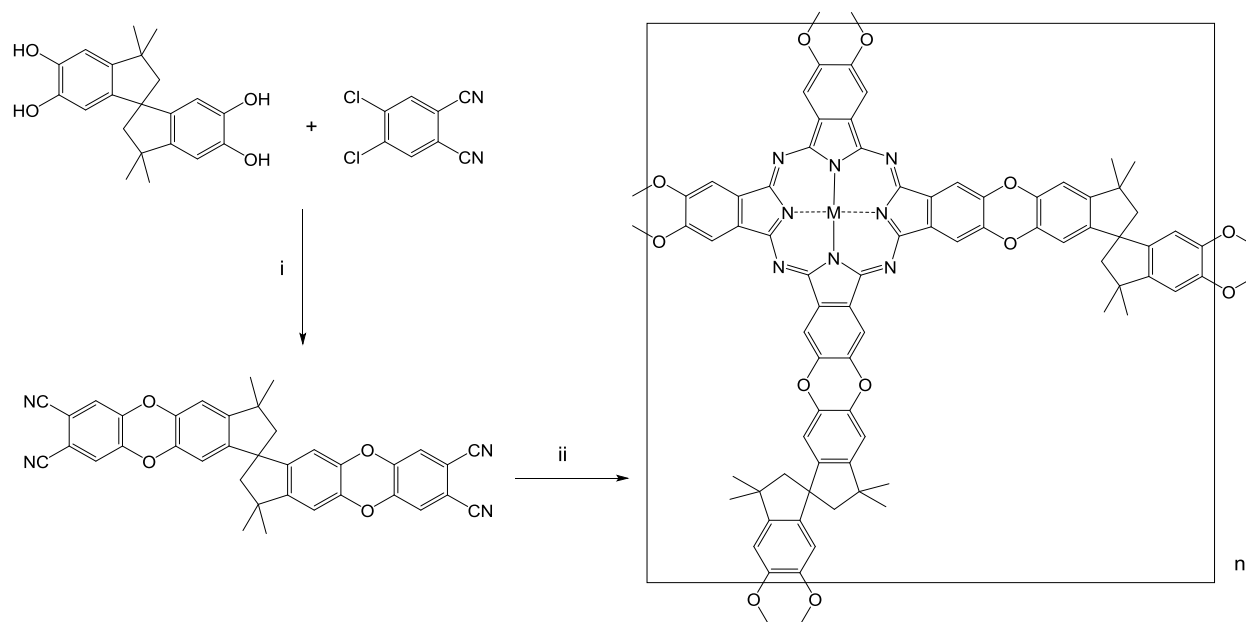
concave faces is highly inefficient due to incomplete mutual interpenetration of concavities.^[72,73] Thus, molecules that possess awkward shapes are expected to pack space inefficiently giving rise to the concept of ‘Intrinsic Microporosity’ (IM).^[74] This concept can be defined as ‘a continuous network of interconnected intermolecular voids which forms as a direct consequence of shape and rigidity of the component macromolecules’.^[75] In general, most polymers pack space efficiently maximizing attractive interactions between component macromolecules and minimizing the amount of void space (since from a molecule’s point of view, ‘empty space is wasted space’^[76]). Most polymers also have sufficient conformational flexibility which allows them to rearrange their shape maximizing intermolecular interactions. Hence, in order to induce IM, it is necessary to design polymers with highly awkward molecular shapes using rigid and contorted molecular components that cannot pack space efficiently. The lack of rotational freedom along the polymer backbone due to fused ring structures also ensures that component macromolecules do not rearrange their conformation and their awkward shape remains fixed during synthesis. In this field, new polymer based microporous materials have found many applications such as in membrane technology^[77,78] including nanofiltration^[79] and gas separation membranes,^[80,81] as adsorbents^[82-84] and sensors,^[85] and in catalysis.^[86-88]

1.7.1 Network PIMs

A wide range of organic network PIMs can be prepared by the general strategy of reacting appropriate fluorinated or chlorinated monomers with complementary monomers containing multiple catechol units^[87,89-92] as will be reviewed below.

1.7.1.1 Pc and Porphyrin based network PIMs

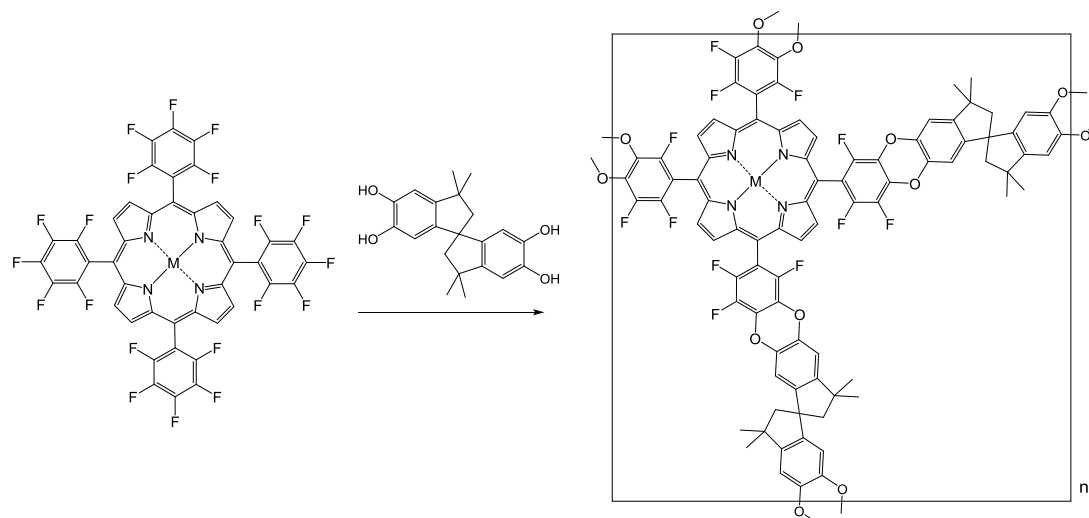
It is well known that Pcs have a strong tendency to form densely packed columnar stacks in which co-facial intermolecular π - π interactions are maximised. Due to this, several Pc based network polymers with different linking groups examined in the past have very low surface areas and are not porous.^[93] However, in 2002, McKeown *et al.* showed that Pc based network polymers constructed using rigid spirocyclic linkers (**Scheme 1.3**) enforce an orthogonal orientation of adjacent Pc units inducing porosity.^[94]



Scheme 1.3: Synthesis of Pc based network PIMs containing spirocyclic linkers. *Reagents and conditions:* (i) K_2CO_3 , DMF, 70 °C; (ii) Metal salt, quinoline, 220 °C (for $M = Zn^{2+}$, Co^{2+} , Cu^{2+}) or lithium pentoxide, pentan-1-ol, reflux (for $M = 2H^+$).

Spectroscopic and structural characterisation of the network polymers confirmed that the rigid spirocyclic linkages prevent close packing of the Pc units due to their orthogonal alignment and the resultant materials were found to have high BET surface areas ranging from 450 – 950 $m^2 g^{-1}$ depending on the metal cation. These Pc based network polymers were actually the first examples of porous materials from which the concept of PIMs originated.

Due to the potential applications of the above mentioned materials in heterogeneous catalysis, it was of interest to extend this investigation into catalytically active porphyrins. Since it is known that the formation of porphyrins from the reaction between pyrrole and a suitable aldehyde is not as efficient as Pc formation,^[95] hence, for network assembly, McKeown *et al.* utilised the commercially available *meso*-tetrakis(pentafluorophenyl)porphyrin monomer which can undergo a nucleophilic aromatic substitution reaction (S_NAr) with two equivalents of the spirocyclic monomer (**Scheme 1.4**) forming rigid dibenzodioxane units.^[96] The resultant network polymers again exhibited large surface areas (900 – 1000 $m^2 g^{-1}$) as revealed by BET nitrogen sorption analysis.



Scheme 1.4: Synthesis of porphyrin based network PIMs containing spirocyclic linkers. *Reagents and conditions:* K_2CO_3 , NMP, 200 °C; 6 h. (M = FeCl or H_2).

Previously it has been established that the most distant fluorine atom (para to the porphyrin core) on each of the *meso*-pentafluorophenyl groups is readily substituted by nucleophiles, ^[97] therefore in order to ensure successful synthesis of the desired porphyrin network PIMs, a model S_NAr reaction was carried out between the porphyrin precursor and four equivalents of catechol. MALDI-MS analysis (**Figure 1.6**) of the crude reaction product confirmed that the only significant product was the tetra-substituted porphyrin containing single benzodioxane units fused to each of the four *meso*-phenyl substituents. Hence, an initial substitution of the para fluorine atom is followed by a rapid substitution of a neighbouring fluorine atom.

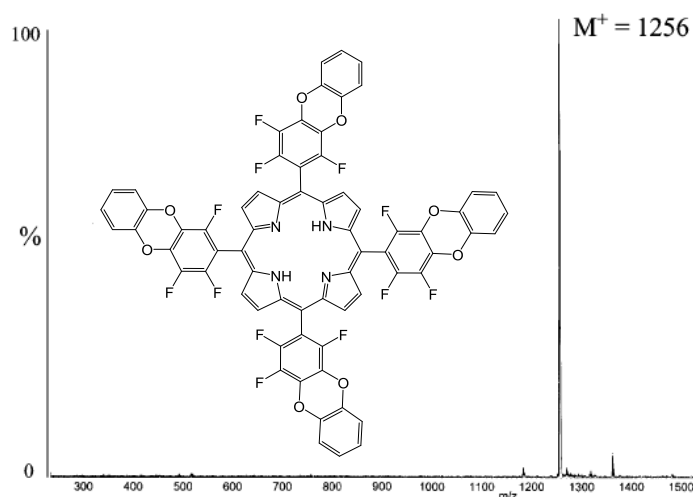


Figure 1.6: MALDI mass spectrum and structure of the tetra-catechol substituted porphyrin.

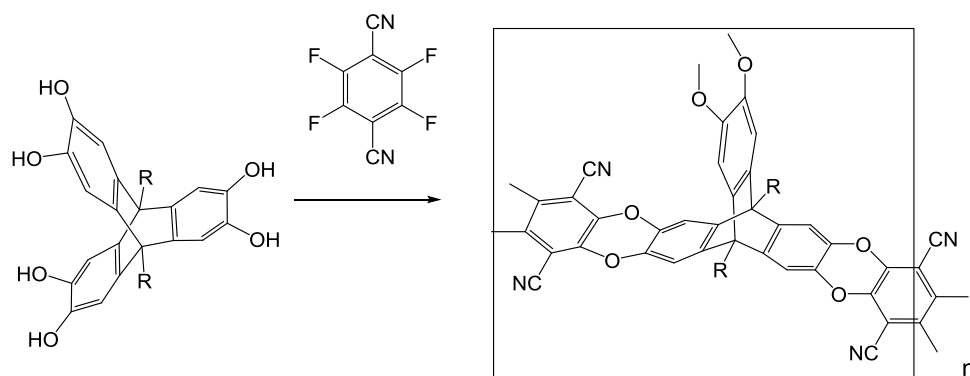
In a further investigation, both of the aforementioned Pc and porphyrin network PIMs containing rigid spirocyclic linkers were found to be efficient catalysts for the decomposition of hydrogen peroxide, the oxidation of cyclohexene and of hydroquinone. ^[98] Hence, these materials are examples of simple biomimetic systems in which an effective isolation of the aromatic Pc or porphyrin core by rigid linkers creates space around the active metal centres, enabling reagents to gain easy access and for reaction to occur.

1.7.1.2 Triptycene based network PIMs

Triptycene is an attractive and highly suitable component for the synthesis of materials of IM due to its rigid, fused ring system and its 3-fold symmetry. Triptycenes have been exploited as components of functional molecular systems such as ligands, ^[99] molecular cages, ^[100] supramolecular receptors ^[101-103] and as materials such as liquid and clathrate crystals, ^[104,105] coordination networks, ^[106,107] and polymers. ^[108,109] For designing microporous materials, triptycene's large internal molecular free volume (IMFV) is of particular interest ^[110,111] and this property can be exploited to obtain suitable materials of spacious cavities with applications as molecular hosts for adsorption ^[112] e.g. 'iptycene' (a term used to describe the extension of the triptycene systems) ^[113] based polymers which are beneficial for adsorbing aromatic molecules for fluorescence based sensors ^[114] or triptycene based oligomers which are capable of significant nitrogen and hydrogen adsorption. ^[115,116]

In this regard, in 2010, Ghanem *et al.* reported the synthesis (**Scheme 1.5**) and properties of network PIMs derived from triptycene monomers with alkyl groups attached to their bridgehead positions (Trip-(R)-PIMs). ^[117] It was found that nitrogen adsorption can be controlled by the length of the alkyl chain with shorter or branched alkyl chains (methyl or isopropyl) giving greater microporosity in contrast to longer alkyl chains which block the pores due to having sufficient conformational freedom to fill the free volume. This variation of alkyl chains allows the apparent BET surface areas to be tuned within the range of 618 – 1760 m² g⁻¹ (**Table 1.1**). The hydrogen adsorption capacities for methyl and isopropyl containing triptycene PIMs at low pressure were also found to be among the highest reported for purely organic polymers. ^[83] Molecular modelling of a fragment of Trip-(Et)-PIM showed that the triptycene components

constrain the growth of the polymer within the same plane and the faces of the ribbon-like ‘struts’ between the triptycenes become oriented perpendicular to the plane of the macromolecular growth. This arrangement blocks any face to face association between the planar struts and can further frustrate the space-efficient packing of the polymer network leading to enhanced microporosity.

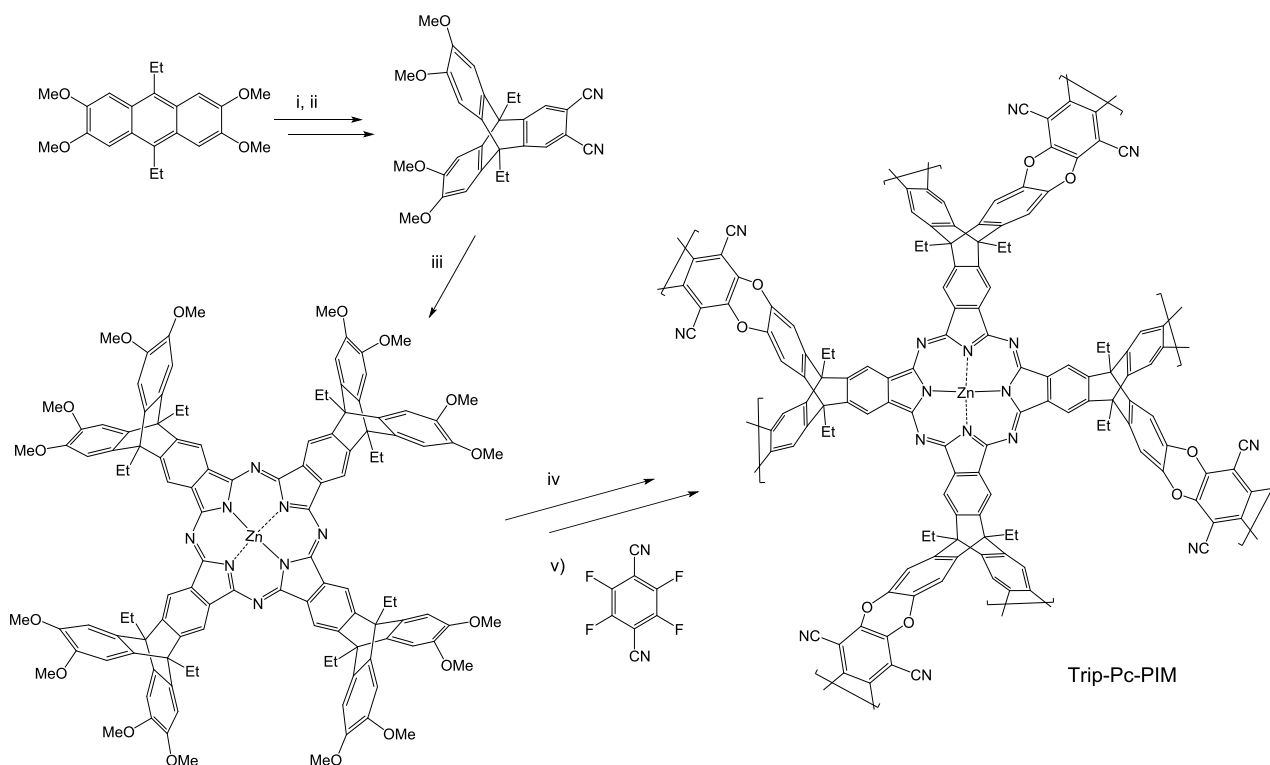


Scheme 1.5: Synthesis of Trip-(R)-PIMs. *Reagents and conditions:* K_2CO_3 , DMF, 80 °C; 24 h.

R group	BET surface area ($m^2 g^{-1}$)
H	1318
Methyl	1760
Ethyl	1416
<i>n</i> -Propyl	1343
<i>i</i> -Propyl	1601
<i>n</i> -Butyl	978
<i>i</i> -Butyl	1076
Pentyl	947
Octyl	618
Benzyl	880

Table 1.1: Variation of R group in Trip-(R)-PIMs and their measured BET surface areas.

The separate developments of Pc based network PIMs and triptycene based network PIMs was followed by the report of a highly rigid network polymer (Trip-Pc-PIM) in 2011, bearing both triptycene and multifunctional Pc components (**Scheme 1.6**).^[118] Nitrogen sorption studies of this polymer revealed an apparent BET surface area of $806 \text{ m}^2 \text{ g}^{-1}$ which is lower than that of the equivalent Trip-(Et)-PIM reported previously^[117] but higher than that of the best characterised Pc PIM^[86] (designated CoPc20) prepared via the bis-phthalonitrile route. Of particular note is the Type-I isotherm of Trip-Pc-PIM with minimal hysteresis between adsorption and desorption isotherms (**Figure 1.7**) suggesting that an extensive 3-D network connectivity as well as component rigidity results in a non-swelling structure of enhanced rigidity for Trip-Pc-PIM which is more characteristic of a crystalline nanoporous material such as a zeolite or a MOF.^[119]



Scheme 1.6: Synthesis of Trip-Pc-PIM. *Reagents and conditions:* i) 1,2,4,5-tetrabromobenzene, *n*-BuLi, toluene, 20 °C, 3 h; ii) CuCN, DMF, reflux, 6 h; iii) Zn(OAc)₂, DMAc, reflux, 48 h; iv) BBr₃, DCM, 20 °C, 24 h; v) K₂CO₃, DMF, 80 °C; 48 h.

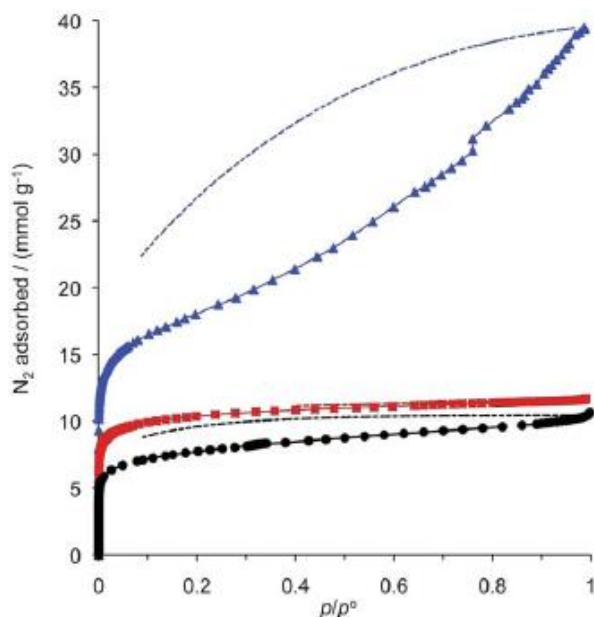
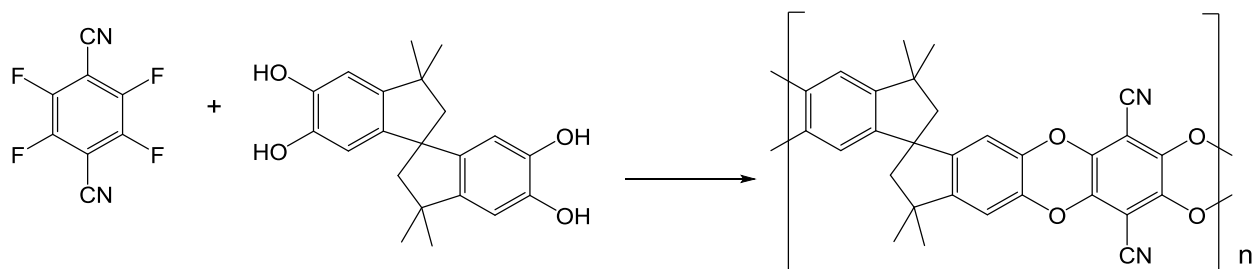


Figure 1.7: The nitrogen sorption isotherms of Trip-Pc-PIM (red); CoPc20 (black) and Trip(Et)-PIM (blue). For Trip-Pc-PIM, the desorption curve is almost indistinguishable from the adsorption curve. (Figure reproduced from Ref. ^[118]).

1.7.2 Ladder PIMs

Due to the high insolubility of network PIMs, the efficiency of dibenzodioxin forming polymerisation reaction was investigated by the development of non-network soluble PIMs. For this purpose, a non-network soluble polymer (PIM-1) was reported in 2004, prepared from tetrahydroxy-tetramethylspirobisindane (biscatechol) and tetrafluoroterphthalonitrile (**Scheme 1.7**), whose randomly contorted shape prevents an efficient packing in the solid state. ^[120] This fluorescent yellow polymer was fully soluble in polar aprotic solvents, high molecular weight of which could be determined by Gel Permeation Chromatography (GPC) and exhibited a high BET surface area of $850 \text{ m}^2 \text{ g}^{-1}$ by nitrogen sorption analysis. The microporosity of this polymer arises from high rigidity combined with a randomly contorted shape (**Figure 1.8**) and was termed ‘intrinsic’ as it arises solely from its molecular structure.



Scheme 1.7: Synthesis of PIM-1. *Reagents and conditions:* K_2CO_3 , DMF, 60 – 120 °C.

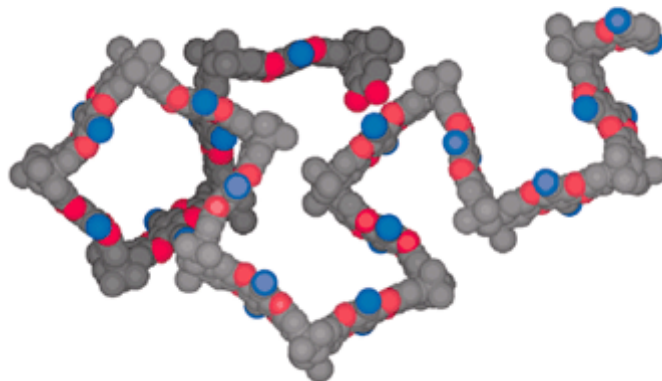
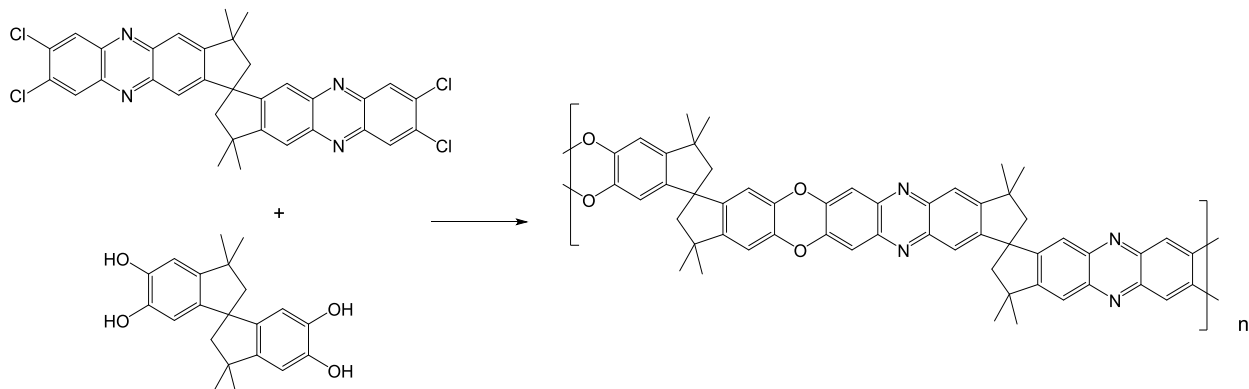


Figure 1.8: Space filling molecular model of a fragment of PIM-1 showing its rigid, randomly contorted structure. (Figure reproduced from Ref. ^[120]).

A similar ladder polymer prepared from the reaction between the bisphenol and a more complex tetrachloride monomer (**Scheme 1.8**) results in the formation of PIM-7, nitrogen sorption analysis of which gave a BET surface area of $750 \text{ m}^2 \text{ g}^{-1}$. ^[92] The phenazine subunits present in the structure of PIM-7 can also be exploited to act as ligands for metal ion coordination such as Pd^{2+} with the resultant microporous materials bearing the potential to be used as efficient heterogeneous catalysts. ^[121]



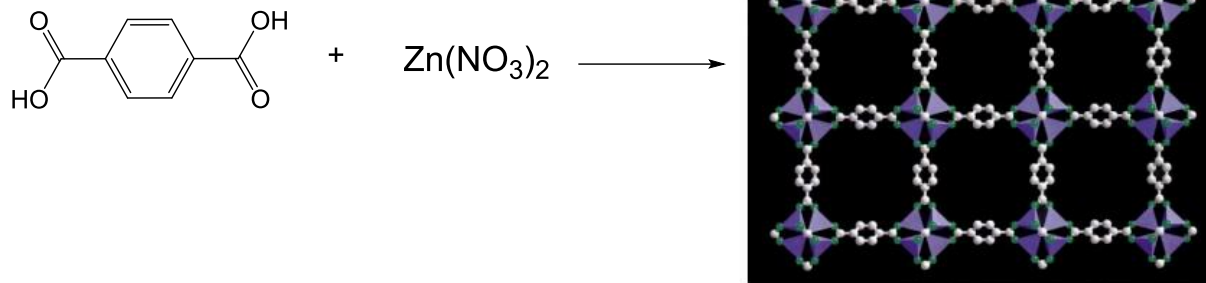
Scheme 1.8: Synthesis of PIM-7. *Reagents and conditions:* K_2CO_3 , DMF, 60 – 120 °C.

The solution processability of these polymers is advantageous over network PIMs in the preparation of solvent-cast membranes for gas separation^[80] with their transport properties further tailored by chemical modifications such as through carboxylation of nitrile groups of PIM-1^[122] or through incorporation of co-monomers.^[123] Moreover, the intrinsic fluorescence of PIM-1 has shown to enable the fabrication of a laser sensor using a thin film of PIM-1 with great sensitivity for the detection of nitrated aromatics.^[124]

1.8 MOFs and COFs

MOFs are hybrid porous solids containing metal ions (inorganic moieties) which are coordinated to organic molecules to form a crystalline 3-D framework. Unlike inorganic zeolites, MOFs have the potential for more flexible and diverse rational design through the use of various organic moieties and metal centres allowing control of architecture and functionalization of pores. MOFs are therefore promising materials of great interest with applications in the field of catalysis,^[125] separation,^[126] gas storage^[127] and molecular recognition.^[128]

Yaghi and co-workers in 1999 firstly reported a MOF (MOF-5) of permanent porosity which remained crystalline and stable to desolvation when heated up to 300 °C.^[129] Previous reports showed the structure of these open frameworks to collapse in the absence of solvent molecules.^[130,131] MOF-5 which was prepared by the reaction of 1,4-benzenedicarboxylate linker with zinc nitrate (**Scheme 1.9**) maintained its periodicity after the evacuation of solvent guest molecules as determined by x-ray single crystal diffraction study. The apparent surface area of MOF-5 determined using gravimetric methods was found to be around 3000 m² g⁻¹ with a Type-I nitrogen sorption isotherm.

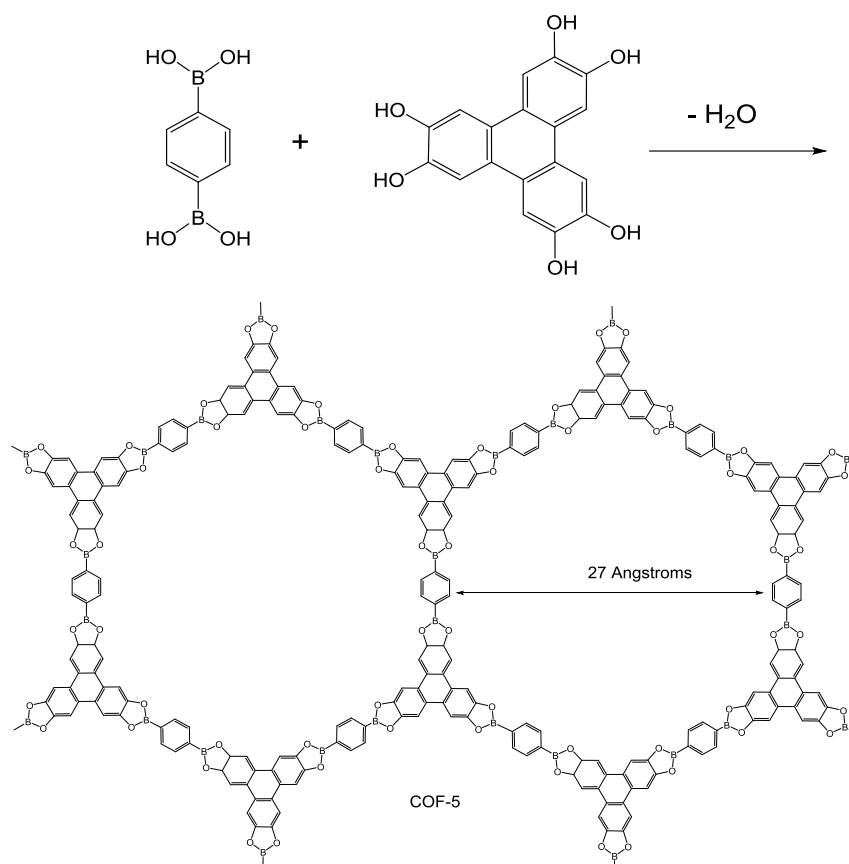


Scheme 1.9: Synthesis and representation of a layer of MOF-5 as determined by single crystal x-ray diffraction study (C, grey; O, green; ZnO₄ tetrahedra are indicated in purple). *Reagents and conditions:* triethylamine, DMF/chlorobenzene, H₂O₂. (Figure reproduced from Ref. ^[129]).

Following the discovery of MOF-5, the researchers went on to develop an ‘isoreticular series’ (one that has a same framework topology) of sixteen further crystalline materials with variable crystal volumes and pore sizes. ^[132] This was done through functionalization of aryl dicarboxylic acid (BDC) units with various groups such as –Br, –NH₂, –OC₃H₇, –C₂H₄ etc. with the pore sizes being expanded by creating longer molecular struts through the replacement of the BDC unit with biphenyl, tetrahydropyrene, pyrene and terphenyl units. This systematic design and construction of a series of frameworks thus allows the targeting of specific properties. For example, out of the compounds prepared, IRMOF-6 demonstrated the highest methane storage capacity attributed to the hydrophobic nature of C₂H₄ groups on the BDC unit.

COFs are purely organic, crystalline extended structures in which the building blocks are linked by strong covalent bonds giving rise to highly rigid porous structures. For example, in 2005 Yaghi *et. al.* reported the synthesis of COF-5, prepared from condensation reaction of phenyldiboronic acid and hexahydroxytriphenylene (**Scheme 1.10**). ^[133] Powder x-ray diffraction (PXRD) studies revealed the porous layers of COF-5 to be stacked in an eclipsed fashion (**Figure 1.9**) with the crystal structure held by strong covalent bonds between B, C and O atoms to form a rigid porous architecture with pore size of up to 27 Å. COF-5 exhibited high thermal stability, permanent porosity and a BET surface area of 1590 m² g⁻¹ with a Type-IV isotherm characteristics of a mesoporous material. Again, by making use of reticular chemistry, the authors also developed 3-D COFs based on tetrahedral shaped boronic acids (such as tetra(4-

dihydroxyborylphenyl)methane) with higher BET surface areas e.g. $3472 \text{ m}^2 \text{ g}^{-1}$ for COF-102 (Figure 1.9) with Type-I Ar gas sorption isotherm. ^[134]



Scheme 1.10: Synthesis and structure of COF-5.

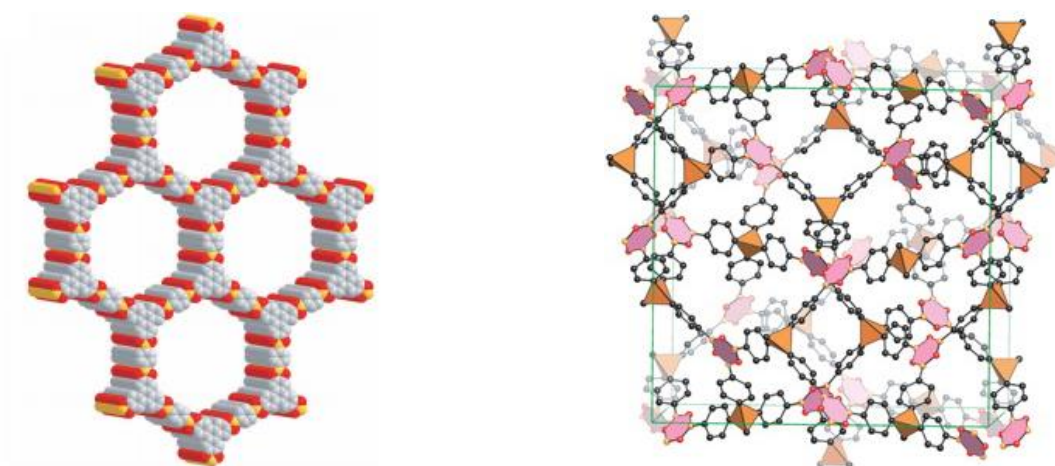


Figure 1.9: Structural representations of COF-5 projected along the c axes (left) and of crystalline product of COF-102 (right) based on powder XRD and modelling. C, B and O atoms are represented as gray, orange, and red spheres respectively. H atoms are omitted. (Figures reproduced from Ref. ^[133] and ^[134] respectively).

In a similar investigation in 2010, Spitler *et. al.* reported the preparation of a 2-D COF composed of Pc macrocycles joined by phenylene bis(boronic acid) linkers.^[135] The synthesis involved Lewis acid catalysed boronate ester formation via deprotection-condensation protocol to give an eclipsed 2-D COF similar to those previously reported by Yaghi and coworkers^[133] but consisting of Pc linkers (**Figure 1.10**). PXRD analysis reveals the Pc-PBBA-COF to be crystalline with long range order and an eclipsed structure due to the strong tendency for Pc units to form co-facial aggregates that are reinforced by stabilizing B–O interactions between adjacent layers. The resulting Pc stacks form pores of 2.3 nm that run parallel to the stacked chromophores. The calculated BET surface area from nitrogen sorption analysis was found to be 450 m² g⁻¹ (Langmiur 506 m² g⁻¹), which is slightly low relative to other reported COFs but still well within the values of other microporous materials.^[136,137] The electronic absorption spectra of dilute solution (~ 10⁻⁶ M) of Pc tetra(acetonide) were typical of a non-aggregating free base Pc with λ_{max} at 653 and 691 nm. In comparison, diffuse reflectance spectra obtained from powders of both Pc-PBBA-COF and Pc tetra(acetonide) show a blue shift of these maxima (11 nm for COF and 66 nm for Pc tetra(acetonide)) as well as broadening of the Q band into the near infrared which is consistent with the formation of co-facially stacked H-aggregates.^[138] Photoluminescence measurements of DCM solutions of Pc tetra(acetonide) fluoresced strongly with a small Stokes shift whereas the solid samples of Pc-PBBA-COF were non-emissive, also suggesting an H-aggregated Pc structure. The changes in absorbance properties exhibited by Pc-PBBA COF, particularly the broadening of the absorbance to enhance absorption in the 450–600 nm region and the tailing into the near infrared, make these materials promising candidates for the collection of solar energy. Also, the material's potential for efficient charge transport through the stacked Pcs, good thermal stability and the modular nature of COF synthesis, show strong promise for applications in organic photovoltaic devices.

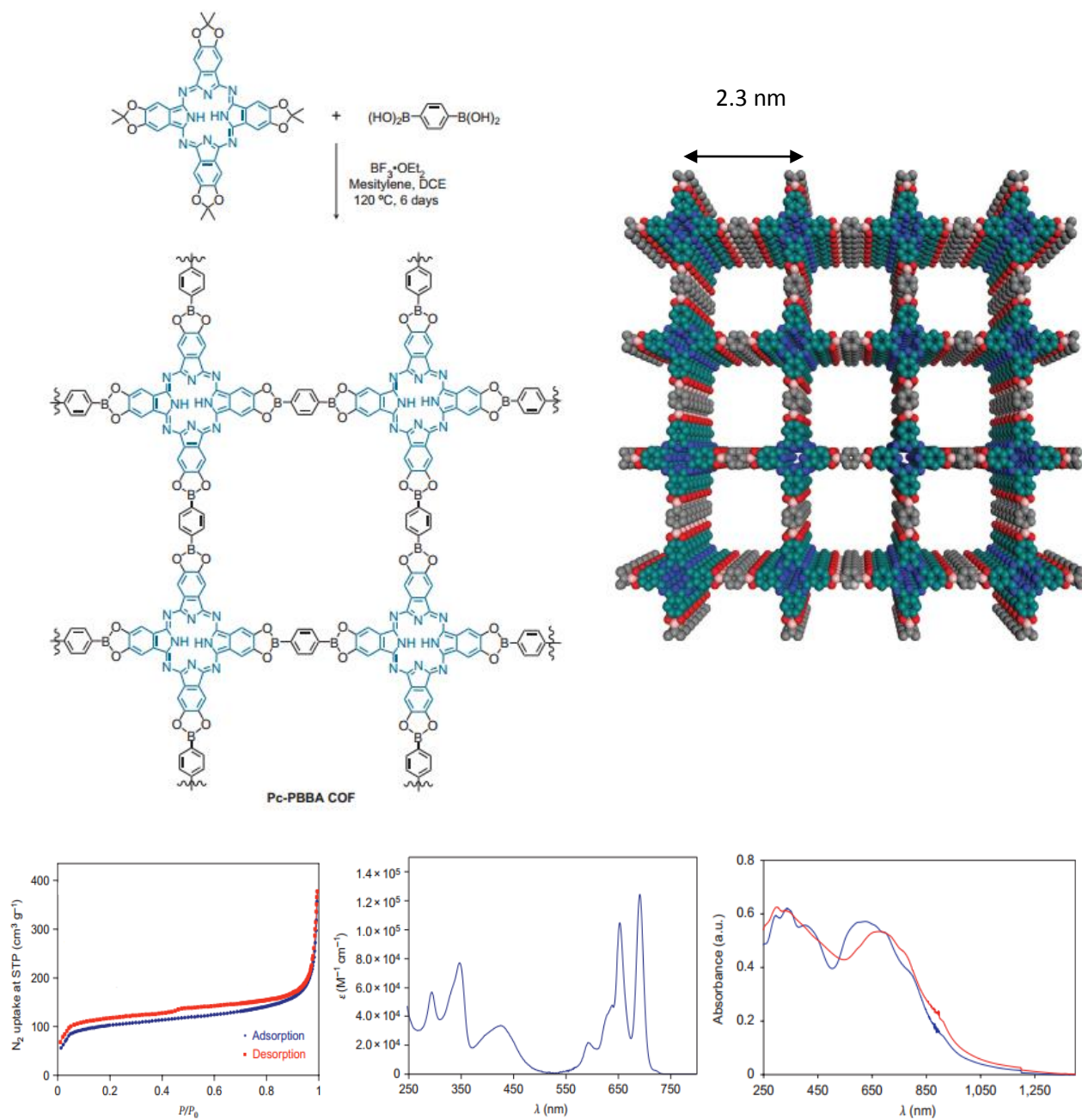


Figure 1.10: Top: Synthesis of Pc-PBBA-COF from Pc tetra(acetonide). Left: A square lattice with 2D sheets that form eclipsed stacks as determined from PXRD. Bottom: Nitrogen sorption isotherm (left), UV-vis spectrum of Pc tetra(acetonide) (middle) and diffuse reflectance spectra of Pc-PBBA-COF (red) and Pc tetra(acetonide) (blue). (Figures reproduced from Ref. ^[135]).

1.9 Microporous Molecular Crystals

1.9.1 Pc based molecular crystals

Nanoporous Molecular Crystals (NMCs) are porous materials composed of discrete molecules between which there are only non-covalent interactions, i.e. they do not possess an extended framework composed of covalent or coordination bonds.^[139] They are formed from removing guest molecules (e.g. solvent molecules) from Inclusion Compounds (ICs) (**Figure 1.11**); a process that for most ICs usually results in the collapse of the open structure of the crystals but in the case of NMCs, the packing of the host molecules is retained and nanoporosity is obtained which can be confirmed by gas adsorption techniques such as BET analysis.

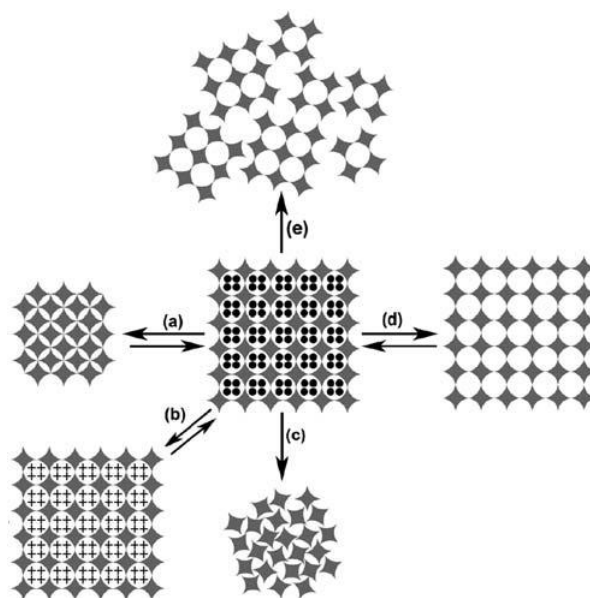


Figure 1.11: Possible processes involving removal or exchange of included solvent within an IC: (a) transformation to a non porous, denser crystal; (b) exchange of included solvent; (c) collapse of crystal structure to a nonporous amorphous solid; (d) formation of a NMC and (e) formation of a NMC accompanied by fragmentation of the crystal due to internal stress caused by a reduction in unit cell size. (Figure reproduced from Ref. ^[139]).

In this context, in 2005, McKeown *et al.* reported a novel zinc 2,3,9,10,16,17,23,24-octa(2',6'-di-*iso*-propylphenoxy)phthalocyanine compound where 2,6-di-*iso*-propylphenoxy groups placed on the peripheral positions of the Pc ring can introduce severe steric crowding to avoid the

cofacial self-association. [21] Slow crystallization of this compound by diffusing acetone into chloroform solution gave large cubic crystals (up to 1 mm³). The packing arrangement as studied by XRD analysis consisted of solvent filled voids of large volume (8 nm³) to be present with each nanovoid being enclosed by a cubic assembly of six Pc molecules and containing 18 and ~65 molecules of water and acetone respectively. In addition, it was found that many other metal complexes of this Pc derivative such as Mg²⁺, Al³⁺, Ti⁴⁺, Mn²⁺, Co²⁺, Ru²⁺, In³⁺ as well as Fe²⁺ (a close analogue of heme) form isomorphous crystals (**Figure 1.12**) even with great variation in size, type and number of axial ligands. [140]

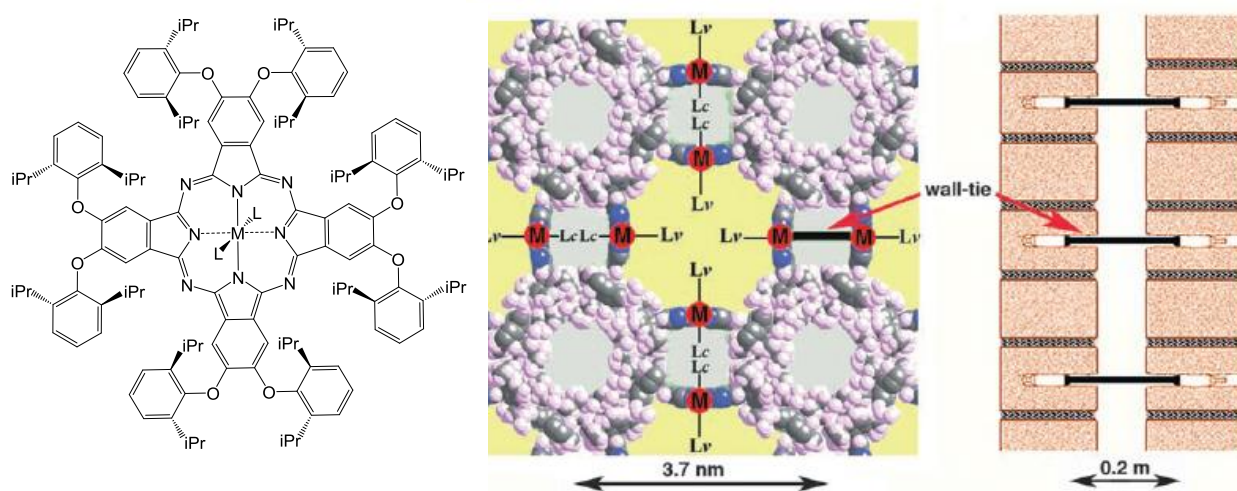


Figure 1.12: The molecular structure of the Pc complexes (left) where L = axial ligand and a space filling model of the crystal structure, of a cross section through the unit cell composed of the Pc complex (middle) and a cross section through a cavity brick wall showing the role of wall ties in maintaining stability (right). (Figures reproduced from Ref. [140]).

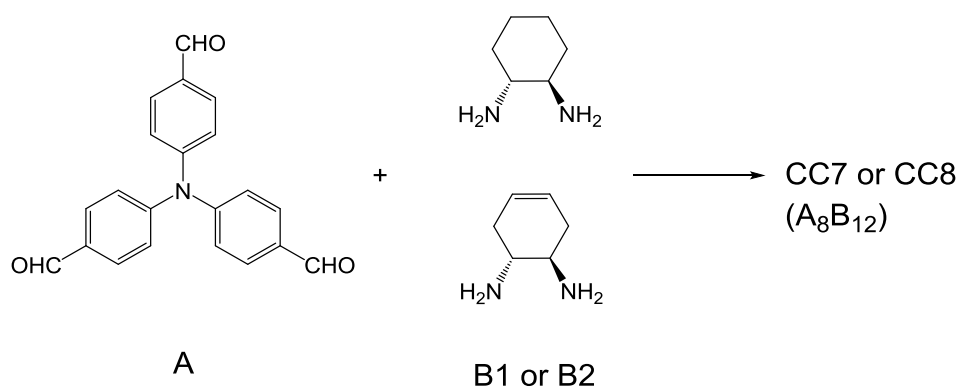
It was found that the original solvent of recrystallisation can be rapidly and reversibly exchanged with other solvents. The crystal structure also differentiated between the axial binding sites of the macrocycle so that ligands could be selectively placed within the nanovoid (Lv) or within the minor cavity that separates the cubic hexa-Pc assemblies (Lc). Hence, suitable bidentate ligands of an appropriate length such as bipy are capable of binding simultaneously to two metal cations across the cavity thus forming a bridge to give a dimeric complex. These architectural “wall ties” stabilize the crystal structure to the removal of included solvent and the molecular crystals

demonstrate permanent nanoporosity and high surface areas ($850 - 1000 \text{ m}^2 \text{ g}^{-1}$) by BET nitrogen sorption analysis.

Initial studies also showed that the related AzaPcs have very similar nanoporous crystal forming properties^[31] so that the reactivity of the transition metal centre within these materials can also be tuned by modifying the macrocycle structure to provide catalytic PUNCs (Pc Unsolvated Nanoporous Crystals) of different reactivity.

1.9.2 Porous organic cage crystals

As an alternative to extended framework materials, porous organic cage crystals have become a major focus recently, since discrete organic molecules offer advantages like solubility, synthetic diversification and post-functionalization in comparison to network materials.^[141] Organic cages are mostly restricted to micropore regime owing to their relatively small molecular size with large structures with big pores being susceptible to structural collapse when desolvated.^[142,143] For example, in 2011, Jelfs *et. al.*^[142] reported the synthesis and structure of two large covalent cage molecules obtained through imine condensation reactions between tris(4-formylphenyl)amine and the chiral diamines (**Scheme 1.11**). Upon desolvation, both cages were found to become amorphous and non-porous to nitrogen at 77 K. A combination of XRD analysis, molecular simulations and DFT calculations revealed that the solvent free cage collapses during simulation causing an increase in dispersive interactions and the formation of multiple π - π stacks of arene species on opposing faces (**Figure 1.13**) which results in an energetically favourable collapsed conformation.



Scheme 1.11: One pot [8+12] synthesis of cages CC7 and CC8.

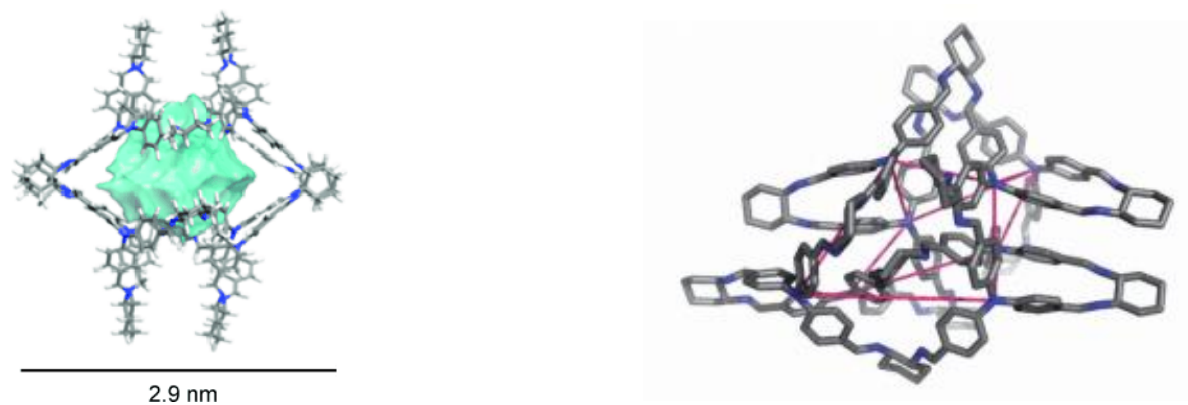
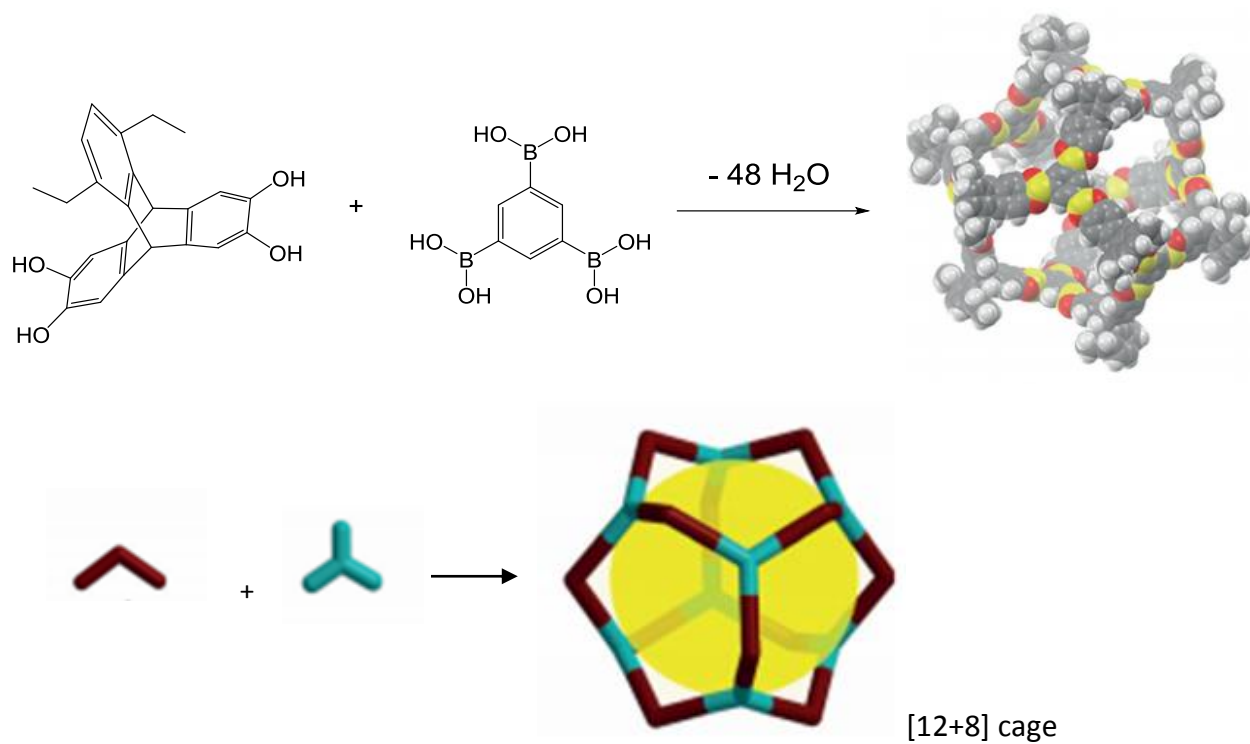


Figure 1.13: Single crystal x-ray structures of CC7 (left) and a representative collapsed cage (right). Distortion of the original cubic topology is illustrated by the pink lines connecting the cage faces. (Figures reproduced from Ref. ^[142]).

In view of this, Zhang *et. al.* ^[144] have recently reported the synthesis of a shape persistent cage compound of cuboctahedral geometry by the reversible formation of boronic ester units starting from triptycene tetraol and triboric acid molecules (**Scheme 1.12**). Single crystal XRD data shows the large cavity of this compound to have an inner diameter of 2.4 – 2.6 nm between two opposite aryl rings of triboronic ester units and 2.9 – 3.1 nm between the bridgehead atoms of two triptycene units. The molecules pack through π - π interactions along the crystallographic *c* axis resulting in a staggered coplanar assembly of boronic ester units of adjacent molecules at 3.2 – 3.4 Å. After removing enclathrated solvent molecules, the molecular cage remains intact and maintains its shape but undergoes a phase change in the assembling of cages as determined by PXRD analysis. The resultant mesoporous material exhibits an exceptionally high BET surface area of 3758 m² g⁻¹ with a pore diameter of 2.3 nm as determined by nitrogen sorption analysis.



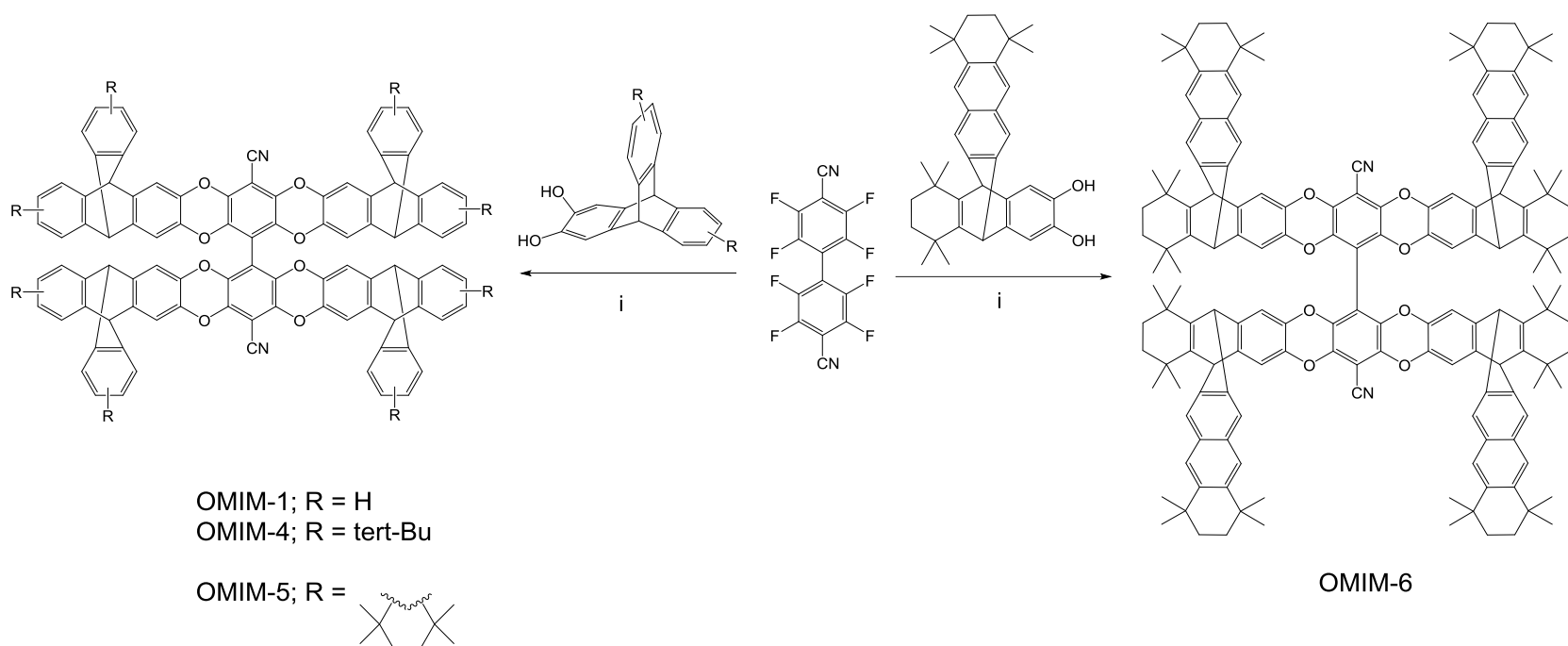
Scheme 1.12: A one step 48-fold condensation reaction of twelve molecules of triptycene tetraol with eight molecules of the triboric acid to give a cuboctahedral [12+8] cage. (Figures reproduced from Ref. [144]).

1.10 Oligomeric Molecules of IM (OMIMs)

Organic Molecules of Intrinsic Microporosity (OMIMs) are a class of discrete molecules of rigid and awkward shapes sharing the same concept as PIMs that achieve porosity through inefficient packing.^[74] These molecules possess large concavities where mutual interpenetration is highly restricted and form microporous glasses.

1.10.1 Triptycene based OMIMs

A mathematical study of geometric shapes by Jiao *et. al.* reveals that the maximum packing density of concave 2-D superdisks and 3-D superballs decreases with increasingly concave faces.^[72,73] In this context, in 2012, Abbott *et. al.* carried out molecular packing simulations of various triptycene based OMIMs containing biphenyl cores and terminal units of various geometries and showed that the addition of bulky substituents such as *tert*-butyl groups to the termini units increase both the amount and accessibility of microporosity.^[145] As reported by Taylor *et. al.*, these OMIMs can be prepared with ease by fusing four dihydroxytriptycene precursors to an octafluorobiphenyl core via an efficient S_NAr reaction (**Scheme 1.13**).^[146] The resultant rigid molecular structures of these OMIMs cause an inefficient packing resulting in the formation of amorphous materials. Apparent BET surface areas measured for the prepared OMIM-1, -4, -5 and -6 were found to be 480, 626, 702 and 622 m² g⁻¹ respectively. In addition, the rate of nitrogen adsorption was found to be much faster for OMIM-4, -5 and -6 compared to OMIM-1 which confirmed the prediction of molecular packing simulations that placing bulky substituents enhances microporosity due to a more open conformation adopted by these molecules. The BET surface area of 702 m² g⁻¹ for OMIM-5 (**Figure 1.14**) is also comparable to microporous amorphous materials based on cages^[147] or PIMs (e.g. PIM-1 ~ 760 m² g⁻¹).^[74]



Scheme 1.13: Synthesis of triptycene based OMIMs. *Reagents and conditions:* (i) K_2CO_3 , DMF, 65 °C, 48 h.

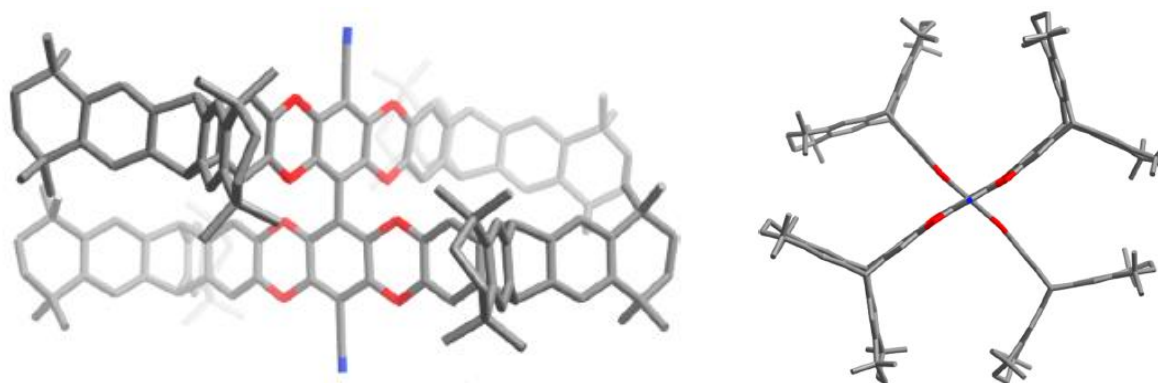
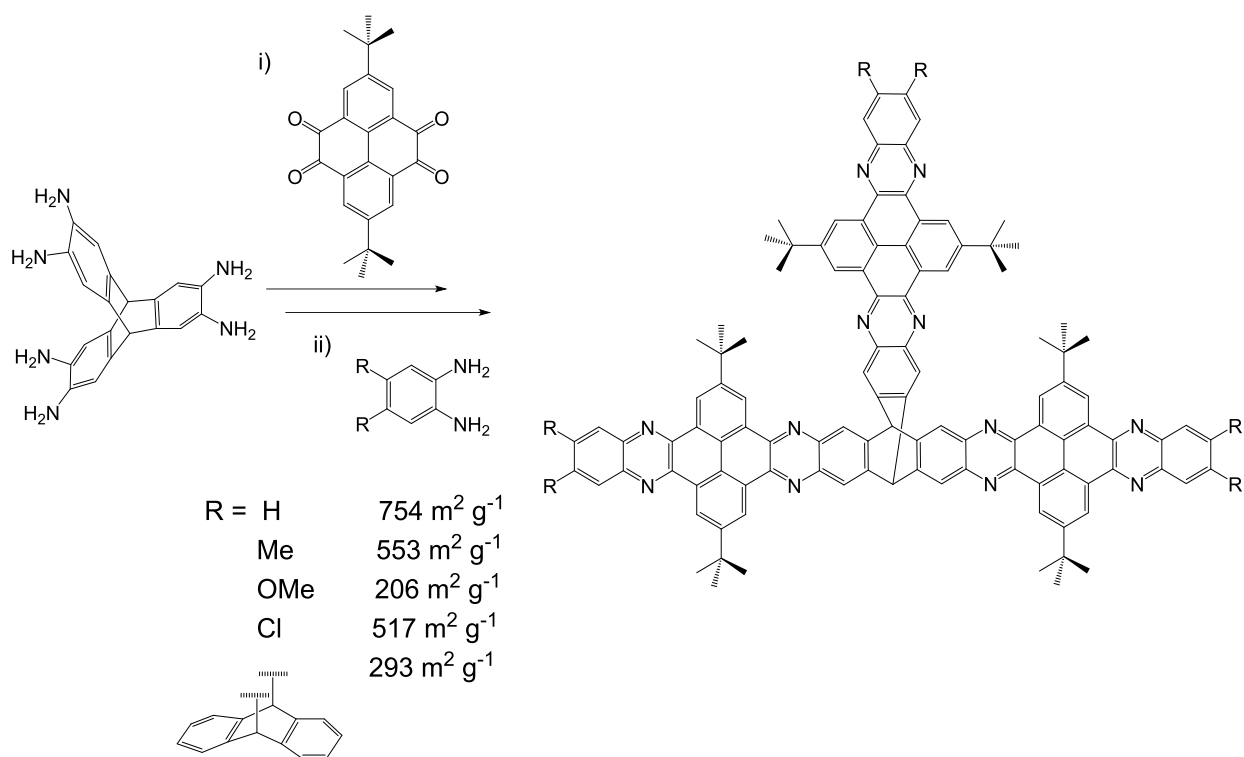


Figure 1.14: Two views of x-ray single crystal structures of OMIM-5. Hydrogen atoms are removed for clarity. (Figure reproduced from Ref. [146]).

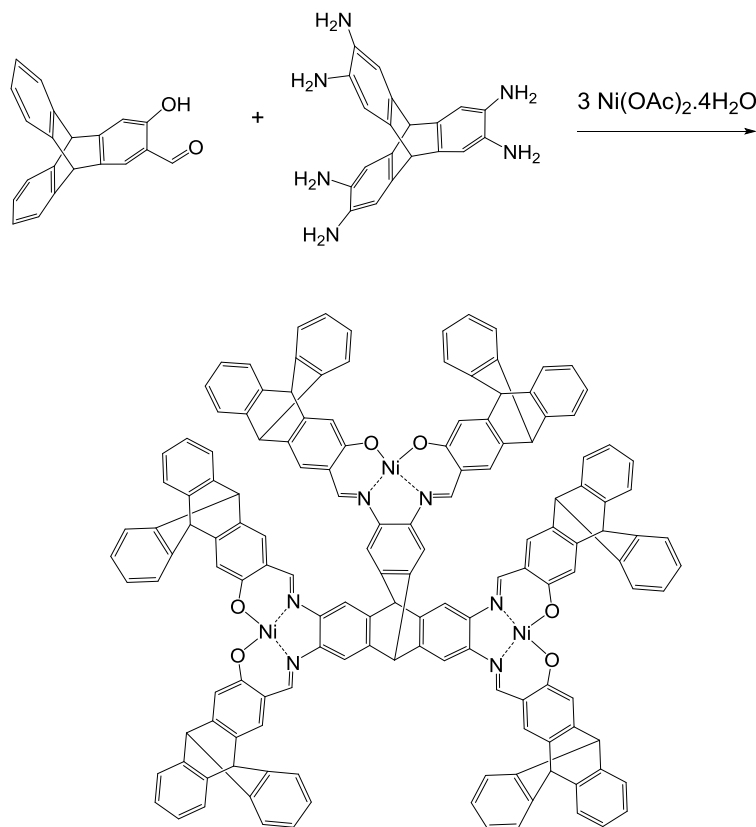
Kohl *et. al.* have also recently reported the synthesis and microporosity of triptycene based molecules which are porous solely due to their inefficient packing in the solid state. ^[148] The synthesis (**Scheme 1.14**) is based on condensation reactions which cause the enlargement of the aromatic arms of the triptycene core to give highly rigid π extended molecules of large IMFVs which are microporous, exhibiting BET surface areas in the range of 206 – 754 m² g⁻¹, depending on the R group. Additionally, these molecules are good electron acceptors as revealed by photophysical measurements with potential application in organic electronics and sensing. ^[149,150]



Scheme 1.14: Synthesis of Kohl's extended triptycene molecule. *Reagents and conditions:* (i) KOAc, AcOH, EtOH/CHCl₃, 85 °C, 16 h; (ii) AcOH, CHCl₃, 70 °C, 15 h.

Similarly, Chong *et. al.* in 2009 reported the synthesis and microporosity of an amorphous trinuclear triptycene based nickel salphen complex, efficient packing of which is hindered by its awkward shape giving rise to a porous solid of high IMFV. ^[116] The complex which can be synthesized via Schiff base condensation (**Scheme 1.15**) was found to have a BET surface area of 403 m² g⁻¹ as determined by nitrogen sorption analysis. The complex also demonstrated hydrogen storage capacity, which is usually facilitated by the number of aromatic rings and

metal centers ^[127] with significant adsorption at low relative pressure, confirming a high population of micropores.

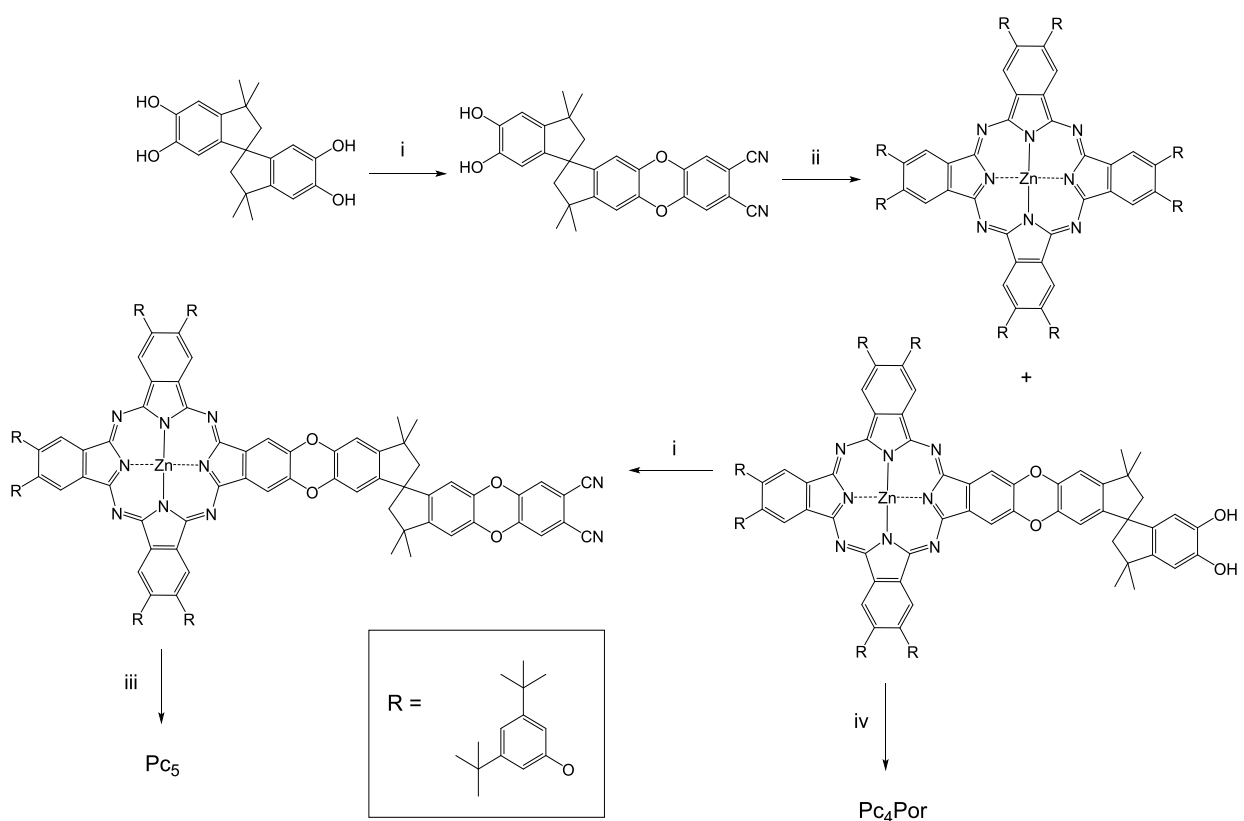


Scheme 1.15: Synthesis of Chong's triptycene based Ni salphen complex.

1.10.2 Pc and porphyrin based oligomers

It is known that strong intermolecular cohesion between the planar faces of the Pc molecule results in unwanted effects on the optical properties of Pcs e.g. broadening and displacement in the position of the Q band in the visible region of the UV-vis spectrum due to exciton coupling. ^[151,152] Co-facial association can result in a blue shift in the position of the Q band from $\lambda_{\max} \sim 680$ nm for the monomer to ~ 635 nm for the dimer and to ~ 615 nm for the higher aggregates. In contrast, edge to edge exciton interactions results in red shifts of the λ_{\max} to higher values. ^[59] These types of aggregation also cause quenching of fluorescence and interference with the formation of singlet oxygen which is an active component of PDT. ^[153] Therefore, it is highly desirable to design materials that act as 'solid solution' in which the Pc units are isolated from one another. ^[154]

In this regard, in 2005, Makhseed *et al.* reported the synthesis and properties of two non-planar and highly rigid pentamers containing four Pc units linked to either a Pc core (**Pc₅**) or a porphyrin core (**Pc₄Por**) via orthogonal spirocyclic units (**Scheme 1.16**).^[155] The pentamers consisted of highly rigid linking groups as well as possessing a randomly contorted shape (**Figure 1.15**) that can discourage any aggregation. Moreover, the presence of *tert*-butyl phenoxy groups around the Pc core provided a high degree of solubility for these pentamers. Analysis by UV-vis absorption spectroscopy showed that the solution spectra of the pentamers are almost identical to the solid state spectra obtained from spin coated films with only slight broadening of the Q band in the latter spectra which suggests a looser amorphous packing of the Pc units. Surprisingly, an assessment of the microporosity of these oligomers by BET revealed no surface area of **Pc₅** (1 m² g⁻¹ measured) and a very low surface area of **Pc₄Por** (100 – 110 m² g⁻¹) suggesting the presence of some microporosity only in the porphyrin containing oligomer.



Scheme 1.16: Synthesis of pentamers **Pc₅** and **Pc₄Por**. *Reagents and conditions:* (i) 4,5-Dichlorophthalonitrile, K₂CO₃, DMF, 60 °C, 24 h; (ii) Excess 4,5-di[3,5-di(*tert*-butyl)phenoxy]phthalonitrile, Zn(OAc)₂, NMP, 150 °C, 24 h; (iii) Zn(OAc)₂, NMP, 150 °C, 24 h; (iv) Tetrakis(pentafluorophenyl)porphyrin, K₂CO₃, DMF, 60 °C, 24 h.

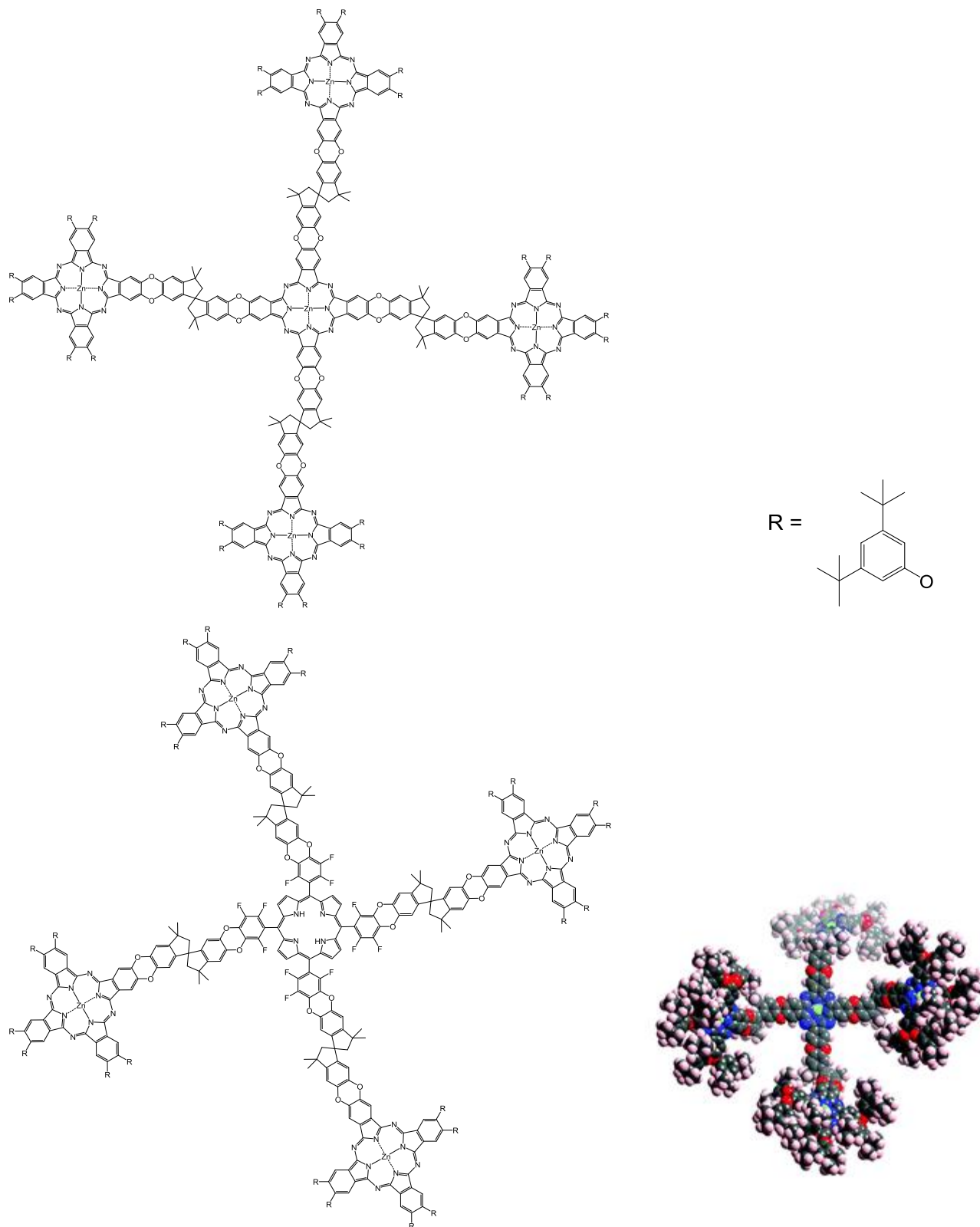


Figure 1.15: Structures of **Pc₄Por** (top) and **Pc₅** (bottom). Also shown below is a space filling molecular model of one of the many possible isomers of **Pc₅**. (Reproduced from Ref. ^[155]).

2. Aims and objectives

The reported triptycene based OMIMs ^[146] and Pc and porphyrin based oligomers ^[155] reviewed previously encouraged us to firstly study the novel octa-*tert*-butyl-tetratriptycene containing Pcs. The specific aim of the project was to design Pc containing molecules of intrinsic microporosity due to their ease of synthesis and reproducibility while offering a well defined structure-property relationship that can be studied in solution, (mainly UV-vis absorption spectroscopy) and as solid state (microporosity measurements). Two other aromatic cores i.e. porphyrazine and porphyrin containing triptycene based molecules were also of interest to look at since they are touched upon only to a limited extent in the literature. ^[155,156]

3. Phthalocyanine containing Molecules of Intrinsic Microporosity

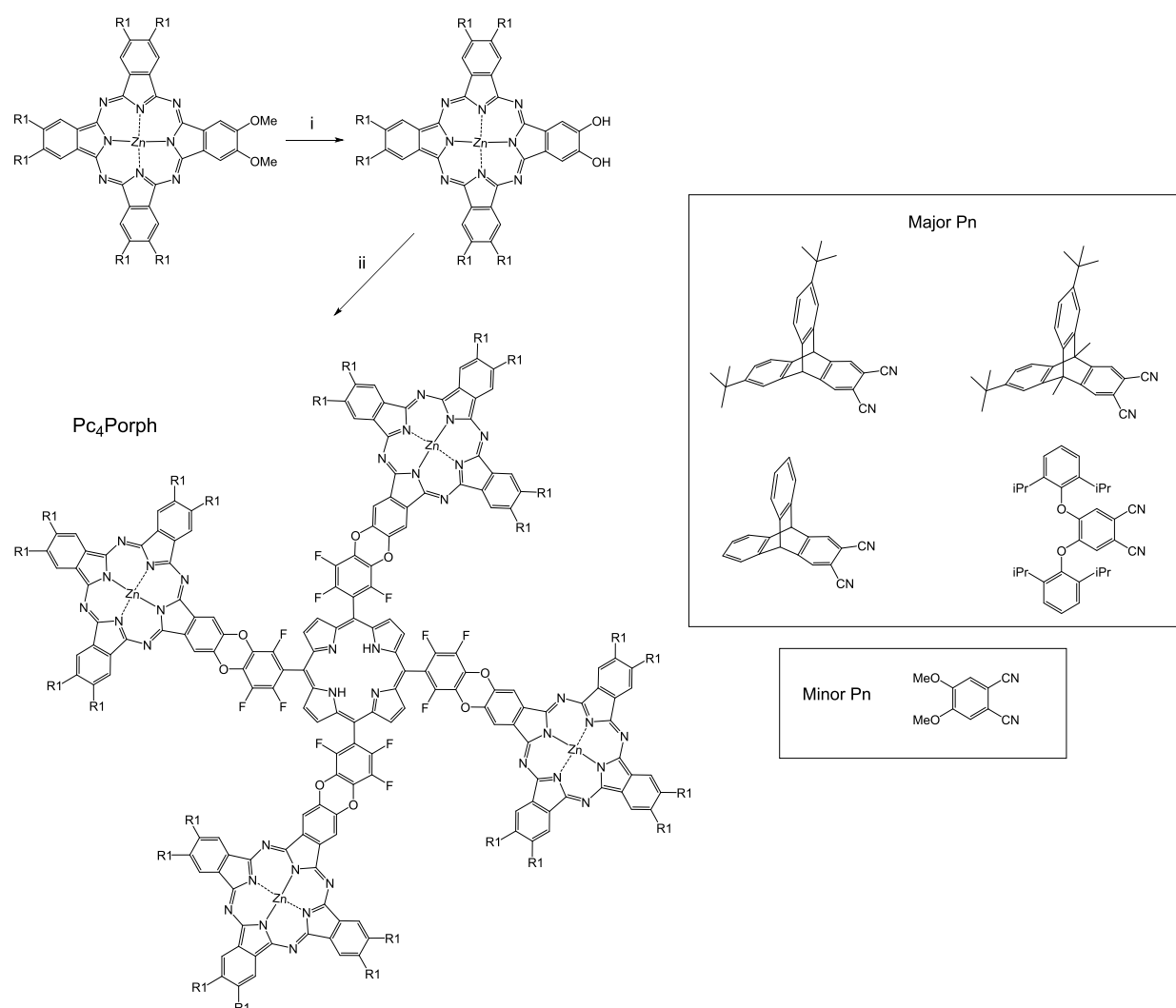
3.1 Introduction

The extended planar shape of the Pc macrocycle results in a strong tendency for it to form densely packed co-facial aggregates ^[157] and this self association has to be prohibited in order to optimise their potential utility for certain optical and electronic devices and for preparing open porous structures that allow access to those active metal centres which are known to impart useful catalytic activity ^[49,158] The concept of IM, whereby a microporous material is formed by the inability of the component macromolecules to pack space efficiently due to their rigid and contorted structure, thus becomes relevant here. ^[74] The preparation of these Pc-based microporous materials has therefore been the main aim of this project.

As reviewed previously, triptycenes are particularly attractive components for designing microporous materials due to their rigidity, relative ease of synthesis and high IMFV. ^[110,159,160] Their trigonal bladed geometry which gives rise to a 120° angle between the three benzene rings is able to hinder efficient packing in the solid state. Since discrete monodisperse molecules of well-defined structure offer reproducible synthesis and properties and are usually more soluble and fully characterisable, a fundamental understanding of structure-function relationship can be achieved. Hence, it was of interest to synthesise and analyse Pc-based molecules with triptycene substituents, similar to OMIMs. ^[146] Similar materials based on the structurally related porphyrazine and porphyrin-based molecules were also synthesised and their microporosity and spectroscopic properties studied. Moreover, some variations in the central metal ions of the aromatic cores were also considered due to their potential catalytic applications.

3.2 Attempts to make Pc OMIMs from unsymmetrical Pcs

One of the preliminary investigations of this project was the preparation of unsymmetrical Pcs with catechol functionality on one side (3:1) which can be used to make tetra Pc based OMIMs via a substitution reaction with fluorinated precursors such as $H_2(PhF_5)_4Porph$ (**Scheme 3.1**). These novel unsymmetric Pcs were synthesised via the cyclotetramerisation reaction using two Pns: first Pn bearing a solubilising group being in a major quantity and the 2nd 4,5-dimethoxyphthalonitrile in a minor quantity (usually 9:1 ratio, statistical mixture) in the presence of zinc(II)acetate according to a reported literature procedure.^[161]



Scheme 3.1: Synthesis of Pc OMIMs. *Reagents and conditions:* i) BBr₃, DCM, 0 °C, 24 h; ii) Tetrakis(pentafluorophenyl)porphyrin, NMP, K₂CO₃, 100 °C. R1 is used for simplicity; see Pns in the figure to match substitution.

Using the Pns shown in **Scheme 3.1**, four novel unsymmetric Pcs bearing methoxy groups at one side were synthesised. The reaction products were purified by column chromatography and fractions analysed by MALDI-MS to isolate the desired unsymmetric Pcs since the reactions yield a complex mixture of symmetric ZnPc and other isomers. An example MALDI mass spectrum of the desired 3:1 isomer (ZnPc(OMe)₂) is shown in **Figure 3.1** below.

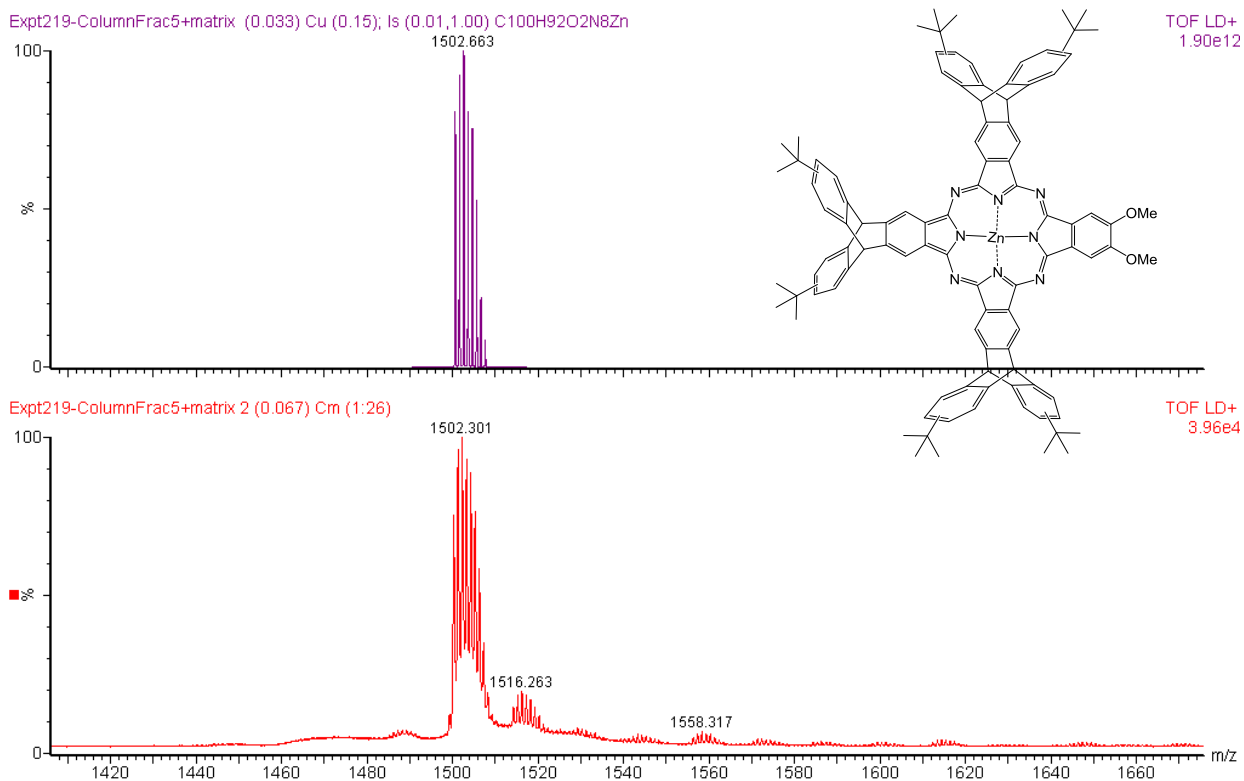


Figure 3.1: Expected isotope model (top) and MALDI mass spectrum (bottom) of 2,3-*o*-benzenedimethoxy-7,8,12,13,17,18-tri(6,15-di-*tert*-butyltritypceno)porphyrinato zinc. Dimer formation at m/z 3007 is also visible.

The Pcs were then demethylated and were subsequently used for substitution reaction. However, these substitution reactions could not yield the desired Pc-OMIMs and MALDI mass spectra only showed the starting demethylated Pcs (ZnPc(OH)₂). This seemed strange at first because we used the same reaction conditions that were used to make tetra triptycene substituted porphyrin molecules.

It was postulated that catechol functionality on the aromatic Pc ring is prone to oxidation and forms an ortho quinone and so, in order to check for this, the Pc(OH)₂ was washed with sodium

dithionite solution. ^[162] UV-vis absorption spectra of the demethylated Pcs before and after the treatment with sodium dithionite show a small change in the appearance of the Q-band (**Figure 3.2**). For example, the absorption spectra of ZnPc(OMe)₂ in CHCl₃ display the typical non-aggregating form with λ_{max} at 680 nm. In contrast, absorption spectra of ZnPc(OH)₂ was found to be very broad with significantly red shifted λ_{max} at 724 nm which could be due to aggregation since MALDI mass spectra and previous work on porphyrazines show the tendency of these molecules to form dimers; or this could be due to oxidation. Upon treatment with sodium dithionite, the appearance of the Q-band changed and λ_{max} shifted back towards 695 nm which could suggest that oxidation was the reason for no substitution reaction.

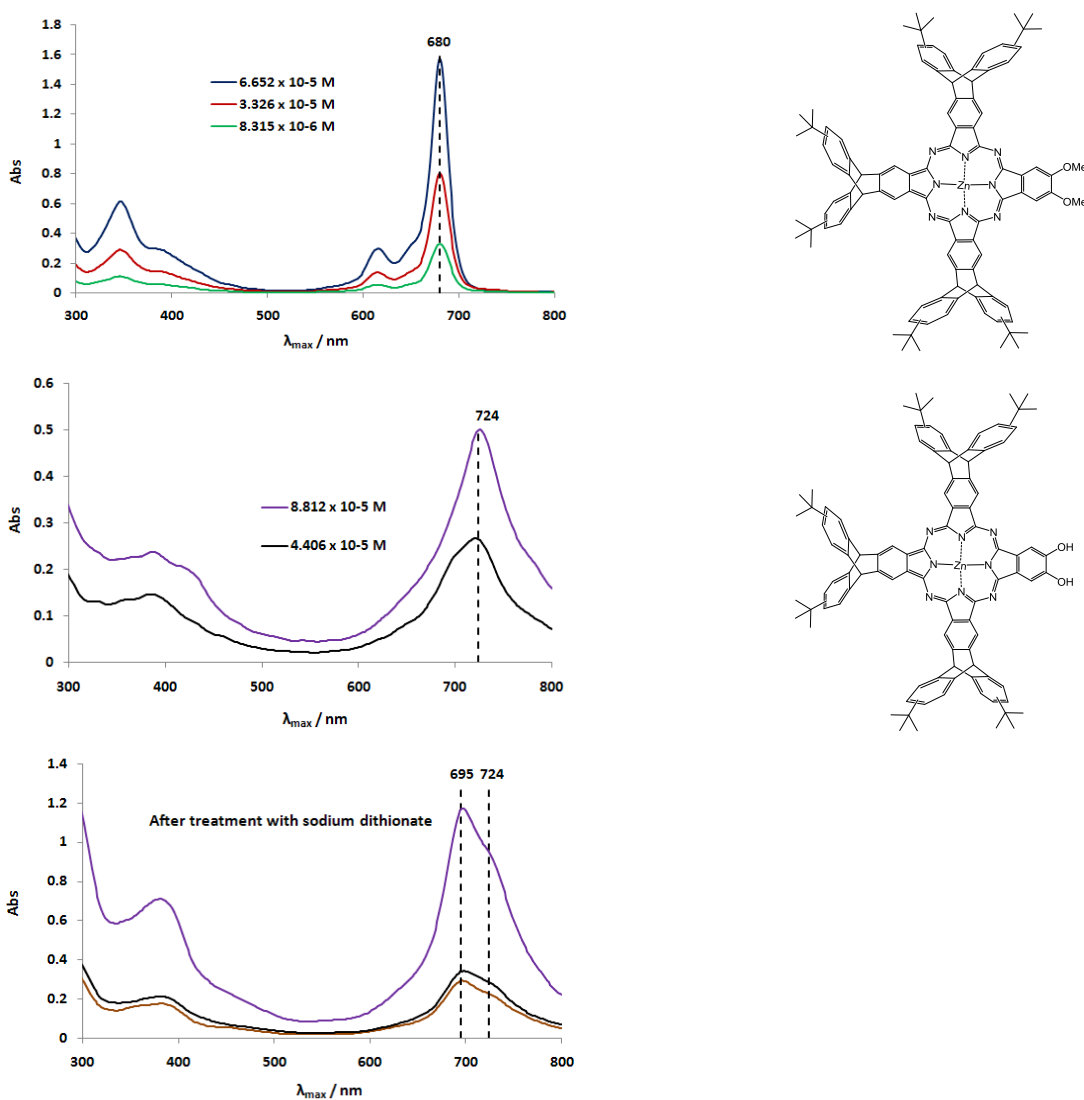
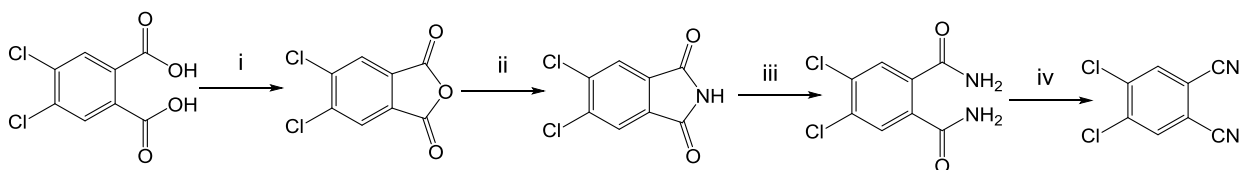


Figure 3.2: UV-vis absorption spectra in CHCl₃ of: **Top:** ZnPc(OMe)₂; **Middle:** ZnPc(OH)₂; **Bottom:** ZnPc(OH)₂ after treatment with sodium dithionite solution.

We therefore decided to try the substitution reaction again and carried out the reduction step prior to this. It was also desired to add minute amounts of sodium dithionite into the reaction. ^[162] Unfortunately, this still did not improve the result and the the desired Pc4Porph could not be formed. No further work in this area was carried out as it could be that the catechol functionality is not sufficiently stable or reactive when placed directly on the Pc ring.

3.3 Pcs from dioxin-phthalonitrile-triptycenes (ZnPc 1 – 4)

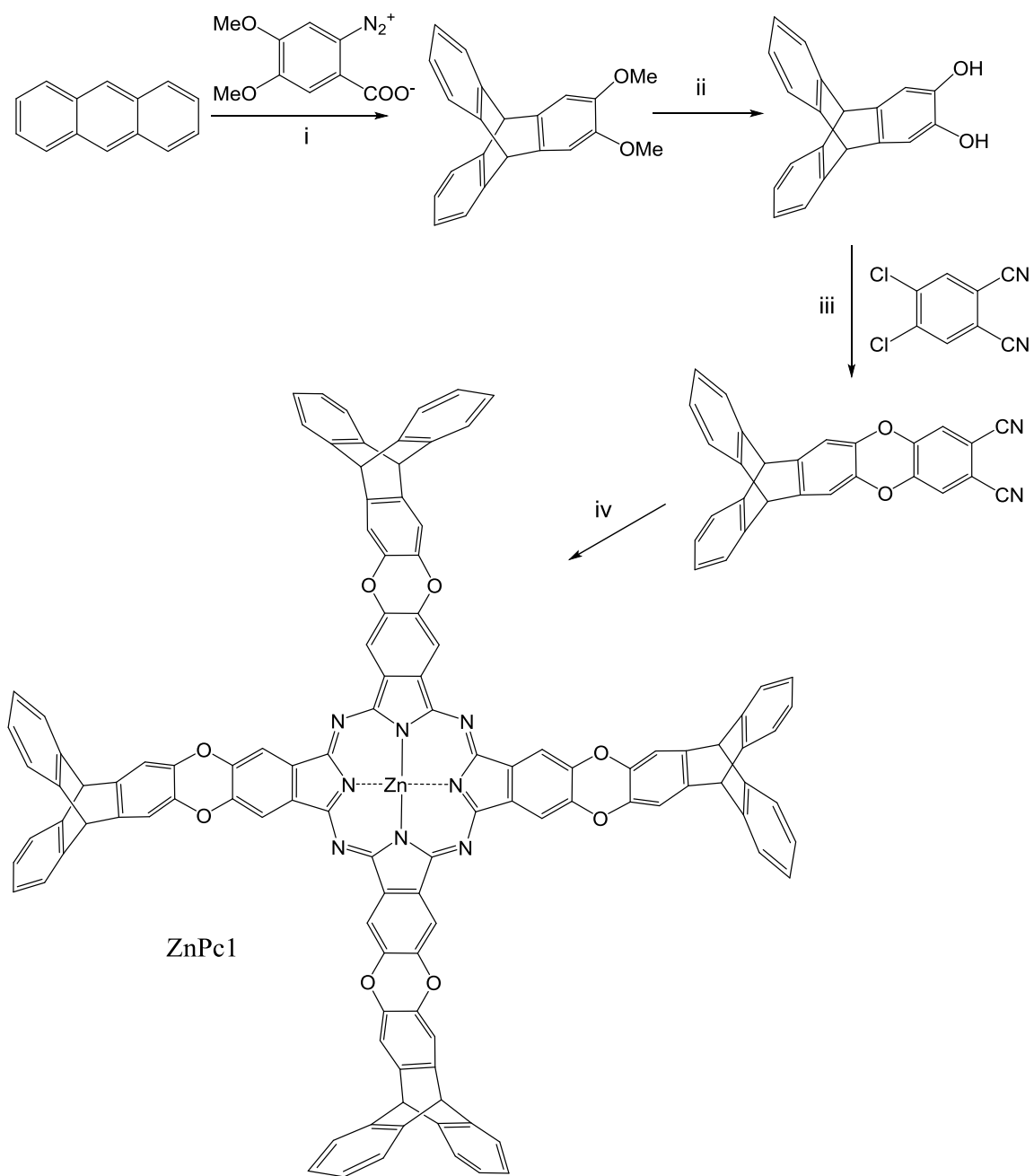
Work was initiated by synthesising 4,5-dichlorophthalonitrile on a large scale so that various substituents can be introduced on to the Pn precursor before it can undergo cyclotetramerisation. The four step procedure ^[163] (**Scheme 3.2**) starts with the dehydration of the inexpensive, commercially available 4,5-dichlorophthalic acid to give the anhydride, which is then reacted with formamide to give the imide. This reacts with ammonium hydroxide to give the diamide which is finally dehydrated to give 4,5-dichlorophthalonitrile.



Scheme 3.2: Synthesis of 4,5-dichlorophthalonitrile. *Reagents and conditions:* i) Ac_2O , reflux, 5 h; ii) Formamide, reflux, 3 h; iii) NH_4OH , RT, 48 h; iv) SOCl_2 , DMF, 0 – 5 °C, 5 h, then RT, 24 h.

Triptycene was introduced onto the Pn precursor via a $\text{S}_{\text{N}}\text{Ar}$ reaction between 2,3-dihydroxytriptycene and 4,5-dichlorophthalonitrile (**Scheme 3.3**). The synthesis of 2,3-dihydroxytriptycene was carried out in two steps: A Diels-Alder reaction between anthracene and 4,5-dimethoxybenzyne (prepared in situ from the diazonium salt of 4,5-dimethoxyanthranilic acid ^[101] gave 2,3-dimethoxytriptycene ^[164] which was then demethylated using BBr_3 to give 2,3-dihydroxytriptycene. ^[102]

The structure of the novel 2,3-dioxin-phthalonitrile-triptycene was confirmed by ^1H and ^{13}C NMR, High Resolution Mass Spectrometry (HRMS) as well as single crystal X-ray diffraction (**Figure 3.3**). Finally, this Pn underwent a cyclotetramerisation reaction using zinc(II)acetate in anhydrous NMP at 180 °C according to the reported literature procedure ^[21] to give **ZnPc1**.



Scheme 3.3: Synthesis of **ZnPc1**. *Reagents and conditions:* i) CH_2Cl_2 , propylene oxide, reflux, 20 h; ii) BBr_3 , DCM, RT, 2h, H_2O ; iii) K_2CO_3 , DMF, 70 °C, 24 h; iv) $\text{Zn}(\text{OAc})_2$, NMP, 180 °C, 20 h.

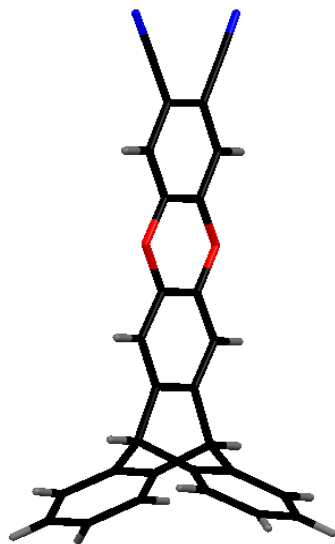


Figure 3.3: Molecular structure for 2,3-dioxin-phthalonitrile-triptycene. Crystals were prepared from slow evaporation of a THF solution.

ZnPc1 was obtained as a dark green/black solid showing only partial solubility in THF and MALDI-MS analysis and UV-vis absorption spectrum (**Figure 3.4, 3.5**) in THF confirmed the presence of the desired product. Purification was achieved by washing the dark coloured solid with refluxing THF using a soxhlet extractor.

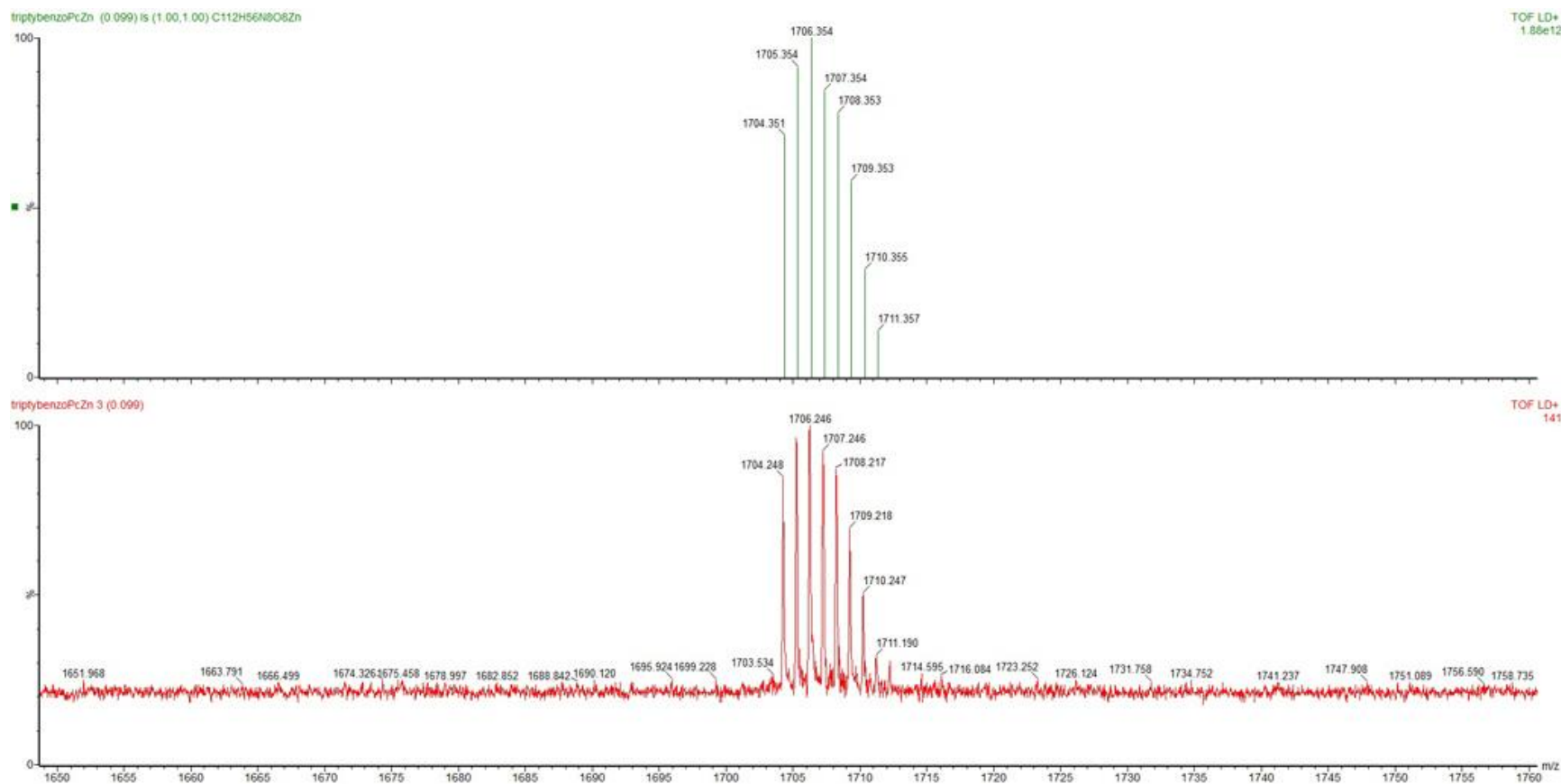


Figure 3.4: Expected isotope model (top) and MALDI mass spectrum (bottom) of ZnPc1.

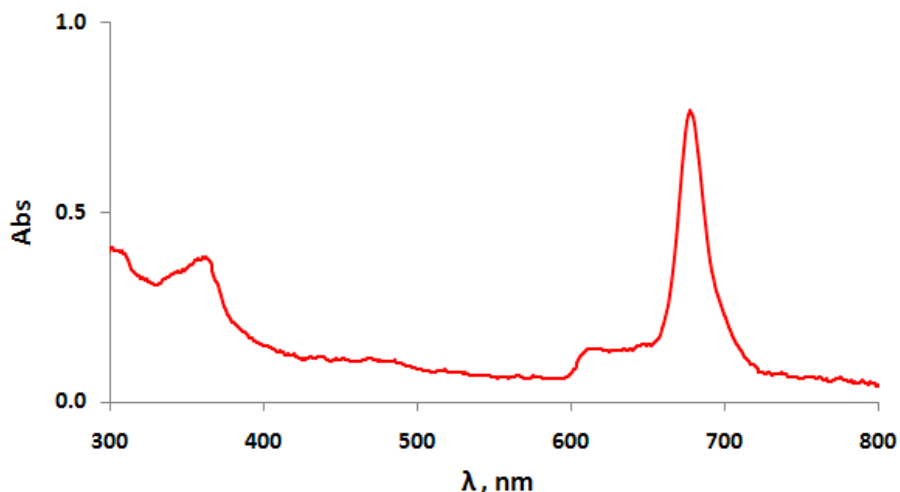


Figure 3.5: UV-vis absorption spectrum of **ZnPc1** in THF.

Due to the lack of solubility of **ZnPc1**, it was decided to introduce *tert*-butyl groups onto the triptycene precursor; since bulky substituents can also induce steric crowding around the Pc ring and prevent self-association. *Tert*-butyl groups were introduced onto the anthracene using TFA and *tert*-butanol according to a reported literature procedure.^[165] The mechanism of the formation of 2,6-di-*tert*-butylanthracene (**Figure 3.6**) involves *tert*-butyl trifluoroacetate as an active intermediate which *tert*-butylates anthracene regioselectively at the 2 position.^[165] This is followed by the energetically favourable aromatization or dehydrogenation and subsequent reaction with a second *tert*-butyl cation at the equivalent position on the other side of the molecule i.e. the 6 position to give the desired product.

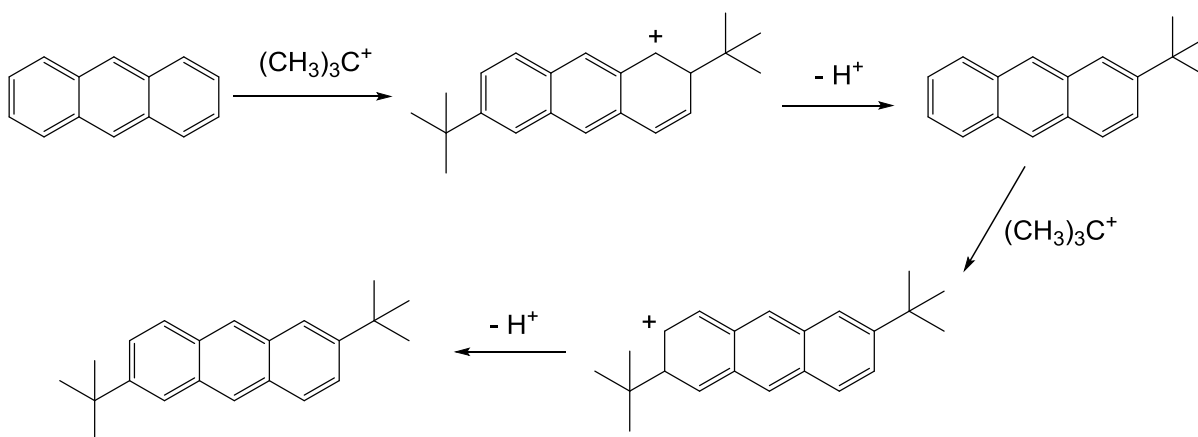
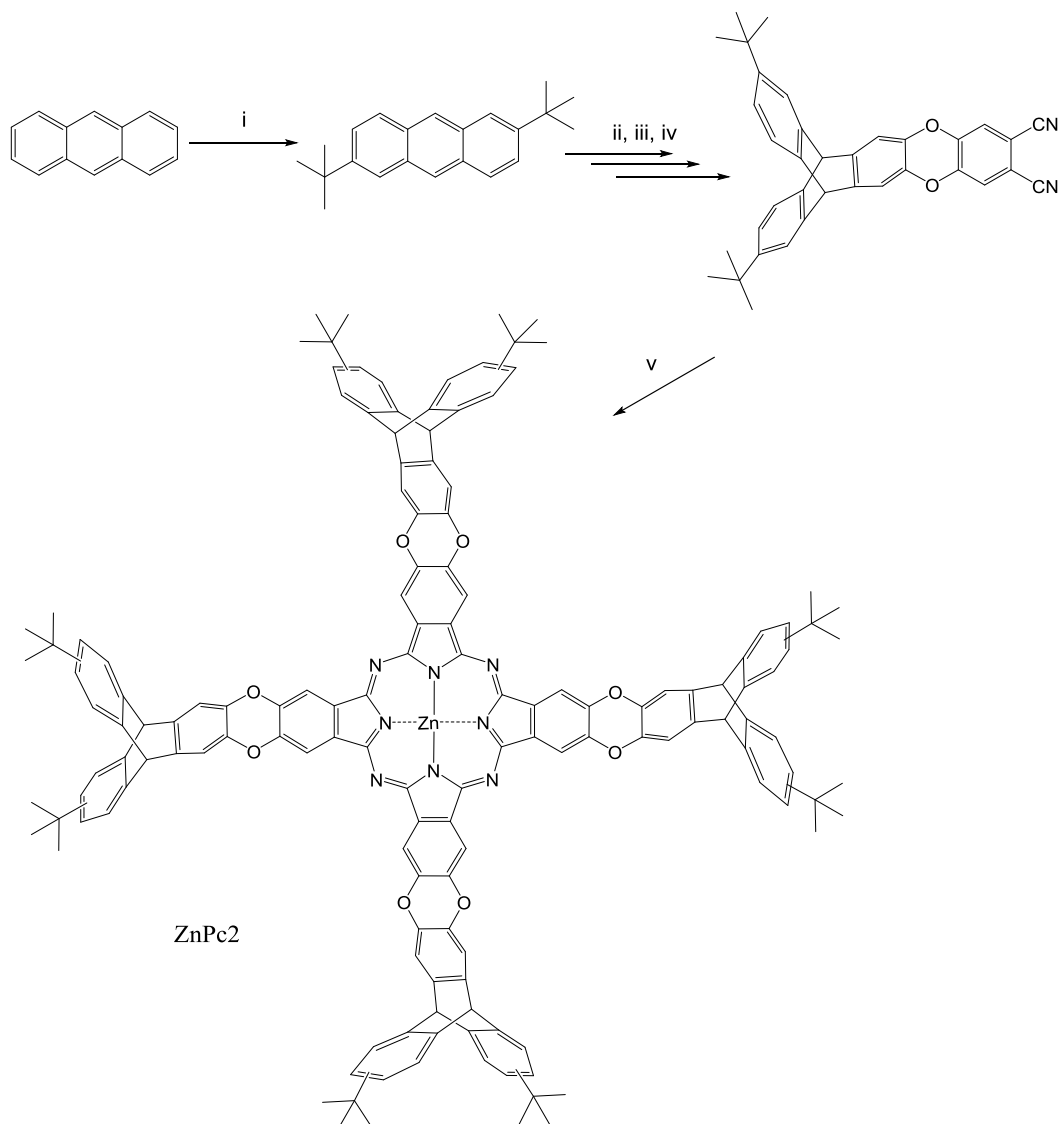


Figure 3.6: Mechanism of the formation of 2,6-di-*tert*-butylanthracene.

The resulting substituted anthracene was then used as the starting material for the synthesis of **ZnPc2** (i.e. the octa-*tert*-butyl analogue of **ZnPc1**), (**Scheme 3.4**); the structure of which was confirmed by MALDI-MS, ^1H NMR, UV-vis absorption spectroscopy and elemental analysis.



Scheme 3.4: Synthesis of **ZnPc2**. Reagents and conditions: i) TFA, *tert*-butanol, reflux, 24 h; Steps (ii), (iii), (iv) and (v) remain the same as for **Scheme 3.3**.

Compared to the previous synthesis, the yield of the Diels-Alder reaction between 2,6-di-*tert*-butylanthracene and 4,5-dimethoxybenzyne was found to be very low (15% as compared to 30% obtained for 2,3-dimethoxytritycene). The corresponding Pn precursor obtained from this

synthesis was reacted with zinc acetate on a small scale to yield just 30 mg (14 % yield) of **ZnPc2**.

Due to the interest in synthesising various metal complexes along with the need to assess these molecules for porosity, we sought to improve the yield of the Diels-Alder reaction since the later steps in the synthesis were very high yielding.

It is known that the presence of electron donating groups on a diene can activate those positions towards Diels-Alder cycloaddition, enhancing yield and regio-control.^[166] So, it was decided to introduce methyl substituents on to the 9- and 10- positions of the anthracene. Since a lack of solubility was already encountered with **ZnPc1**, it was also desired for *tert*-butyl groups to be present. Hence, two further syntheses were carried out:-

As reported in the literature,^[167] starting from 9,10-dichloroanthracene (**Scheme 3.5**), which undergoes a cross coupling reaction with Grignard reagents in the presence of PEPPSI-IPr ([1,3-bis(2,6-di-*iso*-propylphenyl)imidazol-2-ylidene] (3-chloropyridyl) palladium(II)dichloride) catalyst, 9,10-dimethylantracene was prepared in a high yield (91 %). Kumada Corriu coupling mechanism^[168,169] involves firstly, the formation of the diorganopalladium(0) complex via homocoupling of the Grignard reagent. The Pd⁰ species then undergoes oxidative addition into the carbon-chloride bond followed by transmetalation and reductive elimination to generate the desired product as well as the active Pd⁰ catalyst (**Figure 3.7**).

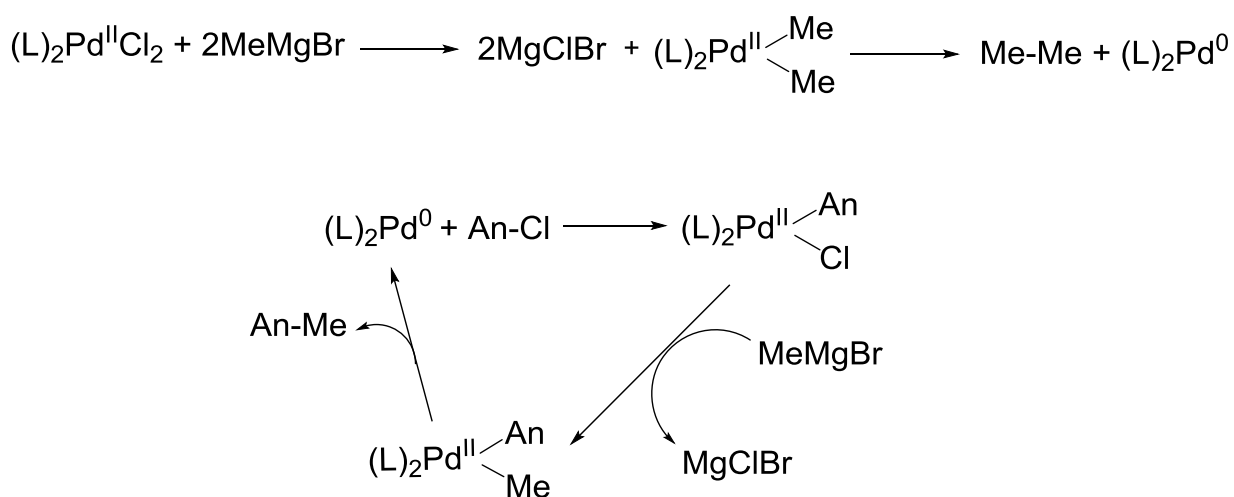
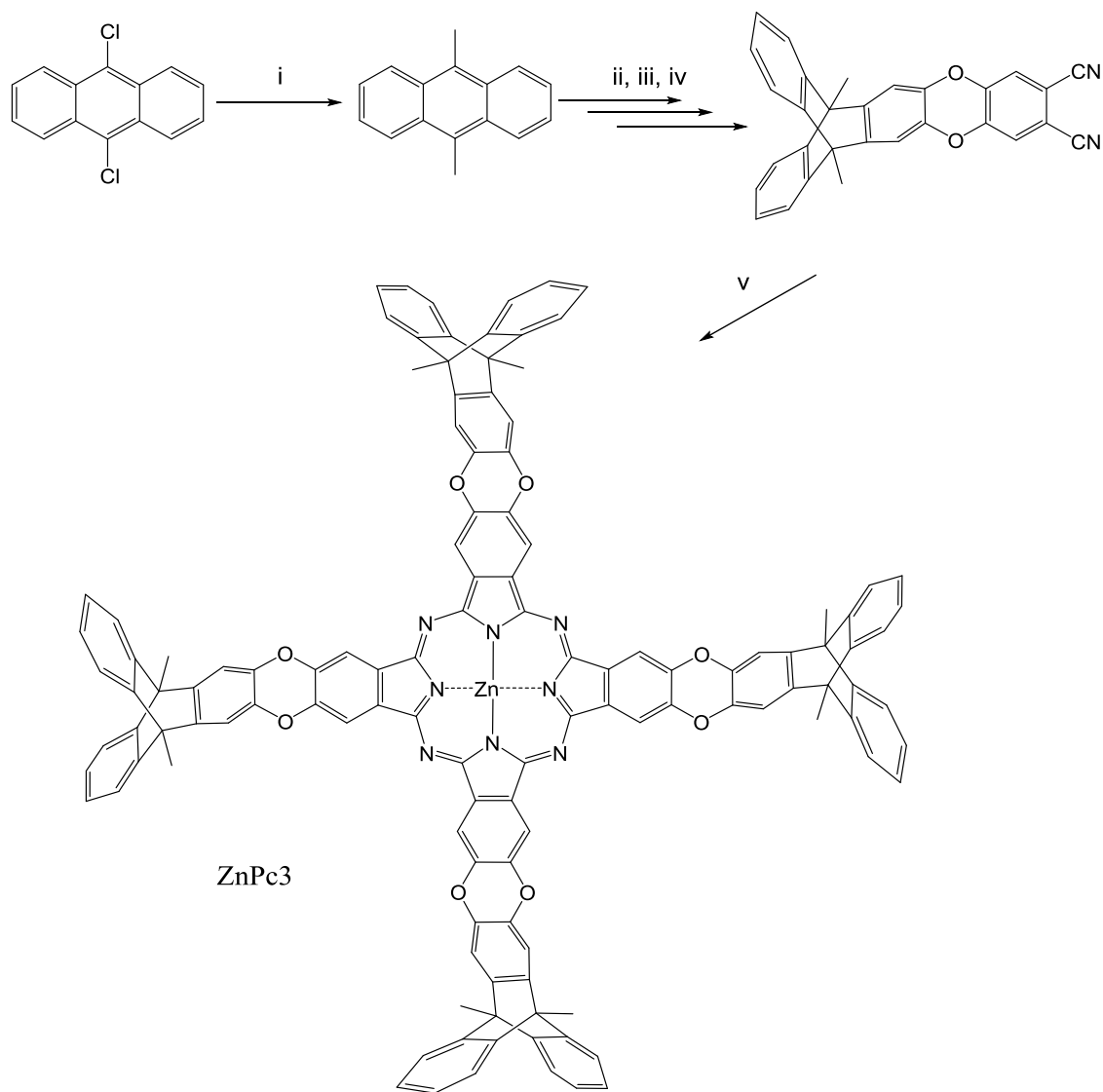


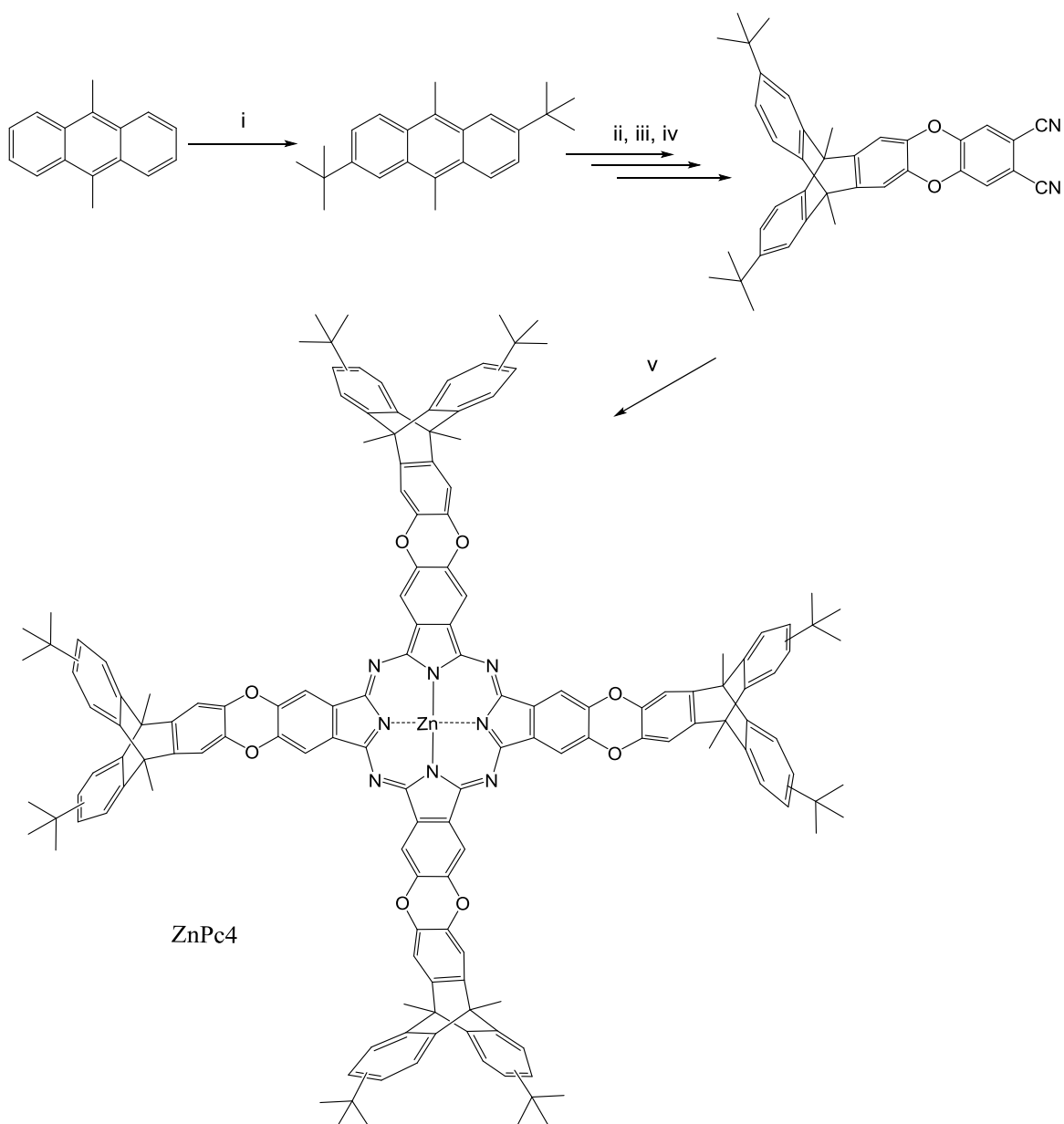
Figure 3.7: Mechanism of the formation of 2,6-di-*tert*-butylantracene.

The yield of the corresponding Diels-Alder reaction to give 2,3-dimethoxy-9,10-dimethyltritycene was improved significantly to 80 % using this anthracene and subsequently **ZnPc3** (octa-methyl analogue of **ZnPc1**) was prepared. However, as expected, the bridgehead methyl groups alone were not sufficient to address the solubility issue.



Scheme 3.5: Synthesis of **ZnPc3**. Reagents and conditions: i) MeMgBr, PEPSI-IPr catalyst, 1,4-dioxane, RT, 24 h; Steps (ii), (iii), (iv) and (v) are same as for **Scheme 3.3**.

Therefore, an additional synthesis (**Scheme 3.6**) involved the *tert*-butylation of 9,10-dimethylantracene which takes place efficiently via the same mechanism as before and subsequent reactions allowed the preparation of **ZnPc4** (**Figure 3.8**). The dimethoxy triptycene and the Pn precursor (**Pn4**) obtained from this latter synthesis formed crystals suitable for analysis by x-ray analysis for which structures are shown in **Figure 3.9**.



Scheme 3.6: Preparation of **ZnPc4**. *Reagents and conditions:* i) TFA, *tert*-butanol, reflux, 20 h; Steps (ii), (iii), (iv) and (v) are same as for **Scheme 3.3**.

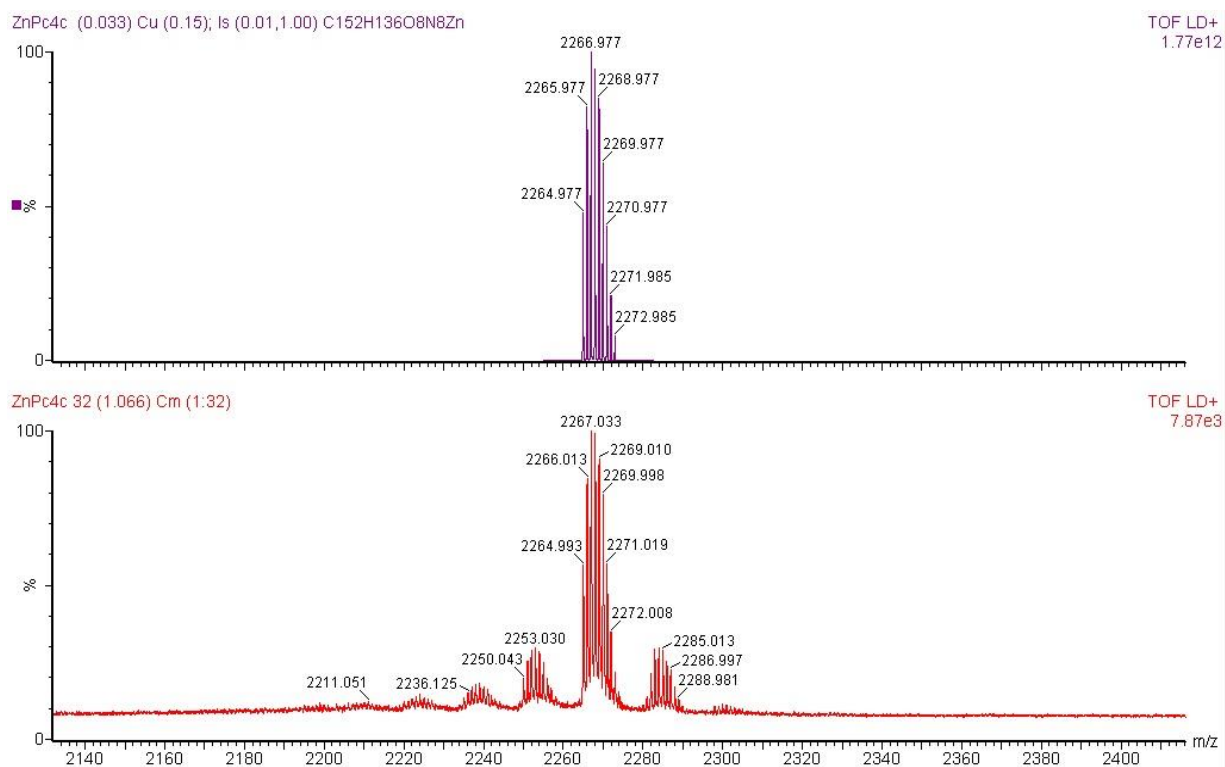


Figure 3.8: Expected isotope model (top) and MALDI mass spectrum (bottom) of **ZnPc4**.

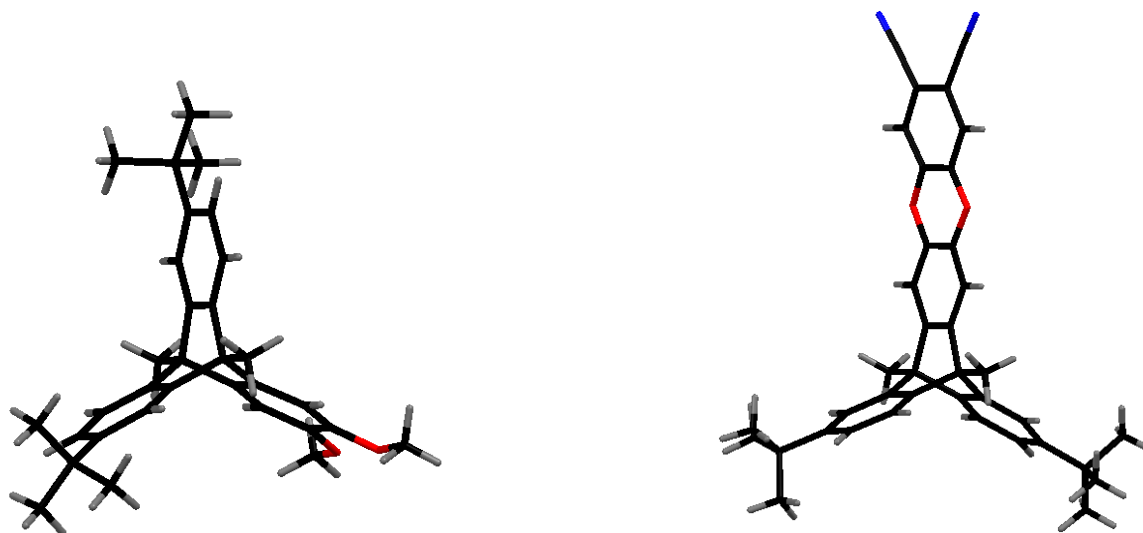


Figure 3.9: Molecular structures for 2,3-dimethoxy-9,10-dimethyl-6,15-di-*tert*-butyltritycene (left) and 2,3-dioxin-phthalonitrile-9,10-dimethyl-6,15-di-*tert*-butyltritycene (**Pn4**) (right). Crystals were prepared from slow diffusion of MeOH into a CHCl_3 solution.

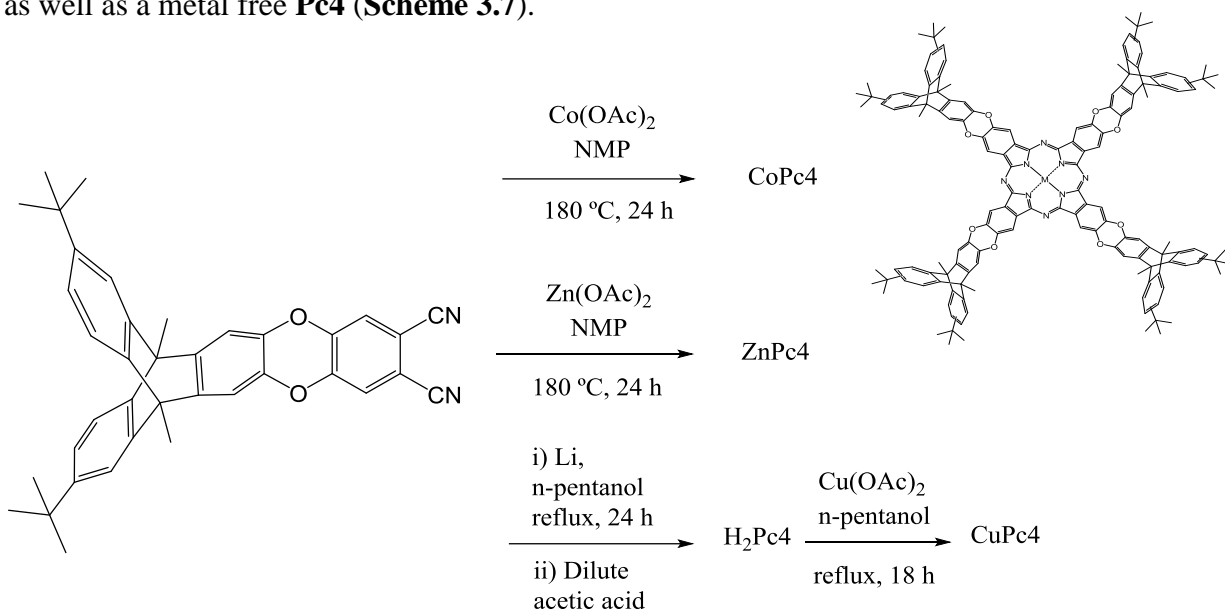
It was found that the presence of *tert*-butyl groups on 9,10-dimethylantracene lowers the yield of the Diels-Alder reaction slightly compared to when 9,10-dimethylantracene is used, nevertheless, the yield was still significantly higher than when started with 2,6-di-*tert*-butylantracene or unsubstituted anthracene. Hence, 9,10-dimethyl-6,15-di-*tert*-butylantracene serves as an optimum precursor for achieving a high overall yield and good solubility. These yields along with those of the corresponding Pns are summarised in **Table 3.1**.

Anthracene precursor	Yield (%) of 2,3-dimethoxytriptycene	Yield (%) of 2,3-dihydroxytriptycene	Yield (%) of the resultant Pn
Anthracene	30	86	79
2,6-Di- <i>tert</i> -butylantracene	15	82	80
9,10-Dimethylantracene	80	96	90
2,6-Di- <i>tert</i> -butyl-9,10-dimethylantracene	71	94	85

Table 3.1: A comparison of the yields of the Diels-Alder reactions and corresponding Pns starting with different anthracene precursors.

3.3.1 Synthesis of MPc4 complexes

For a spectroscopic and porosity investigation, two further metal analogues were also prepared as well as a metal free **Pc4** (Scheme 3.7).



Scheme 3.7: Synthesis of **MPc4** complexes.

CoPc4 was synthesised in the same way as **ZnPc4** via metal ion mediated cyclotetramerisation but using cobalt(II)acetate and **Pn4**.

To make the metal free analogue, ‘The Linstead method’^[14] was followed whereby lithium metal was added to a refluxing solution of **Pn4** in *n*-pentanol. After the reaction was complete, an acidic work up with acetic acid allowed the metal free derivative to be isolated.

CuPc4 was prepared via a metal insertion reaction using **H₂Pc4** and copper(II)acetate in refluxing *n*-pentanol. This method actually resulted in much better yield of 75 % for **CuPc4** as compared to 20 %, 37 % and 55 % yields of **Co**, **Zn** and **H₂Pc4** respectively.

All metal complexes were characterised by MALDI-MS, ¹H NMR spectroscopy (for diamagnetic **ZnPc4** and **H₂Pc4**), UV-vis absorption spectroscopy and elemental analysis. This combined analyses confirmed the desired structures of Pcs.

3.3.2 An assessment of aggregation via UV-vis absorption spectroscopy and BET

A comparison of the UV-vis absorption spectra of **ZnPc1** – **4** in THF (**Figure 3.10**) shows that the position of the main Q-band at 677 nm is unperturbed by the introduction of methyl or *tert*-butyl groups on to the triptycene substituents.

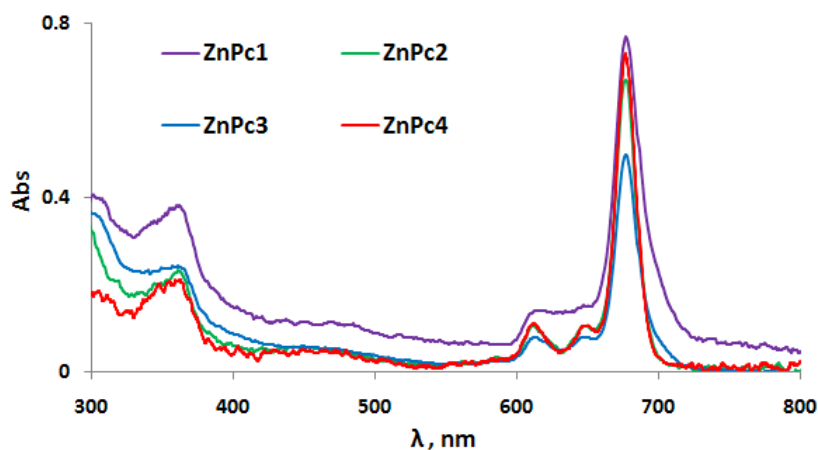


Figure 3.10: UV-vis absorption spectra of **ZnPc 1 – 4** in THF. Concentrations are arbitrary for **ZnPc1** and **ZnPc3** due to partial solubility; **ZnPc2** and **ZnPc4** $\sim 2 \times 10^{-6}$ M.

For **MPc4** complexes ($M = \text{Zn}^{2+}, \text{Cu}^{2+}, \text{Co}^{2+}$) in THF solutions, variation of the metal ion causes a very small shift in the position of the Q-band in the absorption spectra, with λ_{max} ranging from 665 – 677 nm. For **H₂Pc4**, the lower symmetry of the metal free Pc ring causes the Q-band to split with λ_{max} at 667 and 702 nm. This is shown in **Figure 3.11**.

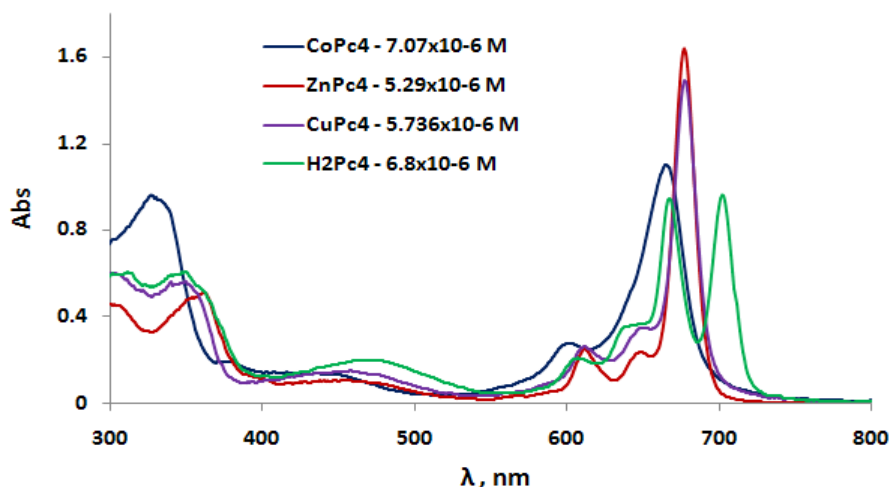


Figure 3.11: UV-vis absorption spectra of **MPc4** complexes in THF.

The excellent solubility of **MPc4** complexes encouraged an assessment of aggregation of these complexes by absorption spectroscopy. For this purpose, spectra were measured in a range of concentrations using different solvents: THF, CHCl_3 and toluene. These spectra showed solvent and concentration dependency of the Pcs and caused broadening of the main Q-band (**Figure 3.12**) and changed the extinction co-efficient values.

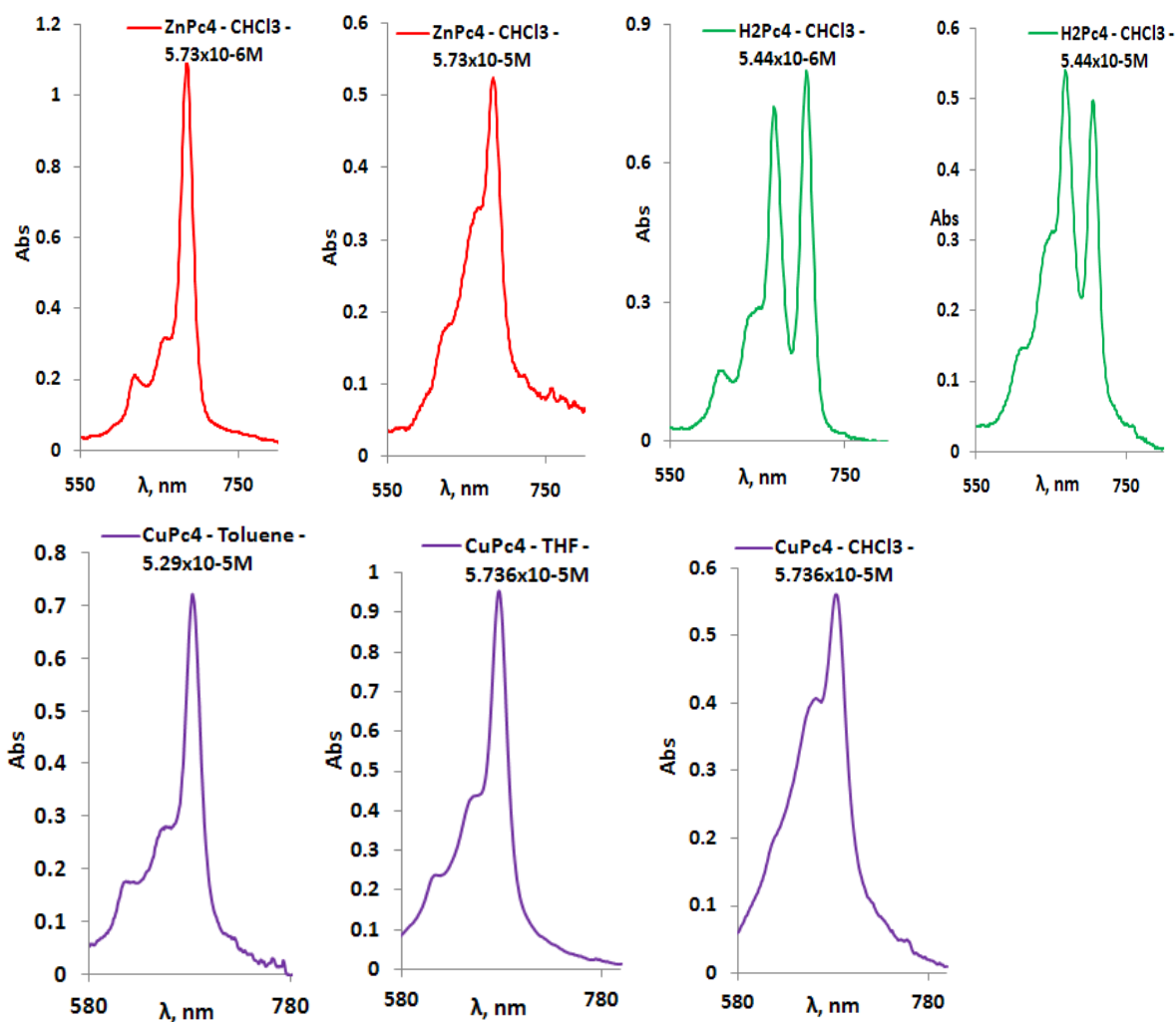


Figure 3.12: A comparison of the UV-vis absorption spectra for **ZnPc4** and **H₂Pc4** to show concentration dependency (top) and UV-vis absorption spectra of **CuPc4** to show solvent dependency (bottom).

For example, a spectrum of a 10⁻⁶ M solution of **ZnPc4** or **H₂Pc4** in CHCl_3 measured using a 1 cm path length cell, displays the classical non aggregated form with sharp intense Q bands.

However, spectra from more concentrated solution (10^{-5} M), measured using a 1 mm path length cell, shows band broadening which results in extinction co-efficient values being lowered. Also, at higher concentrations (10^{-5} M solutions) the appearance of the Q-band changes depending on the solvent. This is shown for **CuPc4** in **Figure 3.12**.

In order to assess the degree of self-association of the Pc units in the solid state, a film was prepared from DCM solution of **ZnPc4**, just on the outside of the quartz cuvette. UV-vis absorption spectrum of this shows the Q-band to be significantly broader than when measured in solution and a good quality spectrum could not be obtained (**Figure 3.13**) which could be due to light scattering from microcrystals.

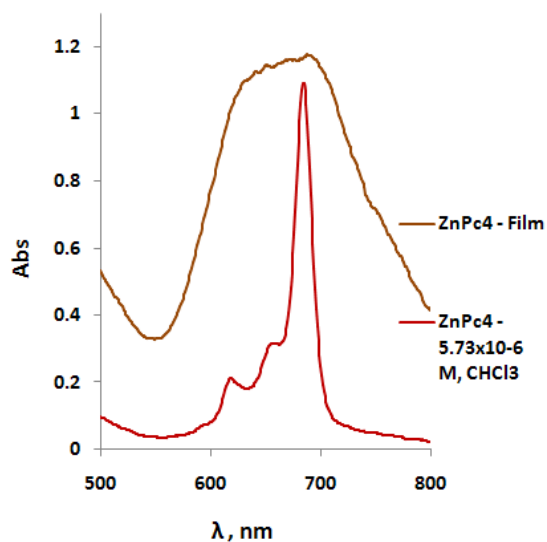


Figure 3.13: UV-vis absorption spectra of **ZnPc4** as a film cast from DCM and in dilute CHCl_3 solution.

The main Q-band in the visible region of the absorption spectra of Pcs results from $\pi\text{-}\pi^*$ transitions and any self association of Pcs causes excitonic coupling to occur between the aromatic cores changing both the position and appearance of this band. A blue-shifted band centred at 620 nm suggests partial columnar co-facial arrangement within the film. ^[59]

Nitrogen adsorption at 77 K allows a quantitative assessment of microporosity within a material and, hence, gives an indication of the efficiency with which molecules pack in the

solid state. As shown in **Figure 3.14** and **Table 3.2**, the apparent BET surface areas of **MPc4** complexes by nitrogen adsorption were measured to be in the range of 400 – 500 m² g⁻¹. The isotherms show significant adsorption at very low relative pressure ($p/p_0 < 0.1$), which is associated with microporosity. These results suggest that even with some degree of aggregation seen for these Pcs in their absorption spectra, the presence of triptycene substituents on the Pc ring give rise to porous materials with significant surface areas, comparable to those reported for triptycene biphenyl OMIMs. ^[146]

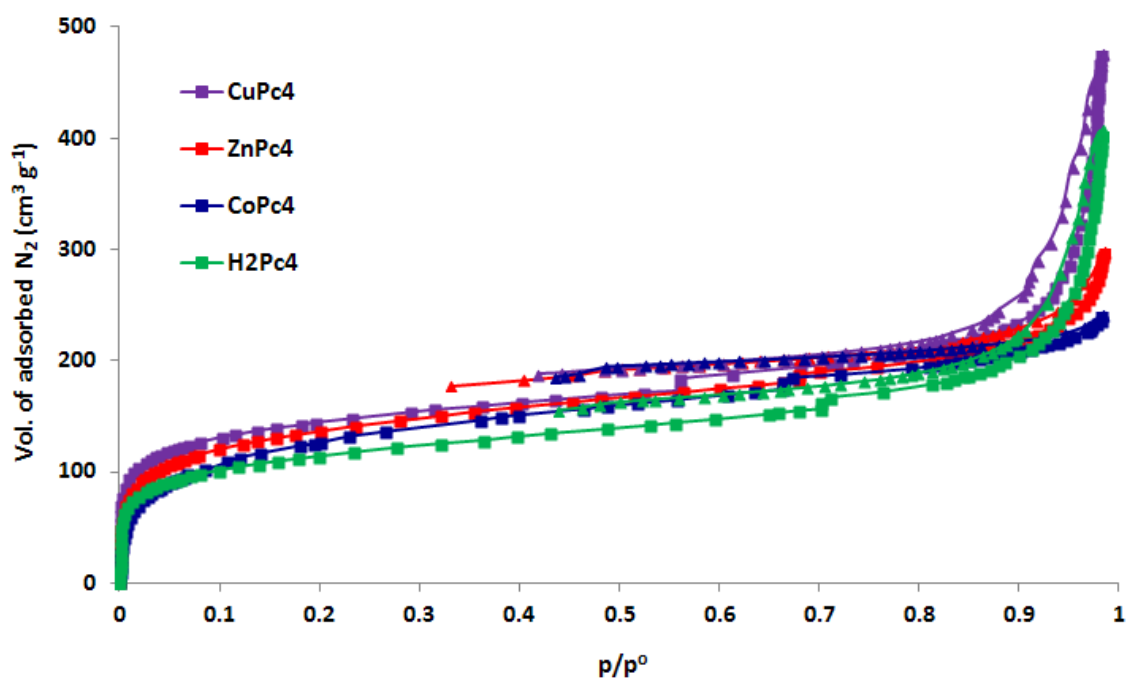


Figure 3.14: BET nitrogen adsorption and desorption isotherms of **MPc4** complexes measured at 77 K.

	Surface area (m ² g ⁻¹)	Total pore volume (cm ³ g ⁻¹)
CuPc4	511	0.73
ZnPc4	488	0.44
CoPc4	463	0.37
H₂Pc4	406	0.61

Table 3.2: BET nitrogen sorption data of **MPc4** complexes.

Comparison between **ZnPc 1 – 4** show large differences in their BET surface areas (**Figure 3.15, Table 3.3**). **ZnPc1** seems to have the lowest surface area of the series suggesting that the high surface areas of **MPC4** complexes are due to the presence of bulky *tert*-butyl and methyl substituents on the triptycenes which hinder self association of these Pcs to a greater extent.

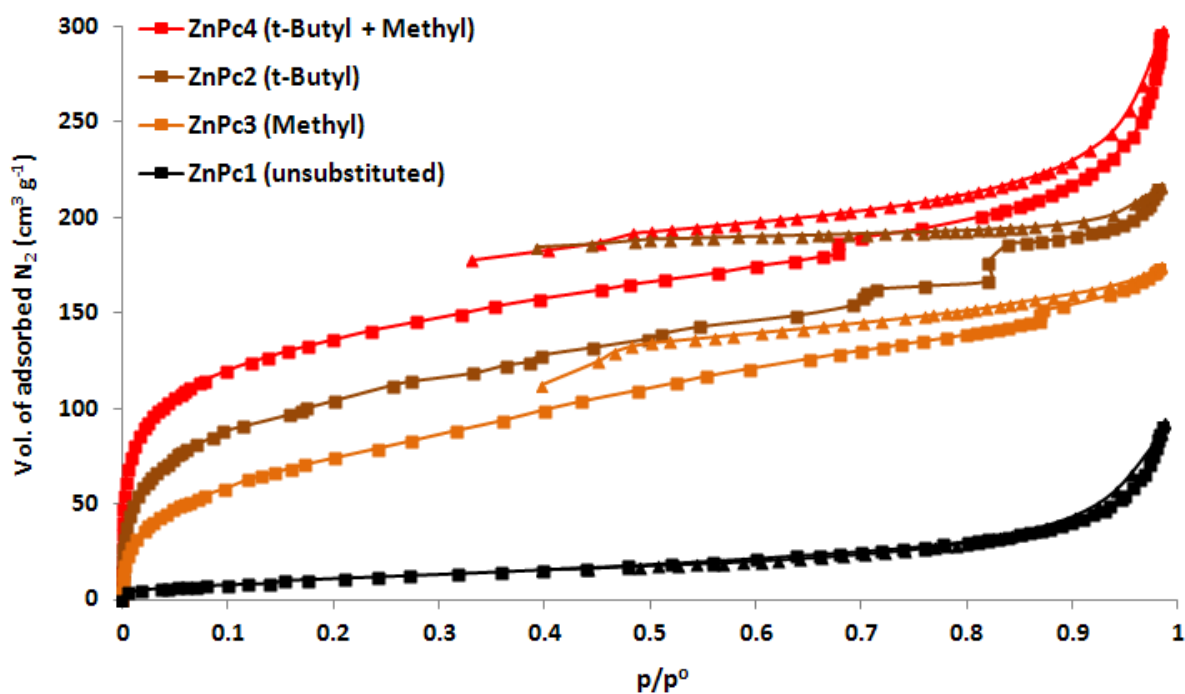


Figure 3.15: BET nitrogen adsorption and desorption isotherms of **ZnPc 1 – 4** measured at 77 K.

	Surface area ($\text{m}^2 \text{g}^{-1}$)	Total pore volume ($\text{cm}^3 \text{g}^{-1}$)
ZnPc1 (Unsubst.)	42	0.13
ZnPc2 (t-Butyl)	378	0.33
ZnPc3 (Methyl)	282	0.27
ZnPc4 (t-Butyl + Methyl)	488	0.44

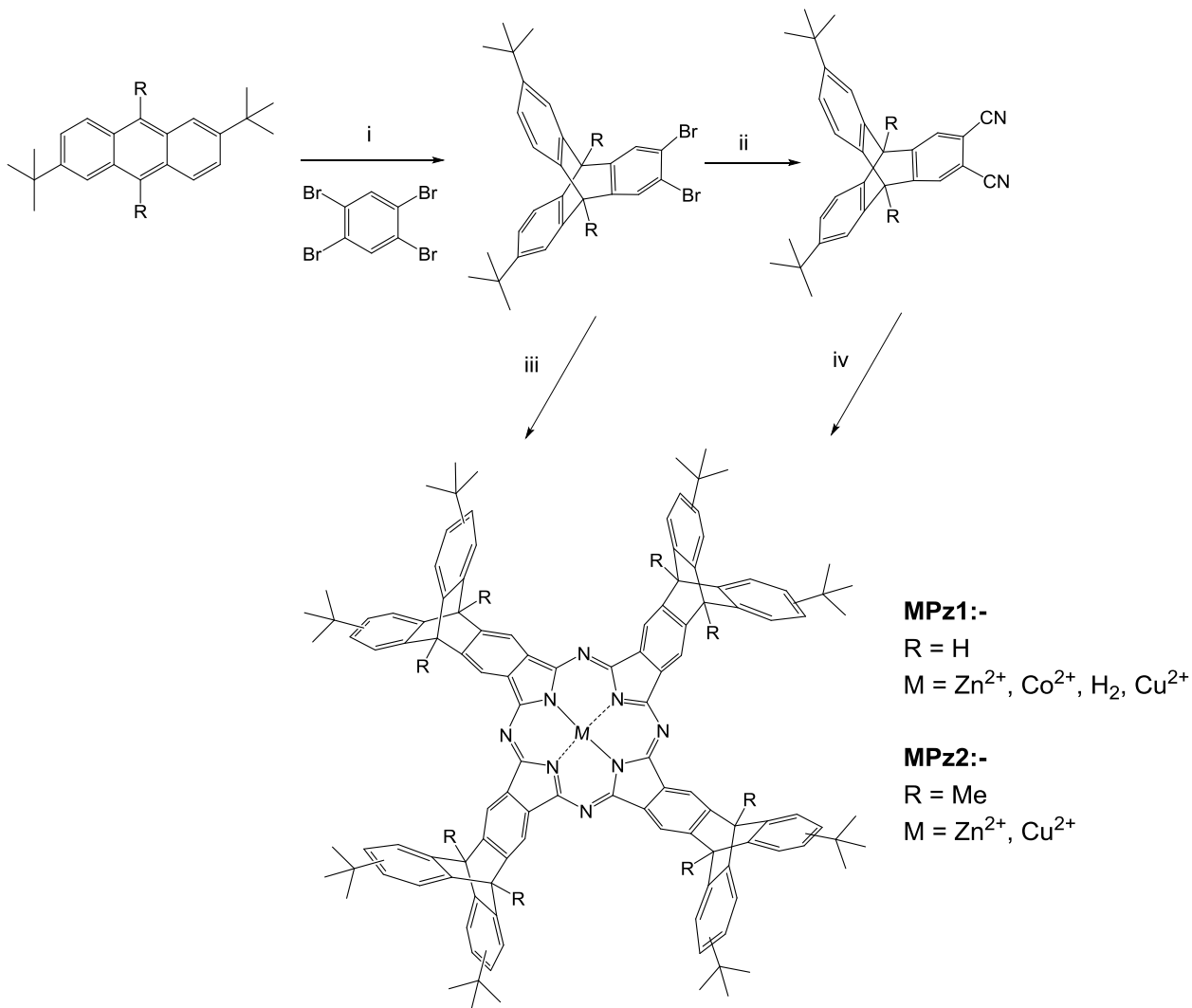
Table 3.3: BET nitrogen sorption data of **ZnPc 1-4**.

3.4 Triptycenoporphyrazines

The investigation into dioxin-triptyceno Pcs encouraged us to reexamine the structurally related octa-*tert*-butyltetra-2,3-triptycenoporphyrazine complexes which were firstly reported by Luk'yanets and co-workers in 1986. ^[156] These complexes differ from the dioxin-triptyceno Pcs (**MPcs 1-4**) in that the *tert*-butylated triptycenes are fused directly to the porphyrazine core. Spectroscopically however, they behave as Pc derivatives. The complexes were thus revisited for a spectroscopic investigation into their very unusual aggregation behaviour.

As can be seen in **Scheme 3.8**, the copper and zinc complexes of octa-*tert*-butyltetra-2,3-triptycenotetraazaporphyrin, previously prepared by Luk'yanets *et al.* ^[156] were synthesized together with the novel metal-free and cobalt derivatives (**MPz1**; M = Cu²⁺, Zn²⁺, Co²⁺, 2H⁺). In addition, two novel copper and zinc complexes containing methyl groups (instead of hydrogens) on the bridgehead positions of the triptycene subunits were also synthesised (**MPz2**; M = Cu²⁺, Zn²⁺). Dibromotriptycenes were prepared from a Diels-Alder reaction between anthracene and tetrabromobenzene with in-situ preparation of the benzyne precursor using BuLi. ^[156] Subsequent cyanation using copper cyanide (CuCN) (Rosenmund von Braun reaction) ^[3,22] gave the Pn precursors which were isolated and then used to prepare the metal complexes (apart from **CuPz1** and **CuPz2**, where it proved convenient to isolate the complexes as by-products from the cyanation reaction). This procedure of preparing **MPzs** from isolated Pns is slightly different to the one used by Lukyanets *et al.* which synthesised **CuPz1** and **ZnPz1** directly from the dibromides using CuCN and ZnCN.

All Pcs were characterised by MALDI-MS, ¹H NMR spectroscopy (for diamagnetic **ZnPz1**, **H₂Pz1** and **ZnPz2**), Electron Paramagnetic Resonance (EPR) spectroscopy (for **CuPz1**), UV-vis absorption spectroscopy, fluorescence spectroscopy and elemental analysis. This combined analysis confirmed the expected structures of **MPzs**. Furthermore, both of the dibromotriptycene precursors as well as 2,3-dicyano-6,15-di-*tert*-butyltriptycene were also characterised by x-ray crystallography (**Figure 3.16**).



Scheme 3.8: Synthesis and structure of **MPz**. *Reagents and conditions:* (i) *n*-BuLi, toluene, RT; (ii), (iii) CuCN, DMF, reflux; (iv) Metal cation mediated cyclotetramerisation (NMP, metal salt, 180 °C).

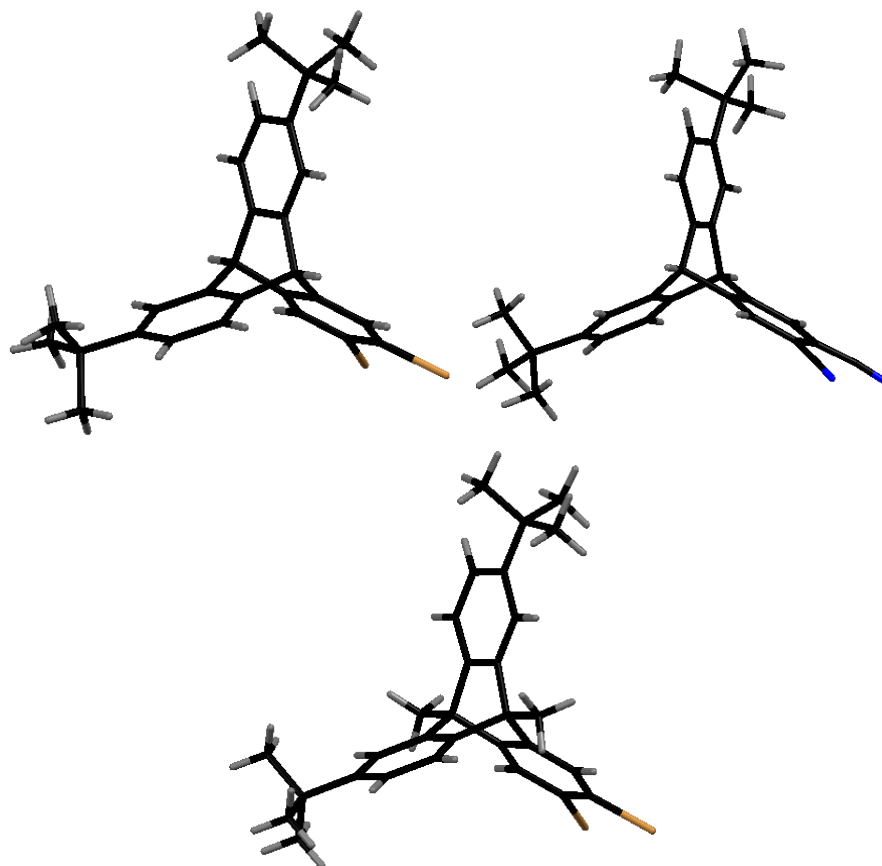


Figure 3.16: Molecular structures of 2,3-dibromo-6,15-di-*tert*-butyltriptycene (top left), 2,3-dicyano-6,15-di-*tert*-butyltriptycene (top right) and 2,3-dibromo-6,15-di-*tert*-butyl-9,10-dimethyltriptycene (centre). Crystals were obtained by slow diffusion of MeOH into a CHCl₃ solution.

3.4.1 UV-vis absorption spectra and Molecular Modelling

UV-vis absorption spectra of **MPz1** complexes in CHCl_3 display the classical non-aggregated form of Pcs, each with sharp intense Q-bands. However, in pentane solutions, an additional sharp peak is present at shorter wavelength, the intensity of which is concentration dependent (**Figure 3.17**, **Table 3.4**). As suggested by Lukyanets *et. al.*, this peak can be attributed to the co-facial dimer formation by **MPz1** complexes.

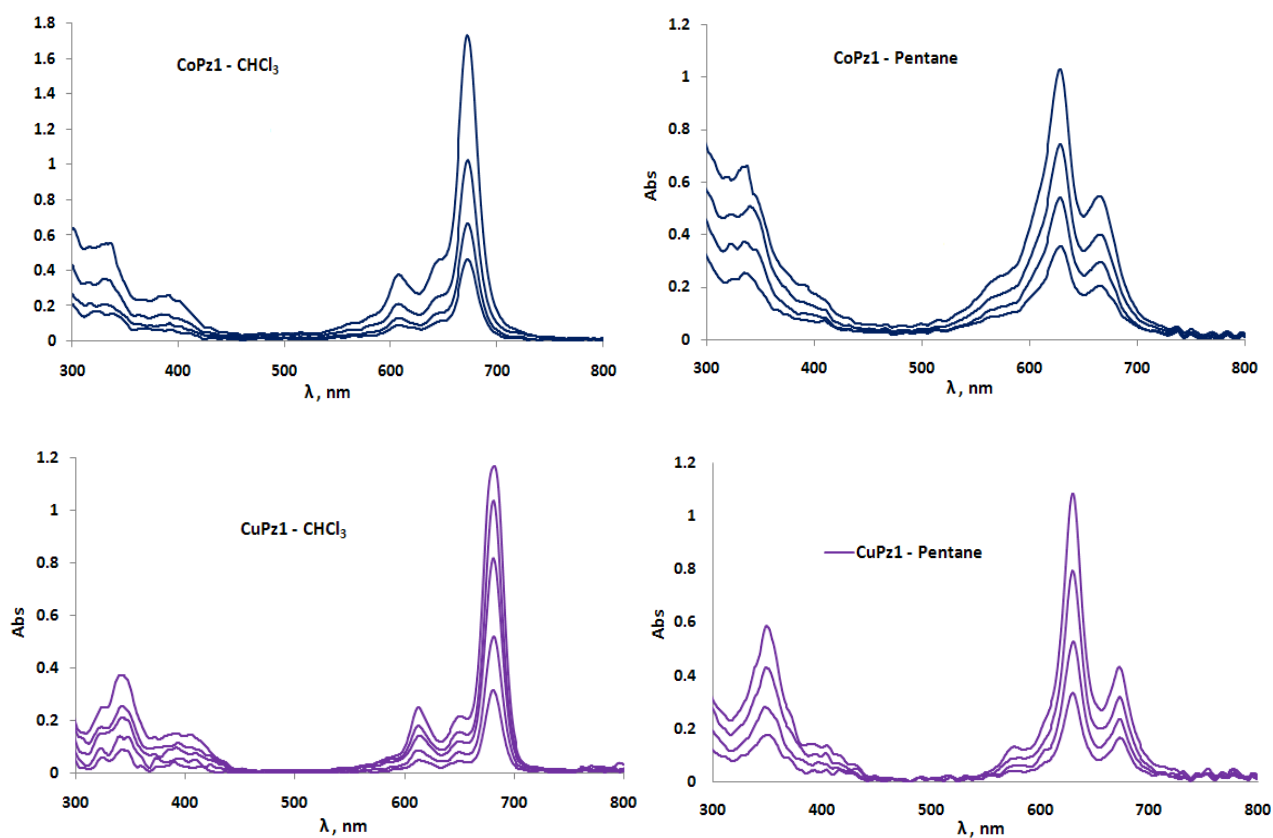


Figure 3.17: UV-vis absorption spectra of **CoPz1** (top) and **CuPz1** (bottom) in CHCl_3 (left) and pentane (right) measured using a 1 mm path length cell. See **Table 3.4** for extinction coefficient values.

Generally, cofacial aggregation of Pcs results in a greatly broadened blue shifted Q-band of much lower intensity relative to that of the monomeric spectrum.^[59] However, in the case of **MPz1**, the band originating from the aggregated species is sharp and intense. It was therefore of interest to model this dimeric species in order to try and explain the unique structural features which may be responsible for this. Modeling of the dimer of **H₂Pz1** was carried out using the

Spartan 10 software package (Version 1.1.0; Wave function Inc. Irvine, CA, USA). Results from molecular modelling (**Figure 3.18**) showed that the lowest energy configuration of the dimer is a self-complementary embrace in which the two Pc cores are staggered at an angle of 45° relative to each other. Further aggregation is prohibited by the *tert*-butylated triptycenes protruding above and below the plane of the Pc ring. This dimerisation results in a remarkably sharp and intense absorption band seen at the shorter wavelength, arising from excitonic coupling within the dimer.^[170] Moreover, this particular configuration of the dimer has also been found previously in μ -oxo-dimers of SiPc.^[171] UV-vis absorption spectra in solution of such dimers in aromatic solvents display an intense absorption band at ~ 639 nm, which was attributed to the conformer of *D_{4h}* symmetry, in which the two Pc components are staggered at an angle of 45° .

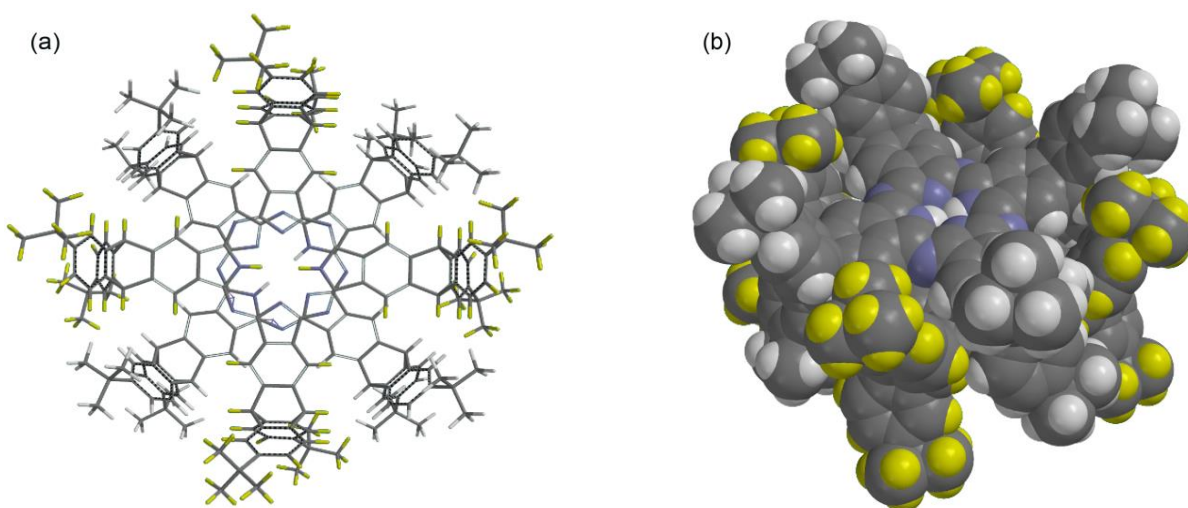


Figure 3.18: Molecular models of the cofacial dimer of **H₂Pz1** showing (a) the close embrace that results in each Pc ring being staggered at an angle of 45° relative to its partner and (b) a space-filling model showing the interlocking peripheral fused 9,10-dihydroanthracene substituents within the dimer. Note that the hydrogens on the two Pc molecules are coloured yellow on one and white on the other.

Interestingly, modelling suggested that placing methyl substituents onto the bridgehead positions of the triptycene subunits raises the energy of the dimer to ~ 50 kJ mol⁻¹, which is greater than the various values for the enthalpy of association of Pcs reported in the literature,^[172] and caused energetically unfavourable distortions in both the Pc and triptycene units. Hence, the most convenient way to check if this prediction holds true was to analyse **MPz2** complexes by UV-vis absorption spectroscopy.

Absorption spectra of **MPz2** in CHCl_3 solution display the monomeric behaviour as also seen for **MPz1** complexes. However in pentane solution, no evidence of dimer formation is seen (absence of peak at shorter wavelength) (**Figure 3.19**), which confirms the prediction from modelling that substitution of bridgehead positions by methyl groups prohibits co-facial association.

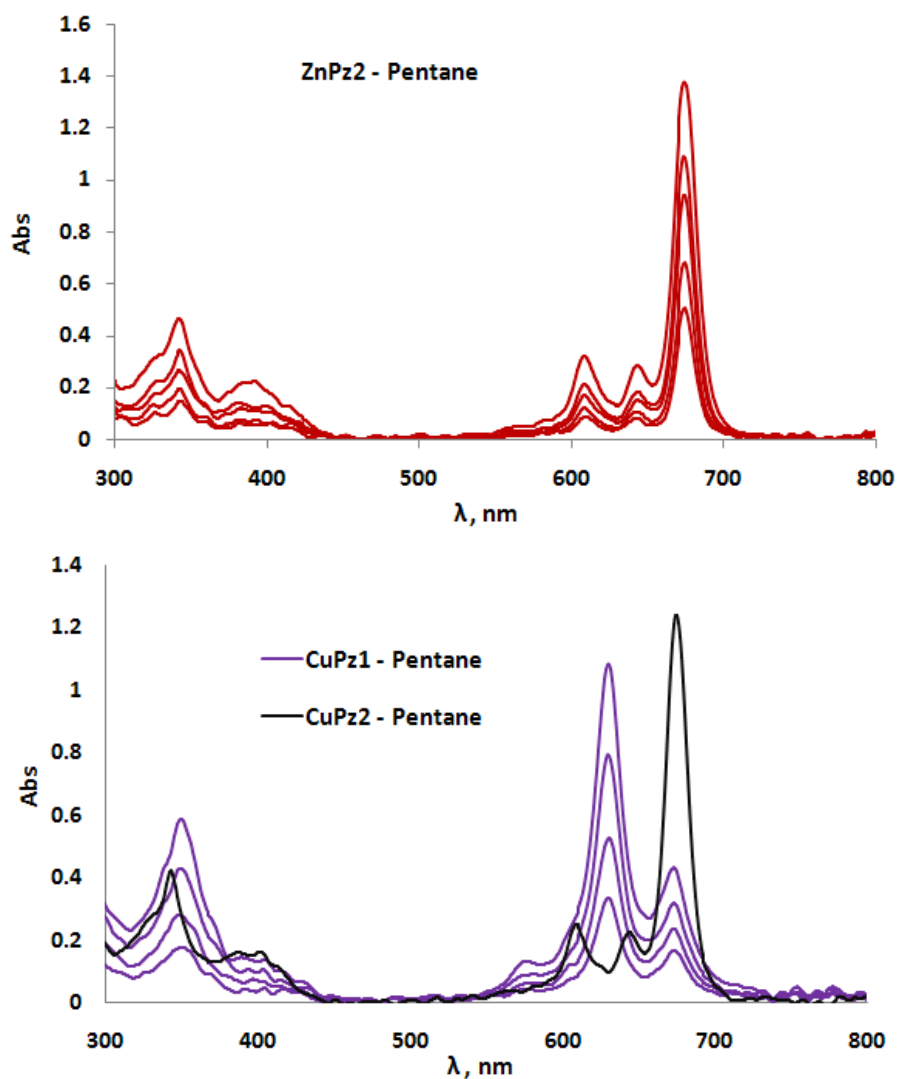


Figure 3.19: Top: UV-vis absorption spectra of **ZnPz2** in pentane. **Bottom:** A comparison of **CuPz1** and **CuPz2** in pentane. See **Table 3.4** for extinction coefficient values. **CuPz2** = 9.8×10^{-5} M.

3.4.2 Luminescence Spectroscopy

Steady state luminescence spectra of **MPz1** ($M = \text{Zn}^{2+}$ and 2H^+) showed emission only from the non-aggregated form from both chloroform and pentane solutions (**Figure 3.20**). Surprisingly, only very weak fluorescence was observed for **ZnPz2** in chloroform, but none was displayed from pentane solution, suggesting an efficient quenching of the excited state. The paramagnetic complexes were not emissive.

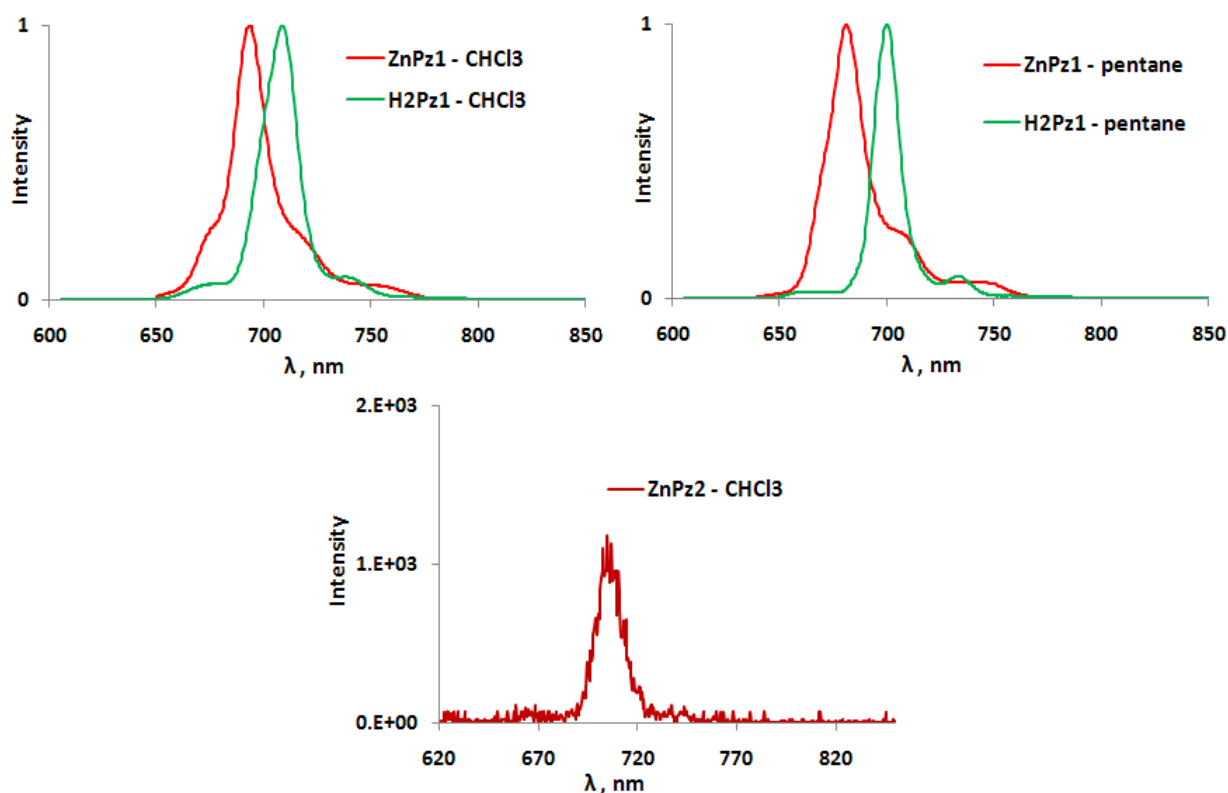


Figure 3.20: Normalised luminescence spectra for **ZnPz1** and **H₂Pz1** in CHCl_3 and pentane (top) and luminescence spectrum of **ZnPz2** in CHCl_3 (bottom). $\lambda_{\text{ex}} = 600$ nm.

These results from luminescence along with those obtained from UV-vis absorption spectroscopy for **MPz1** and **MPz2** are summarized in **Table 3.4**. The extinction coefficients calculated from the non-aggregated spectra of **MPz2** in pentane were used to calculate the concentration of the non-aggregated components of the solutions of **MPz1** ($M = \text{Cu}^{2+}$ and Zn^{2+})

in the same solvent. This analysis allowed the dimerization constants (K_d) of **MPz1** ($M = \text{Cu}^{2+}$ and Zn^{2+}) to be calculated together with the molar extinction coefficient of the dimers ($\epsilon = \sim 4.0 \times 10^5 \text{ M}^{-1} \text{ cm}^{-1}$). The larger K_d value for **CuPz1** as compared to that of **ZnPz1** may reflect the greater tendency of the Zn^{2+} cation in Pcs to possess an axial ligand (*e.g.* H_2O), which may hinder dimerization.

	λ_{max} , nm chloroform ($\epsilon \times 10^5 \text{ M}^{-1} \text{ cm}^{-1}$)	λ_{max} , nm pentane ($\epsilon \times 10^5 \text{ M}^{-1} \text{ cm}^{-1}$)	K_d , M^{-1}	λ_{em}^b , nm CHCl ₃	λ_{em}^b , nm pentane
CuPz1	681 (2.27)	675 (2.24) ^a ; 632 (4.20) ^a	9.0×10^4 ^a	---	---
ZnPz1	683 (3.30)	675 (3.04) ^a ; 636 (3.8) ^a	3.7×10^4 ^a	691	680
CoPz1	673 (1.44)	668 (-); 629 (-)	(-)	---	---
H₂Pz1	702 (3.0), 665 (2.5)	698(-); 656 (-); 625 (-)	(-)	707	698
CuPz2	681 (2.14)	675 (2.24)	N/A	---	---
ZnPz2	682 (3.43)	675 (2.40)	N/A	701 (w)	---

Table 3.4: Data from UV-vis absorption and fluorescence spectra of the Pcs. **Notes:** ^a calculated assuming that the values of ϵ of the monomer of **MPz1** ($M = \text{Cu}^{2+}$ and Zn^{2+}) in pentane are identical to those of **MPz2** in pentane. ^b Excitation at 600 nm. (w) = weak.

3.4.3 EPR spectra of CuPz1 complex

Further evidence of this discrete dimer formation came from EPR spectroscopic analysis (**Figure 3.21**, **Table 3.5**), carried out by Dr. Emma Carter, of **CuPz1** in CHCl_3 and pentane solutions which agrees with that reported previously by Selyutin *et al.* in 1995. ^[173] As can be seen, in chloroform solution, the classic Cu^{2+} Pc monomer spectrum ($S = 1/2$) is obtained, showing hyperfine splitting from the nitrogens whereas in pentane solution, the spectrum is

dominated by an apparent $S = 1$ spin state. An effective $S = 1$ spin state can arise due to a close association between two $S = 1/2$ spin states as would be expected from the copper-containing cofacial dimer. Evidence of the formally forbidden $\Delta M_s = \pm 2$ transition at $g \sim 4$, referred to as the half-field transition, further confirms the presence of $S = 1$ state (see inset to **Figure 3.21**).

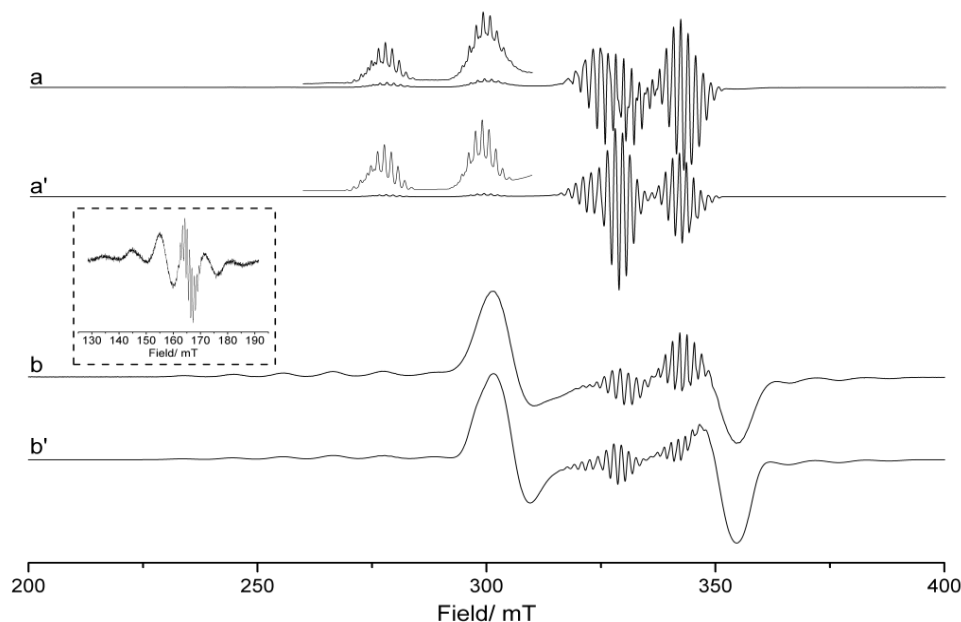


Figure 3.21: X-band CW EPR spectra (140 K) of **CuPz1** dissolved in (a) chloroform and (b) pentane at a concentration of 5.8×10^{-3} M. Corresponding simulations are given in a' and b'. The half field transition is shown in the inset.

	g_{\perp}	g_{\parallel}	${}^{\text{Cu}}A_{\perp}$	${}^{\text{Cu}}A_{\parallel}$	${}^{\text{N}}A_x$	${}^{\text{N}}A_y$	${}^{\text{N}}A_z$	$ D $
Chloroform	2.052 ^a	2.161 ^a	90 ^b	647 ^b	50 ^c	43 ^c	45 ^c	--
Pentane	2.040 ^a	2.155 ^a	35 ^b	325 ^b	--	--	--	1335 ^d

^a ± 0.005 ; ^b ± 3 MHz; ^c ± 2 MHz; ^d ± 5 MHz.

Table 3.5: Spin Hamiltonian parameters for **CuPz1** in chloroform and pentane solution (all hyperfine and zero-field values are given in MHz).

The above study thus concludes that fine-tuning of rigid and contorted substituents on the Pc ring can prevent the degree of self-association and could allow preparation of microporous molecules. A nitrogen sorption isotherm was also measured for **ZnPz2** but the analysis was carried out on a very small amount of sample (~ 23 mg as opposed to 80 – 100 mg) which means that a greater error is associated with the surface area value calculated. However, the shape of the isotherm (**Figure 3.22**) could be an indication of microporosity.

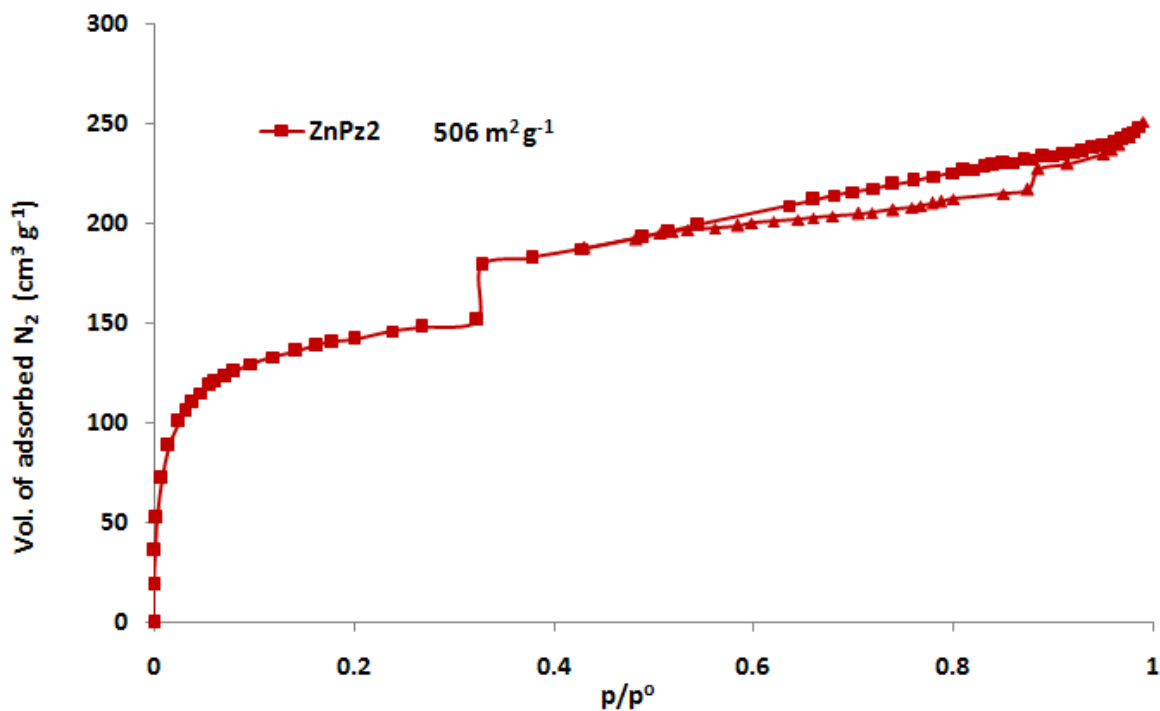
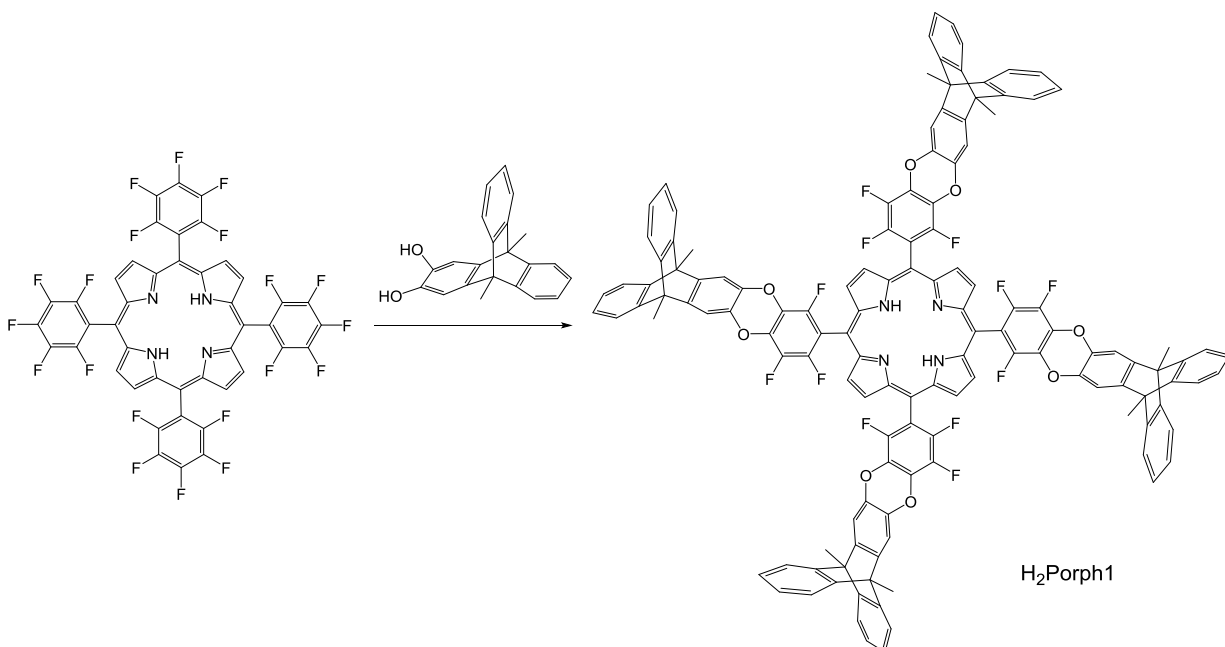


Figure 3.22: BET nitrogen adsorption and desorption isotherms of **ZnPz2** complex measured at 77 K.

3.5 Triptycene-substituted porphyrins

An investigation into metalloporphyrin molecules of IM was prompted by their similarities to Pcs and the ease of obtaining appropriate pre-formed precursors such as the commercially available tetrakis(pentafluorophenyl)porphyrin ($H_2(PhF_5)_4Porph$). Based on previous work by the group, it was anticipated that this precursor will undergo a substitution reaction with dihydroxytriptycenes to give molecules bearing some structure similarity to the biphenyl-based OMIMs^[146] and the Pc and Pz complexes prepared earlier in this project.

To begin with, a tetra-triptycene substituted porphyrin molecule (**H₂Porph1**) was synthesised (**Scheme 3.9**) from S_NAr reaction between $H_2(PhF_5)_4Porph$ and four equivalents of 2,3-dihydroxy-9,10-dimethyltriptycene, according to the reported procedure.^[96]



Scheme 3.9: S_NAr reaction to make **H₂Porph1**. *Reagents and conditions:* K_2CO_3 , NMP, 100 °C, 18 h.

The novel porphyrin molecule was firstly characterised by MALDI-MS (**Figure 3.23**) and 1H and ^{19}F NMR spectroscopy (**Figure 3.24**), all of which confirmed the presence of the tetra-substituted species with the expected symmetry as the major product. As reported previously,^[97] the most distant fluorine atoms (at para position) of the pentafluorophenyl groups at the meso positions of the porphyrin core, are readily substituted by nucleophiles. In the case of

tritycene catechol, the initial substitution of the para fluorine atom is followed by the substitution of the neighbouring fluorine atom.

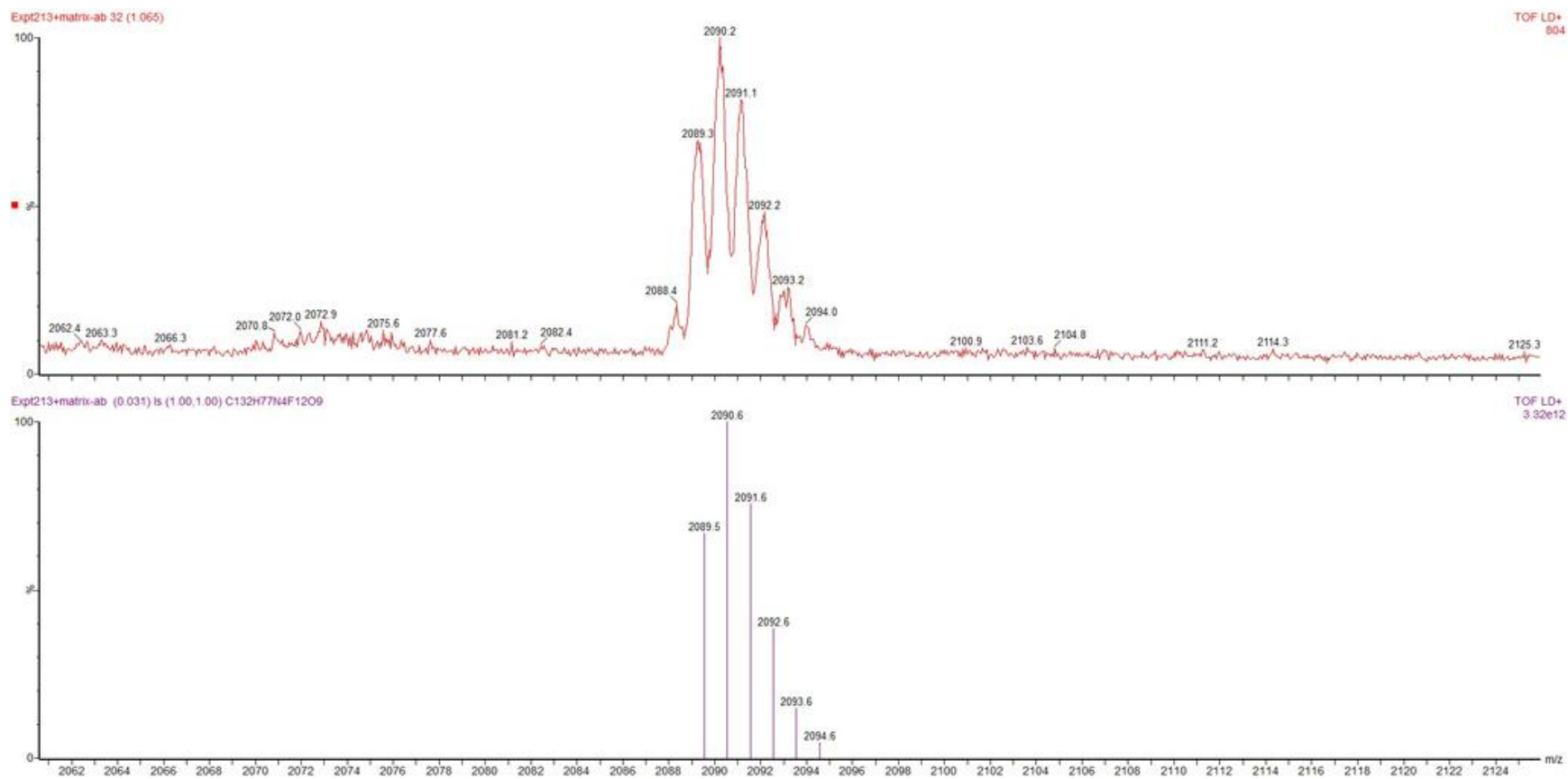


Figure 3.23: Expected isotope model (top) and MALDI mass spectrum (bottom) of **H₂Porph1**.

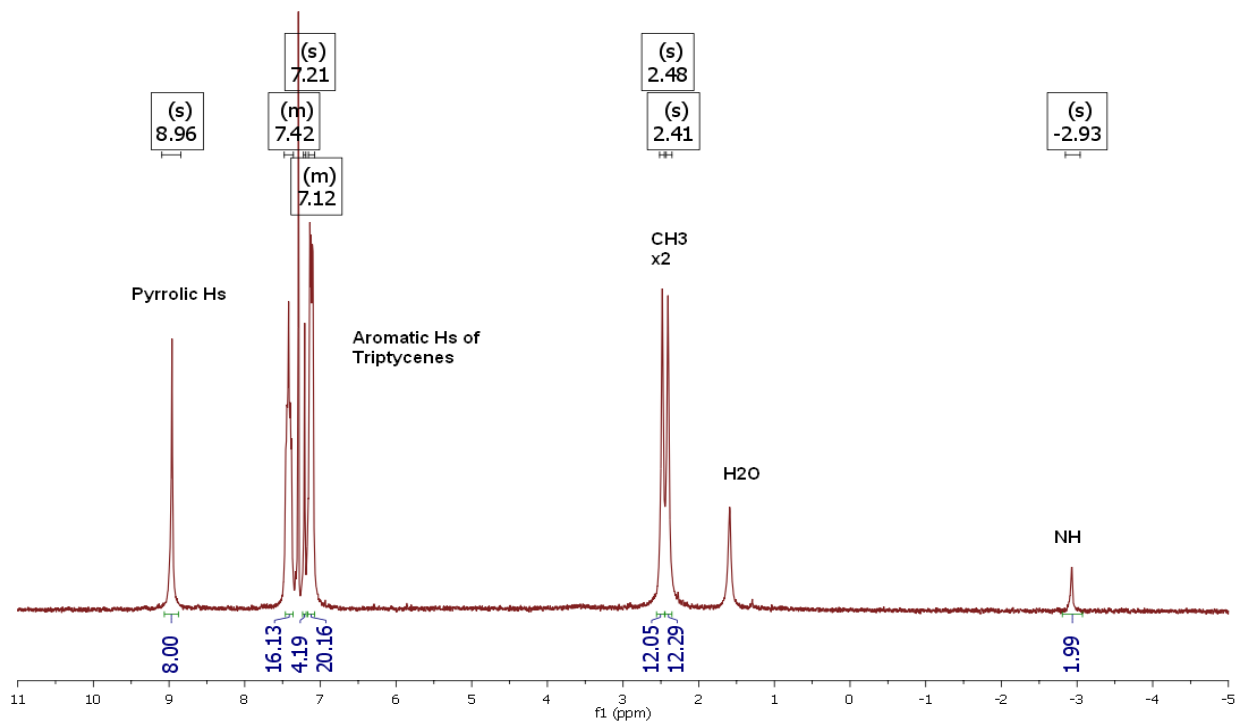
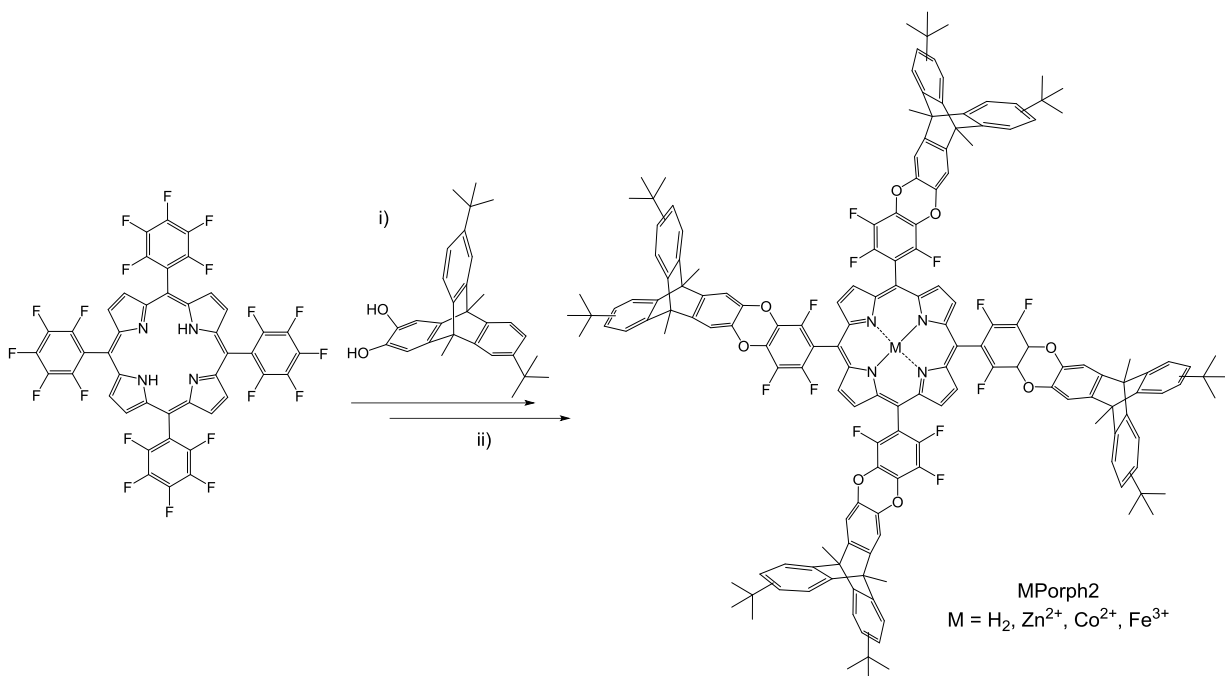


Figure 3.24: ^1H NMR spectrum of $\text{H}_2\text{Porph1}$ recorded at 250 MHz in CDCl_3 .

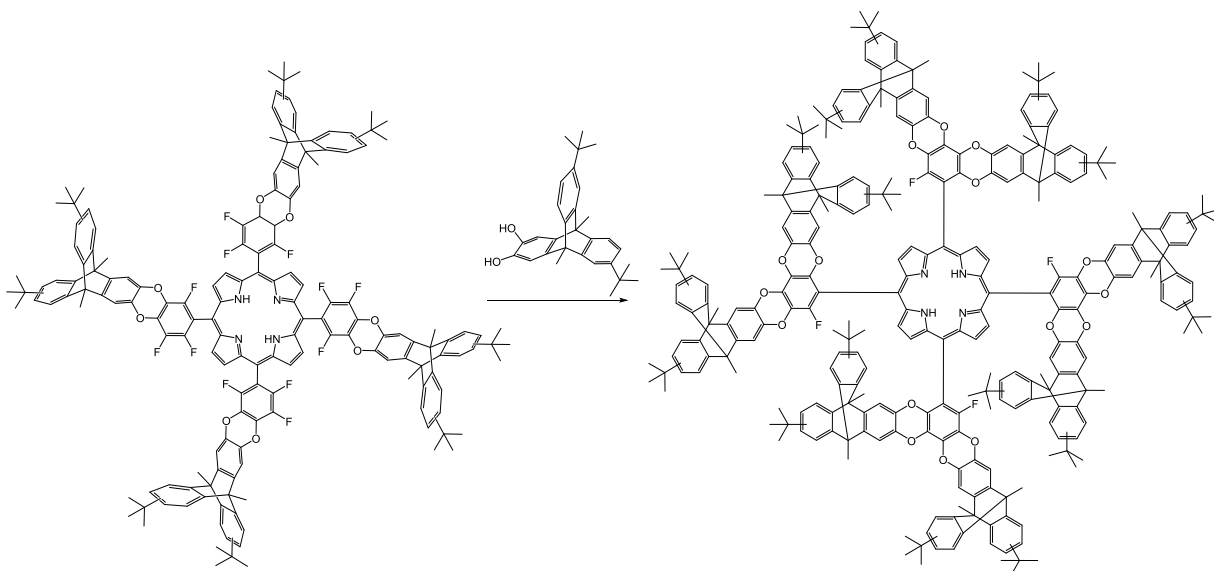
Since it is known that *tert*-butyl groups induce significant steric crowding around the aromatic core and also improve surface area of OMIMs, a *tert*-butylated analogue ($\text{H}_2\text{Porph2}$) was also synthesised. Moreover, three metal analogues (MPorph2 , $\text{M} = \text{Zn}^{2+}$, Co^{2+} and Fe^{3+}) were also prepared via metal insertion reaction using $\text{H}_2\text{Porph2}$ and an appropriate metal salt (**Scheme 3.10**). MALDI-MS, ^1H and ^{19}F NMR spectroscopy and UV-vis absorption spectroscopy (see later) all confirmed the successful preparation of MPorph2 .



Scheme 3.10: Synthesis of **MPorph2**. *Reagents and conditions:* i) K₂CO₃, NMP, 100 °C, 18 h; ii) **H₂Porph2**, NMP, anhydrous Zn(OAc)₂, Co(OAc)₂ or FeCl₃, 140 °C, ~ 18 h.

3.5.1 Attempts to make octa-triptycene substituted porphyrin

Attempts to make an octa-triptycene substituted porphyrin (**Scheme 3.11**) only resulted in a mixture of products being isolated. For example, **H₂Porph2** was reacted with 5 equivalents (slight excess) of 2,3-dihydroxy-9,10-dimethyl-6,15-di-*tert*-butyltriptycene using the same reaction conditions as before. However, MALDI-MS analysis after 24 h showed only the starting **H₂Porph2** to be present. Temperature was thus increased to 150 °C and the reaction stirred for another 24 h. This time, the MALDI mass spectrum (**Figure 3.25**) showed a mixture of hepta- and octa- with small traces of tetra- and penta- triptycene substituted porphyrin to be present which was difficult to separate by column chromatography. This mixture of compounds was isolated and reacted with an excess of catechol at 165 °C for the third time, however, this did not improve the result as determined by MALDI-MS. Despite the orthogonality of the meso-pentafluorophenyl groups around the planar porphyrin core, it could be that there is still significant steric crowding towards further substitution.



Scheme 3.11: Synthesis of octa-triptycene subst. porphyrin. *Reagents and conditions:* i) K_2CO_3 , NMP, $100\text{ }^\circ\text{C}$, 18 h.

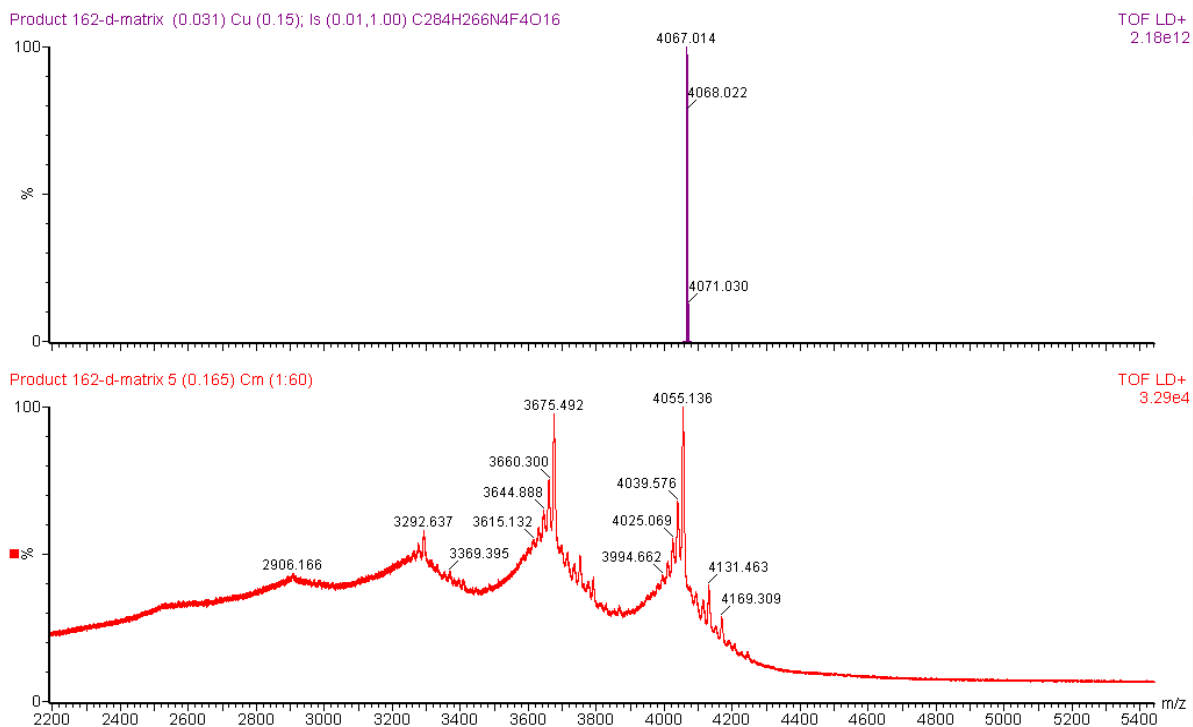


Figure 3.25: Expected isotope model (top) and MALDI mass spectrum (bottom) of an octa-substituted porphyrin molecule.

3.5.2 UV-vis absorption and luminescence spectroscopy

As reported in the literature, ^[174-177] UV-vis absorption spectra of the prepared meso-substituted porphyrins consist of an intense Soret or B band at 410 – 420 nm and a set of weakly intense Q bands at longer wavelengths at 500 – 650 nm (**Figure 3.26, Table 3.6**) arising due to $\pi - \pi^*$ transitions.

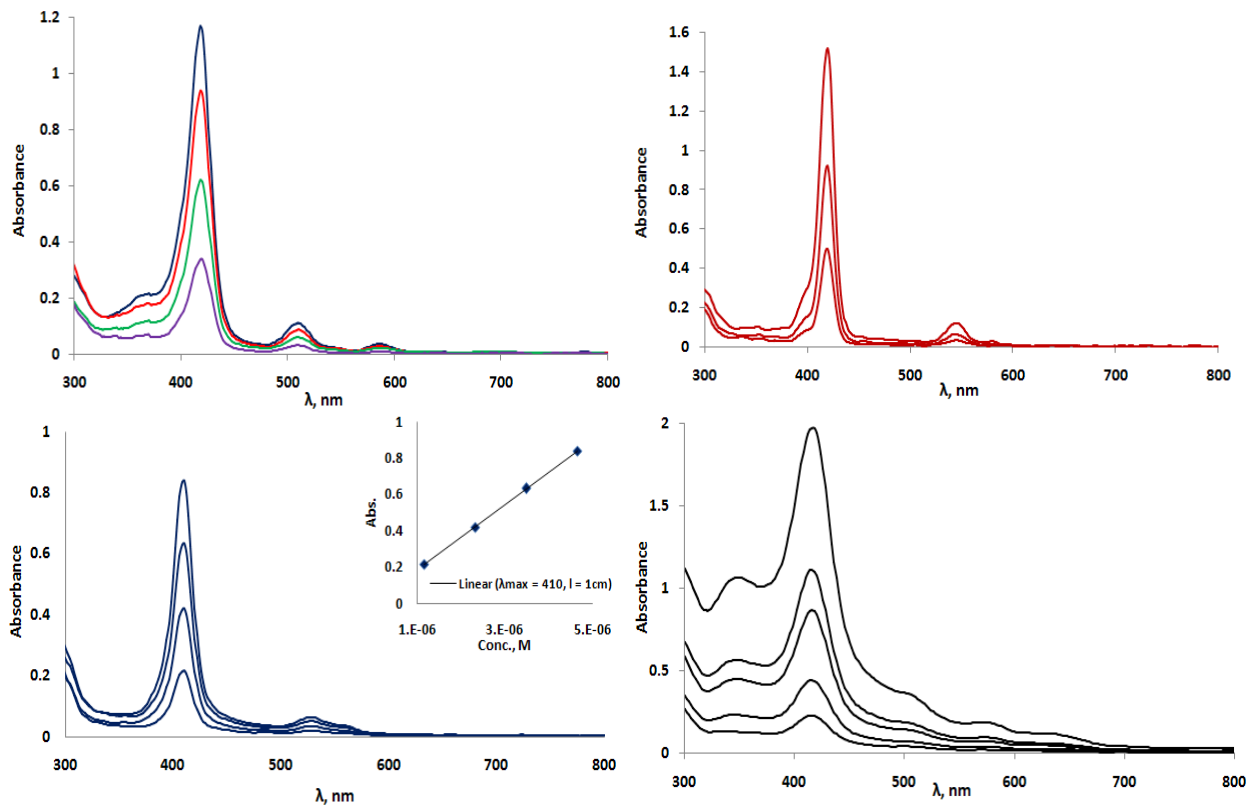


Figure 3.26: UV-vis absorption spectra of **H₂Porph1** (top left), **ZnPorph2** (top right), **CoPorph2** (bottom left with inset: A plot of absorbance vs. concentration) and **FePorph2** (bottom right) recorded in CHCl₃ at varying concentrations.

λ_{\max} , nm, (ϵ , $M^{-1} \text{ cm}^{-1}$)	
CHCl ₃	
H₂Porph1	418 (2.36×10^5), 510 (2.36×10^5), 544 (5.45×10^3), 584 (7.20×10^3), 634 (2.0×10^3)
H₂Porph2	419 (2.90×10^5), 508 (2.67×10^4), 543 (6.64×10^3), 585 (9.67×10^3), 645 (1.86×10^3)
ZnPorph2	419 (3.66×10^5), 544 (2.59×10^4), 576 (6.71×10^3)
CoPorph2	410 (1.80×10^5), 528 (1.40×10^4), 560 (7.87×10^3)
FePorph2	416 (8.34×10^4), 504 (1.38×10^4), 574 (7.31×10^3), 636 (4.53×10^3)

Table 3.6: Data from UV-vis absorption spectroscopy.

The subtle difference in the position of the B band depends on the nature of central metal ion: Absorption spectra of **H₂Porph1** and **H₂Porph2** contain B band at ~ 419 nm, while that of **FePorph2** and **CoPorph2** are slightly blue shifted to 416 and 410 nm respectively and the position of the B band for **ZnPorph2** remains unchanged at 419 nm. Moreover, the number and the intensity of the Q bands in the absorption spectra of porphyrins also depend upon the nature of the metal ion. As reported in the literature, ^[174-176] this dependence is due to the extent to which the metal d orbitals interact with the porphyrin π system. As Zn^{2+} is a closed shell metal ion, there is little interaction with the porphyrin ligand, whereas with partly filled metal d orbitals or paramagnetic metal ions (Co^{2+} and Fe^{3+}), charge transfer absorption bands can arise ($d - \pi^*$ or $\pi - d$) as well as ‘tripmultiplet transitions’ can occur which complicates the absorption spectra of porphyrins. The recorded UV-vis absorption spectra of all porphyrin compounds remained unchanged at varying concentrations in CHCl₃ suggesting an absence of aggregation (inset **Figure 3.26**).

An absence of aggregation in metalloporphyrins was further confirmed by luminescence spectroscopy. At 298 K in CHCl₃ solutions (**Figure 3.27**, **Table 3.7**), **H₂Porph1**, **H₂Porph2** and **ZnPorph2** exhibit strong fluorescence (lifetimes: 4.4, 4.7 and 1.25 ns respectively)

whereas **FePorph2** showed a very weak and poorly resolved emission spectrum and **CoPorph2** was non luminescent. As reported, for metal free and zinc analogues, the excited states can be regarded as purely $\pi - \pi^*$ in nature but in the case of paramagnetic complexes, the absence or inefficiency of luminescence could be the result of complicated non-radiative decay processes occurring within different excited states and can also be due to an efficient quenching by triplet oxygen. ^[174-176]

Hence, further luminescence measurements were carried out in frozen toluene glasses and also in solid state to avoid the problem of oxygen quenching in solution. It was found that **FePorph2** gives more resolved spectra both in toluene glass and in solid state compared to at RT whereas **CoPorph2** remained non-emissive.

It is also reported in the literature that metal free, Zn^{2+} and Fe^{3+} porphyrin complexes exhibit low temperature phosphorescence in frozen glasses. ^[174,175,177] Unfortunately, we did not find any clear evidence of emission peaks present at longer wavelengths in our recorded spectra for the metal free and zinc analogues to confirm that phosphorescence is seen alongside fluorescence. This could be due to the phosphorescent peaks being very low in intensity in the case of **ZnPorph2** (peak at ~ 750 nm **Figure 3.27, top right**).

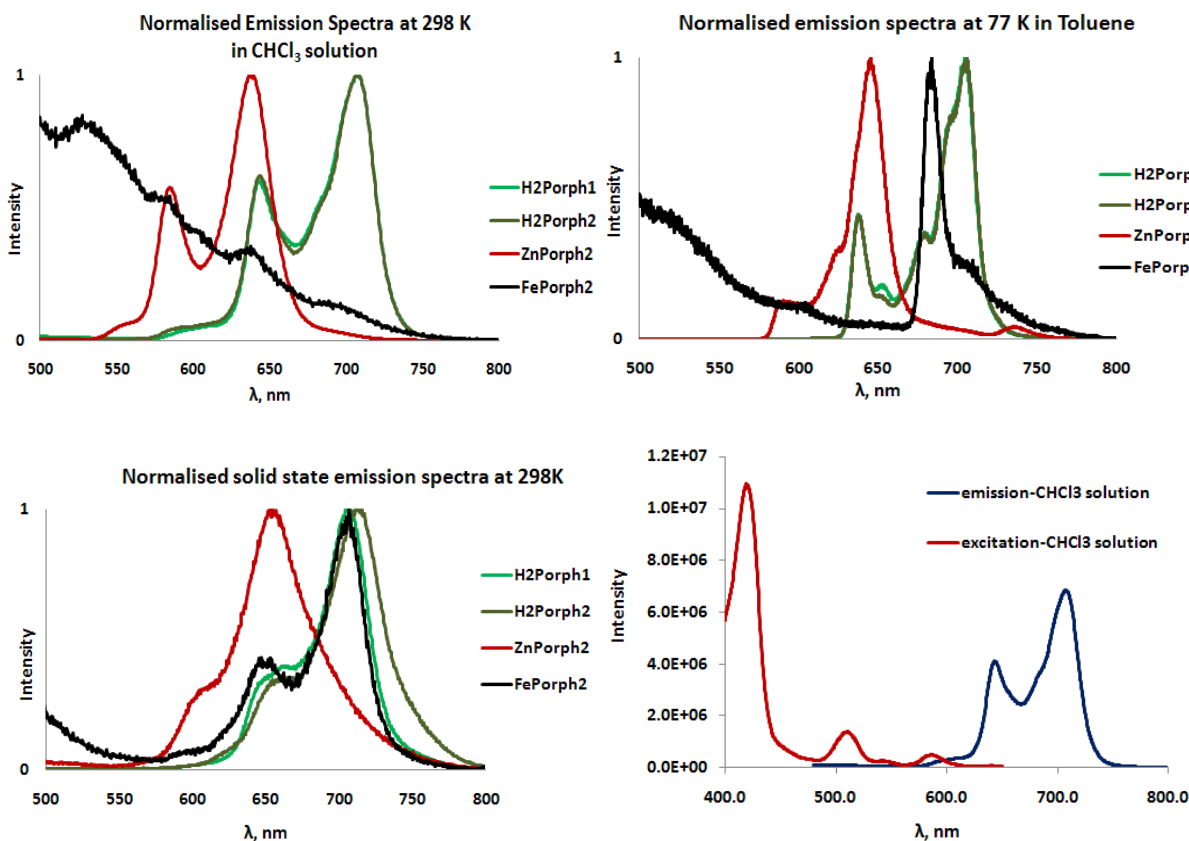


Figure 3.27: Luminescence spectra recorded in various conditions. **Bottom left:** An example of excitation vs. emission spectra of **H₂Porph1**. λ_{ex} : 410 – 420 nm.

	λ_{max} , nm, CHCl ₃	λ_{em} , nm, solid state, 298 K	λ_{em} , nm, CHCl ₃ , 298 K	λ_{em} , nm, Toluene, 77 K
H₂Porph1	418, 510, 544, 584, 634	657, 713	644, 708	632, 709
H₂Porph2	419, 508, 543, 585, 645	658, 706	643, 708	637, 705
ZnPorph2	419, 544, 576	655	585, 638	646
CoPorph2	410, 528, 560	644 (v. weak)	---	---
FePorph2	416, 504, 574, 636	650, 707	Weak, poorly resolved	684

Table 3.7: Data from luminescence spectroscopy with absorption spectroscopy data for comparison.

λ_{ex} : 410 nm.

3.5.3 Nitrogen adsorption analysis

Nitrogen adsorption isotherms (**Figure 3.28**) measured at 77 K for tetratriptycenoporphyrins demonstrate significant uptake at low relative pressures indicative of microporosity. The apparent BET surface areas calculated for these porphyrins ranged from 450 – 600 m² g⁻¹ (**Table 3.8**). It was found that the presence of *tert*-butyl groups improve the surface area by ~ 80 m² g⁻¹ for **H₂Porph2** as compared to **H₂Porph1**. The rate of nitrogen adsorption was also found to be much faster for **H₂Porph2** as compared to **H₂Porph1** which could be because the pores are more readily accessible in **H₂Porph2** due to the presence of bulky *tert*-butyl groups which further prevent any possible aggregation occurring and increase the amount of free space available in the solid state packing. In general however, these **MPorph2** complexes were slow at adsorbing nitrogen compared to **MPc4** complexes prepared previously. This could be due to the fact that **MPorph2** contain single bonds (linking the porphyrin ring and phenyl groups at the *meso* positions) which could rotate or are flexible which slows down adsorption kinetics. Out of the metal analogues, **ZnPorph2** was found to have the highest surface area possibly due to the presence of axial ligands which are usually removed on degassing the sample. **H₂Porph1**, **H₂Porph2** and **ZnPorph2** were also found to have quite high pore volumes compared to **FePorph2** and **CoPorph2**.

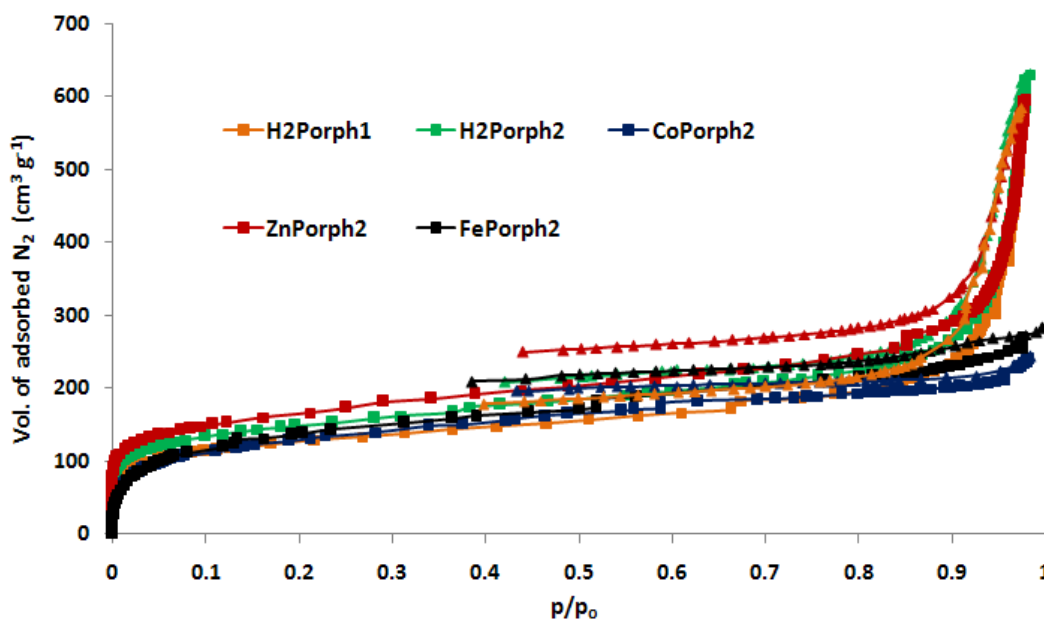


Figure 3.28: BET nitrogen adsorption and desorption isotherms for the porphyrin complexes measured at 77 K.

	Surface area (m ² g ⁻¹)	Total pore volume (cm ³ g ⁻¹)
H₂Porph1	455	0.90
H₂Porph2	531	0.97
ZnPorph2	595	0.99
FePorph2	506	0.42
CoPorph2	467	0.37

Table 3.8: BET surface areas and total pore volumes of the prepared porphyrin complexes.

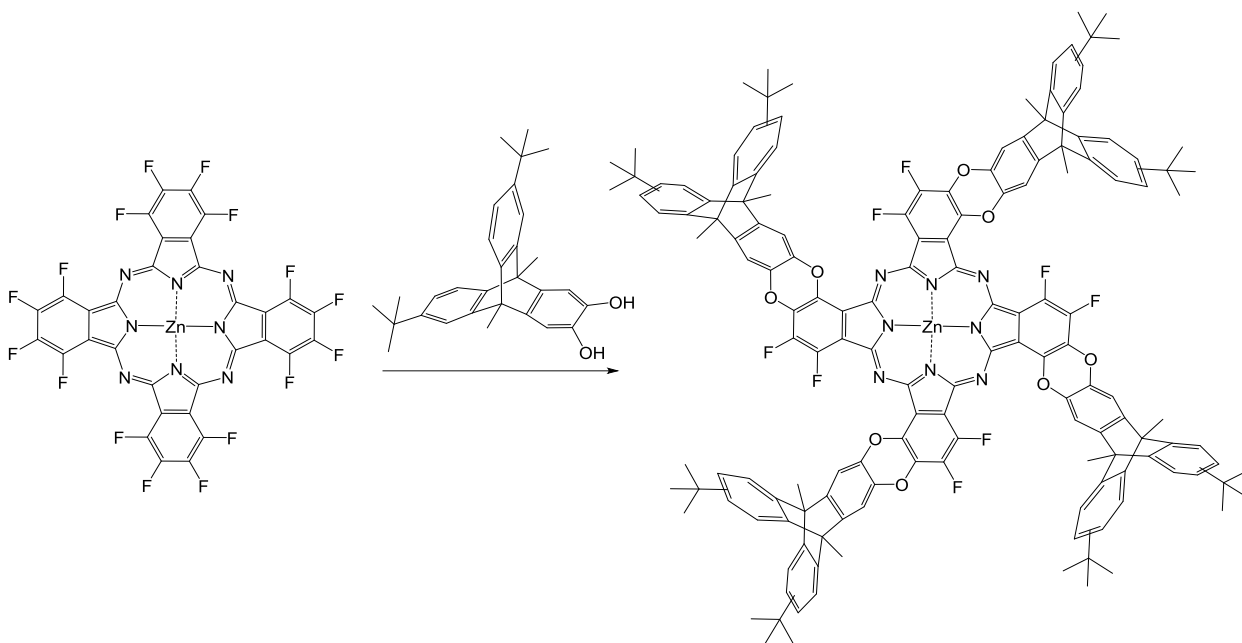
It is worth comparing these materials with the two highly rigid pentamers containing four Pc units linked via a spirocyclic fused ring system to a central Pc and porphyrin core that were reported in 2005. ^[155] The 1st of these had no surface area while Pc₄Porph exhibited a surface area of 100 – 110 m² g⁻¹. In contrast, this investigation clearly demonstrates that the presence of triptycenes as rigid substituents of high IMFV can significantly improve surface area in the case of Pc complexes e.g. **MPc4** complexes or porphyrin complexes e.g. **H₂Porph1** and **MPorph2**.

3.6 Molecules from hexadecafluoroMPcs

A related, commercially available and much cheaper precursor as compared to tetrakis(pentafluorophenyl)porphyrin is zinc(II)1,2,3,4,8,9,10,11,15,16,17,18,22,23,24,25-hexadecafluorophthalocyanine and its other metal analogues (hexadecafluoroMPcs). A publication in 2004 by Leznoff *et. al.* [178] reports the synthesis of poly-substituted Pc materials by reacting the preformed hexadecafluoroZnPc with a range of O, N, C and S nucleophiles via S_NAr reaction. The obtained reaction products had good solubility and consisted of a narrow distribution of polysubstituted Pcs with the degree of substitution dependant markedly on the steric effect of the nucleophile, its nucleophilicity, the temperature and time required to complete the reaction. A second relevant publication in 2008 on catalysis by Pc and porphyrin network PIMs [98] describes the preparation of a spiro-linked CoPc network PIM made from preformed hexadecachloroCoPc and two equivalents of tetrahydroxyspirobisindane. The network PIM consisted of tetrasubstituted Pc cores as evident from elemental analysis. Both papers therefore showed scope for similar reactions using preformed Pcs and triptycene catechols to make OMIM-like materials.

3.6.1 Reaction to make tetra substituted Pc

Firstly, we tried to make a tetra substituted molecule using hexadecafluoroZnPc and four equivalents of 2,3-dihydroxy-9,10-dimethyl-6,15-di-*tert*-butyltriptycene (**Scheme 3.12**). After quenching, MALDI-MS analysis of the reaction showed a mixture of tetra and penta substituted Pc to be present in almost a 1:1 ratio as well as some hexa substituted Pc (**Figure 3.29**). Also higher molecular weight products were seen which could be due to aggregation phenomena. Little information could be obtained from ¹H NMR analysis due to poor solubility and this mixture of products was not seperable by TLC analysis.



Scheme 3.12: Attempted synthesis of tetra substituted Pc. *Reagents and conditions:* i) K_2CO_3 , NMP, $100\text{ }^\circ\text{C}$, 18 h.

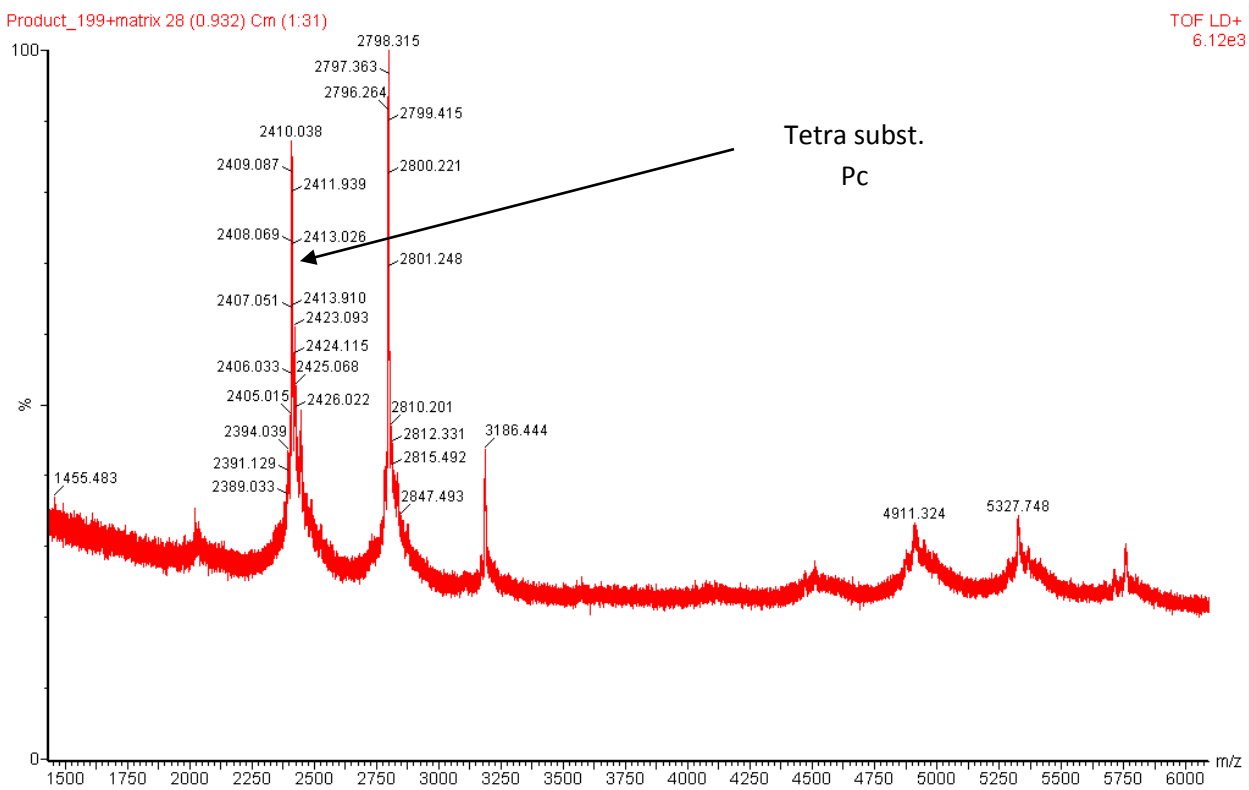


Figure 3.29: MALDI mass spectrum of the reaction to make tetra subst. Pc. Tetra, penta and hexa subst. Pc products are clearly visible.

It was thought that the high temperature reaction results in a greater degree of substitution and so lower temperature reactions (71 °C) were attempted. MALDI-MS indicated a product mixture of tri and tetra substituted products with traces of penta substitution (**Figure 3.30**).

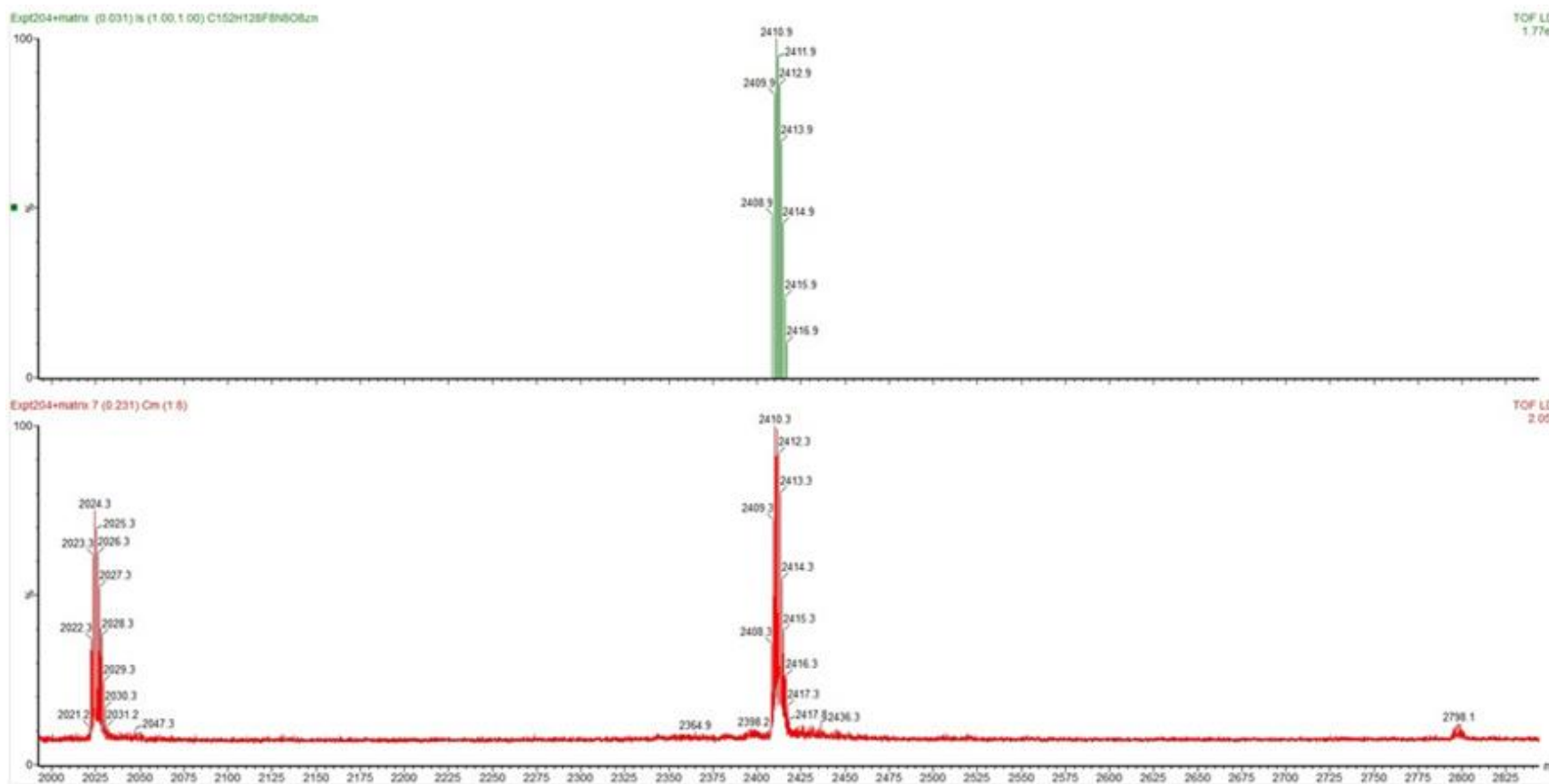
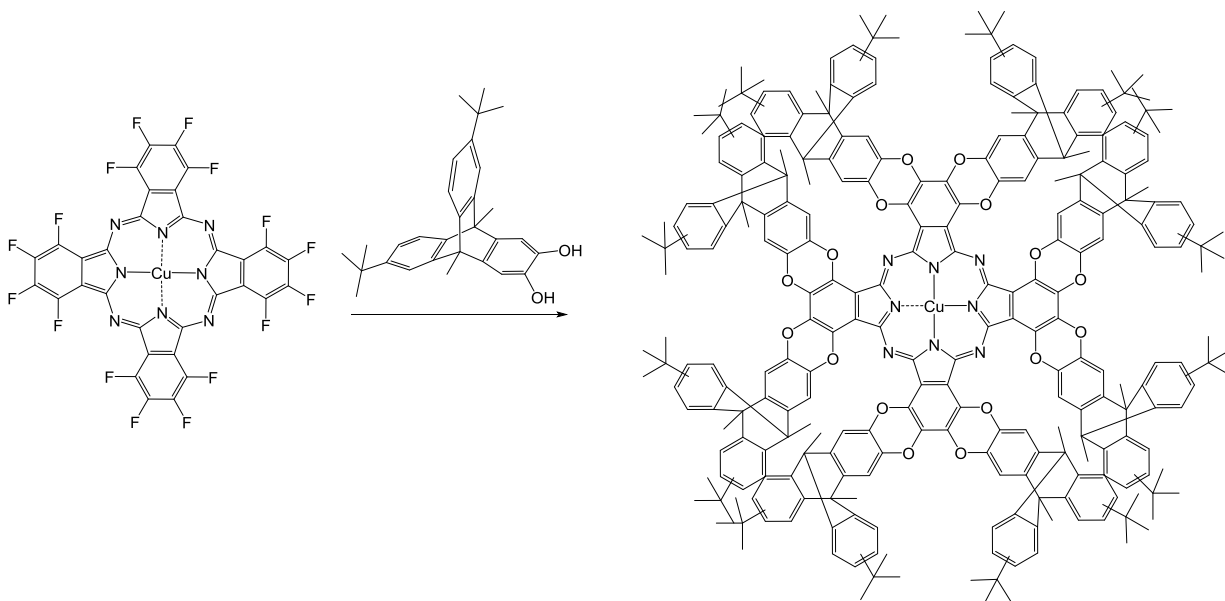


Figure 3.30: Expected isotope model (top) of tetra substituted Pc and MALDI mass spectrum (bottom) of the reaction at 71 °C.

3.6.2 Reaction to make an octa substituted Pc

The previous two attempts to make a tetra substituted Pc resulted only in mixtures of products. Therefore full octa substitution of the Pc was attempted. For this purpose, ten equivalents of 2,3-dihydroxy-9,10-dimethyl-6,15-di-*tert*-butyltritycene were reacted with hexadecafluoroCuPc (**Scheme 3.13**). To push the reaction to completion, the temperature was also increased to 165 °C and the reaction left stirring for ~ 72 hours. After quenching, the crude product was washed with methanol to remove any unreacted triptycene. To our surprise, MALDI mass spectrum of the reaction product showed octa to be present as the major product with only traces of hepta and hexa substituted Pcs (**Figure 3.31**).



Scheme 3.13: Attempted synthesis of octa substituted Pc. *Reagents and conditions:* i) K_2CO_3 , NMP, 100 °C, 18 h.

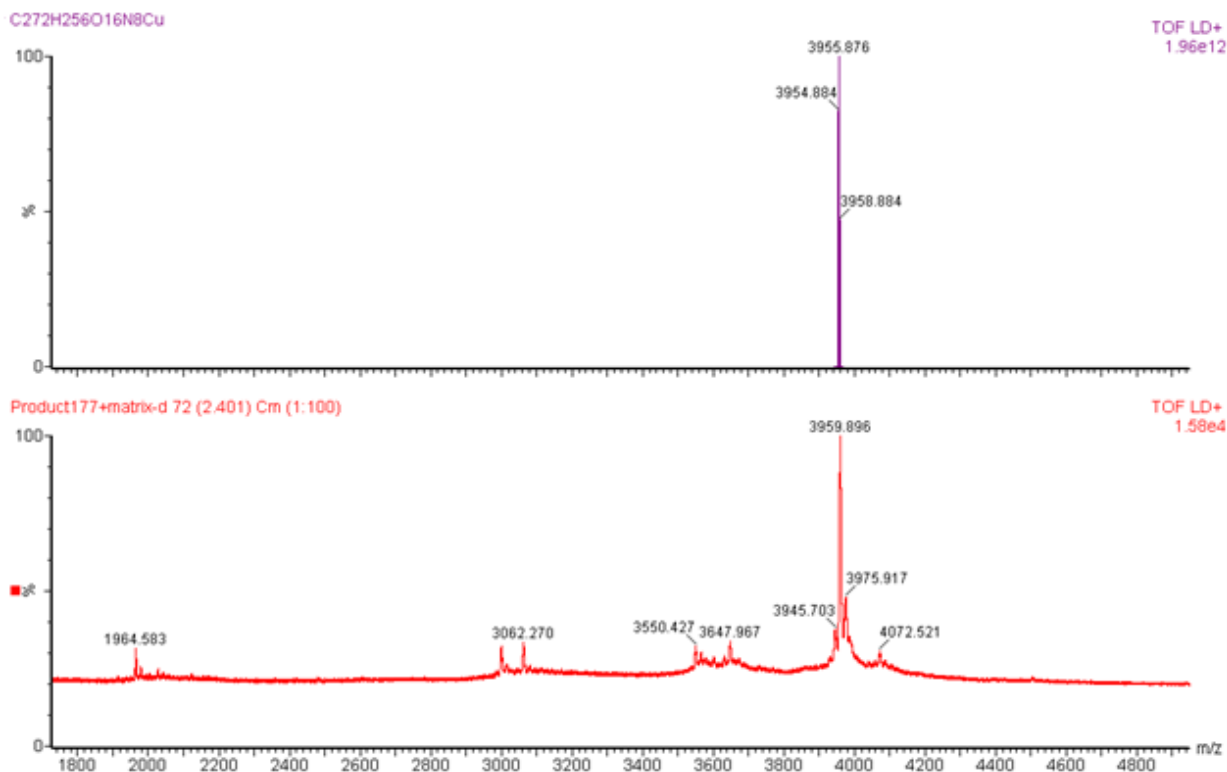


Figure 3.31: Theoretical (top) and obtained (bottom) MALDI mass spectrum of octa substituted CuPc.

UV-vis absorption spectrum of this reaction product showed the Q band to be very broad with low extinction co-efficient which could be because it is a mixture of products and not completely pure (**Figure 3.32**). More importantly, the Q band was red shifted compared to **CuPc4** complex which was prepared from cyclotetramerisation of **Pn4** previously (**Scheme 3.7**). This is expected since it is known that the non-peripheral sites on hexadecafluoroPcs are substituted 1st which results in a shift in the λ_{\max} from ~ 670 nm for peripheral substituted Pc to ~ 750 nm for non-peripheral substituted Pc. ^[179]

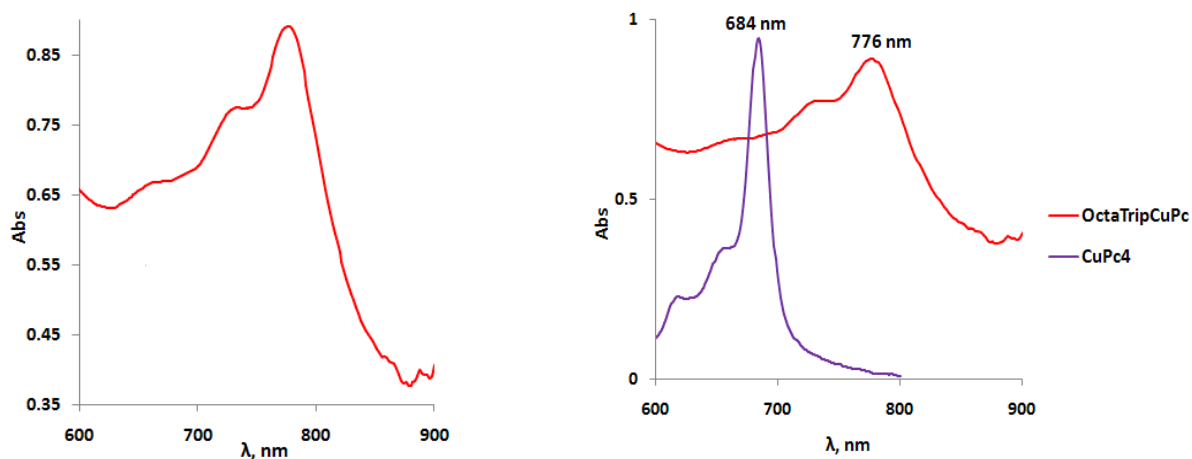


Figure 3.32: UV-vis absorption spectrum of the octa triptycene substituted CuPc in CHCl_3 of 3.79×10^{-5} M concentration (left) and a comparison of absorption spectra with the peripheral substituted **CuPc4** of 5.736×10^{-6} M concentration in CHCl_3 (right).

The reaction products from hexadecafluoroMPc molecules were not purified due to their poor solubility but it was of interest to assess one of the reaction products for porosity. BET analysis of the octa subst. CuPc reaction product gave a good surface area of $484 \text{ m}^2 \text{ g}^{-1}$ which is comparable with that of **CuPc4** ($511 \text{ m}^2 \text{ g}^{-1}$). However, the isotherm (**Figure 3.33**) differentiates from that of **CuPc4** in its shape and is a type (IV) isotherm according to the IUPAC classification.^[68] Also it consists of a hysteresis loop which tries to close in at low relative pressure ($p/p_0 \sim 0.5$) and could be due to mesoporosity or it could be that the material swells at high relative pressure.

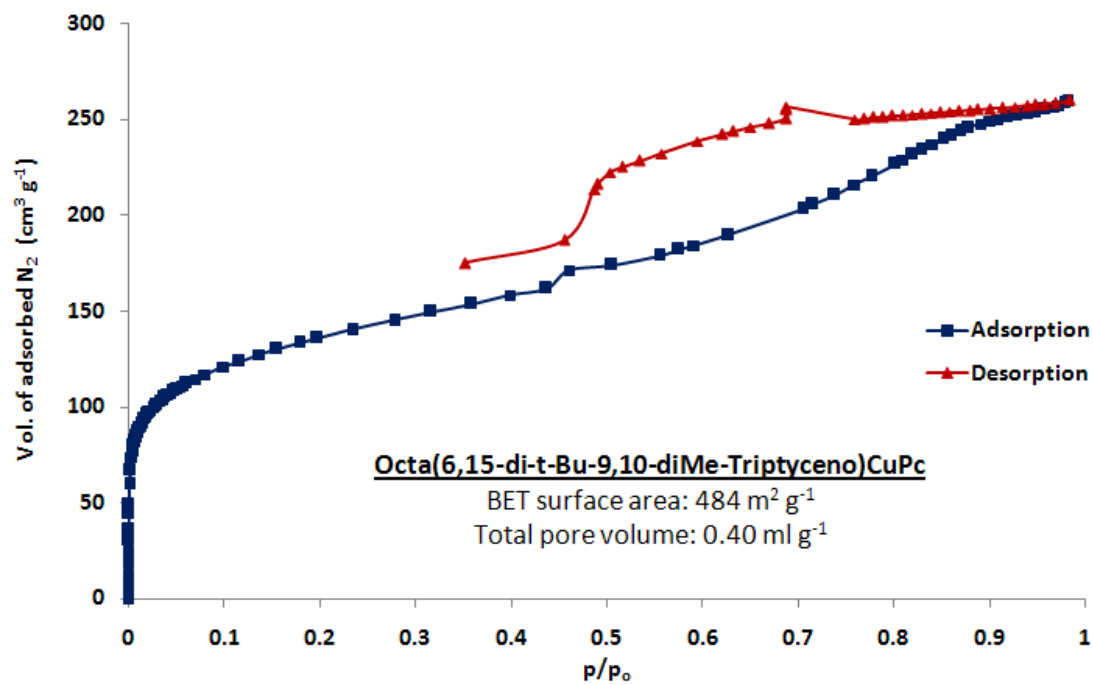


Figure 3.33: BET nitrogen adsorption and desorption isotherm of octa subst. CuPc.

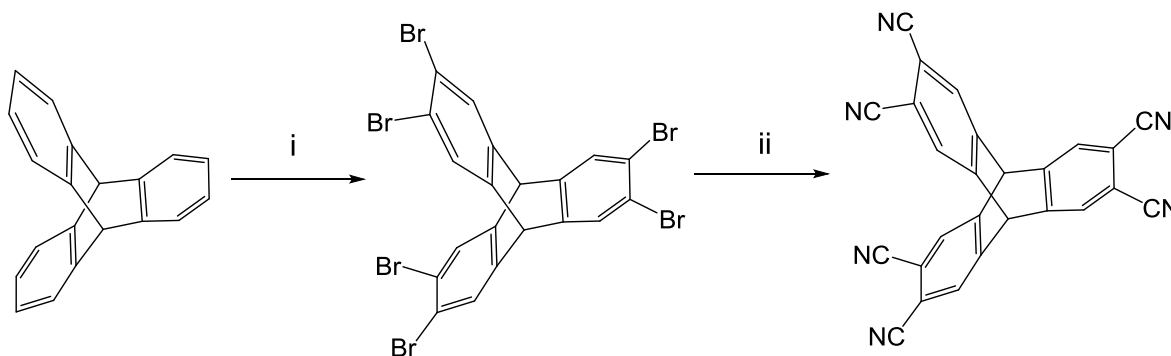
3.7 Attempts to make Pc-dimer and trimer molecules of intrinsic microporosity

It was anticipated that OMIM-like Pc-based materials could be prepared from rigid precursor “cores” bearing two or more Pn functional groups which can undergo cyclotetramerisation reaction with a second monofunctional Pn (e.g. 2,3- dicyano-6,15-di- *tert*-butyltritycene).

3.7.1 Synthesis of cores

3.7.1.1 Hexacyanotriptycene

Perhaps the most obvious precursor core to synthesise was 2,3,6,7,14,15-hexacyanotriptycene which can be prepared starting from the unsubstituted triptycene by bromination ^[111] and then cyanation ^[180] (**Scheme 3.14**).

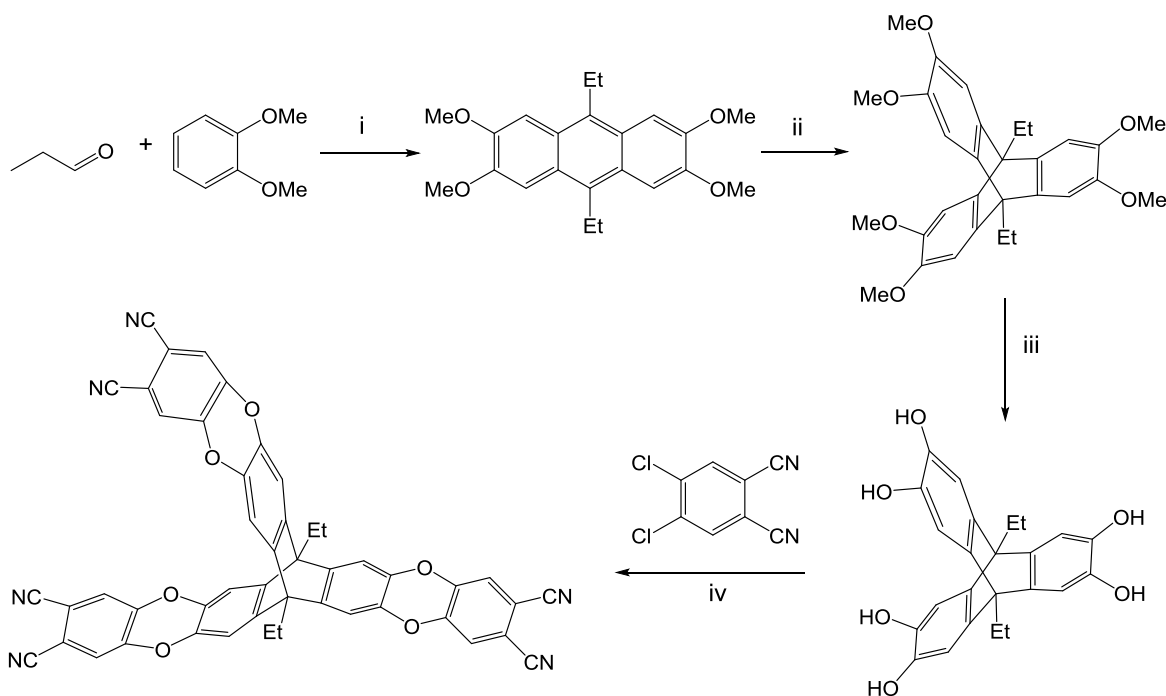


Scheme 3.14: Synthesis of hexacyanotriptycene. *Reagents and conditions:* (i) Br₂, DCM, reflux; (ii) CuCN, DMF, reflux.

The isolation of hexacyanotriptycene was particularly challenging mainly due to its low solubility and problems with purification and because the reaction intermediates undergo network polymer formation during the reaction producing a complex product mixture. Nevertheless, a small amount of hexacyanotriptycene was isolated, confirmed by its ¹H NMR and mass spectrum.

3.7.1.2 Alternative triptycene core

An alternative precursor to hexacyanotriptycene is the trisphthalonitrile derived from 2,3,6,7,14,15-hexahydroxy-9,10-diethyltriptycene which can be prepared starting from 2,3,6,7-tetramethoxy-9,10-diethylantracene (**Scheme 3.15**). The anthracene precursor can be prepared using veratrole and propanal under acidic conditions ^[117,181] which then undergoes cycloaddition with dimethoxybenzynes intermediate to give dimethoxy triptycene which is then, demethylated and substituted with dichlorophthalonitrile to give the novel **trisPn triptycene** for which a crystal structure was also obtained (**Figure 3.34**). Previously, the hexahydroxy-9,10-diethyltriptycene precursor from this synthesis was used to prepare organic triptycene-based PIMs with high surface areas for gas adsorption. ^[117]



Scheme 3.15: Synthesis of **TrisPn triptycene**. *Reagents and conditions:* (i) H_2SO_4 , RT; (ii) Diazonium salt of 4,5-dimethoxyanthranilic acid, Propylene oxide, 1,2-DCE, reflux; (iii) BBr_3 , DCM, RT; (iv) K_2CO_3 , DMF, $80\text{ }^\circ\text{C}$.

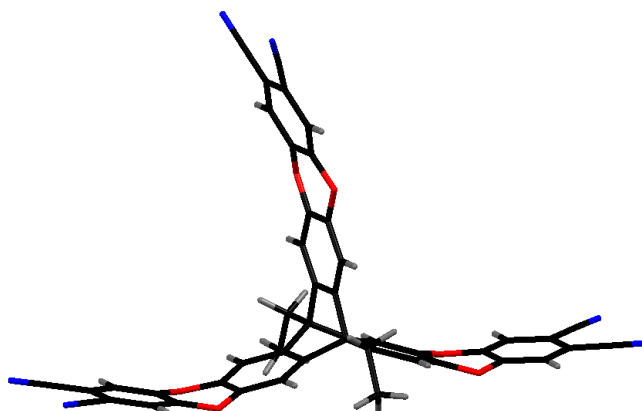


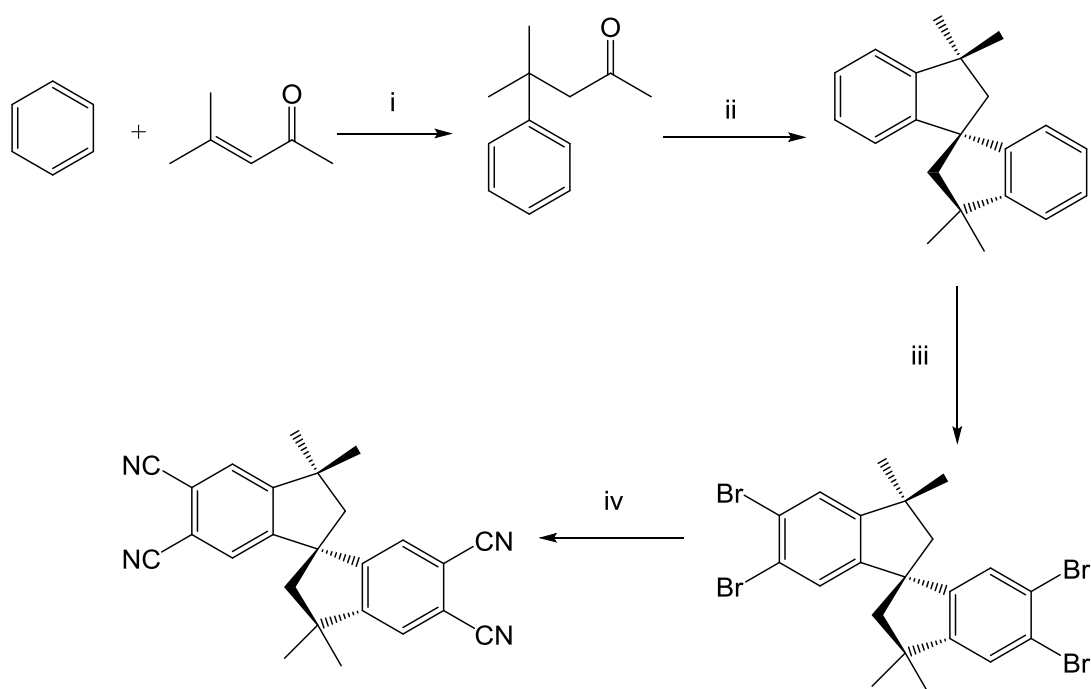
Figure 3.34: Molecular structure for TrisPn triptycene. Crystals were obtained by slow evaporation of a THF solution.

3.7.1.3 Tetracyanospirobisindane and tetracyanoethanoanthracene

As noted, spirobisindane (SBI) containing monomers have been synthesised previously to prepare Pc and porphyrin based network PIMs with high surface areas. ^[94,96] But, a recent publication from the group has demonstrated that in comparison to the relatively flexible SBI molecule, a ladder polymer consisting of ethanoanthracene (EA) linking groups provides a much higher BET surface area of 1028 m² g⁻¹ in comparison to 745 m² g⁻¹ for SBI polymer due to the shape persistency and inflexibility of EA. ^[182] Hence, for a comparison between microporosity of Pc-based molecules from different cores, we also decided to make tetracyanospirobisindane and tetracyanoethanoanthracene.

To make the novel tetracyanospirobisindane core (**Scheme 3.16**), firstly, mesityl oxide is added to benzene in the presence of AlCl₃ to give 4-methyl-4-phenyl-2-pentanone, ^[183] which undergoes a cyclodehydration reaction in the presence of zinc chloride to give the SBI hydrocarbon. ^[184] Subsequent bromination and cyanation of SBI gave the novel tetracyanospirobisindane for which a crystal structure was also obtained (**Figure 3.35**).

The full mechanism of SBI formation as postulated by Barclay and co-workers ^[184] is shown in **Figure 3.36**. The starting ketone can undergo two simultaneous reactions. It can either eliminate acetone by acid cleavage to give the protonated α -methylstyrene and it can undergo cyclodehydration to give the indene. This indene is in equilibrium with its exocyclic form in the acid medium. The bulky protonated α -methylstyrene can attack the exocyclic form more readily than the endocyclic form due to sterics and this produces the carbonium ion with the positive charge that is suitably situated to alkylate the second aromatic ring to produce 3,3,3',3'-tetramethyl-1,1'-spirobisindane.



Scheme 3.16: Synthesis of tetracyanospirobisindane. *Reagents and conditions:* (i) AlCl_3 , RT; (ii) ZnCl_2 , $180\text{ }^\circ\text{C}$; (iii) Br_2 , DCM, reflux; (iv) CuCN , DMF, reflux.

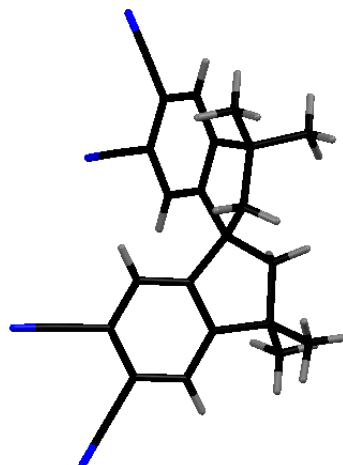


Figure 3.35: Molecular structure for tetracyanospirobisindane. Crystals were obtained from slow diffusion of MeOH into a CHCl_3 solution.

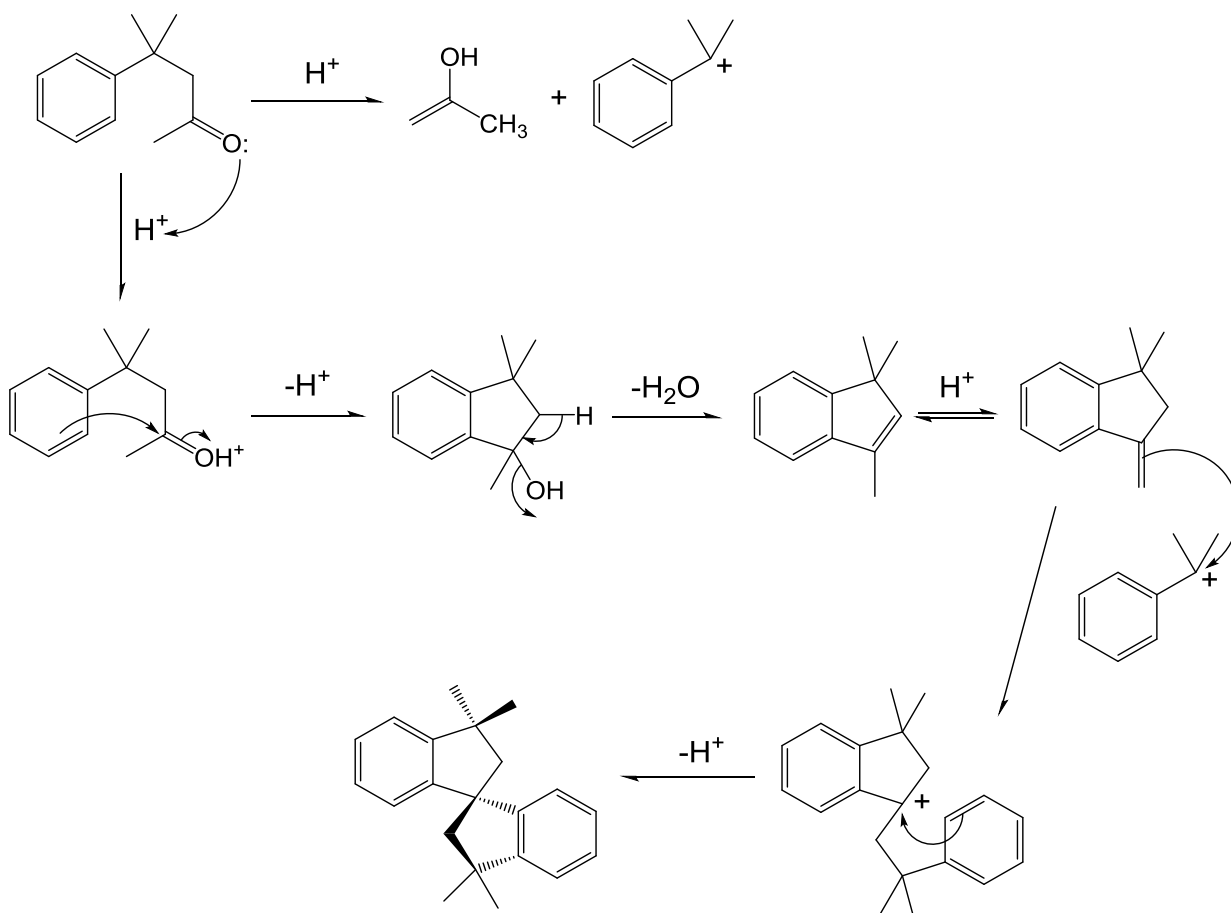
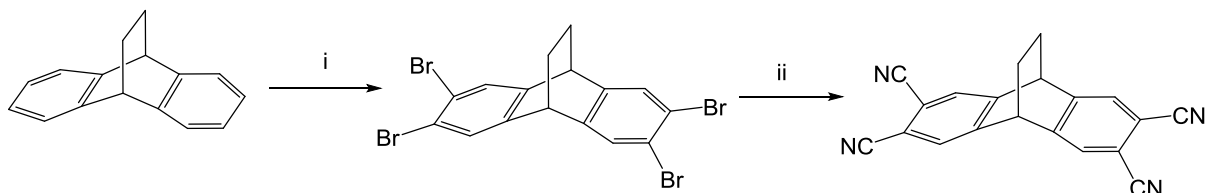


Figure 3.36: Mechanism of the SBI formation.

Tetracyanoethanoanthracene was prepared similarly (bromination and cyanation) starting from purchased 9,10-dihydro-9,10-ethanoanthracene (**Scheme 3.17**). Moreover, three crystal structures were also obtained for the brominated and cyanated products (**Figure 3.37** and **3.38**).



Scheme 3.17: Synthesis of tetracyanoethanoanthracene. *Reagents and conditions:* (i) Br_2 , DCM, reflux; (ii) CuCN , DMF, reflux.

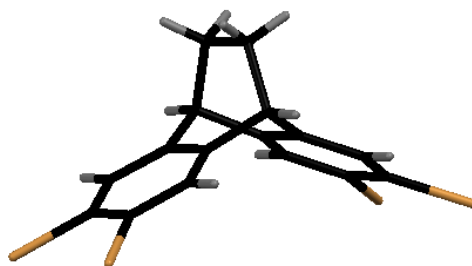
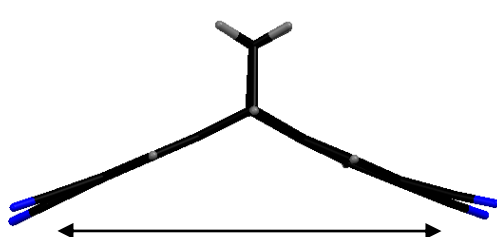
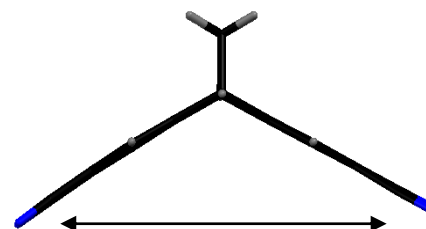


Figure 3.37: Molecular structure for tetrabromoethanoanthracene. Crystals were obtained from slow diffusion of MeOH into a CHCl_3 solution.



N-N distances: 10.89, 11.10 Å.

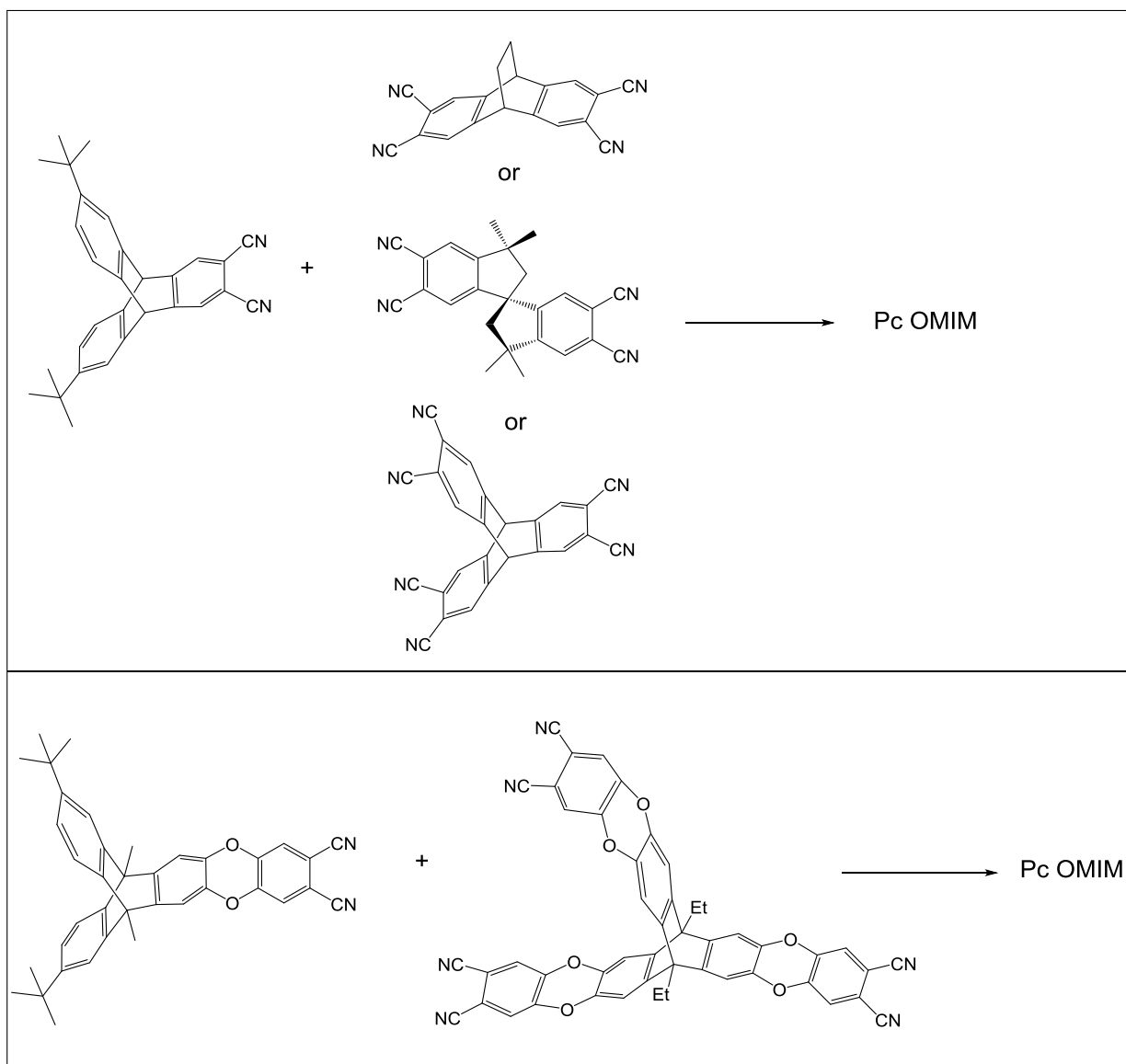


N-N distances: 10.36, 10.34 Å.

Figure 3.38: Molecular structures of two polymorphs of tetracyanoethanoanthracene. Crystals were obtained from slow evaporation of a CHCl_3 solution.

3.7.2 Reactions to make Pc-based OMIMs

Each of the synthesised cores then underwent a cyclotetramerisation reaction with an appropriate Pn (statistical mixture; **Scheme 3.18**) under the same reaction conditions used to make ZnPc molecules. In the case of hexacyanotriptycene, tetracyanospirobisindane and tetracyanoethanoanthracene, 2,3-dicyano-6,15-di-*tert*-butyltriptycene was used as the second Pn. In the case of **TrisPn triptycene**, **Pn4** was used as the second Pn taking into account the presence of dioxin functionality in both precursors.



Scheme 3.18: Synthesis of Pc OMIMs. *Reagents and conditions:* NMP, Zn(OAc)₂, 180 °C, 20 h.

Unfortunately, the yields of the desired Pc OMIMs from these reactions were very low and in some cases, MALDI-MS analysis showed no evidence of the desired molecules in the crude product or in the column fractions. Where MALDI showed evidence of traces of the desired products (see **Figure 3.39** and **3.40** for example), problems were encountered in separation and a pure product could not be isolated. The major product was always the symmetric **ZnPz1** or **ZnPc4** complex.

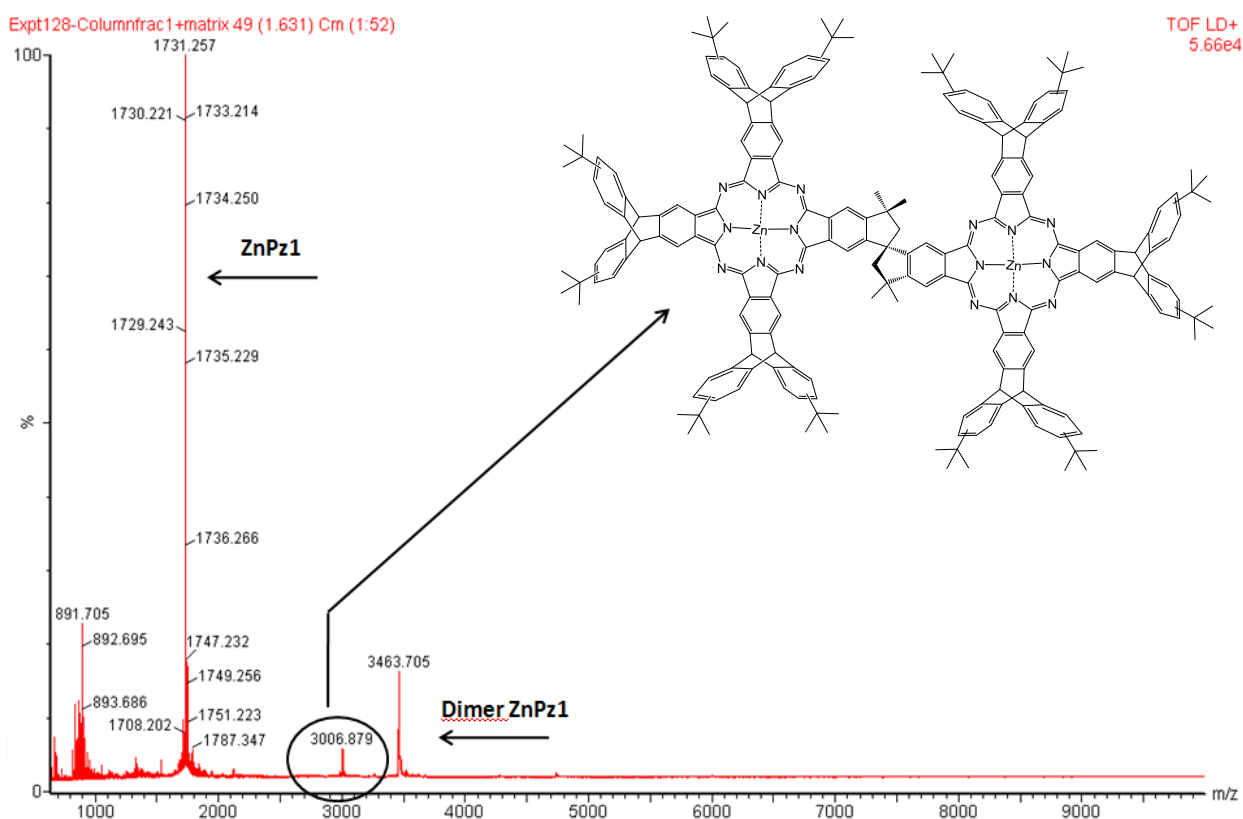


Figure 3.39: MALDI mass spectrum of one of the column fractions for the SBI based Pc OMIM.

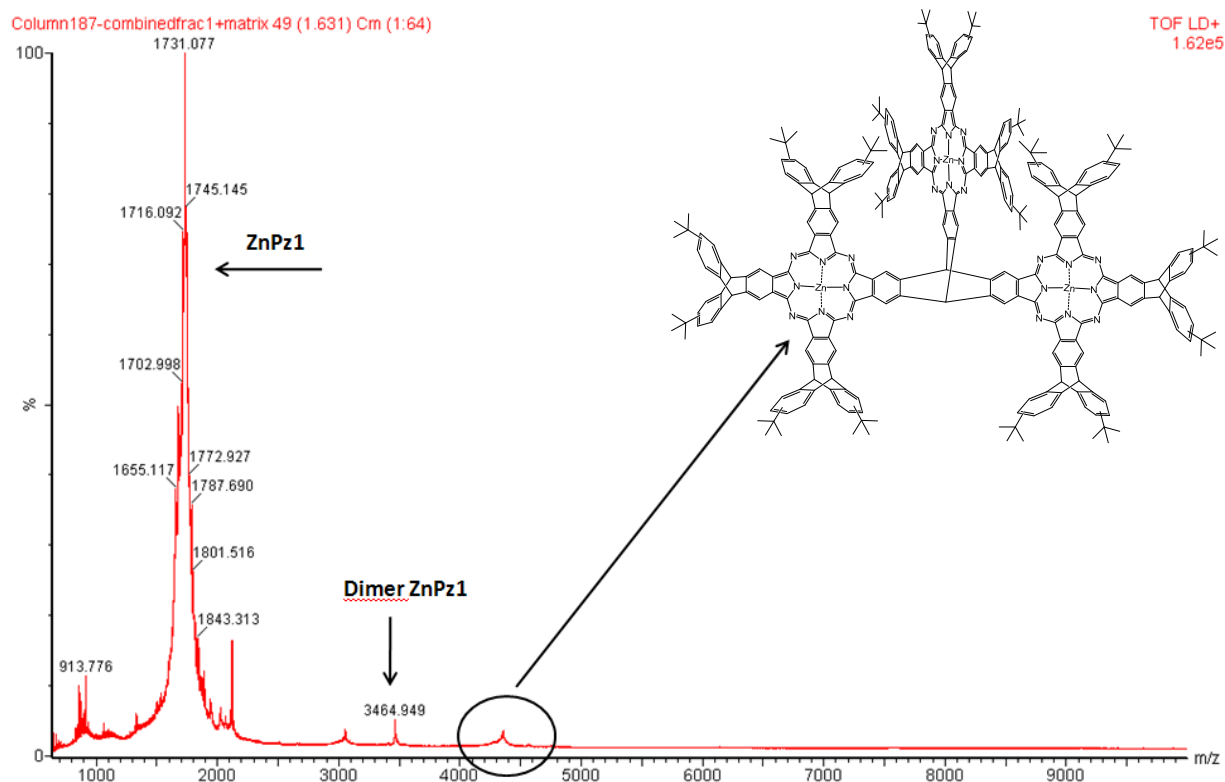


Figure 3.40: MALDI mass spectrum of one of the column fractions for the triptycene based Pc OMIM from hexacyanotriptycene. Desired product at m/z 4349.

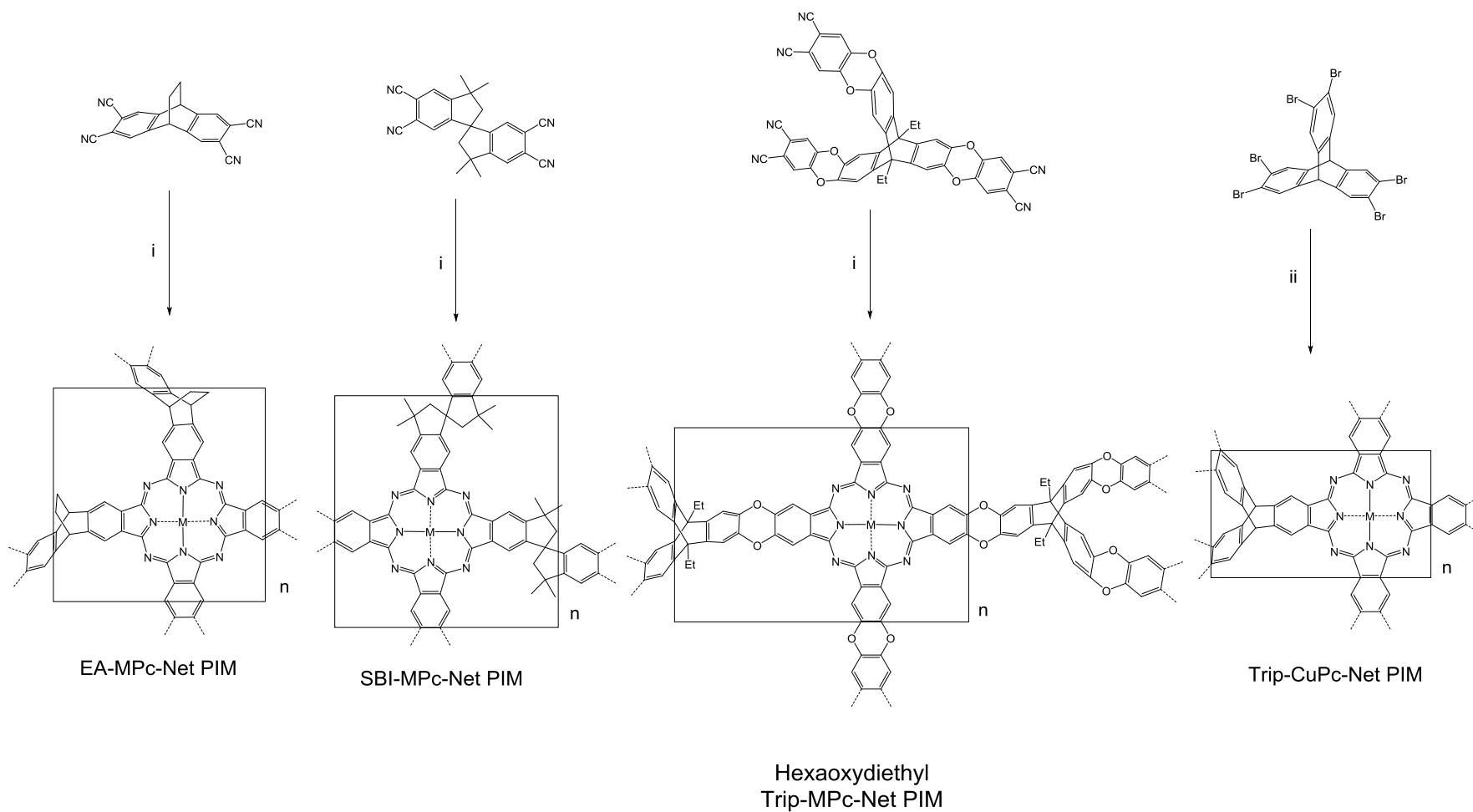
4 Pc and porphyrin containing network-PIMs

4.1 Introduction

It was noted that some of the precursors used for making OMIM-type materials could also be exploited to make the related novel Pc and Porph based network PIMs. Thus, for a comparative study and due to their potential applications in heterogeneous catalysis and gas adsorption, we decided to make these phthalocyanine-based network PIMs (MPc-Net PIMs).

4.2 Network PIMs from cyclotetramerisation reactions

MPc-Net PIMs were prepared by heating the previously prepared bis and tris Pns in the presence of an appropriate metal salt at temperature above 200 °C in quinoline (**Scheme 4.1**) with the exception of **Trip-CuPc-Net PIM** which was prepared directly from hexabromotriptycene by refluxing in DMF over several days with an excess of copper(I) cyanide. In all cases, after 3 – 4 hours, the reaction mixture became thick and sometimes became impossible to stir due to the conversion of the reaction mixture to a solid. The resulting green solids were obtained in high yields and were purified by the removal of low molecular weight impurities by immersion in a range of refluxing solvents.



Scheme 4.1: Synthesis of **MPc-NetPIMs** via cyclotetramerisation. *Reagents and conditions:* (i) An appropriate metal salt: $\text{Zn}(\text{OAc})_2$, $\text{Co}(\text{OAc})_2$ or $\text{Cu}(\text{OAc})_2$, quinoline, 210 °C, 20 h; (ii) CuCN , DMF, reflux, 72 h.

The nitrogen isotherms for **MPc-Net PIMs** from bis and tris Pns gave surface area values within the range of $88 - 585 \text{ m}^2 \text{ g}^{-1}$ (**Figure 4.1, Table 4.1**). The highest surface area was obtained for **HexaoxydiethylTrip-CuPc-Net PIM**, the isotherm of which also had a prominent hysteresis which could either be due to swelling of the polymer as it fills with nitrogen or it could be due to mesoporosity. This shape of isotherm was also observed for the remaining metal analogues of this type of polymer and also for **EA-CoPc-Net PIM** (surface area $462 \text{ m}^2 \text{ g}^{-1}$). For the remaining polymers, the obtained BET isotherms lacked hysteresis which indicates rigidity and presence of a non-swelling 3-D network structure or a lack of mesoporosity and is characteristic of a rigid framework.^[119] Surprisingly, **HexaoxydiethylTrip-ZnPc-Net PIM** had the lowest surface area, in contrast with its copper analogue bearing the highest surface area. This inconsistency could be due to the fact that cyclotetramerisation reaction to make Pc based network polymers does not always proceed successfully due to the requirements of high temperature (above $200 \text{ }^\circ\text{C}$) and concentration.

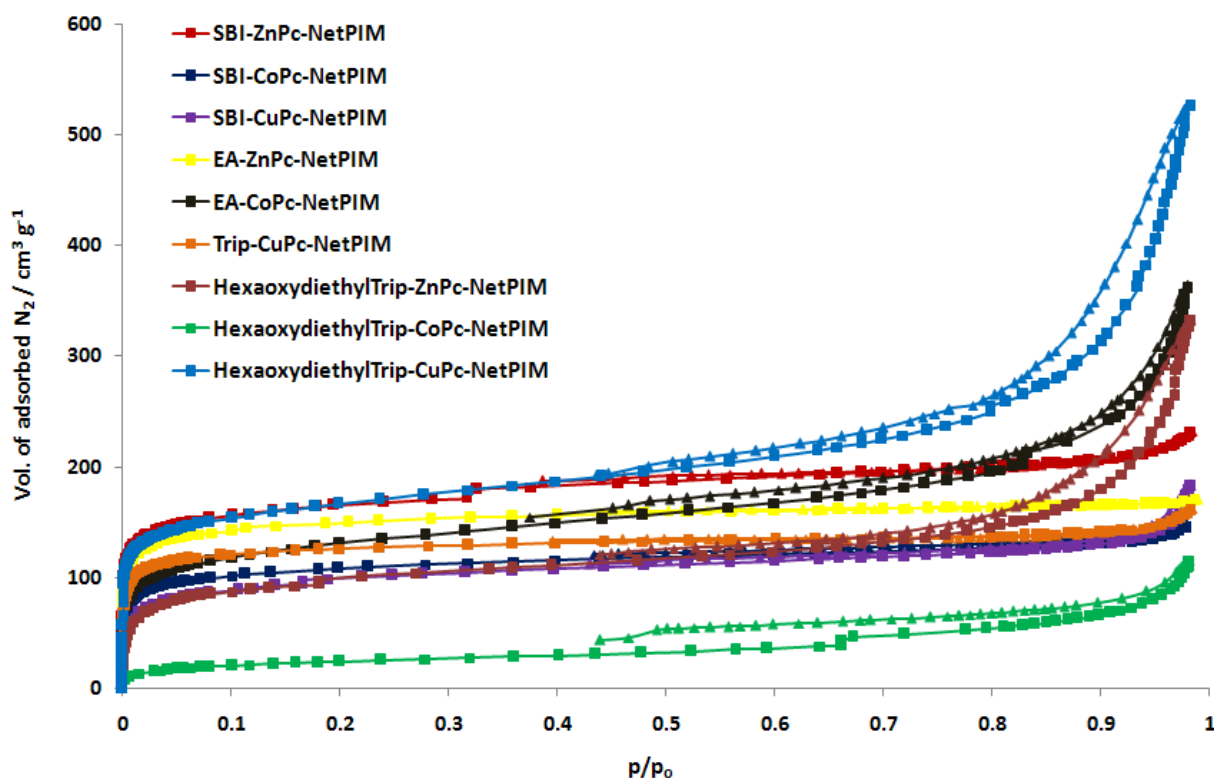


Figure 4.1: Nitrogen adsorption and desorption isotherms of various **MPc-NetPIMs** measured at 77 K.

Polymer	Metal	Surface area (m ² g ⁻¹)	Total pore volume (cm ³ g ⁻¹)
Trip-MPc-Net PIM	Cu	436	0.25
HexaoxydiethylTrip-MPc-Net PIMs	Zn	343	0.51
	Co	88	0.17
	Cu	585	0.81
SBI-MPc-Net PIMs	Zn	577	0.35
	Co	377	0.23
	Cu	352	0.28
EA-MPc-Net PIMs	Zn	511	0.26
	Co	462	0.57

Table 4.1: BET surface areas and pore volumes from nitrogen sorption data measured for various **MPc-NetPIMs**.

UV-vis absorption spectroscopic characterisation of most of the network PIMs proved difficult due to their extreme insolubility and particle scattering effects. In some cases, good UV-vis absorption spectra were obtained in DMF or 1-chloronaphthalene demonstrating the non-aggregated form of Pcs with an absence of exciton coupling (**Figure 4.2**).

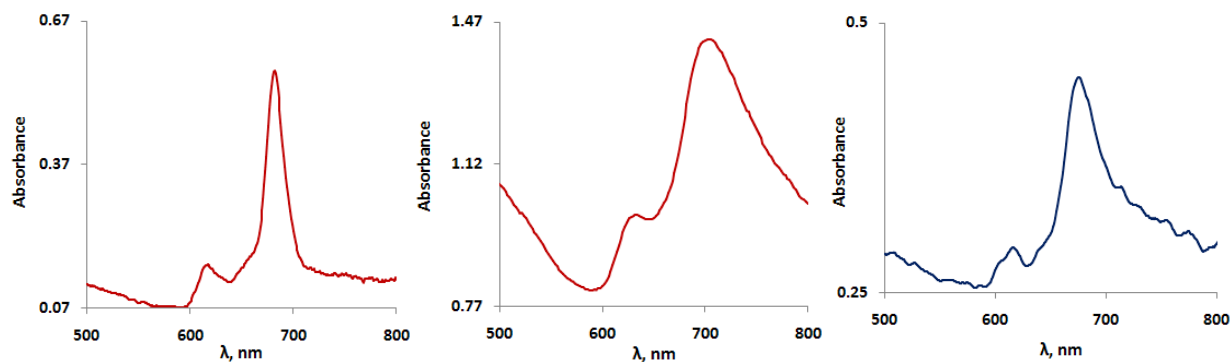


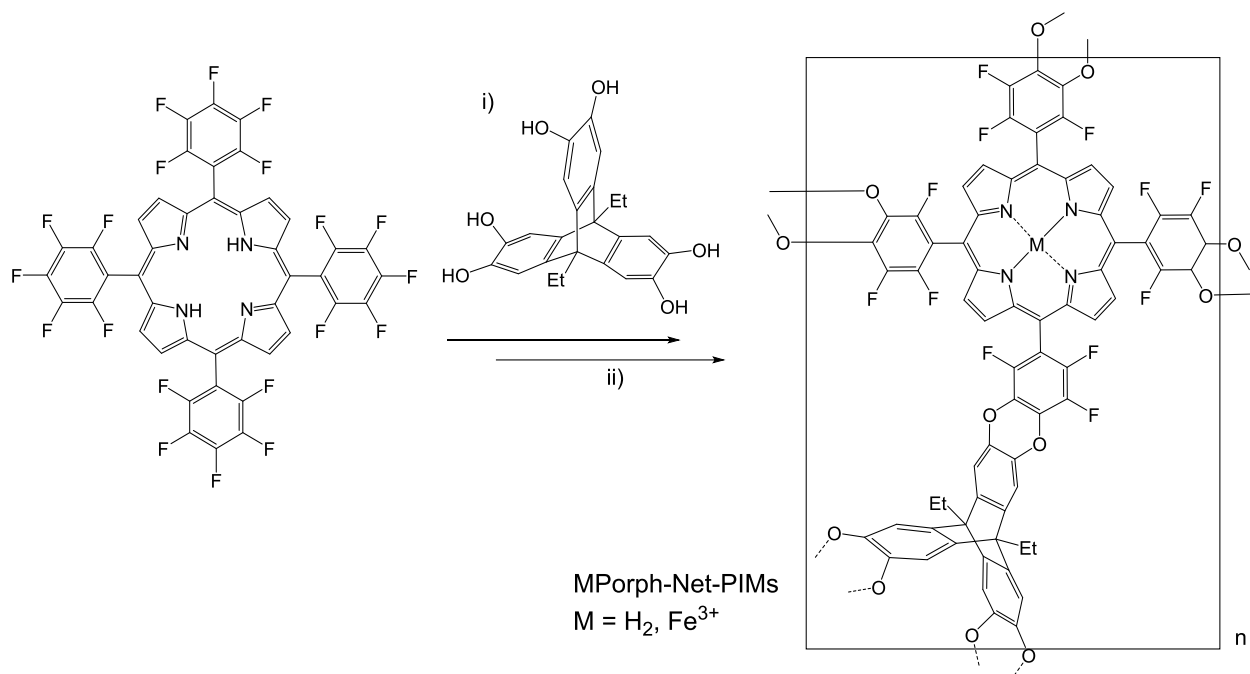
Figure 4.2: UV-vis absorption spectra of **SBI-ZnPc-Net PIM** in DMF (left), **hexaoxydiethylTrip-ZnPc-Net PIM** in 1-chloronaphthalene (centre) and **SBI-CoPc-Net PIM** in DMF (right).

4.3 Network PIMs from nucleophilic substitution reactions

4.3.1 From tetrakis(pentafluorophenyl)porphyrin

In line with the work carried out on porphyrin molecules, it was noticed that using a multiple functional triptycene such as hexahydroxydiethyltriptycene, porphyrin based Net PIM could also be prepared.

It was anticipated that using hexahydroxydiethyltriptycene as co-monomer, a porphyrin based network PIM could also be prepared directly from $\text{H}_2(\text{PhF}_5)_4\text{Porph}$. In order to prepare the network polymer, 1.33 equivalents of the freshly prepared hexahydroxydiethyltriptycene was reacted with $\text{H}_2(\text{PhF}_5)_4\text{Porph}$ at 180 °C (**Scheme 4.2**).^[96] Within minutes of the start, the reaction mixture turned solid. After quenching and washing the resulting purple solid in a range of refluxing solvents, **H₂Porph-Net-PIM** was isolated in a high yield (98 %). Due to its usefulness in catalysis,^[98] an iron analogue of this polymer was also prepared via metal insertion reaction. The % amount of fluorine found in both polymers from elemental analysis agrees well with the calculated values (within ~ 2.5 %) although carbon content was much lower possibly due to a high char yield.



Scheme 4.2: Synthesis of **MPorph-Net-PIMs**; (M = H₂, Fe). *Reagents and conditions:* i) K₂CO₃, NMP, 180 °C, 18 h; ii) **H₂Porph-Net-PIM**, NMP, anhydrous FeCl₃, 140 °C, 24 h.

Nitrogen adsorption analysis (**Figure 4.3, Table 4.2**) shows that the porphyrin based network PIMs have reproducibly high surface areas in the range of 860 – 1000 m² g⁻¹. BET analysis of tetratriptycenoporphyrin molecules showed that for some molecules, the rate of nitrogen sorption was slow which could be due to the rotation of single bonds linking the aromatic porphyrin core and the phenyl groups at the meso positions. In contrast, porphyrin PIMs adsorbed and desorbed nitrogen continuously without delay, indicating an open porous structure. This is expected due to the extensive 3-D network connectivity present in these polymers which restricts any bond rotation and thus prohibits any structural relaxation or flexibility. This is also evident from the shape of the isotherm (Type -1) with minimum hysteresis which suggests that the extensive 3-D network connectivity and component rigidity gives rise to a non swelling structure. The surface areas are also comparable with the previously prepared porphyrin polymers from H₂(PhF₅)₄Porph and 5,5',6,6'-tetrahydroxy-3,3',3'-tetramethyl-1,1'-spirobisindane ^[96] which ranged from 910 – 980 m² g⁻¹, indicating the ease with which highly rigid network polymers with large surface areas can be reproducibly prepared from H₂(PhF₅)₄Porph.

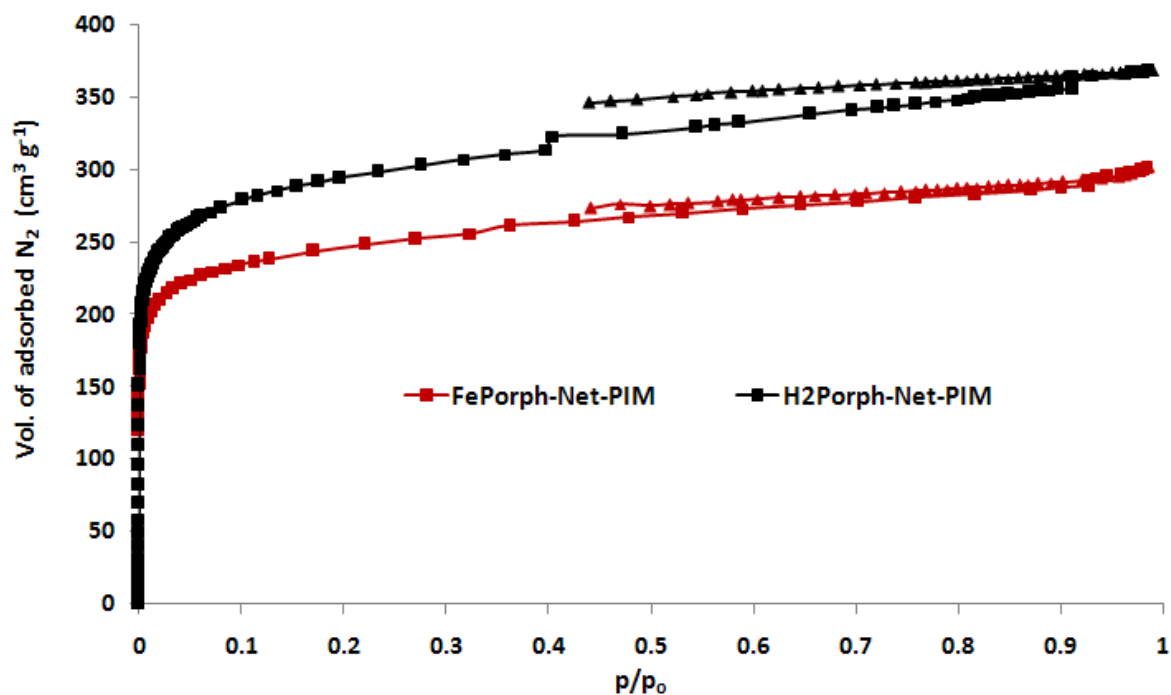


Figure 4.3: BET nitrogen adsorption and desorption isotherms of **MPorph-Net-PIMs** measured at 77 K.

Polymer	Metal	Surface area ($\text{m}^2 \text{g}^{-1}$)	Total pore volume ($\text{cm}^3 \text{g}^{-1}$)
MPorph-Net-PIM	H ₂	1028	0.57
	Fe	867	0.46

Table 4.2: BET nitrogen sorption data of **MPorph-Net-PIMs** measured at 77 K.

Luminescence spectroscopic analysis showed **H₂Porph-Net-PIM** to be weakly fluorescent (**Figure 4.4**) which could indicate that the aromatic porphyrin cores are sufficiently isolated from one another despite the 3-D network connectivity.

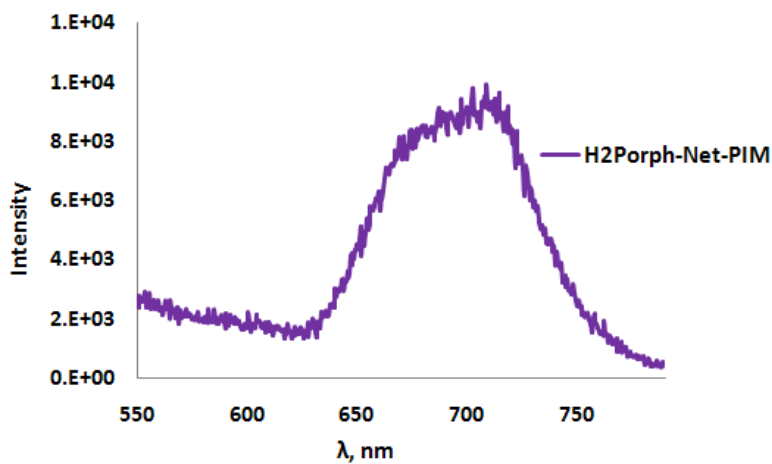


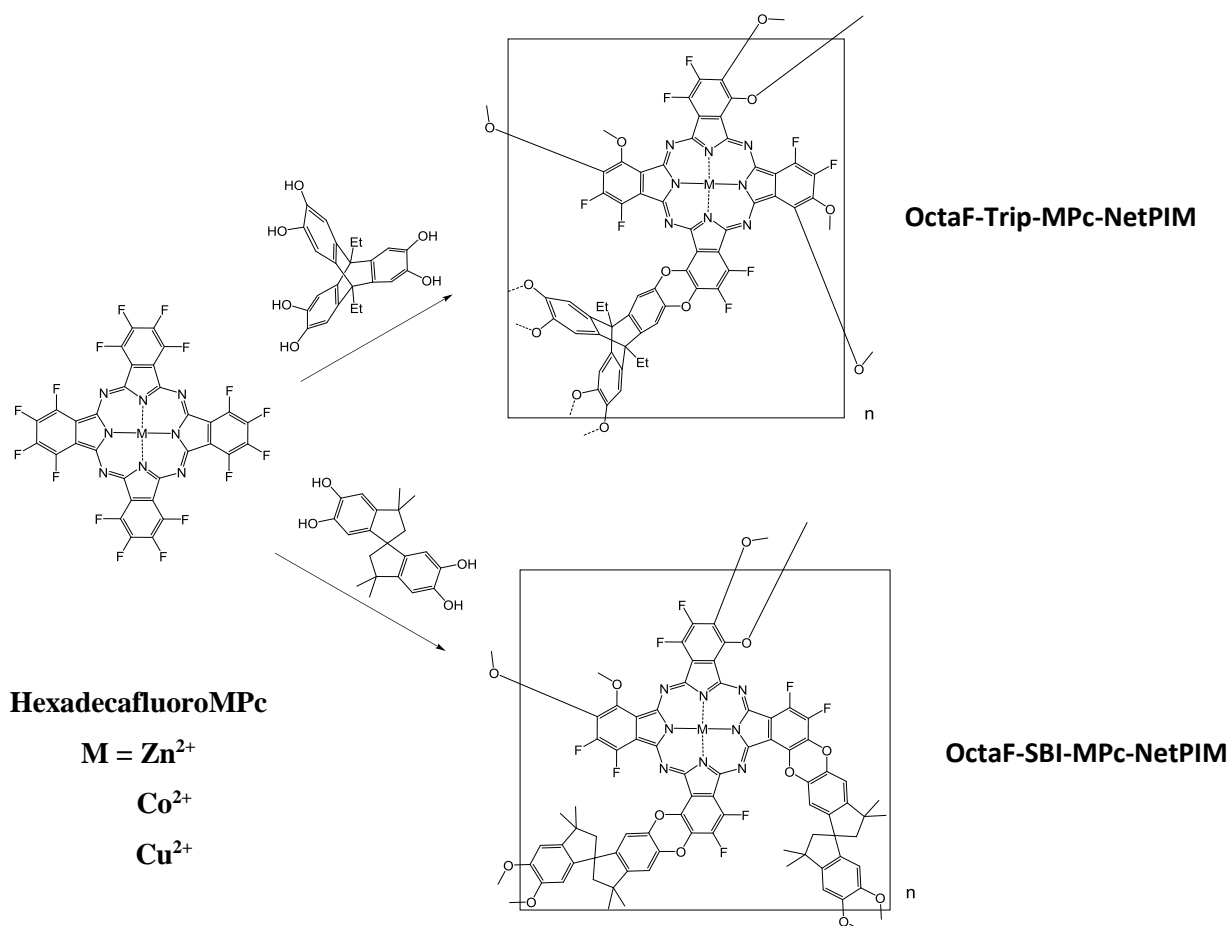
Figure 4.4: Luminescence spectrum of **H₂Porph-Net-PIM** measured as solid state. λ_{ex} : 419 nm

4.3.2 Pc polymers from hexadecafluoroMPcs

It was also of interest to investigate the related hexadecafluoroMPc precursors for the preparation of phthalocyanine-based network PIMs. There is some literature precedence for this reaction where hexadecachloroCoPc was reacted with 2 equivalents of 5,5',6,6'-tetrahydroxy-3,3,3',3'-tetramethyl-1,1'-spirobisindane to give a network polymer with BET surface area of 201 $\text{m}^2 \text{g}^{-1}$ and the resultant polymer was investigated for its catalytic usefulness. [98]

Two types of novel polymers were investigated (**Scheme 4.3**):

- 1) Reaction between hexadecafluoroMPc and 2 equivalents of 5,5',6,6'-tetrahydroxy-3,3,3',3'-tetramethyl-1,1'-spirobisindane at 180 °C to give **OctaF-SBI-MPc-NetPIMs**.
- 2) Reaction between hexadecafluoroMPc and 1.33 equivalents of 2,3,6,7,14,15-hexahydroxy-9,10-diethyltriptycene at 180 °C to give **OctaF-Trip-MPc-NetPIMs**.



Scheme 4.3: Synthesis of **OctaF-SBI & Trip-MPc-NetPIMs**. *Reagents and conditions:* K_2CO_3 , NMP, 180 °C.

The reaction conditions used were the same as the ones used to make porphyrin polymers. The fluorinated Pc polymers were purified by refluxing in a range of solvents and were obtained in high yields (91 – 98 %). Results from elemental analysis showed that in contrast to the porphyrin polymers prepared in the previous section, these fluorinated Pc polymers were deficient in fluorine as compared to the expected content (see experimental) suggesting that substitution on the Pc ring occurs to a greater extent than expected for tetrasubstitution. Nevertheless, the obtained polymers were investigated for porosity.

From the nitrogen adsorption analysis, the obtained BET surface areas for **OctaF-SBI-MPc-NetPIMs** ranged from 520 – 680 m² g⁻¹ while for **OctaF-Trip-MPc-NetPIMs**, surface areas ranged from 480 – 570 m² g⁻¹ (**Figure 4.5, Table 4.3**). In general, all isotherms contained minimal hysteresis indicating the rigidity of these network PIMs.

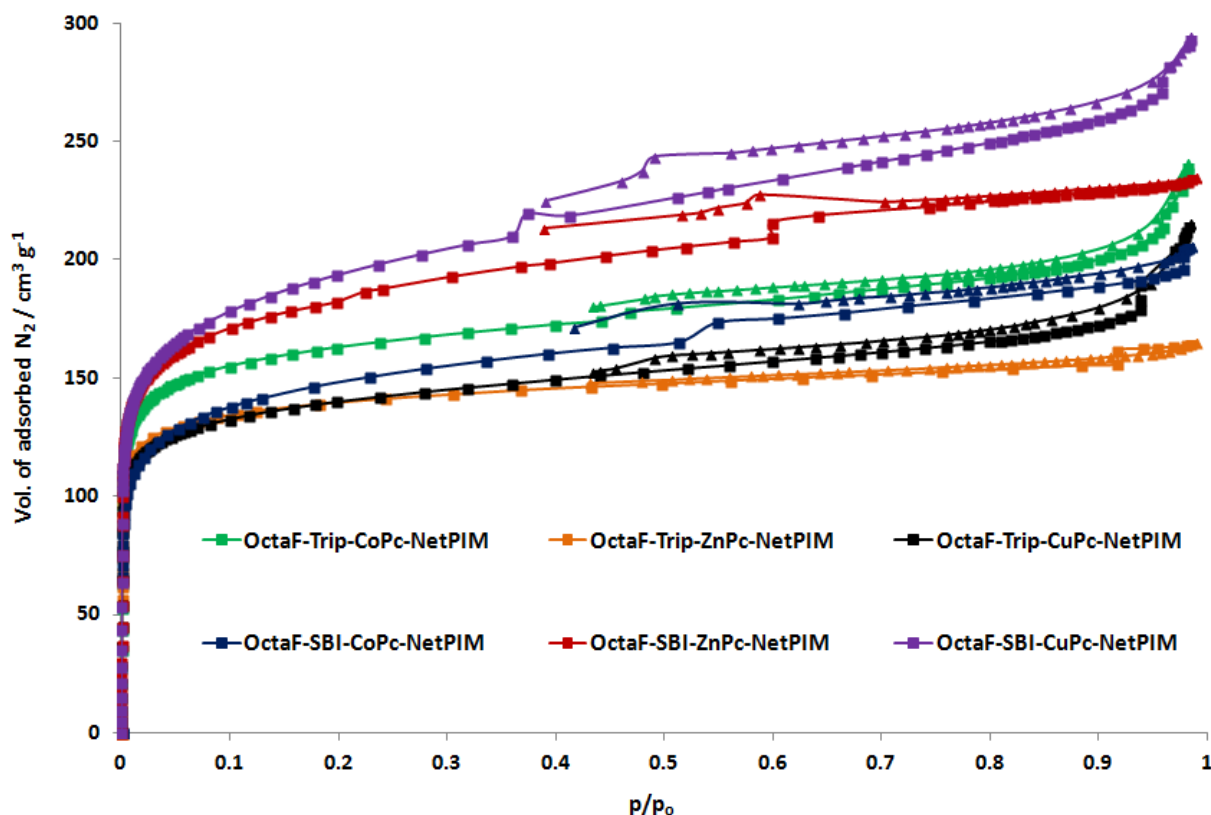


Figure 4.5: BET nitrogen adsorption and desorption isotherms of **OctaF-SBI & Trip-MPc-NetPIMs** measured at 77 K.

Polymer	Metal	Surface area (m ² g ⁻¹)	Total pore volume (cm ³ g ⁻¹)
OctaF-Trip-MPc-NetPIM	Co	565	0.37
	Zn	482	0.25
	Cu	485	0.33
OctaF-SBI-MPc-NetPIM	Co	524	0.32
	Zn	636	0.36
	Cu	680	0.45

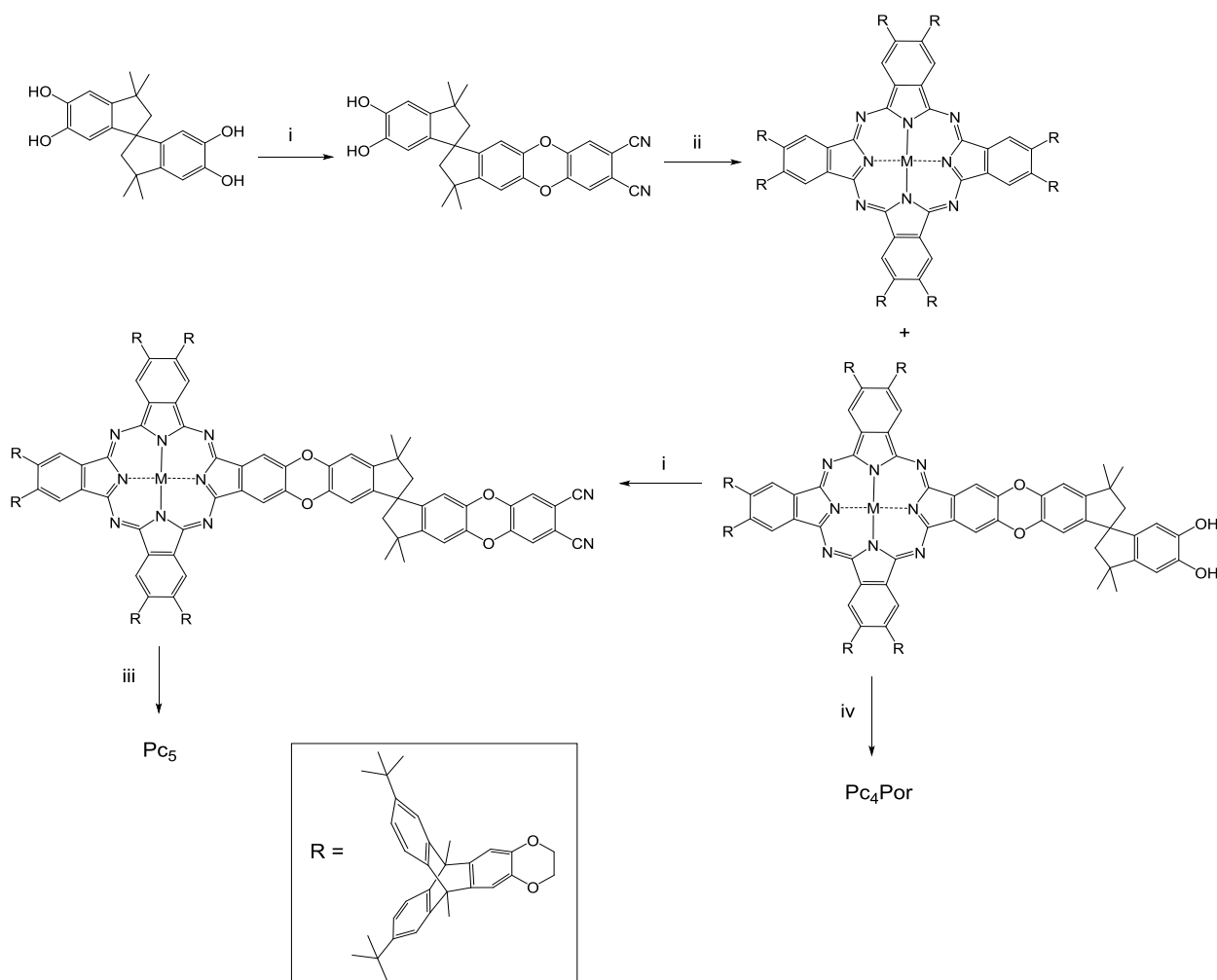
Table 4.3: BET nitrogen sorption data for **OctaF-SBI-** & **OctaF-Trip-MPc-NetPIMs**.

4.4 Conclusion

In conclusion, a good amount of discrete molecules and polymers were prepared containing Pc and porphyrin aromatic cores. Variation of structural units (i.e. SBI, ethanoanthracene and triptycenes) allowed the study of structure-function relationship by looking at their microporosity and photophysical properties. In comparison to MPc molecules, it was noticed that Pc based network PIMs from cyclotetramerisation did not give competitive BET surface areas. In contrast, bigger differences in BET sorption kinetics and surface areas were found between porphyrin based molecules and network polymers, which might suggest that substitution reaction on a preformed aromatic core works much more effectively and allows for a better comparison between molecules and polymers than cyclotetramerisation. In the latter case, requirements of high temperature for the formation of an extensive 3-D Pc containing network polymer and problems with insolubility during the reaction might be the limiting factors. In general, all molecules and polymers have competitive BET surface areas which could suggest their potential to be exploited as effective heterogeneous catalysts.

5. Future Work

One of the areas where future work is required is the synthesis of Pc and porphyrin based oligomers containing triptycene substituents (**Scheme 5.1**). Previous work in this area (cf. **Scheme 1.16**) used *tert*-butyl phenoxy groups as substituents which were good at imparting solubility and preventing aggregation as shown by UV-vis absorption spectroscopy ^[155] however, the obtained BET surface areas of the resultant oligomers were low. It is hoped that the presence of triptycene substituents with *tert*-butyl groups will improve the surface areas of the oligomers.



Scheme 5.1: Synthesis of pentamers Pc_5 and Pc_4Por . *Reagents and conditions:* (i) 4,5-Dichlorophthalonitrile, K_2CO_3 , DMF, 60 °C, 24 h; (ii) Excess 2,3-dioxin-linked 9,10-dimethyl-6,15-di-*tert*-butyltriptycene phthalonitrile, $Zn(OAc)_2$, NMP, 150 °C, 24 h; (iii) $Zn(OAc)_2$, NMP, 150 °C, 24 h; (iv) Tetrakis(pentafluorophenyl)porphyrin, K_2CO_3 , DMF, 60 °C, 24 h.

Another area of work could be the preparation of mixed-matrix membranes. Since Pc and porphyrin based network polymers cannot be cast into films, incorporation of these PIMs into solution processable polymers such as PIM-1 could enhance or modify the gas separation performance of these membranes. ^[185]

6. Experimental

6.1 General Remarks

Commercially available reagents were used without further purification. Anhydrous toluene was dried either over molecular sieves or obtained from a solvent purification system and anhydrous NMP and DMF were bought from Aldrich. TLC analysis refers to analytical thin layer chromatography, using aluminium-backed plates coated with Merck Kieselgel 60 GF₂₅₄. Column chromatography was performed on silica gel with pore size of 60 Å (particle size 40 – 63 µm) technical grade (Aldrich). Removal of solvent under vacuum refers to evaporation at reduced pressure using a rotary evaporator and diaphragm pump, followed by the removal of trace volatiles using a vacuum oven.

Melting Point

Melting points were recorded using a Gallenkamp melting point apparatus and are uncorrected.

UV-vis Spectroscopy

UV-vis absorption spectra were recorded in the range 200 – 800 nm using a Jasco V-570 UV/vis/NIR spectrophotometer.

Infra Red Spectroscopy (IR)

Infrared absorption spectra were recorded in the range 4000 - 600 cm⁻¹ using a Perkin-Elmer 660 plus FTIR instrument or Shimadzu IR Affinity-1 8400s FTIR instrument, either as a thin film between sodium chloride plates or as solid state.

Nuclear Magnetic Resonance Spectroscopy (NMR)

¹H NMR spectra were recorded in a suitable deuterated solvent using an Avance Bruker DPX 500, 400 and 250 instruments (500, 400 and 250 MHz respectively) with ¹³C NMR spectra

recorded on the same machines at 125, 100 and 62.5 MHz respectively. ^{19}F NMR spectra were recorded on a Jeol JNM-ECP 300 instrument at 282 MHz. Chemical shifts (δ_{H} or δ_{C}) were recorded in parts per million (ppm) and corrected according to the following solvent peaks for ^1H and ^{13}C NMR respectively:

7.25 and 77.18 (CDCl_3);

2.05 and 29.84, 206.3 ($(\text{CD}_3)_2\text{CO}$);

2.50 and 39.52 ($(\text{CD}_3)_2\text{SO}$);

3.31 and 49.10 (CD_3OD);

4.79 (D_2O);

2.09, 6.98, 7.00, 7.10 (C_7D_8)

7.22, 7.58, 8.74 (pyridine- d_5)

The abbreviations s, d, dd, t, q, sept, m and br. denote singlet, doublet, doubled doublet, triplet, quartet, septet, multiplet and broadened resonances; all coupling constants (J) were recorded in Hertz (Hz).

Mass Spectrometry

Low-resolution mass spectrometric data (LRMS) were determined using a Fisons VG Platform II quadrupole instrument using electron impact (EI) or electrospray ionisation (ES) unless otherwise stated. High-resolution mass spectrometric data (HRMS) were obtained in electrospray (ES) mode or electron impact (EI) mode unless otherwise reported, on a Waters Q-TOF micromass spectrometer. MALDI-TOF mass spectroscopic analysis was performed with a Waters MALDI Micro MX spectrometer.

Nitrogen adsorption analysis

Low-temperature (77 K) nitrogen adsorption/desorption isotherms were obtained using a Coulter SA3100 surface area analyser. Samples of about 0.10 g were weighed accurately (unless

otherwise stated) and degassed for about 14 – 15 h at 135 °C under high vacuum prior to analysis.

Elemental analysis

Elemental analysis was carried out by Medac Ltd.

Thermo Gravimetric Analysis (TGA)

Thermo-gravimetric analyses were carried out on a Thermal Analysis SDT Q600 system, heating samples at a rate of 10 °C/min from room temperature (RT) to 1000 °C.

Luminescence Spectroscopy

Photophysical data were obtained on a Jobin Yvon-Horiba Fluorolog spectrometer fitted with a JY TBX picoseconds photodetection module in solution. Emission spectra were uncorrected and excitation spectra were instrument corrected.

X-ray crystallography

Single crystal X-ray structures were determined at Cardiff University using a Bruker-Nonius Kappa CCD area-detector diffractometer equipped with an Oxford Cryostream low temperature cooling device operating at 150(2) K ($\lambda = 0.71073 \text{ \AA}$).

Electron Paramagnetic Resonance Spectroscopy (EPR)

The CW EPR spectra of **CuPz1** were recorded on an X-band *Bruker EMX* spectrometer operating at 100 kHz field modulation, 10 mW microwave power and fitted with a high sensitivity cavity (ER 4119HS). The *g* values were determined using a DPPH standard. Computer simulations of the EPR spectra were performed using the EasySpin programme.^[186]

6.2 Some general procedures

a) Synthesis of dimethoxytriptycenes via Diels-Alder reaction

In a typical procedure, anthracene (1 mmol) was dissolved in 1,2-dichloroethane (200 ml) at ~ 50 °C under a nitrogen atmosphere followed by the addition of 2-carboxy-4,5-dimethoxy benzenediazonium chloride (3.5 mmol) and propylene oxide (45 ml). The resulting mixture was stirred under reflux for 24 h. After cooling RT, the solvent was removed under vacuum and the crude residue was subjected to column chromatography to isolate the desired product.

b) Synthesis of dihydroxytriptycenes via demethylation

In general, to a solution of 2,3-dimethoxytriptycene (1 mmol) in DCM (7 ml) at 0 °C under a nitrogen atmosphere, BBr₃ (2 mmol) was added. The reaction mixture was stirred for 2 h at RT and monitored by TLCs. Upon completion, the reaction was quenched with water and the product extracted with ether. The organic extracts were combined, dried over MgSO₄ and solvent removed under vacuum.

c) Synthesis of phthalonitrile (Pn) precursors from substitution with dichlorophthalonitrile

2,3-Dihydroxytriptycene (1 mmol) and 4,5-dichlorophthalonitrile (1 mmol) were stirred in anhydrous DMF (25 ml) at 77 °C under a nitrogen atmosphere. To this solution, anhydrous potassium carbonate (6 mmol) was added and the reaction mixture stirred usually for 18 hours. The reaction was then cooled to RT, poured into water and filtered to dryness.

d) Synthesis of dibromotriptycenes via Diels-Alder reaction

To a stirred mixture of anthracene (1 mmol) and 1,2,4,5-tetrabromobenzene (1.36 mmol) in anhydrous toluene (250 ml) under a nitrogen atmosphere, was added *n*-BuLi (1.57 mmol) in anhydrous toluene (50 ml) dropwise at RT. The reaction mixture was stirred for 20 h after which, the solvent was removed under vacuum. Water (200 ml) was then added to the residue and the organics extracted with DCM (3 x 100 ml). The organic layer was then washed with 1M NaOH (200 ml) before the removal of solvent under vacuum to give the crude product which was purified via column chromatography.

e) Synthesis of phthalonitrile (Pn) precursors from cyanation (Rosenmund von Braun reaction)

In general, to a solution of bromine containing starting material in anhydrous DMF under a nitrogen atmosphere at 61 °C, about five equivalents of copper cyanide were added for each bromide group present in the starting material. The reaction was then stirred at reflux and monitored by TLCs. Upon completion, the reaction was cooled to RT, poured into conc. ammonia, stirred for about half an hour and then filtered. The crude mixture was purified by column chromatography to isolate the desired product.

f) Synthesis of metal phthalocyanine molecules from cyclotetramerisation

A mixture of an appropriate Pn (1 mmol) and metal salt (1 mmol) were stirred in anhydrous NMP at 180 °C for 24 hours under a nitrogen atmosphere. The reaction mixture was then cooled to RT, poured into distilled water (~ 200 ml) and filtered. The crude product was purified by column chromatography.

g) Synthesis of metalloporphyrins via metal insertion

Free base porphyrin (1 mmol) and an appropriate metal salt (20 mmol) were stirred in anhydrous NMP (3 ml) at 140 °C for 18 hrs. Upon cooling to RT, the mixture was poured into distilled water, stirred and filtered.

h) Synthesis of unsymmetric phthalocyanines (3:1 isomers) with methoxy substituents

A mixture of 4,5-dimethoxyphthalonitrile (1 mmol) and a second appropriate Pn (7 mmol) and metal salt (7 mmol) were stirred in anhydrous NMP at 180 °C for 24 hours under a nitrogen atmosphere. The reaction mixture was then cooled to RT, poured into distilled water (~ 200 ml) and filtered. The desired product was isolated from the crude mixture by column chromatography.

i) Synthesis of metal phthalocyanine network polymers via cyclotetramerisation

A mixture of an appropriate bis or tris Pn (1 mmol) and metal salt (1 mmol) were stirred in quinoline at 210 °C for 24 hours under a nitrogen atmosphere. The reaction mixture was then

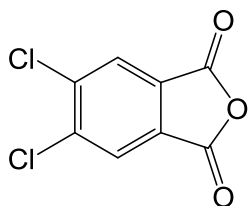
cooled to RT, poured into a 1:1 mixture of methanol and distilled water (~ 200 ml), filtered and dried.

j) Synthesis of fluorinated metal phthalocyanine network polymers

Pre-formed metal (II)1,2,3,4,8,9,10,11,15,16,17,18,22,23,24,25-hexadecafluoro-29*H*,31*H* phthalocyanine (1 mmol) and either 2,3,6,7,14,15-hexahydroxy-9,10-diethyltriptycene (1.33 mmol) or 5,5',6,6'-tetrahydroxy-3,3',3'-tetramethyl-1,1'-spirobisindane (2 mmol) were stirred in anhydrous NMP (3.5 ml) with anhydrous potassium carbonate under a nitrogen atmosphere at 180 °C for ~ 20 hours. The reaction mixture was then cooled to RT, poured into distilled water and filtered.

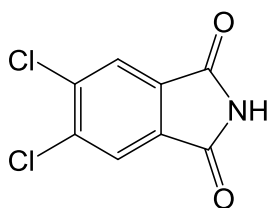
6.3 Synthesis of precursors

4,5-Dichlorophthalic anhydride ^[163]

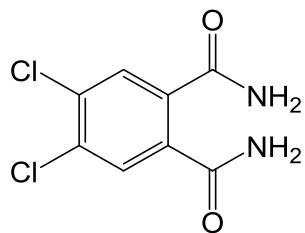


4,5-Dichlorophthalic acid (90 g, 380 mmol) and acetic anhydride (150 ml) were stirred under weak reflux for 5 h with slow distilling off of solvent. After cooling, the solid was filtered, washed with petroleum ether and dried under vacuum to give **4,5-dichlorophthalic anhydride** as a white solid (80 g, 96 %). Mp 185 – 187 °C, (lit. mp ^[163] 184 – 186 °C); IR (film): ν , cm^{-1} 1835, 1789, 1600, 1383, 1310, 1247, 1094, 915, 733; ¹H NMR (400 MHz; CDCl_3): δ_{H} , ppm 8.15 (s, 2H, ArH); ¹³C NMR (100 MHz; CDCl_3): δ_{C} , ppm 161.1, 142.1, 130.7, 127.9; LRMS (EI) found m/z 216.98 ($[\text{M}]^+$, 100 %).

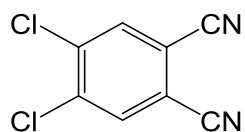
4,5-Dichlorophthalimide ^[163]



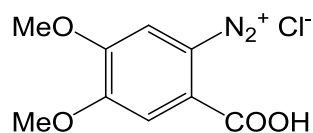
4,5-Dichlorophthalic anhydride (79 g, 360 mmol) was stirred at reflux in formamide (110 ml) for 3 hours. After cooling, the precipitate formed was filtered, washed with water and dried under vacuum to give **4,5-dichlorophthalimide** as a yellow crystalline solid (77 g, 98 %). Mp 217 – 218 °C, (lit. mp ^[163] 193 – 195 °C); IR (film): ν , cm^{-1} 3425, 1777, 1716, 1643, 1384, 1055, 906, 737; ¹H NMR (400 MHz; CDCl_3): δ_{H} , ppm 7.98 (s, 2H, ArH); ¹³C NMR (62.5 MHz; CDCl_3): δ_{C} , ppm 167.0, 137.1, 132.5, 125.7; LRMS (EI) found m/z 214.96 ($[\text{M}]^+$, 85 %).

4,5-Dichlorobenzene-1,2-diamide ^[163]

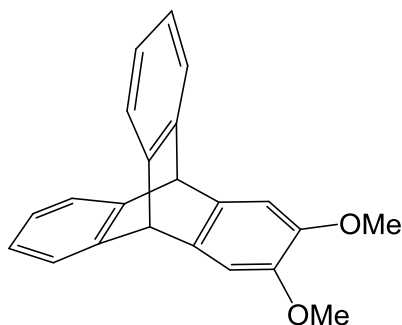
4,5-Dichlorophthalimide (76 g, 350 mmol) was stirred for 24 h in 25 % NH₄OH (900 ml); 33 % NH₄OH (300 ml) was added and stirring was continued for another 24 h. The precipitate was filtered, washed with water and dried under vacuum to give **4,5-dichlorobenzene-1,2-diamide** as a white solid (61 g, 74 %). Mp 225 – 227 °C, (lit. mp ^[163] 245 – 247 °C); IR (film): ν , cm⁻¹ 3423, 3296, 3126, 1653, 1606, 1407, 1120, 915, 897; ¹H NMR (400 MHz; DMSO-d₆): δ _H, ppm 7.92 (s, 2H, NH₂), 7.71 (s, 2H, ArH), 7.52 (s, 2H, NH₂); ¹³C NMR (100 MHz; DMSO-d₆): δ _C, ppm 168.1, 137.0, 132.0, 130.0; LRMS (ES) found m/z 231.96 ([M]⁻, 100 %).

4,5-Dichlorophthalonitrile ^[163]

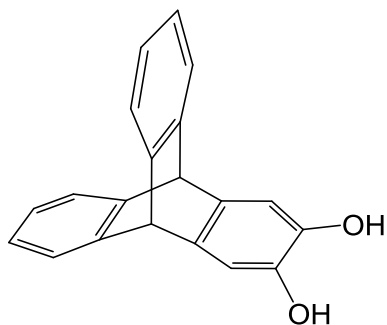
At 0 °C, SOCl₂ (200 ml) was added under stirring and under nitrogen to anhydrous DMF (300 ml). After 2 hours, 4,5-dichlorobenzene-1,2-diamide (40 g, 170 mmol) was added and the mixture was stirred at 0 – 5 °C for 5 h and then at RT for 24 h. The mixture was slowly added to ice water to quench the excess SOCl₂, the precipitate was filtered, washed with water and recrystallized twice from methanol to give **4,5-dichlorophthalonitrile** (20 g, 59 %). Mp 183 – 184 °C, (lit. mp ^[163] 182 – 184 °C); IR (film): ν , cm⁻¹ 3015, 2239, 1467, 1347, 1142, 913, 681; ¹H NMR (400 MHz; CDCl₃): δ _H, ppm 7.94 (s, 2H, ArH); ¹³C NMR (62.5 MHz; CDCl₃): δ _C, ppm 136.9, 132.8, 112.9, 111.4; LRMS (EI) found m/z 195.95 ([M]⁺, 90 %).

2-Carboxy-4,5-dimethoxy benzenediazonium chloride ^[101]

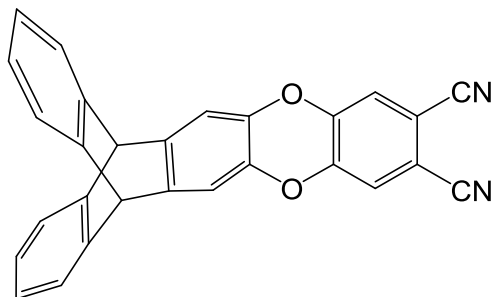
Concentrated hydrochloric acid (8 ml) then isoamyl nitrite (16 ml, 119 mmol) were added to a suspension of 4,5-dimethoxy anthranilic acid (14 g, 71 mmol) in ethanol (150 ml) at 0 °C. The mixture was stirred for 30 mins at RT before ether (250 ml) was added, stirred further for 15 mins, filtered, washed with ether and dried to give **2-carboxy-4,5-dimethoxy benzenediazonium chloride** as a beige solid (16.5 g, 95 %). ¹H NMR (400 MHz; D₂O): δ_H, ppm 8.0 (s, 1H, ArH), 7.72 (s, 1H, ArH), 3.99 (s, 3H, OCH₃), 3.88 (s, 3H, OCH₃); ¹³C NMR (125 MHz; D₂O): δ_C, ppm 163.9, 159.3, 152.0, 132.6, 115.1, 114.5, 102.8, 57.8, 57.4.

2,3-Dimethoxytryptene ^[164]

Anthracene (3.5 g, 20 mmol), 1,2-dichloroethane (250 ml) 2-carboxy-4,5-dimethoxy benzenediazonium chloride (17.2 g, 70 mmol) and propylene oxide (45 ml) were reacted according to the general procedure (a). Purification by column chromatography on silica (DCM:hexane, 6:4) gave a yellow oil which was triturated in methanol to give **2,3-dimethoxytryptene** as a white solid (1.88 g, 30 %). Mp 180 – 182 °C, (lit. mp ^[164] 181 – 183 °C); IR (film): ν, cm⁻¹ 3065, 2956, 2830, 1614, 1601, 1501, 1294, 1222, 1082, 1022, 987, 842, 739; ¹H NMR (400 MHz; CDCl₃): δ_H, ppm 7.41 (dd, 4H, ³J_{HH} = 5.2 Hz, ⁴J_{HH} = 3.3 Hz, ArH), 7.06 (s, 2H, ArH), 7.02 (dd, 4H, ³J_{HH} = 5.2 Hz, ⁴J_{HH} = 3.3 Hz, ArH), 5.38 (s, 2H, CH), 3.87 (s, 6H, OCH₃); ¹³C NMR (62.5 MHz; CDCl₃): δ_C, ppm 146.0, 145.7, 138.0, 125.1, 123.4, 108.6, 56.2, 53.8; LRMS (APCI) found *m/z* 315.14 ([MH]⁺, 100 %).

2,3-Dihydroxytriptycene ^[102]

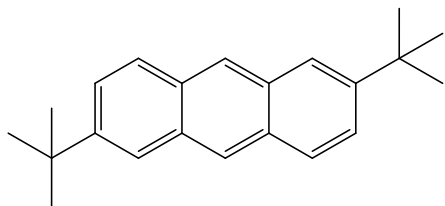
BBr_3 (1.1 ml, 11 mmol) was reacted with 2,3-dimethoxytriptycene (1.6 g, 5 mmol) in DCM (25 ml) according to the general procedure (b). The obtained solid was dissolved in a small amount of ether and reprecipitated from hexane to give **2,3-dihydroxytriptycene** as a white powder (1.25 g, 86 %). Mp decomposed over 70 °C; ^[102] IR (film): ν , cm^{-1} 3390, 2959, 1622, 1500, 1457, 1307, 1154, 1060, 740, 627; ¹H NMR (400 MHz; CDCl_3): δ_{H} , ppm 7.37 (m, 4H, ArH), 7.0 (m, 4H, ArH), 6.96 (s, 2H, ArH), 5.01 (s, 2H, CH); ¹³C NMR (62.5 MHz; CDCl_3): δ_{C} , ppm 145.5, 140.1, 138.4, 125.1, 123.4, 112.0, 53.4; LRMS (ES) found m/z 285.13 ($[\text{M}]^-$, 100 %).

2,3-Dioxin-phthalonitrile-triptycene

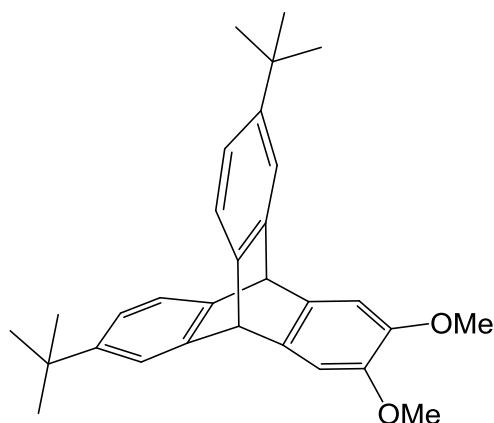
2,3-Dihydroxytriptycene (1.25 g, 4.4 mmol) and 4,5-dichlorophthalonitrile (0.86 g, 4.4 mmol) were reacted in anhydrous DMF (15 ml) at 77 °C under a nitrogen atmosphere with anhydrous potassium carbonate (3.6 g, 26 mmol) according to the general procedure (c). The crude product was recrystallised from methanol to give **2,3-dioxin-phthalonitrile triptycene** as a light green solid (1.42 g, 79 %). Mp > 300 °C; IR (film): ν , cm^{-1} 3080, 2960, 2236, 1635, 1566, 1466, 1342, 1316, 1171, 889, 738; ¹H NMR (400 MHz; CDCl_3): δ_{H} , ppm 7.40 (dd, 4H, ³ $J_{\text{HH}} = 5.3$ Hz, ⁴ $J_{\text{HH}} = 3.2$ Hz, ArH), 7.12 (s, 2H, ArH), 7.05 (dd, 4H, ³ $J_{\text{HH}} = 5.3$ Hz, ⁴ $J_{\text{HH}} = 3.2$ Hz, ArH), 6.95 (s, 2H,

ArH), 5.37 (s, 2H, *CH*); ^{13}C NMR (62.5 MHz; CDCl_3): δ_{C} , ppm 146.1, 144.3, 143.0, 137.0, 125.6, 123.7, 121.2, 114.7, 112.8, 111.5, 53.2; HRMS (EI) found m/z 410.1060 $[\text{M}]^+$, calculated 410.1055 for $\text{C}_{28}\text{H}_{14}\text{N}_2\text{O}_2$; Crystallography data (THF): Monoclinic, $P2_1/c$, $a = 19.884(5)$ Å, $b = 8.044(5)$ Å, $c = 30.274(5)$ Å, $\beta = 96.255(5)$, $V = 4813(3)$ Å³, $Z = 4$, $R_I = 8.23$.

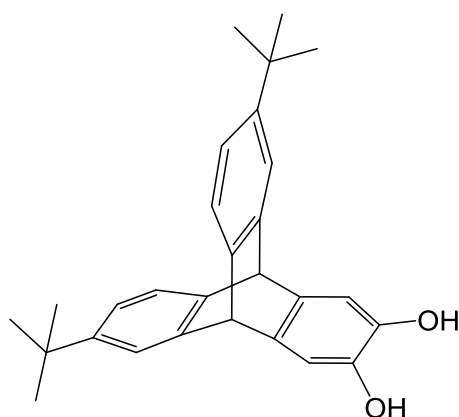
2,6-Di-*tert*-butylanthracene ^[165]



tert-Butanol (10.8 g, 146 mmol) was added to a stirring suspension of anthracene (7.13 g, 40 mmol) and trifluoroacetic acid (40 ml) and the resulting mixture was heated at reflux for 24 h. Upon cooling to RT, the reaction mixture was quenched with ice cold water and filtered. The obtained precipitate was dissolved in DCM, washed with water and brine, dried over MgSO_4 and solvent evaporated. The off white/yellow solid was recrystallised from methanol to give **2,6-di-*tert*-butylanthracene** as a white solid (3.50 g, 30 %). Mp 248 – 250 °C, (lit. mp ^[187] 250.2 °C); IR (film): ν , cm^{-1} 3025, 2973, 2952, 2866, 1660, 1641, 1459, 1365, 898, 742, 612; ^1H NMR (400 MHz; CDCl_3): δ_{H} , ppm 8.22 (s, 2H, *ArH*), 7.83 (d, 2H, $^3J_{\text{HH}} = 8.9$ Hz, *ArH*), 7.76 (d, 2H, $^4J_{\text{HH}} = 1.8$ Hz, *ArH*), 7.44 (dd, 2H, $^3J_{\text{HH}} = 8.9$ Hz, $^4J_{\text{HH}} = 1.8$ Hz, *ArH*), 1.35 (s, 18H, $\text{C}(\text{CH}_3)_3$); ^{13}C NMR (62.5 MHz; CDCl_3): δ_{C} , ppm 147.0, 131.5, 130.5, 127.7, 125.4, 124.8, 122.3, 34.9, 31.0; LRMS (EI) found m/z 290.2 ($[\text{M}]^+$, 70 %).

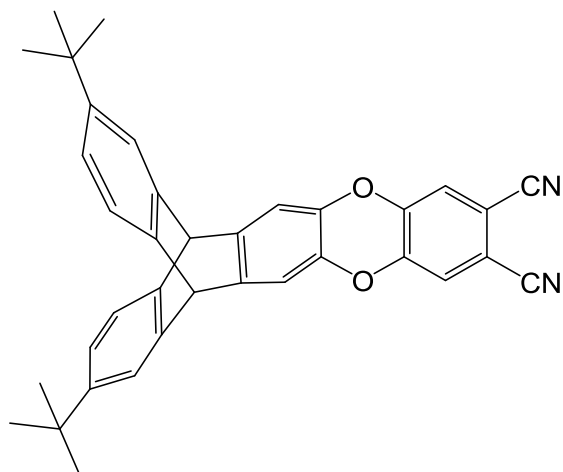
2,3-Dimethoxy-6,15-di-*tert*-butyltritycene ^[146]

2,6-Di-*tert*-butylantracene (3.5 g, 12 mmol), 1,2-dichloroethane (250 ml), 2-carboxy-4,5-dimethoxy benzenediazonium chloride (10.3 g, 42 mmol) and propylene oxide (45 ml) were reacted according to general procedure (a). Purification by column chromatography on silica (DCM:hexane, 1:1) gave a yellow oil which was triturated in methanol to give **2,3-dimethoxy-6,15-di-*tert*-butyltritycene** as a white solid (0.8 g, 15 %). Mp 257 – 259 °C, (lit. mp ^[146] 257 – 259 °C); IR (film): ν , cm^{-1} 2959, 2905, 2867, 2830, 1644, 1481, 1291, 1222, 1088, 751; ¹H NMR (400 MHz; CDCl₃): δ_{H} , ppm 7.42 (d, 2H, ⁴ J_{HH} = 1.9 Hz, ArH), 7.30 (d, 2H, ³ J_{HH} = 7.7 Hz, ArH), 7.03 (s, 2H, ArH), 7.01 (dd, ³ J_{HH} = 7.7 Hz, ⁴ J_{HH} = 1.9 Hz, ArH), 5.30 (s, 2H, CH), 3.86 (s, 6H, OCH₃), 1.28 (s, 18H, C(CH₃)₃); ¹³C NMR (62.5 MHz; CDCl₃): δ_{C} , ppm 147.9, 145.9, 145.7, 142.9, 138.6, 122.7, 121.5, 120.7, 108.6, 56.2, 53.7, 34.6, 31.6; HRMS (EI) found m/z 426.2558 [M]⁺, calculated 426.2559 for C₃₀H₃₄O₂.

2,3-Dihydroxy-6,15-di-*tert*-butyltritycene ^[146]

BBr_3 (0.4 ml, 4 mmol) was reacted with 2,3-dimethoxy-6,15-di-*tert*-butyltritycene (0.78 g, 1.8 mmol) in DCM (18 ml) according to the general procedure (b) to give **2,3-dihydroxy-6,15-di-*tert*-butyltritycene** as an off-white solid (0.6 g, 82 %). Mp > 300 °C, (lit. mp ^[146] > 300 °C); IR (film): ν , cm^{-1} 3408, 2961, 2904, 2868, 1691, 1613, 1502, 1481, 1306, 1262, 1182, 1062, 843; ^1H NMR (400 MHz; CDCl_3): δ_{H} , ppm 7.30 (d, 2H, $^4J_{\text{HH}} = 1.8$ Hz, ArH), 7.18 (m, 2H, ArH), 6.90 (dd, 2H, $^3J_{\text{HH}} = 7.7$ Hz, $^4J_{\text{HH}} = 1.8$ Hz, ArH), 6.85 (s, 2H, ArH), 5.15 (s, 2H, CH), 1.17 (s, 18H, $\text{C}(\text{CH}_3)_3$); ^{13}C NMR (62.5 MHz; CDCl_3): δ_{C} , ppm 149.7, 148.0, 145.5, 142.7, 139.9, 122.7, 121.6, 120.7, 111.9, 53.3, 34.6, 31.6; HRMS (EI) found m/z 398.2257 $[\text{M}]^+$, calculated 398.2246 for $\text{C}_{28}\text{H}_{30}\text{O}_2$.

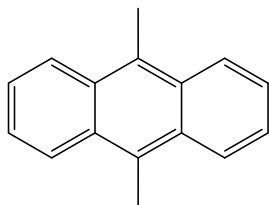
2,3-Dioxin-phthalonitrile-6,15-di-*tert*-butyltritycene



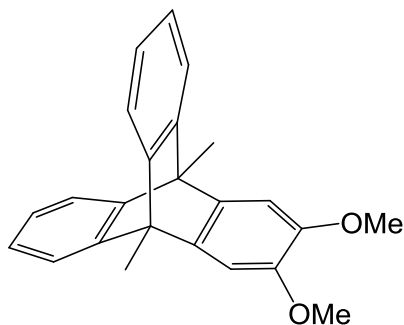
2,3-Dihydroxy-6,15-di-*tert*-butyltritycene (0.5 g, 1.3 mmol) and 4,5-dichlorophthalonitrile (0.25 g, 1.3 mmol) were reacted in anhydrous DMF (8 ml) at 77 °C under a nitrogen atmosphere with anhydrous potassium carbonate (1.1 g, 8 mmol) according to the general procedure (c). The crude product was purified by reprecipitation of a DCM solution with methanol to give **2,3-dioxin-phthalonitrile-6,15-di-*tert*-butyltritycene** as an off-white solid (0.53 g, 80 %). Mp > 300 °C; IR (film): ν , cm^{-1} 3079; 2962, 2869, 2236, 1635, 1566, 1503, 1472, 1340, 1265, 1038, 898, 795; ^1H NMR (400 MHz; CDCl_3): δ_{H} , ppm 7.32 (d, 2H, $^4J_{\text{HH}} = 1.8$ Hz, ArH), 7.22 (d, 2H, $^3J_{\text{HH}} = 7.7$ Hz, ArH), 7.01 (s, 2H, ArH), 6.95 (dd, 2H, $^3J_{\text{HH}} = 7.7$ Hz, $^4J_{\text{HH}} = 1.8$ Hz, ArH), 6.83 (s, 2H, ArH), 5.20 (s, 2H, CH), 1.18 (s, 18H, $\text{C}(\text{CH}_3)_3$); ^{13}C NMR (100 MHz; CDCl_3): δ_{C} , ppm

149.0, 146.6, 144.7, 143.9, 141.9, 137.3, 123.5, 122.5, 121.6, 121.4, 115.1, 113.1, 111.8, 53.5, 35.0, 31.9; HRMS (EI) found m/z 522.2302 $[M]^+$, calculated 522.2307 for $C_{36}H_{30}N_2O_2$.

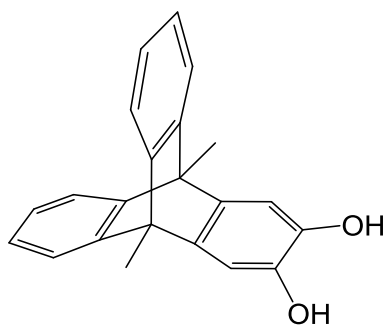
9,10-Dimethylantracene ^[167]



9,10-Dichloroanthracene (7.5 g, 30.4 mmol) and PEPSI-IPr catalyst (1.34 g, 2 mmol) were stirred in 1,4-dioxane (500 ml) at RT for an hour under a nitrogen atmosphere. Then, methylmagnesium bromide (3 M solution in diethyl ether, 60.7 ml, 182 mmol) was added dropwise and the resultant mixture was stirred for 24 h. The reaction was quenched by pouring into a mixture of water (500 ml) and ethyl acetate (200 ml) and stirred for 30 mins. Ethyl acetate layer was then separated and the aqueous layer extracted two more times with ethyl acetate (2 x 200 ml). The organic extracts were combined, washed with sodium chloride solution and filtered. The solvent was removed under vacuum and the crude product was stirred in acetone (100 ml) and filtered to give **9,10-dimethylantracene** as a green/yellow solid (5.70 g, 91 %). Mp 180 – 182 °C, (lit. mp ^[167] 181 – 183 °C); IR (film): ν , cm^{-1} 3081, 3031, 2925, 2863, 1696, 1618, 1443, 1025, 751, 743; ¹H NMR (250 MHz; CDCl₃): δ_H , ppm 8.39 (dd, 4H, ³ J_{HH} = 6.9 Hz, ⁴ J_{HH} = 3.3 Hz, ArH), 7.57 (dd, 4H, ³ J_{HH} = 6.9 Hz, ⁴ J_{HH} = 3.3 Hz, ArH), 3.15 (s, 6H, OCH₃); ¹³C NMR (62.5 MHz; CDCl₃): δ_C , ppm 129.9, 128.4, 125.4, 124.7, 14.1; LRMS (EI) found m/z 206.09 ($[M]^+$, 50 %).

2,3-Dimethoxy-9,10-dimethyltriptycene

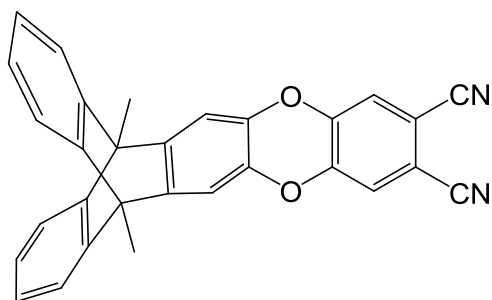
9,10-Dimethylantracene (3.3 g, 16 mmol), 1,2-dichloroethane (250 ml), 2-carboxy-4,5-dimethoxy benzenediazonium chloride (13.7 g, 56 mmol) and propylene oxide (45 ml) were reacted according to the general procedure (a). Purification by column chromatography on silica (DCM:hexane, 1:1) gave a yellow oil which was reprecipitated with methanol to give **2,3-dimethoxy-9,10-dimethyltriptycene** as a white solid (4.4 g, 80 %). Mp 190 – 192 °C; IR (film): ν , cm^{-1} 3063, 2969, 2947, 2925, 2825, 1597, 1506, 1461, 1288, 1200, 1041, 835, 742; ^1H NMR (250 MHz; CDCl_3): δ_{H} , ppm 7.39 (dd, 4H, $^3J_{\text{HH}} = 5.2$ Hz, $^4J_{\text{HH}} = 3.2$ Hz, ArH), 7.07 (dd, 4H, $^3J_{\text{HH}} = 5.2$ Hz, $^4J_{\text{HH}} = 3.2$ Hz, ArH), 7.01 (s, 2H, ArH), 3.89 (s, 6H, OCH_3), 2.46 (s, 6H, CH_3); ^{13}C NMR (62.5 MHz; CDCl_3): δ_{C} , ppm 148.7, 145.9, 141.3, 124.7, 120.2, 106.2, 56.4, 48.3, 13.7; HRMS (EI) found m/z 342.1618 $[\text{M}]^+$, calculated 342.1620 for $\text{C}_{24}\text{H}_{22}\text{O}_2$.

2,3-Dihydroxy-9,10-dimethyltriptycene

BBr_3 (2.42 ml, 25.2 mmol) was reacted with 2,3-dimethoxy-9,10-dimethyltriptycene (4.3 g, 12.6 mmol) in DCM (25 ml) according to the general procedure (b). The obtained solid was dissolved in a small amount of ether and reprecipitated from hexane to give **2,3-dihydroxy-9,10-dimethyltriptycene** as a white powder (3.8 g, 96 %). Mp decomposed over 70 °C; IR (film): ν ,

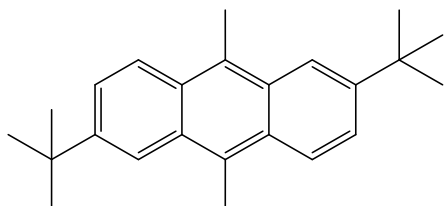
cm⁻¹ 3382, 3064, 2971, 2880, 1697, 1612, 1506, 1447, 1365, 1304, 1156, 838, 744; ¹H NMR (250 MHz; CDCl₃): δ_H, ppm 7.35 (dd, 4H, ³J_{HH} = 5.5 Hz, ⁴J_{HH} = 3.2 Hz, ArH), 7.05 (dd, 4H, ³J_{HH} = 5.5 Hz, ⁴J_{HH} = 3.2 Hz, ArH), 6.91 (s, 2H, ArH), 2.36 (s, 6H, CH₃); ¹³C NMR (62.5 MHz; CDCl₃): δ_C, ppm 148.4, 141.7, 139.8, 124.7, 120.2, 109.4, 48.0, 13.7; HRMS (EI) found *m/z* 314.1301 [M]⁺, calculated 314.1307 for C₂₂H₁₈O₂.

2,3-Dioxin-phthalonitrile-9,10-dimethyltritycene



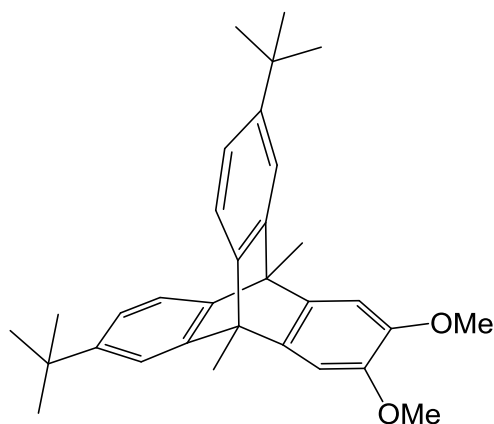
2,3-Dihydroxy-9,10-dimethyltritycene (3.75 g, 12 mmol) and 4,5-dichlorophthalonitrile (2.35 g, 12 mmol) were reacted in anhydrous DMF (40 ml) at 77 °C under a nitrogen atmosphere with anhydrous potassium carbonate (10 g, 72 mmol) according to the general procedure (c). The crude product was purified by reprecipitation of a DCM solution with methanol to give **2,3-dioxin-phthalonitrile-9,10-dimethyltritycene** as an off-white solid (4.7 g, 90 %). Mp > 300 °C; IR (film): ν, cm⁻¹ 3045, 2978, 2238, 1564, 1503, 1449, 1337, 1318, 900, 881, 742; ¹H NMR (400 MHz; CDCl₃): δ_H, ppm 7.37 (dd, 4H, ³J_{HH} = 5.5 Hz, ⁴J_{HH} = 3.2 Hz, ArH), 7.11 (s, 2H, ArH), 7.09 (dd, 4H, ³J_{HH} = 5.5 Hz, ⁴J_{HH} = 3.2 Hz, ArH), 6.90 (s, 2H, ArH), 2.38 (s, 6H, OCH₃); ¹³C NMR (62.5 MHz; CDCl₃): δ_C, ppm 147.3, 146.3, 146.2, 136.9, 125.2, 121.2, 120.5, 114.7, 111.5, 110.2, 48.2, 13.5; HRMS (EI) found *m/z* 438.1362 [M]⁺, calculated 438.1368 for C₃₀H₁₈N₂O₂.

2,6-Di-*tert*-butyl-9,10-dimethylantracene ^[165]



tert-Butanol (9.9 g, 134 mmol) was added to a stirring suspension of 9,10-dimethylantracene (6.89 g, 33.4 mmol) and trifluoroacetic acid (50 ml) and the resulting mixture was heated at reflux for 20 h. Upon cooling to RT, the reaction mixture was quenched with ice cold water and extracted with DCM (3 x 150 ml). The DCM layer was washed with water and brine, dried over MgSO₄ and solvent evaporated. The addition of acetone to the residual oil resulted in precipitation of the product which was collected by filtration, stirred again in a minimum amount of more acetone and then filtered to give **2,6-di-*tert*-butyl-9,10-dimethylantracene** as an off-white solid (3.90 g, 37 %). Mp 246 – 247 °C, (lit. mp ^[165] 245 – 247 °C); IR (film): ν , cm⁻¹ 3070, 2956, 2930, 2869, 1631, 1457, 1378, 1265, 875, 805, 738; ¹H NMR (250 MHz; CDCl₃): δ _H, ppm 8.31 (d, 2H, ³J_{HH} = 9.3 Hz, ArH), 8.22 (d, 2H, ⁴J_{HH} = 1.9 Hz, ArH), 7.64 (dd, 2H, ³J_{HH} = 9.3 Hz, ⁴J_{HH} = 1.9 Hz, ArH), 3.12 (s, 6H, CH₃), 1.52 (s, 18H, C(CH₃)₃); ¹³C NMR (62.5 MHz; CDCl₃): δ _C, ppm 146.3, 129.5, 128.6, 127.5, 125.1, 124.0, 119.4, 35.1, 31.1, 14.0; LRMS (APCI) found *m/z* 319.24 ([MH]⁺, 100 %).

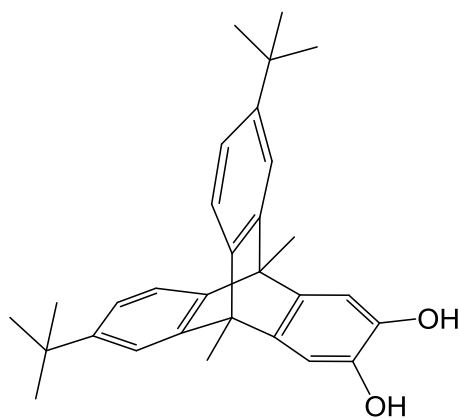
2,3-Dimethoxy-9,10-dimethyl-6,15-di-*tert*-butyltriptycene



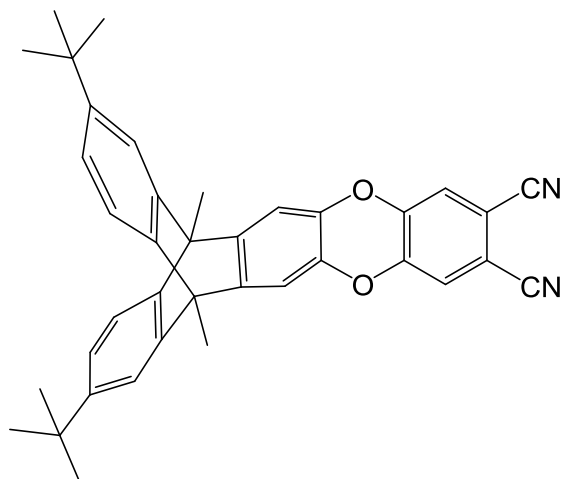
2,6-Di-*tert*-butyl-9,10-dimethylantracene (3.5 g, 11 mmol), 1,2-dichloroethane (250 ml) 2-carboxy-4,5-dimethoxy benzenediazonium chloride (9.4 g, 38.5 mmol) and propylene oxide (45 ml) were reacted according to the general procedure (a). The crude residue was purified by column chromatography on silica (DCM:hexane, 1:1) to obtain a yellow oil which was triturated with methanol to give **2,3-dimethoxy-9,10-dimethyl-6,15-di-*tert*-butyltriptycene** as a white solid (3.56 g, 71 %). Mp 233 – 235 °C; IR (film): ν , cm⁻¹ 3100, 2964, 2905, 2865, 1601, 1507, 1481, 1361, 1291, 1200, 1044, 735; ¹H NMR (250 MHz; CDCl₃): δ _H, ppm 7.39 (d, 2H, ⁴J_{HH} =

1.8 Hz, *ArH*), 7.29 (d, 2H, $^3J_{\text{HH}} = 7.9$ Hz, *ArH*), 7.06 (dd, 2H, $^3J_{\text{HH}} = 7.9$ Hz, $^4J_{\text{HH}} = 1.8$ Hz, *ArH*), 6.99 (s, 2H, *ArH*), 3.88 (s, 6H, OCH_3), 2.44 (s, 6H, CH_3), 1.30 (s, 18H, $\text{C}(\text{CH}_3)_3$); ^{13}C NMR (62.5 MHz; CDCl_3): δ_{C} , ppm 148.4, 147.4, 145.9, 145.8, 141.7, 121.1, 119.6, 117.5, 106.1, 56.4, 48.1, 34.6, 31.6, 13.7; HRMS (EI) found m/z 454.2880 $[\text{M}]^+$, calculated 454.2872 for $\text{C}_{32}\text{H}_{38}\text{O}_2$; Crystallography data ($\text{CHCl}_3/\text{methanol}$): Monoclinic, $C2/c$, $a = 11.2766(2)$ Å, $b = 18.5541(6)$ Å, $c = 25.0651(6)$ Å, $\beta = 100.732(2)$, $V = 5152.6(2)$ Å³, $Z = 8$, $R_1 = 6.31$.

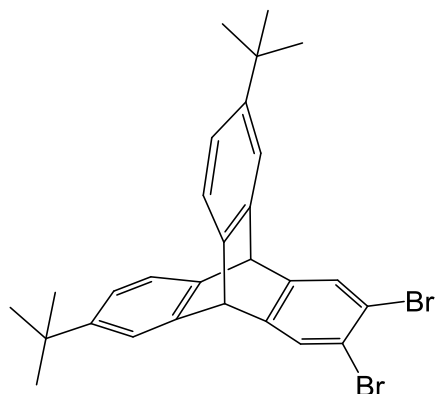
2,3-Dihydroxy-9,10-dimethyl-6,15-di-*tert*-butyltriptycene



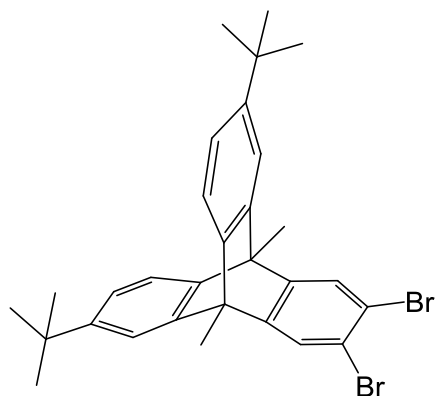
BBr_3 (1.44 ml, 15 mmol) was reacted with 2,3-dimethoxy-9,10-dimethyl-6,15-di-*tert*-butyltriptycene (3.4 g, 7.5 mmol) in DCM (25 ml) according to the general procedure (b) to give **2,3-dihydroxy-9,10-dimethyl-6,15-di-*tert*-butyltriptycene** as an off-white powder (3.0 g, 94 %). Mp > 300 °C; IR (film): ν , cm^{-1} 3390, 3068, 2965, 2903, 2868, 1616, 1480, 1456, 1362, 1303, 1245, 989, 841, 736; ^1H NMR (250 MHz; Acetone- d_6): δ_{H} , ppm 7.53 (s, 2H, *OH*), 7.43 (d, 2H, $^4J_{\text{HH}} = 1.9$ Hz, *ArH*), 7.26 (d, 2H, $^3J_{\text{HH}} = 7.9$ Hz, *ArH*), 7.03 (dd, 2H, $^3J_{\text{HH}} = 7.9$ Hz, $^4J_{\text{HH}} = 1.9$ Hz, *ArH*), 6.91 (s, 2H, *ArH*), 2.35 (s, 6H, CH_3), 1.27 (s, 18H, $\text{C}(\text{CH}_3)_3$); ^{13}C NMR (62.5 MHz; Acetone- d_6): δ_{C} , ppm 148.2, 147.4, 145.7, 142.0, 139.8, 121.1, 119.6, 117.5, 109.2, 47.8, 34.6, 31.6, 13.7; HRMS (EI) found m/z 425.2485 $[\text{M}]^+$, calculated 425.2481 for $\text{C}_{30}\text{H}_{33}\text{O}_2$.

2,3-Dioxin-phthalonitrile-9,10-dimethyl-6,15-di-*tert*-butyltritycene

2,3-Dihydroxy-9,10-dimethyl-6,15-di-*tert*-butyltritycene (2.09 g, 4.9 mmol) and 4,5-dichlorophthalonitrile (0.97 g, 4.9 mmol) were reacted in anhydrous DMF (25 ml) at 77 °C under a nitrogen atmosphere with anhydrous potassium carbonate (5.8 g, 42 mmol) according to the general procedure (c). The crude product was purified by reprecipitation of its DCM solution with methanol to give **2,3-dioxin-phthalonitrile-9,10-dimethyl-6,15-di-*tert*-butyltritycene** as a light green solid (2.30 g, 85 %). Mp > 300 °C; IR (film): ν , cm^{-1} 3053, 2965, 2905, 2871, 2237, 1634, 1566, 1501, 1456, 1339, 1313, 1271, 1174, 885, 737; ^1H NMR (400 MHz; CDCl_3): δ_{H} , ppm 7.38 (d, 2H, $^4J_{\text{HH}} = 1.4$ Hz, ArH), 7.28 (d, 2H, $^3J_{\text{HH}} = 7.8$ Hz, ArH), 7.09 (m, 4H, ArH), 6.89 (s, 2H, ArH), 2.38 (s, 6H, CH_3), 1.29 (s, 18H, $\text{C}(\text{CH}_3)_3$); ^{13}C NMR (62.5 MHz; CDCl_3): δ_{C} , ppm 148.1, 147.1, 146.8, 146.3, 144.5, 136.8, 121.6, 121.2, 120.0, 117.7, 114.7, 111.5, 110.0, 48.1, 34.7, 31.5, 13.5; HRMS (EI) found m/z 568.2939 $[\text{M}+\text{NH}_4]^+$, calculated 568.2964 for $\text{C}_{38}\text{H}_{34}\text{N}_2\text{O}_2\cdot\text{NH}_4$; Crystallography data ($\text{CHCl}_3/\text{MeOH}$): Monoclinic, $P2_1/c$, $a = 18.9292(4)$ Å, $b = 14.6433(2)$ Å, $c = 11.1365(2)$ Å, $\beta = 101.540(2)$, $V = 3024.48(9)$ Å³, $Z = 4$, $R_1 = 4.96$.

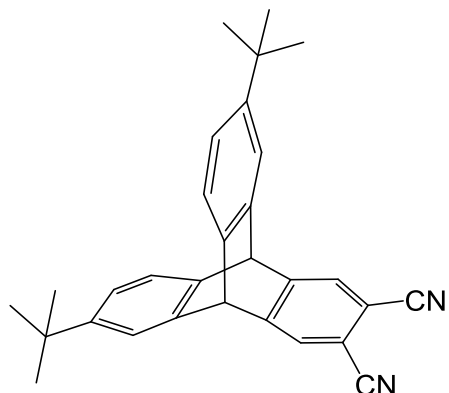
2,3-Dibromo-6,15-di-*tert*-butyltritycene ^[156]

2,6-Di-*tert*-butylanthracene (3.7 g, 12.7 mmol) and 1,2,4,5-tetrabromobenzene (6.8 g, 17.3 mmol) were reacted with *n*-BuLi (2.5 M in hexane, 8 ml, 20 mmol) in anhydrous toluene (250 according to the general procedure (d). Purification via column chromatography on silica eluting with hexane:DCM (9:1) gave **2,3-dibromo-6,15-di-*tert*-butyltritycene** as a white solid (2.20 g, 33 %). Mp 263 – 265 °C, (lit. mp ^[156] 286 °C); IR (film): ν , cm^{-1} 2962, 2899, 2868, 1641, 1481, 1445, 1363, 1263, 1098, 891, 738, 648; ¹H NMR (400 MHz; CDCl₃): δ_{H} , ppm 7.42 (2H, s, ArH), 7.22 (2H, d, ⁴ J_{HH} = 1.8 Hz, ArH), 7.11 (2H, d, ³ J_{HH} = 7.8 Hz, ArH), 6.84 (2H, dd, ³ J_{HH} = 7.8 Hz, ⁴ J_{HH} = 1.8 Hz, ArH), 5.12 (2H, s, CH), 1.07 (18H, s, C(CH₃)₃); ¹³C NMR (62.5 MHz; CDCl₃): δ_{C} , ppm 148.7, 146.9, 144.1, 141.3, 128.5, 123.3, 122.2, 121.2, 120.4, 53.1, 34.6, 31.5; HRMS (EI) found m/z 522.0565 [M]⁺, calculated 522.0558 for C₂₈H₂₈⁷⁹Br₂; Crystallography data (CHCl₃/MeOH): Monoclinic, $P2_1/c$, $a = 18.6134(10)$ Å, $b = 11.1479(5)$ Å, $c = 12.0010(5)$ Å, $\beta = 98.439(5)$, $V = 2463.2(2)$ Å³, $Z = 4$, $R_1 = 5.30$.

2,3-Dibromo-6,15-di-*tert*-butyl-9,10-dimethyltritycene

2,6-Di-*tert*-butyl-9,10-dimethylantracene (3.4 g, 10.7 mmol) and 1,2,4,5-tetrabromobenzene (5.7 g, 14.6 mmol) were reacted with *n*-BuLi (2.5 M in hexane, 6.8 ml, 17 mmol) in anhydrous toluene (250 ml) according to the general procedure (d). Purification by column chromatography on silica eluting with hexane:DCM (9:1) gave **2,3-dibromo-6,15-di-*tert*-butyl-9,10-dimethyltritycene** as a white solid (1.65 g, 28 %). Mp 260 – 263 °C; IR (film): ν , cm^{-1} 3078, 2965, 2903, 2867, 1636, 1554, 1413, 1264, 1113, 890, 738; ^1H NMR (400 MHz; CDCl_3): δ_{H} , ppm 7.44 (2H, s, ArH), 7.28 (2H, d, $^4J_{\text{HH}} = 1.8$ Hz, ArH), 7.18 (2H, d, $^3J_{\text{HH}} = 7.9$ Hz, ArH), 6.99 (2H, dd, $^3J_{\text{HH}} = 7.9$ Hz, $^4J_{\text{HH}} = 1.8$ Hz, ArH), 2.29 (6H, s, CH_3), 1.18 (18H, s, $\text{C}(\text{CH}_3)_3$); ^{13}C NMR (125 MHz; CDCl_3): δ_{C} , ppm 150.1, 148.2, 146.9, 144.4, 125.8, 121.7, 120.4, 120.2, 117.9, 48.1, 34.7, 31.5, 13.4; HRMS (EI) found m/z 550.0861 $[\text{M}]^+$, calculated 550.0871 for $\text{C}_{30}\text{H}_{32}^{79}\text{Br}_2$; Crystallography data ($\text{CHCl}_3/\text{MeOH}$): Monoclinic, $P2_1/c$, $a = 14.5821(3)$ Å, $b = 20.1342(3)$ Å, $c = 10.3225(2)$ Å, $\beta = 100.426(2)$, $V = 2980.64(10)$ Å³, $Z = 4$, $R_1 = 4.94$.

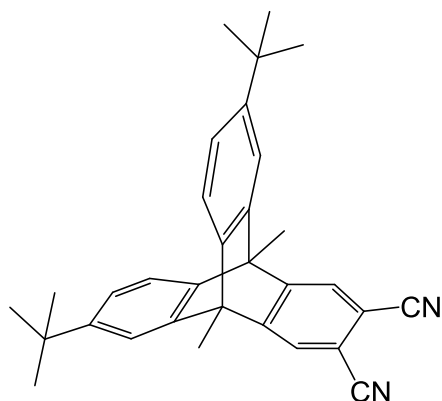
2,3-Dicyano-6,15-di-*tert*-butyltritycene



2,3-Dibromo-6,15-di-*tert*-butyltritycene (9 g, 17.2 mmol) and copper cyanide (15.4 g, 172 mmol) were stirred at reflux in anhydrous DMF (150 ml) under a nitrogen atmosphere according to the general procedure (e). The crude product was extracted by washing the obtained solid with DCM and was purified via column chromatography on silica eluting with DCM:hexane (1:1) to give **2,3-dicyano-6,15-di-*tert*-butyltritycene** as a pale blue solid (3.5 g, 49 %). Mp > 300 °C; IR (film): ν , cm^{-1} 2964, 2904, 2868, 2234, 1618, 1559, 1471, 1364, 1327, 1265, 1166, 1084, 845; ^1H NMR (250 MHz; CDCl_3): δ_{H} , ppm 7.76 (2H, s, ArH), 7.50 (2H, s, ArH), 7.40 (2H, d, $^3J_{\text{HH}} = 7.8$ Hz, ArH), 7.13 (2H, d, $^3J_{\text{HH}} = 7.8$ Hz, ArH), 5.54 (2H, s, CH), 1.30 (18H, s, $\text{C}(\text{CH}_3)_3$); ^{13}C NMR (62.5 MHz; CDCl_3): δ_{C} , ppm 151.9, 149.6, 142.7, 139.9, 127.9, 123.8, 122.9, 121.6, 115.8,

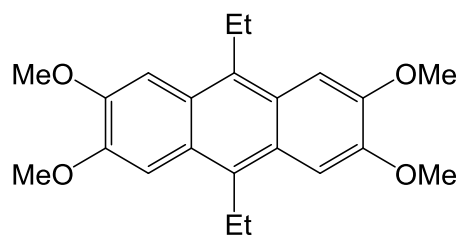
112.8, 53.6, 34.7, 31.5; HRMS (EI) found m/z 416.2254 $[M]^+$, calculated 416.2252 for $C_{30}H_{28}N_2$; Crystallography data ($CHCl_3/MeOH$): Monoclinic, $P2_1/c$, $a = 34.815(3)$ Å, $b = 11.7189(6)$ Å, $c = 11.5941(12)$ Å, $\beta = 90.070(8)$, $V = 4730.3(7)$ Å³, $Z = 8$, $R_I = 13.48$.

2,3-Dicyano-6,15-di-*tert*-butyl-9,10-dimethyltriptycene



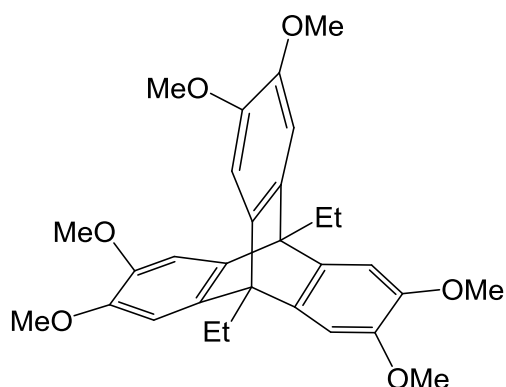
2,3-Dibromo-6,15-di-*tert*-butyl-9,10-dimethyltriptycene (3.5 g, 6.3 mmol) and copper cyanide (5.7 g, 63 mmol) were stirred at reflux in anhydrous DMF (70 ml) under a nitrogen atmosphere according to the general procedure (e). Purification via column chromatography on silica eluting with hexane:DCM (7:3) gave **2,3-dicyano-6,15-di-*tert*-butyl-9,10-dimethyltriptycene** as an off-white solid (1.15 g, 41 %). Mp > 300 °C; IR (film): ν , cm⁻¹ 2964, 2871, 2232, 1642, 1455, 1413, 1363, 1256, 902; ¹H NMR (250 MHz; $CDCl_3$): δ_H , ppm 7.72 (2H, s, ArH), 7.43 (2H, d, ⁴ $J_{HH} = 1.7$ Hz, ArH), 7.35 (2H, d, ³ $J_{HH} = 7.9$ Hz, ArH), 7.16 (2H, dd, ³ $J_{HH} = 7.9$ Hz, ⁴ $J_{HH} = 1.7$ Hz, ArH), 2.48 (6H, s, CH_3), 1.30 (18H, s, $C(CH_3)_3$); ¹³C NMR (62.5 MHz; $CDCl_3$): δ_C , ppm 155.1, 149.0, 145.6, 143.0, 125.0, 122.4, 120.8, 118.4, 116.0, 112.6, 48.9, 34.8, 31.5, 13.2; HRMS (EI) found m/z 444.2575 $[M]^+$, calculated 444.2565 for $C_{32}H_{32}N_2$.

2,3,6,7-Tetramethoxy-9,10-diethylantracene ^[117]



A solution of veratrole (27.6 g, 200 mmol) and propanal (29.0 g, 500 mmol) was added dropwise to concentrated sulfuric acid (200 ml) at 0 – 5 °C. The reaction mixture was then stirred at RT for 16 hours, quenched with water and neutralised with 35 % aqueous ammonia solution. After cooling, the organics were extracted with DCM (3 x 300 ml), washed with water and brine, dried over MgSO₄ and solvent evaporated. The crude product was triturated in ethanol to give **2,3,6,7-tetramethoxy-9,10-diethylanthracene** as a yellow powder (12.0 g, 34 %). Mp 247 – 249 °C, (lit. mp ^[117] 232 – 234 °C); IR (film): ν , cm⁻¹ 2951, 2832, 1636, 1535, 1495, 1433, 1240, 1200, 1167, 1061, 1034, 982, 935, 833, 779, 750; ¹H NMR (250 MHz; CDCl₃): δ_{H} , ppm 7.44 (4H, s, ArH), 4.11 (12H, s, OCH₃), 3.50 (4H, q, ³J_{HH} = 7.6 Hz, CH₂CH₃), 1.48 (6H, t, ³J_{HH} = 7.6 Hz, CH₂CH₃); ¹³C NMR (62.5 MHz; CDCl₃): δ_{C} , ppm 148.9, 130.6, 125.0, 102.3, 55.7, 21.9, 14.5; LRMS (EI) found m/z 354.17 ([M]⁺, 100 %).

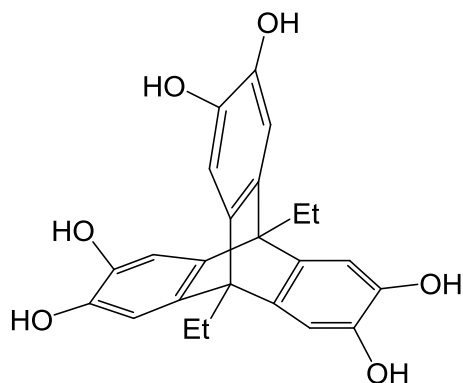
2,3,6,7,14,15-Hexamethoxy-9,10-diethyltriptycene ^[117]



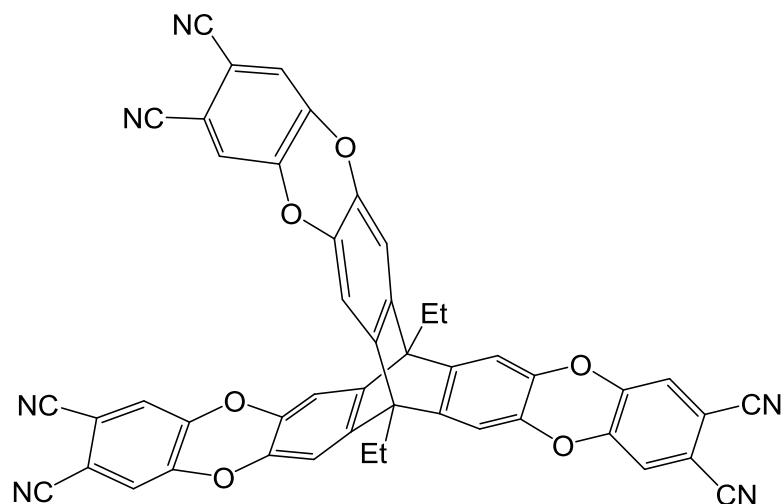
2,3,6,7-Tetramethoxy-9,10-diethylanthracene (3.5 g, 10 mmol) was dissolved in 1,2-dichloroethane (250 ml) at ~ 50 °C followed by the addition of 2-carboxy-4,5-dimethoxy benzenediazonium chloride (8.6 g, 35 mmol) and propylene oxide (45 ml) and the resulting mixture was stirred under reflux according to the general procedure (a). The crude residue was purified by column chromatography on silica eluting with DCM to obtain a yellow oil which was triturated in methanol to give **2,3,6,7,14,15-hexamethoxy-9,10-diethyltriptycene** as an off-white solid (2.24 g, 46 %). Mp 230 – 232 °C, (lit. mp ^[117] 274 – 276 °C); IR (film): ν , cm⁻¹ 2990, 2938, 2826, 1609, 1584, 1487, 1466, 1437, 1404, 1265, 1250, 1152, 1078, 1043, 912, 860, 785, 752; ¹H NMR (400 MHz; CDCl₃): δ_{H} , ppm 7.35 (6H, s, ArH), 4.20 (18H, s, OCH₃), 3.33 (4H, q, ³J_{HH} = 7.1 Hz, CH₂CH₃), 2.10 (6H, t, ³J_{HH} = 7.1 Hz, CH₂CH₃); ¹³C NMR (125 MHz; CDCl₃): δ_{C} ,

ppm 145.3, 107.5, 56.3, 52.7, 20.2, 11.2, one C missing; LRMS (EI) found m/z 490.25 ($[M]^+$, 60 %).

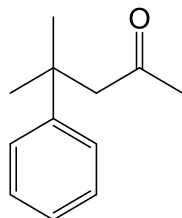
2,3,6,7,14,15-Hexahydroxy-9,10-diethyltriptycene ^[117]



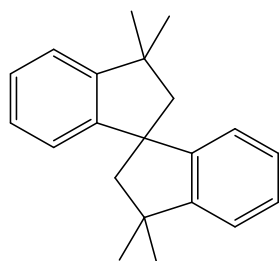
To a solution of 2,3,6,7,14,15-hexamethoxy-9,10-diethyltriptycene (2 g, 4 mmol) in DCM (25 ml) at 0 °C under a nitrogen atmosphere, BBr_3 (2.35 ml, 24 mmol) was added and the reaction mixture was stirred for 2 h at RT and monitored by TLCs. Upon completion, the reaction was quenched with water and DCM evaporated. The organics were extracted into ethyl acetate (2 x 100 ml), washed with water, dried over MgSO_4 and solvent reduced in volume under vacuum. Recipitation of this solution with hexane gave **2,3,6,7,14,15-hexahydroxy-9,10-diethyltriptycene** as a pink powder (1.45 g, 88 %). Mp > 300 °C, (lit. mp ^[117] > 300 °C); IR (film): ν , cm^{-1} 3289, 1697, 1618, 1485, 1445, 1373, 1294, 1202, 1136, 1040, 1007, 920, 860, 789, 760; ^1H NMR (250 MHz; CD_3OD): δ_{H} , ppm 6.83 (6H, s, ArH), 2.74 (4H, q, $^3J_{\text{HH}} = 7.1$ Hz, CH_2CH_3), 1.63 (6H, t, $^3J_{\text{HH}} = 7.1$ Hz, CH_2CH_3); ^{13}C NMR (125 MHz; CD_3OD): δ_{C} , ppm 141.5, 111.4, 53.0, 21.3, 11.5, one C missing; HRMS (EI) found m/z 406.1420 $[M]^+$, calculated 406.1416 for $\text{C}_{24}\text{H}_{22}\text{O}_6$.

2,3,6,7,14,15-tris(dioxinphthalonitrile)-9,10-diethyltritycene

2,3,6,7,14,15-Hexahydroxy-9,10-diethyltritycene (0.085 g, 0.2 mmol) and 4,5-dichlorophthalonitrile (0.12 g, 0.6 mmol) were stirred in anhydrous DMF (20 ml) at 60 °C under a nitrogen atmosphere. To this solution, anhydrous potassium carbonate (0.3 g, 2.1 mmol) was added in and the reaction mixture stirred for 22 h at 77 °C. Upon cooling to room temperature, the mixture was poured into water and filtered to dryness. The crude product was purified by reprecipitation of its DCM solution with methanol to give **2,3,6,7,14,15-tris(dioxinphthalonitrile)-9,10-diethyltritycene** as a light green solid (0.12 g, 75 %). Mp > 300 °C; IR (film): ν , cm^{-1} 3040, 2850, 2237, 1564, 1502, 1466, 1327, 1254, 1173, 999, 926, 887, 845, 800, 748; ^1H NMR (400 MHz; CDCl_3): δ_{H} , ppm 7.07 (6H, s, ArH), 6.83 (6H, s, ArH), 2.72 (4H, q, $^3J_{\text{HH}} = 7.0$ Hz, CH_2CH_3), 1.56 (6H, t, $^3J_{\text{HH}} = 7.0$ Hz, CH_2CH_3); ^{13}C NMR (125 MHz; CDCl_3): δ_{C} , ppm 145.8, 137.2, 121.3, 114.5, 111.8, 52.6, 19.7, 10.5, two Cs missing; HRMS (EI) found m/z 778.1602, calculated 778.1601 for $\text{C}_{48}\text{H}_{22}\text{N}_6\text{O}_6$; Crystallography data (THF): Triclinic, *P*-1, $a = 10.7268(4)$ Å, $b = 15.3620(6)$ Å, $c = 18.6391(7)$ Å, $\alpha = 93.123(3)$, $\beta = 97.338(3)$, $\gamma = 105.212(4)$, $V = 2927.10(19)$ Å³, $Z = 2$, $R_1 = 7.04$.

4-Methyl-4-phenyl-2-pentanone ^[182,183]

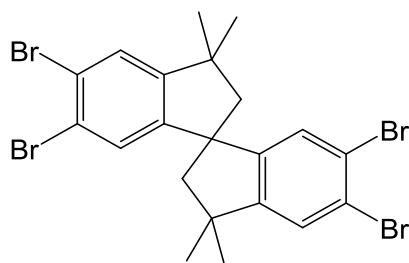
Under a nitrogen atmosphere, mesityl oxide (40 ml, 350 mmol) was added dropwise to an ice bath cooled suspension of aluminium trichloride (60 g, 450 mmol) in anhydrous benzene (140 ml, 1571 mmol). After the addition, the reaction was stirred at room temperature for 4 hours, poured over ice water (700 ml) and extracted into diethyl ether (3 x 200 ml). The organics were washed with water, dried over MgSO₄ and solvent evaporated under vacuum. The crude yellow oil was then purified by distillation, collecting the fraction that boiled between 120 – 125 °C to give **4-methyl-4-phenyl-2-pentanone** as colourless oil (52.7 g, 86 %). IR (film): ν , cm⁻¹ 3088, 3059, 3024, 2955, 2878, 1705, 1602, 1496, 1444, 1358; ¹H NMR (500 MHz; CDCl₃): δ _H, ppm 7.34 (3H, m, ArH), 7.19 (2H, t, ³J_{HH} = 7.0 Hz, ArH), 2.74 (2H, s, CH₂), 1.78 (3H, s, O=CCH₃), 1.44 (6H, s, PhC(CH₃)₂); ¹³C NMR (62.5 MHz; CDCl₃): δ _C, ppm 207.6, 148.2, 128.3, 126.0, 125.5, 56.9, 37.3, 31.7, 28.9; LRMS (EI) found m/z 176.12 ([M]⁺, 75 %).

3,3,3',3'-Tetramethyl-1,1'-spirobisindane ^[182-184]

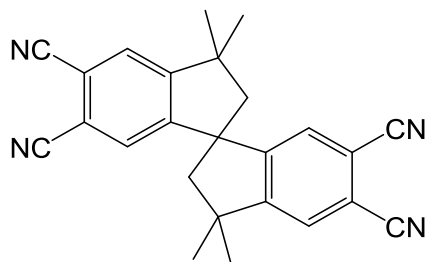
A mixture of zinc chloride (40.73 g, 299 mmol) and 4-methyl-4-phenyl-2-pentanone (52.7 g, 299 mmol) were heated to 180 °C under a nitrogen atmosphere. After the resultant violent reaction has taken place, the mixture was cooled to room temperature and extracted with hexane (3 x 300 ml). The organic extracts were combined, solvent removed under vacuum to give yellow oil which was stirred in methanol. The crude yellow solid was then recrystallised from hexane to give **3,3,3',3'-tetramethyl-1,1'-spirobisindane** as white needles (15.0 g, 36 %). Mp 132 – 134

°C, (lit. mp ^[184] 133 – 134 °C); IR (film): ν , cm^{-1} 3017, 2943, 2920, 2857, 1582, 1476, 1447, 1360, 1312, 1153, 1020, 762; ¹H NMR (250 MHz; CDCl₃): δ_{H} , ppm 7.34 – 7.17 (6H, m, ArH), 6.88 (2H, d, ³*J*_{HH} = 7.4 Hz, ArH), 2.43 (2H, d, ²*J*_{HH} = 13.1 Hz, CHH), 2.32 (2H, d, ²*J*_{HH} = 13.1 Hz, CHH), 1.48 (6H, s, CH₃), 1.43 (6H, s, CH₃); ¹³C NMR (62.5 MHz; CDCl₃): δ_{C} , ppm 152.2, 150.8, 127.2, 127.0, 124.4, 121.8, 59.4, 57.7, 43.6, 31.8, 30.3; LRMS (EI) found *m/z* 276.01 ([M]⁺, 70 %).

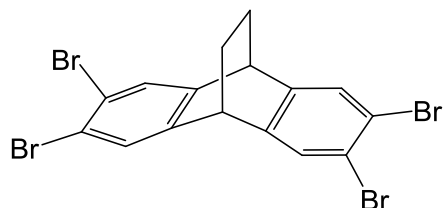
5,5',6,6'-Tetrabromo-3,3,3',3'-tetramethyl-1,1'-spirobisindane



3,3,3',3'-Tetramethyl-1,1'-spirobisindane (2.47 g, 9 mmol) and iron powder (~ 30 mg) were stirred in anhydrous DCM (45 ml). To this bromine (6.1 g, 38.2 mmol) was added and the reaction was stirred under reflux for 18 hours. The reaction was then cooled to room temperature, washed with water, the organics extracted with DCM, dried over MgSO₄ and solvent removed under vacuum. The crude product was triturated in hexane and filtered to give **5,5',6,6'-tetrabromo-3,3,3',3'-tetramethyl-1,1'-spirobisindane** as a light brown powder (4.75 g, 89 %). Mp 234 – 236 °C; IR (film): ν , cm^{-1} 2956, 2923, 2863, 1464, 1385, 1363, 1349, 1310, 1282, 1264, 1210, 1100, 925, 875, 750; ¹H NMR (250 MHz; CDCl₃): δ_{H} , ppm 7.45 (2H, s, ArH), 7.04 (2H, s, ArH), 2.37 (2H, d, ²*J*_{HH} = 13.3 Hz, CHH), 2.22 (2H, d, ²*J*_{HH} = 13.3 Hz, CHH), 1.41 (6H, s, CH₃), 1.35 (6H, s, CH₃); ¹³C NMR (125 MHz; CDCl₃): δ_{C} , ppm 153.4, 150.6, 129.3, 127.5, 123.6, 123.2, 59.1, 57.0, 43.6, 31.4, 29.9; LRMS (EI) found *m/z* 591.84 ([M]⁺, 40 %).

5,5',6,6'-Tetracyano-3,3,3',3'-tetramethyl-1,1'-spirobisindane

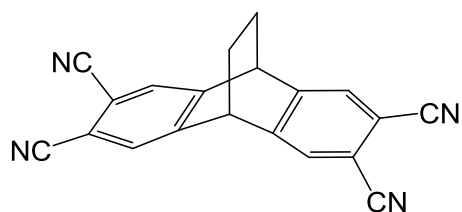
5,5',6,6'-Tetrabromo-3,3,3',3'-tetramethyl-1,1'-spirobisindane (4.5 g, 7.6 mmol) and copper cyanide (13.6 g, 152 mmol) were stirred at reflux in anhydrous DMF (~ 70 ml) under a nitrogen atmosphere according to the general procedure (e). The crude product was extracted by washing the obtained solid with DCM (~ 700 ml) and was purified via column chromatography on silica eluting with DCM:hexane (8:2) to give **5,5',6,6'-tetracyano-3,3,3',3'-tetramethyl-1,1'-spirobisindane** as a light blue solid (1.25 g, 44 %). Mp > 300 °C; IR (film): ν , cm^{-1} 3031, 2963, 2927, 2867, 2233, 1598, 1560, 1483, 1367, 1250, 1198, 1100, 898; ^1H NMR (400 MHz; CDCl_3): δ_{H} , ppm 7.31 (2H, s, ArH), 6.82 (2H, s, ArH), 2.15 (2H, d, $^2J_{\text{HH}} = 13.5$ Hz, CHH), 1.92 (2H, d, $^2J_{\text{HH}} = 13.5$ Hz, CHH), 1.13 (6H, s, CH_3), 1.05 (6H, s, CH_3); ^{13}C NMR (125 MHz; CDCl_3): δ_{C} , ppm 158.2, 153.9, 129.4, 128.3, 115.4, 58.3, 44.8, 31.1, 29.2, some Cs missing; HRMS (EI) found m/z 376.1692 $[\text{M}]^+$, calculated 376.1688 for $\text{C}_{25}\text{H}_{20}\text{N}_4$; Crystallography data ($\text{CHCl}_3/\text{MeOH}$): Triclinic, $P-1$, $a = 10.0893(5)$ Å, $b = 10.3879(4)$ Å, $c = 13.5531(6)$ Å, $\alpha = 108.661(4)$, $\beta = 99.168(4)$, $\gamma = 107.874(4)$, $V = 1227.47(9)$ Å³, $Z = 2$, $R_I = 4.97$.

2,3,6,7-Tetrabromo-9,10-dihydro-9,10-ethanoanthracene

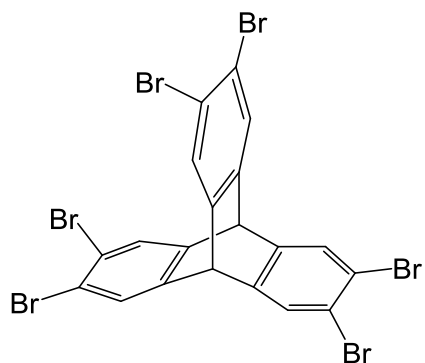
9,10-Dihydro-9,10-ethanoanthracene (3 g, 14.5 mmol) (Apollo Chemicals) and iron powder (~ 30 mg) were stirred in anhydrous DCM (45 ml). To this bromine (9.78 g, 61 mmol) was added and the reaction was stirred under reflux for 18 hours. The reaction was then cooled to room temperature, washed with water, the organics extracted with DCM, dried over MgSO_4 and

solvent removed under vacuum. The crude product was triturated in hexane and filtered to give **2,3,6,7-tetrabromo-9,10-dihydro-9,10-ethanoanthracene** as a white powder (5.6 g, 74 %). Mp 264 – 267 °C; IR (film): ν , cm^{-1} 2957, 2930, 2857, 1593, 1474, 1449, 1435, 1360, 1302, 1136, 1094, 1016, 953, 887, 839, 826, 787; ^1H NMR (250 MHz; CDCl_3): δ_{H} , ppm 7.54 (4H, s, ArH), 4.25 (2H, s, CH), 1.72 (4H, s, CH_2); ^{13}C NMR (62.5 MHz; CDCl_3): δ_{C} , ppm 143.5, 128.6, 121.6, 42.4, 25.8; HRMS (EI) found m/z 517.7525 $[\text{M}]^+$, calculated 517.7516 for $\text{C}_{16}\text{H}_{10}^{79}\text{Br}_4$; Crystallography data ($\text{CHCl}_3/\text{MeOH}$): Monoclinic, $P2_1/c$, $a = 14.5275(3)$ Å, $b = 6.55070(10)$ Å, $c = 16.2667(4)$ Å, $\beta = 93.456(2)$, $V = 1545.21(6)$ Å³, $Z = 4$, $R_I = 3.65$.

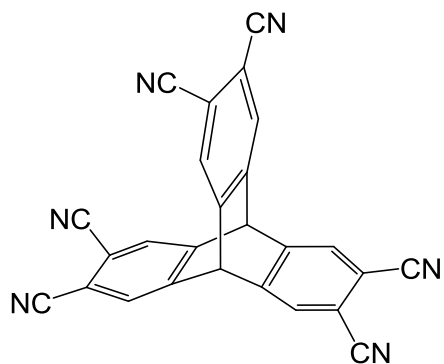
2,3,6,7-Tetracyano-9,10-dihydro-9,10-ethanoanthracene



2,3,6,7-Tetrabromo-9,10-dihydro-9,10-ethanoanthracene (9.4 g, 18 mmol) and copper cyanide (32 g, 360 mmol) were stirred at reflux in anhydrous DMF (~ 150 ml) under a nitrogen atmosphere according to the general procedure (e). The crude product was extracted by washing the obtained solid with DCM (~ 700 ml) and was purified via column chromatography on silica eluting with DCM to give **2,3,6,7-tetracyano-9,10-dihydro-9,10-ethanoanthracene** as a light blue solid (2.41 g, 44 %). Mp > 300 °C; IR (film): ν , cm^{-1} 3034, 2947, 2876, 2230, 1605, 1560, 1474, 1335, 1310, 1261, 1234, 1142, 1015, 905, 854, 841, 799, 737; ^1H NMR (250 MHz; $\text{DMSO-}d_6$): δ_{H} , ppm 8.19 (4H, s, ArH), 4.89 (2H, s, CH), 1.69 (4H, s, CH_2); ^{13}C NMR (62.5 MHz; $\text{DMSO-}d_6$): δ_{C} , ppm 147.7, 129.3, 116.0, 112.6, 42.3, 24.2; HRMS (EI) found m/z 306.0906 $[\text{M}]^+$, calculated 306.0905 for $\text{C}_{20}\text{H}_{10}\text{N}_4$; Crystallography data: First polymorph (CHCl_3): Orthorhombic, $Pbca$, $a = 6.9455(2)$ Å, $b = 15.5407(4)$ Å, $c = 28.3868(8)$ Å, $V = 3064.01(15)$ Å³, $Z = 8$, $R_I = 5.23$. Second polymorph (CHCl_3): Monoclinic, $P2_1/n$, $a = 6.6157(5)$ Å, $b = 14.5927(8)$ Å, $c = 15.6830(10)$ Å, $\beta = 96.449(7)$, $V = 1504.47(17)$ Å³, $Z = 4$, $R_I = 6.15$.

2,3,6,7,14,15-Hexabromotriptycene ^[111]

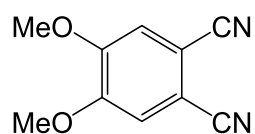
Triptycene (3 g, 11.8 mmol) and iron powder (~ 50 mg) were stirred in anhydrous DCM (45 ml). To this, bromine (11.86 g, 74 mmol) was added and the reaction stirred under reflux for 17 hours. The reaction was then cooled to room temperature, washed with water, the organics extracted with DCM, dried over MgSO₄ and solvent removed under vacuum. The crude product was triturated in hexane and filtered to give **2,3,6,7,14,15-hexabromotriptycene** as a white powder (6.8 g, 79 %). Mp > 300 °C, (lit. mp ^[111] > 350 °C); IR (film): ν , cm⁻¹ 3062, 2968, 1678, 1607, 1526, 1441, 1358, 1290, 1175, 1098, 926, 885, 837, 802; ¹H NMR (250 MHz; CDCl₃): δ _H, ppm 7.65 (6H, s, ArH), 5.26 (2H, s, CH); ¹³C NMR (62.5 MHz; CDCl₃): δ _C, ppm 144.0, 129.1, 121.8, 51.1; LRMS (EI) found m/z 727.57 ([M]⁺, 30 %).

2,3,6,7,14,15-Hexacyanotriptycene ^[180]

2,3,6,7,14,15-Hexabromotriptycene (1.50 g, 2.06 mmol) and copper cyanide (5 g, 55.8 mmol) were stirred at reflux in anhydrous DMF (45 ml) under a nitrogen atmosphere according to the general procedure (e). The desired product was obtained from the crude green solid by refluxing the crude solid in DMF, filtering and then reprecipitating the DMF solution with a mixture of

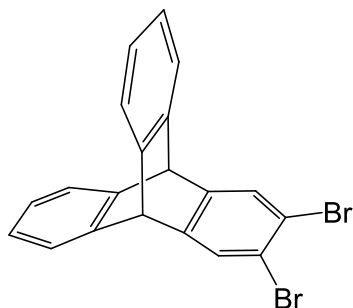
methanol and water to give **2,3,6,7,14,15-hexacyanotriptycene** as a pale blue solid (0.084 g, 10 %). Mp > 300 °C; IR (solid): ν , cm^{-1} 3028, 2971, 2234, 1738, 1670, 1560, 1472, 1366, 1316, 1263, 1231, 1217, 1206, 1090, 909, 808, 745, 719, 631; ^1H NMR (400 MHz; $\text{DMSO-}d_6$): δ_{H} , ppm 8.33 (6H, s, ArH), 6.40 (2H, s, CH); ^{13}C NMR (125 MHz; $\text{DMSO-}d_6$): δ_{C} , ppm 147.4, 130.1, 115.6, 113.2, 50.8; HRMS (EI) found m/z 404.0805 $[\text{M}]^+$, calculated 404.0810 for $\text{C}_{26}\text{H}_8\text{N}_6$.

4,5-Dimethoxyphthalonitrile ^[188]



2,3-Dibromoveratrole (5 g, 17 mmol) and copper cyanide (15 g, 167 mmol) were stirred at reflux in anhydrous DMF (140 ml) under a nitrogen atmosphere according to the general procedure (e). Purification was achieved via column chromatography on silica using DCM as the eluent to give **4,5-dimethoxyphthalonitrile** as a white powder (1.8 g, 56 %). Mp 182 – 184 °C, (lit. mp ^[188] 179 – 181 °C); IR (film): ν , cm^{-1} 3067, 2989, 2862, 2228, 1645, 1590, 1521, 1459, 1296, 1235, 1090, 877, 830, 731; ^1H NMR (400 MHz; CDCl_3): δ_{H} , ppm 7.19 (2H, s, ArH), 3.99 (6H, s, OCH_3); ^{13}C NMR (100 MHz; CDCl_3): δ_{C} , ppm 153.0, 116.2, 115.2, 109.3, 57.1; LRMS (EI) found m/z : 188.03 ($[\text{M}]^+$, 100 %).

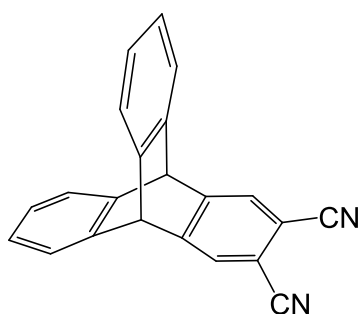
2,3-Dibromotriptycene ^[189]



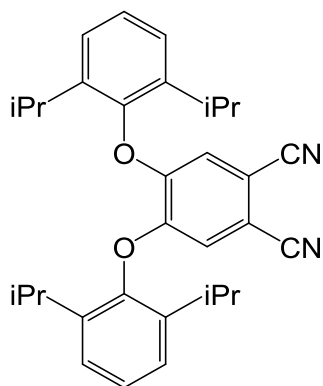
Anthracene (4 g, 22 mmol) and 1,2,4,5-tetrabromobenzene (12 g, 30 mmol) were reacted with $n\text{-BuLi}$ (2.5 M in hexane, 14 ml, 35 mmol) in anhydrous toluene (70 ml) according to the general procedure (d). The crude residue was purified via column chromatography on silica

(hexane:DCM, 9:1) to give **2,3-dibromotriptycene** as a pale yellow solid (3 g, 32 %). M.p.: 186 – 188 °C; (lit. mp ^[189] 191 – 192 °C); IR (film): ν , cm^{-1} 3066, 3020, 2962, 1589, 1556, 1458, 1442, 1264, 1097, 922, 886, 748, 641, 628; ¹H NMR (400 MHz; CDCl₃): δ_{H} , ppm 7.66 (2H, s, ArH), 7.41 (4H, dd, ³J_{HH} = 5.3 Hz, ⁴J_{HH} = 3.2 Hz, ArH), 7.06 (4H, dd, ³J_{HH} = 5.3 Hz, ⁴J_{HH} = 3.2 Hz, ArH), 5.40 (2H, s, CH); ¹³C NMR (100 MHz; CDCl₃): δ_{C} , ppm 146.7, 144.5, 129.1, 126.1, 124.3, 121.0, 53.5; LRMS (EI) found m/z : 411.92 ([M]⁺, 90 %).

2,3-Dicyanotriptycene ^[190]



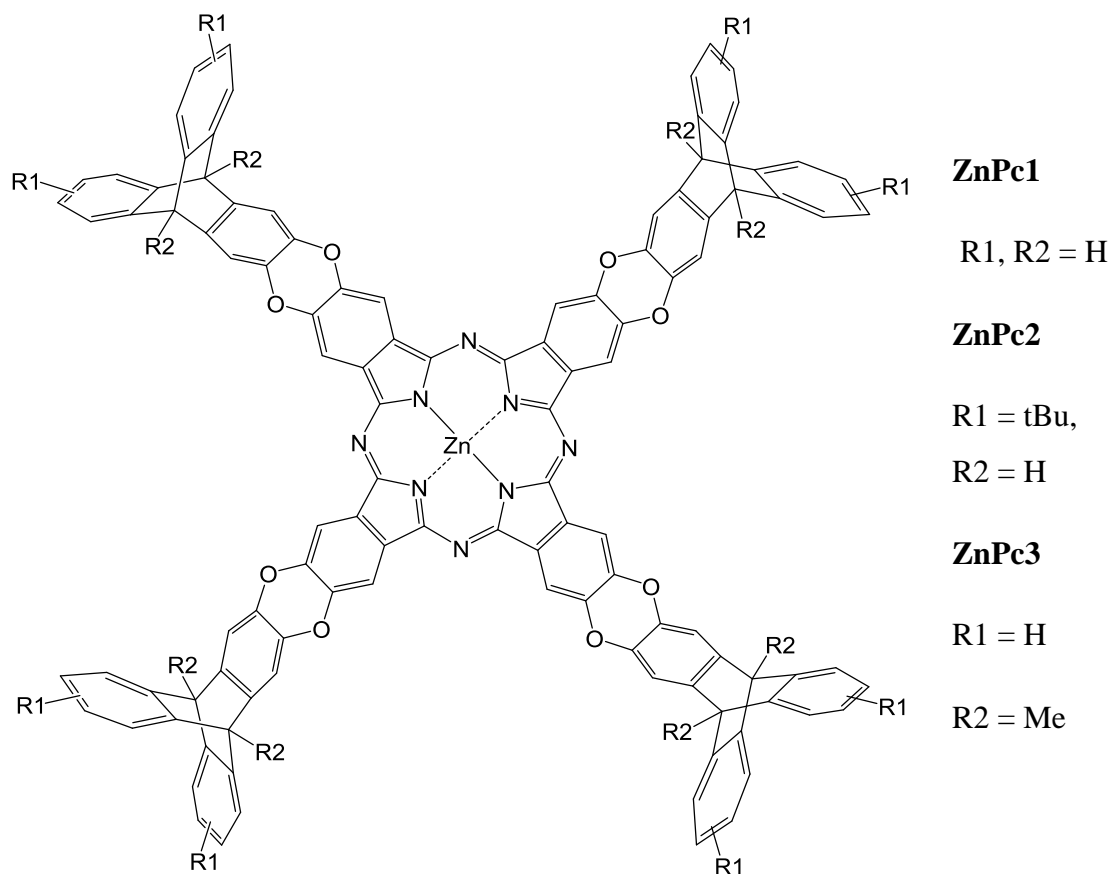
2,3-Dibromotriptycene (2.9 g, 7 mmol) and copper cyanide (6.5 g, 70 mmol) were stirred at reflux in anhydrous DMF (70 ml) under a nitrogen atmosphere according to the general procedure (e). The crude product was collected by filtration and was purified via column chromatography on silica eluting with DCM:hexane (7:3) to give **2,3-dicyanotriptycene** as a light green powder (1.4 g, 65 %). M.p.: 237 – 239 °C, (lit. mp ^[190] 235 – 238 °C); IR (film): ν , cm^{-1} 3071, 3038, 2986, 2237, 1563, 1457, 1328, 1264, 1152, 904, 758, 629; ¹H NMR (500 MHz; CDCl₃): δ_{H} , ppm 7.68 (2H, s, ArH), 7.36 (4H, dd, ³J_{HH} = 5.4 Hz, ⁴J_{HH} = 3.2 Hz, ArH), 7.01 (4H, dd, ³J_{HH} = 5.4 Hz, ⁴J_{HH} = 3.2 Hz, ArH), 5.48 (2H, s, CH); ¹³C NMR (125 MHz; CDCl₃): δ_{C} , ppm 151.4, 142.7, 128.0, 126.3, 124.3, 115.6, 113.1, 53.6; LRMS (EI) found m/z : 304.09 ([M]⁺, 90 %).

4,5-Di-(2,6-di-*iso*-propylphenoxy)phthalonitrile ^[21]

4,5-Dichlorophthalonitrile (6 g, 30 mmol) and 2,6-di-*iso*-propyl phenol (16.9 ml, 90 mmol) were dissolved in anhydrous DMF (80 ml) at 77 °C under a nitrogen atmosphere. To this solution, anhydrous potassium carbonate (17 g, 123 mmol) was added and the reaction mixture stirred for 72 h. Upon cooling to RT, the mixture was poured into water (300 ml) and extracted with DCM (3 x 300 ml). The organic layer was dried over MgSO₄, filtered and solvent removed under vacuum. The crude product was recrystallised from methanol to give **4,5-di-(2,6-di-*iso*-propylphenoxy)phthalonitrile** as a green solid (8.3 g, 57 %). M.p.: 182 – 183 °C; IR (film): ν , cm⁻¹ 3070, 2965, 2930, 2871, 2231, 1595, 1502, 1400, 1286, 1207, 1078, 795; ¹H NMR (400 MHz; CDCl₃): δ_{H} , ppm 7.25 (6H, m, ArH), 6.68 (2H, s, ArH), 2.87 (4H, sept, ³J_{HH} = 6.7 Hz, CH₃CHCH₃), 1.18 (12H, d, ³J_{HH} = 6.7 Hz, CH₃CHCH₃), 1.10 (12H, d, ³J_{HH} = 6.7 Hz, CH₃CHCH₃); ¹³C NMR (100 MHz; CDCl₃): δ_{C} , ppm 151.9, 147.6, 141.1, 127.8, 125.6, 118.3, 115.7, 109.6, 27.9, 24.6, 22.9; LRMS (EI) found m/z : 480.26 ([M]⁺, 100 %).

6.4 Synthesis of Pc and porphyrin molecules

ZnPc



2,3,9,10,16,17,23,24-octa(2',3'-dioxitriptyceno)phthalocyaninato zinc (ZnPc1)

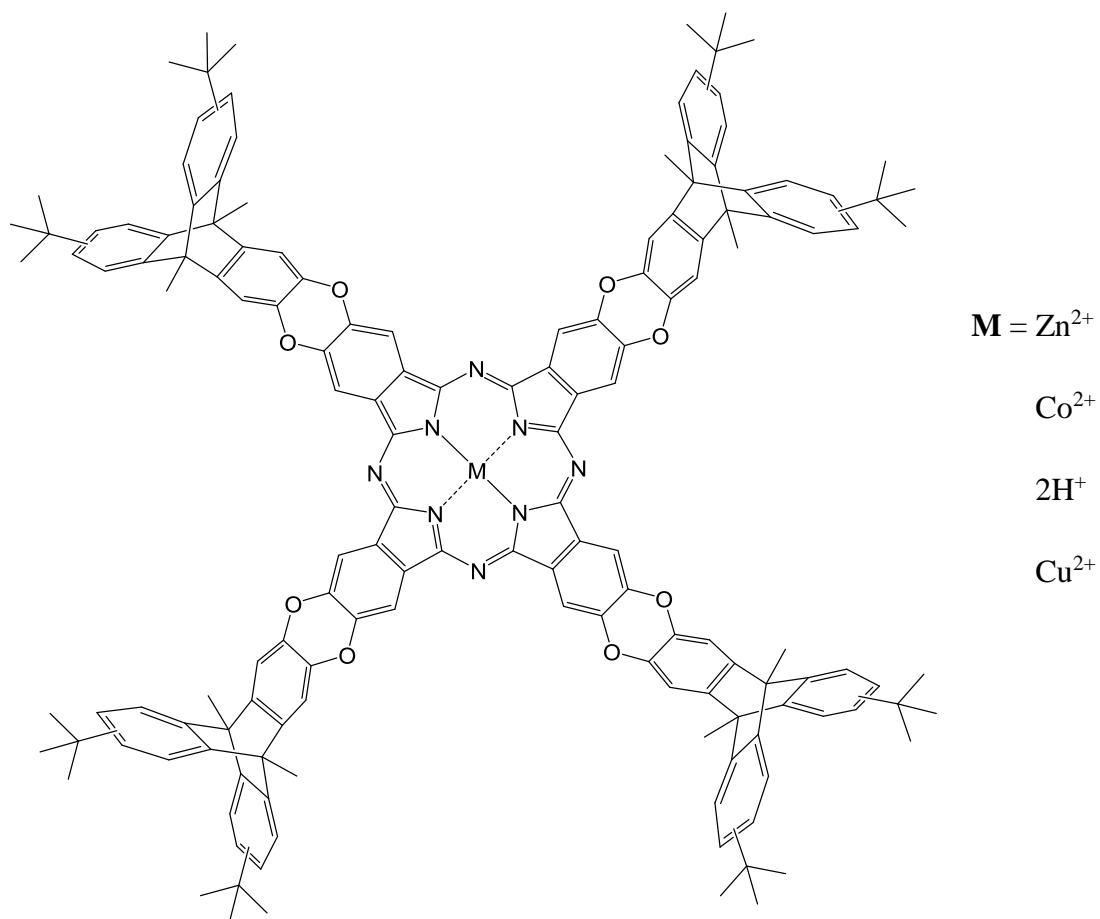
2,3-Dioxin-phthalonitrile-triptycene (0.4 g, 1 mmol) and zinc(II)acetate (0.22 g, 1 mmol) were reacted in anhydrous NMP (1.5 ml) according to the general procedure. Purification was achieved by refluxing the crude black solid in chloroform, then THF to isolate **ZnPc1** as a dark green-black solid (0.1 g, 24 %). Mp > 300 °C; UV-vis (THF): λ_{max} , nm 677, 611, 363, 304; IR (solid): ν , cm^{-1} 3173, 1583, 1306, 1083, 1017, 891, 848, 769; MS (MALDI-TOF): cluster centred at m/z 1706.5 (calcd. for $[\text{M}]^+$ 1706.4); BET surface area = 42 $\text{m}^2 \text{g}^{-1}$; total pore volume = 0.13 $\text{cm}^3 \text{g}^{-1}$ at $p/p^0 = 0.98$.

2,3,9,10,16,17,23,24-octa(2',3'-dioxy-6',15'-di-*tert*-butyltritypceno)phthalocyaninato zinc (ZnPc2)

2,3-Dioxin-phthalonitrile-6,15-di-*tert*-butyltritypcene (0.2 g, 0.38 mmol) and zinc(II)acetate (0.07 g, 0.38 mmol) were reacted in anhydrous NMP (1.5 ml) according to the general procedure (f). Purification was achieved via column chromatography on silica (hexane:DCM:EtOAc, 7:2:1) to give **ZnPc2** as a green solid (0.03 g, 14%). Mp > 300 °C; Elemental analysis (%) calcd. for C₁₄₄H₁₂₀N₈O₈Zn.H₂O: C 79.56, H 5.66, N 5.15, found C 79.34, H 5.85, N 5.00; UV-vis (THF): λ_{\max} , nm 677, 649, 611, 362, 307; IR (film): ν , cm⁻¹ 3082, 2954, 2924, 2853, 1638, 1585, 1463, 1402, 1377, 1334, 1283, 1136, 1087, 1017, 903, 801, 721; ¹H NMR (400 MHz; CDCl₃): δ_{H} , ppm 7.8 – 7.45 (16H, br m, ArH), 7.33 (8H, br s, ArH), 7.05 (8H, br s, ArH), 5.45 (8H, br s, CH), 1.35 (72H, br m, C(CH₃)₃); MS (MALDI-TOF): cluster centred at m/z 2155.5 (calcd. for [M]⁺ 2154.9); BET surface area = 378 m² g⁻¹; total pore volume = 0.33 cm³ g⁻¹ at p/p° = 0.98.

2,3,9,10,16,17,23,24-octa(2',3'-dioxy-9',10'-dimethyltritypceno)phthalocyaninato zinc (ZnPc3)

2,3-Dioxin-phthalonitrile-9,10-dimethyltritypcene (0.9 g, 2.1 mmol) and zinc(II)acetate (0.38 g, 2.1 mmol) were reacted in anhydrous NMP (3 ml) according to the general procedure (f). Purification was achieved by refluxing the crude black solid in chloroform to isolate **ZnPc3** as a dark greenish solid (0.1 g, 11 %). Mp > 300 °C; UV-vis (THF): λ_{\max} , nm 677, 647, 612, 362, 302; IR (solid): ν , cm⁻¹ 3180, 1638, 1604, 1579, 1329, 1284, 1161, 1081, 1030, 978, 902, 876, 744; ¹H NMR (400 MHz; DMSO-d₆): δ_{H} , ppm 7.37 (dd, 16H, ³J_{HH} = 5.4 Hz, ⁴J_{HH} = 3.4 Hz, ArH), 7.29 (s, 8H, ArH), 7.06 (dd, 16H, ³J_{HH} = 5.4 Hz, ⁴J_{HH} = 3.4 Hz, ArH), 7.04 (s, 8H, ArH), 2.31 (s, 24H, OCH₃); MS (MALDI-TOF): cluster centred at m/z 1819.1 (calcd. for [M]⁺ 1818.5); BET surface area = 282 m² g⁻¹; total pore volume = 0.27 cm³ g⁻¹ at p/p° = 0.98.

MPc4

2,3,9,10,16,17,23,24-octa(2',3'-dioxo-9',10'-dimethyl-6',15'-di-*tert*-butyltriptyceno) phthalocyaninato zinc (ZnPc4)

2,3-Dioxin-phthalonitrile-9,10-dimethyl-6,15-di-*tert*-butyltriptycene (1 g, 1.8 mmol) and zinc(II)acetate (0.33 g, 1.8 mmol) were reacted in anhydrous NMP (3 ml) according to the general procedure (f). Purification was achieved via column chromatography on silica eluting with hexane:DCM:EtOAc (7:2:1) to give **ZnPc4** as a green solid (0.37 g, 37 %). Mp > 300 °C; Elemental analysis (%) calcd. for C₁₅₂H₁₃₆N₈O₈Zn: C 80.49, H 6.04, N 4.94, found C 81.23, H 6.18, N 4.75; UV-vis (Toluene): λ_{max}, nm 684, 650, 615, 467, 371, 303; IR (film): ν, cm⁻¹ 3041, 2966, 2903, 2865, 1616, 1581, 1456, 1402, 1331, 1271, 1175, 1084, 1033, 980, 902, 765, 744; ¹H NMR (400 MHz; pyridine-*d*₅): δ_H, ppm 8.55 (8H, br s, ArH), 7.64 (8H, br s, ArH), 7.42 (8H, br s, ArH), 7.10 (8H, br m, ArH), 2.51 (24H, br s, CH₃), 1.10 (72H, br m, C(CH₃)₃); MS

(MALDI-TOF): cluster centred at m/z 2267.0 (calcd. for $[M]^+$ 2267.0); BET surface area = 488 $m^2 g^{-1}$; total pore volume = 0.44 $cm^3 g^{-1}$ at $p/p^o = 0.98$.

2,3,9,10,16,17,23,24-octa(2',3'-dioxy-9',10'-dimethyl-6',15'-di-*tert*-butyltrityceno) phthalocyaninato cobalt (CoPc4)

2,3-Dioxin-phthalonitrile-9,10-dimethyl-6,15-di-*tert*-butyltritycene (1 g, 1.8 mmol) and cobalt(II)acetate (0.32 g, 1.8 mmol) were reacted in anhydrous NMP (3 ml) according to the general procedure (f). Purification was achieved via column chromatography on silica eluting with hexane:DCM:EtOAc (7:2:1) to give **CoPc4** as a dark green solid (0.20 g, 20 %). Mp > 300 °C; Elemental analysis (%) calcd. for $C_{152}H_{136}N_8O_8Co$: C 80.72, H 6.06, N 4.95, found C 81.05, H 6.36, N 4.72; UV-vis (Toluene): λ_{max} , nm 673, 643, 606, 449, 321; IR (film): ν , cm^{-1} 2969, 1641, 1471, 1415, 1329, 1308, 1096, 1049, 905, 865; MS (MALDI-TOF): cluster centred at m/z 2260.4 (calcd. for $[M]^+$ 2261.0); BET surface area = 463 $m^2 g^{-1}$; total pore volume = 0.37 $cm^3 g^{-1}$ at $p/p^o = 0.98$.

2,3,9,10,16,17,23,24-octa(2',3'-dioxy-9',10'-dimethyl-6',15'-di-*tert*-butyltrityceno) phthalocyanine (H₂Pc4)

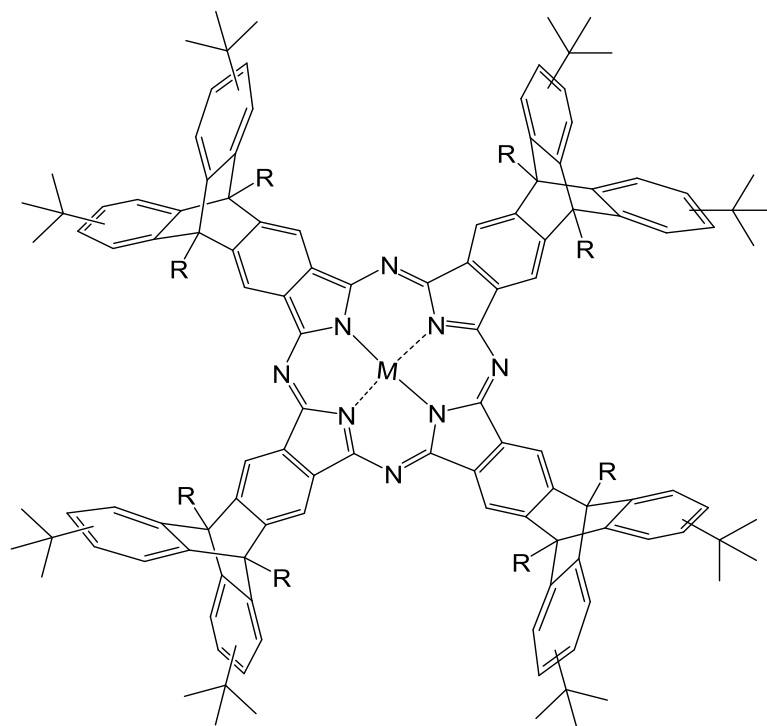
To a solution of 2,3-dioxin-phthalonitrile-9,10-dimethyl-6,15-di-*tert*-butyltritycene (1 g, 1.8 mmol) in refluxing anhydrous *n*-pentanol (10 ml) under a nitrogen atmosphere, was added lithium metal (~ 100 mg). The reaction mixture was stirred for 18 h, after which the solvent was evaporated. Dilute acetic acid was then added to this and the crude product extracted with DCM, dried over $MgSO_4$ and solvent evaporated. Purification was achieved via column chromatography on silica eluting with hexane:DCM:EtOAc (7:2:1) to give **H₂Pc4** as a green solid (0.55 g, 55 %). Mp > 300 °C; Elemental analysis (%) calcd. for $C_{152}H_{138}N_8O_8 \cdot 2H_2O$: C 81.47, H 6.39, N 5.00, found C 81.07, H 6.31, N 4.87; UV-vis (Toluene): λ_{max} , nm 706, 669, 639, 604, 471, 349, 308; IR (film): ν , cm^{-1} 2965, 2904, 2871, 1635, 1580, 1456, 1442, 1331, 1308, 1288, 1084, 1016, 895, 749; 1H NMR (400 MHz; $CDCl_3$): δ_H , ppm 7.89 (8H, br s, ArH), 7.45 (8H, br s, ArH), 7.20 (8H, br s, ArH), 2.55 (24H, br s, CH_3), 1.24 (72H, br m, $C(CH_3)_3$), -0.95

(2H, s, NH); MS (MALDI-TOF): cluster centred at m/z 2204.1 (calcd. for $[M]^+$ 2204.1); BET surface area = $406 \text{ m}^2 \text{ g}^{-1}$; total pore volume = $0.61 \text{ cm}^3 \text{ g}^{-1}$ at $p/p^o = 0.98$.

2,3,9,10,16,17,23,24-octa(2',3'-dioxo-9',10'-dimethyl-6',15'-di-*tert*-butyltritypceno) phthalocyaninato copper (CuPc4)

To a solution of **H₂Pc4** (0.2 g, 0.1 mmol) in refluxing anhydrous *n*-pentanol (7 ml) under a nitrogen atmosphere, was added excess Cu(II)acetate (0.8 g, 4.5 mmol). The reaction mixture was stirred for 18 h, after which the solvent was evaporated. Water was then added to this and the crude product extracted with DCM, dried over MgSO₄ and solvent evaporated. Purification was achieved via reprecipitation of a DCM solution with methanol to give **CuPc4** as a green solid (0.15 g, 75 %). Mp > 300 °C; Elemental analysis (%) calcd. for C₁₅₂H₁₃₆N₈O₈Cu.2H₂O: C 79.29, H 6.13, N 4.87, found C 79.52, H 6.17, N 4.85; UV-vis (Toluene): λ_{max} , nm 683, 650, 613, 463, 317; IR (film): ν , cm⁻¹ 2966, 2906, 2869, 1612, 1585, 1456, 1412, 1330, 1308, 1094, 1041, 903, 743; MS (MALDI-TOF): cluster centred at m/z 2266.1 (calcd. for $[M]^+$ 2266.0); BET surface area = $511 \text{ m}^2 \text{ g}^{-1}$; total pore volume = $0.73 \text{ cm}^3 \text{ g}^{-1}$ at $p/p^o = 0.98$.

MPz

**MPz1, R = H****M = Cu²⁺**Zn²⁺Co²⁺2H⁺**MPz2, R = Me****M = Cu²⁺**Zn²⁺**Tetra-2,3-(6,15-di-*tert*-butyltriptyceno)porphyrazinato copper** ^[156] (**CuPz1**)

Obtained as an additional product from the preparation of 2,3-dicyano-6,15-di-*tert*-butyltriptycene. Column chromatography on silica eluting with hexane:DCM (6:4) gave **CuPz1** as a bright blue solid (0.13 g). Mp > 300 °C; Elemental analysis (%) calcd. for C₁₂₀H₁₁₂N₈Cu.2H₂O: C 81.62, H 6.62, N 6.35, found C 81.88, H 6.61, N 6.16; UV-vis (CHCl₃): λ_{max}, nm 681, 651, 613, 395, 338, 288; IR (film): ν, cm⁻¹ 2961, 2868, 1481, 1456, 1402, 1263, 1092, 1019, 897, 750; MS (MALDI-TOF): clusters centred at *m/z* 1729.0 (calcd. for [M]⁺ 1729.8) and 3458.5 (calcd. for [M₂]⁺ 3459.7).

Tetra-2,3-(6,15-di-*tert*-butyltriptyceno)porphyrazinato zinc ^[156] (**ZnPz1**)

A mixture of 2,3-dicyano-6,15-di-*tert*-butyltriptycene (1 g, 2.4 mmol) and zinc(II)acetate (0.44 g, 2.4 mmol) were reacted in anhydrous NMP (3 ml) according to the general procedure (f). Purification was achieved via column chromatography on silica eluting with hexane:DCM:EtOAc (7:2:1) to give **ZnPz1** as a green solid (0.40 g, 40 %). Mp > 300 °C; Elemental analysis (%) calcd. for C₁₂₀H₁₁₂N₈Zn.2H₂O: C 81.54, H 6.61, N 6.35, found C 81.59,

H 6.75, N 6.12; UV-vis (CHCl_3): λ_{max} , nm 683, 653, 615, 393, 348, 290; IR (film): ν , cm^{-1} 2960, 2868, 1596, 1481, 1394, 1362, 1263, 1090, 1010, 899, 747; ^1H NMR (250 MHz; C_7D_8): δ_{H} , ppm 9.67 (8H, s, ArH), 7.58 (8H, br s, ArH), 7.38 (8H, d, $^3J_{\text{HH}} = 7.7$ Hz, ArH), 6.84 (8H, br s, ArH), 5.88 (8H, s, CH), 1.05 (72H, m, $\text{C}(\text{CH}_3)_3$); MS (MALDI-TOF): clusters centred at m/z 1730.7 (calcd. for $[\text{M}]^+$ 1730.8) and 3461.7 (calcd. for $[\text{M}_2]^+$ 3461.4).

Tetra-2,3-(6,15-di-*tert*-butyltriptyceno)porphyrazinato cobalt (CoPz1)

A mixture of 2,3-dicyano-6,15-di-*tert*-butyltriptycene (1 g, 2.4 mmol) and cobalt(II)acetate (0.42 g, 2.4 mmol) were reacted in anhydrous NMP (3 ml) according to the general procedure (f). Purification was achieved via column chromatography on silica eluting with hexane:DCM:EtOAc (7:2:1) to give **CoPz1** as a dark blue/black solid (0.25 g, 25 %). Mp > 300 °C; Elemental analysis (%) calcd. for $\text{C}_{120}\text{H}_{112}\text{N}_8\text{Co}\cdot\text{H}_2\text{O}$: C 82.68, H 6.59, N 6.43, found C 82.41, H 6.64, N 6.18; UV-vis (CHCl_3): λ_{max} , nm 673, 607, 387, 295; IR (film): ν , cm^{-1} 2961, 2867, 1483, 1457, 1407, 1362, 1263, 1158, 1094, 1027, 897, 755; MS (MALDI-TOF): clusters centred at m/z 1724.6 (calcd. for $[\text{M}]^+$ 1724.8) and 3448.4 (calcd. for $[\text{M}_2]^+$ 3449.7).

Tetra-2,3-(6,15-di-*tert*-butyltriptyceno)porphyrazine ($\text{H}_2\text{Pz1}$)

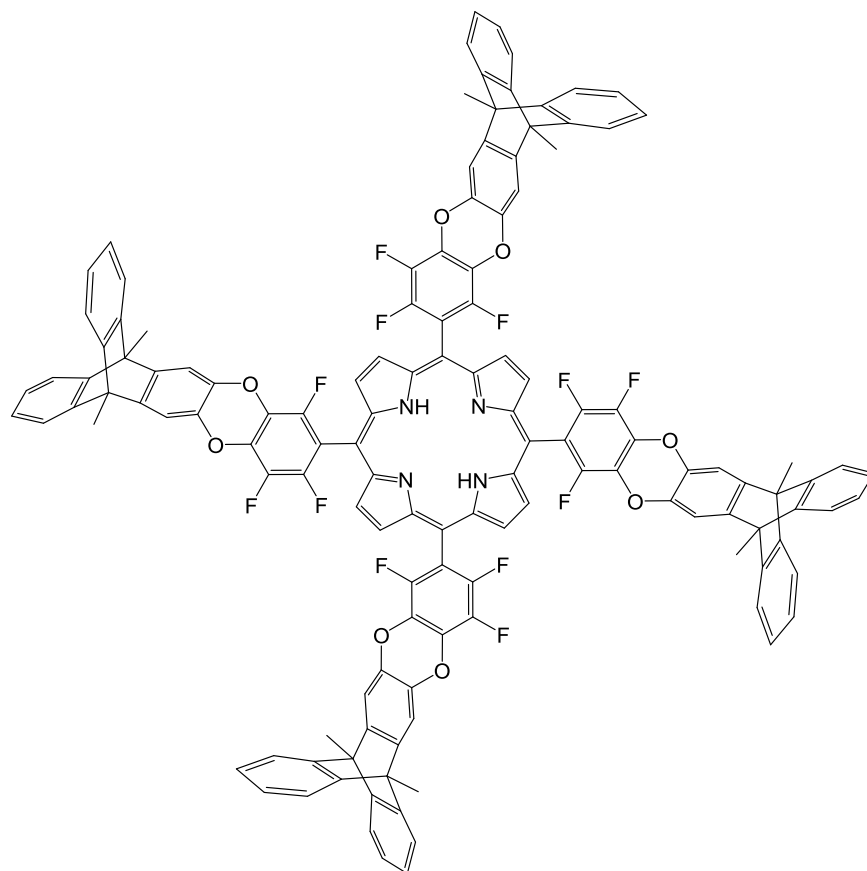
To a solution of 2,3-dicyano-6,15-di-*tert*-butyltriptycene (1 g, 2.4 mmol) in refluxing anhydrous *n*-pentanol (10 ml) under a nitrogen atmosphere, was added lithium metal (~ 100 mg). The reaction mixture was stirred for 18 h, cooled to room temperature and acetic acid (10 ml, 0.1 M) added. The crude product was extracted with DCM, dried over MgSO_4 and solvent evaporated. Purification was achieved via column chromatography on silica eluting with hexane:DCM (7:3) to give **$\text{H}_2\text{Pz1}$** as a dark green solid (0.55 g, 55 %). Mp > 300 °C; Elemental analysis (%) calcd. for $\text{C}_{120}\text{H}_{114}\text{N}_8\cdot\text{H}_2\text{O}$: C 85.47, H 6.93, N 6.65, found C 85.38, H 6.79, N 6.50; UV-vis (CHCl_3): λ_{max} , nm 702, 665, 603, 403, 352, 292; IR (film): ν , cm^{-1} 3295, 2962, 2867, 1481, 1430, 1393, 1362, 1263, 1161, 1089, 1016, 996, 898, 751; ^1H NMR (400 MHz; CDCl_3): δ_{H} , ppm 9.25 (8H, s, ArH), 7.44 (8H, br m, ArH), 7.30 (8H, br m, ArH), 6.88 (8H, br m, ArH), 5.76 (8H, s, CH), 1.07 (72H, m, $\text{C}(\text{CH}_3)_3$), -0.77 (2H, s, NH); MS (MALDI-TOF): clusters centred at m/z 1667.7 (calcd. for $[\text{M}]^+$ 1667.9) and 3335.5 (calcd. for $[\text{M}_2]^+$ 3335.8).

Tetra-2,3-(6,15-di-*tert*-butyl-9,10-dimethyltriptyceno)porphyrazinato copper (CuPz2)

Obtained as an additional product from the preparation of 2,3-dicyano-6,15-di-*tert*-butyl-9,10-dimethyltriptycene. Column chromatography on silica eluting with hexane:DCM (7:3) gave **CuPz2** as a bright green solid (0.04 g). Mp > 300 °C; Elemental analysis (%) calcd. for C₁₂₈H₁₂₈N₈Cu.H₂O: C 82.65, H 7.04, N 6.02, found C 82.87, H 7.68, N 4.63; UV-vis (CHCl₃): λ_{max}, nm 681, 652, 614, 398, 347, 289; IR (film): ν, cm⁻¹ 3073, 2964, 2868, 1598, 1480, 1456, 1398, 1362, 1270, 1104, 1064, 975, 889, 754; MS (MALDI-TOF): cluster centred at *m/z* 1841.3 (calcd. for [M]⁺ 1841.0).

Tetra-2,3-(6,15-di-*tert*-butyl-9,10-dimethyltriptyceno)porphyrazinato zinc (ZnPz2)

A mixture of 2,3-dicyano-6,15-di-*tert*-butyl-9,10-dimethyltriptycene (0.2 g, 0.45 mmol) and zinc(II)acetate (0.08 g, 0.45 mmol) were reacted in anhydrous NMP (1 ml) according to the general procedure (f). Purification was achieved via column chromatography on silica eluting with hexane:DCM (1:1) to give **ZnPz2** as a dark green solid (0.07 g, 33 %). Mp > 300 °C; Elemental analysis (%) calcd. for C₁₂₈H₁₂₈N₈Zn.2H₂O: C 81.78, H 7.08, N 5.98, found C 81.76, H 6.94, N 5.67; UV-vis (CHCl₃): λ_{max}, nm 682, 656, 613, 406, 345, 289; IR (film): ν, cm⁻¹ 3070, 2964, 2871, 1605, 1480, 1447, 1398, 1377, 1347, 1271, 1154, 1104, 1082, 1064, 975, 889, 753; ¹H NMR (400 MHz; CDCl₃): δ_H, ppm 7.43 (8H, br s, ArH), 7.29 (16H, br s, ArH), 2.55 (24H, br s, CH₃), 1.20 (72H, m, C(CH₃)₃); MS (MALDI-TOF): cluster centred at *m/z* 1841.5 (calcd. for [M]⁺ 1842.0); BET surface area = 506 m² g⁻¹; total pore volume = 0.38 cm³ g⁻¹ at *p/p*^o = 0.98 (data obtained on 25 mg of sample).

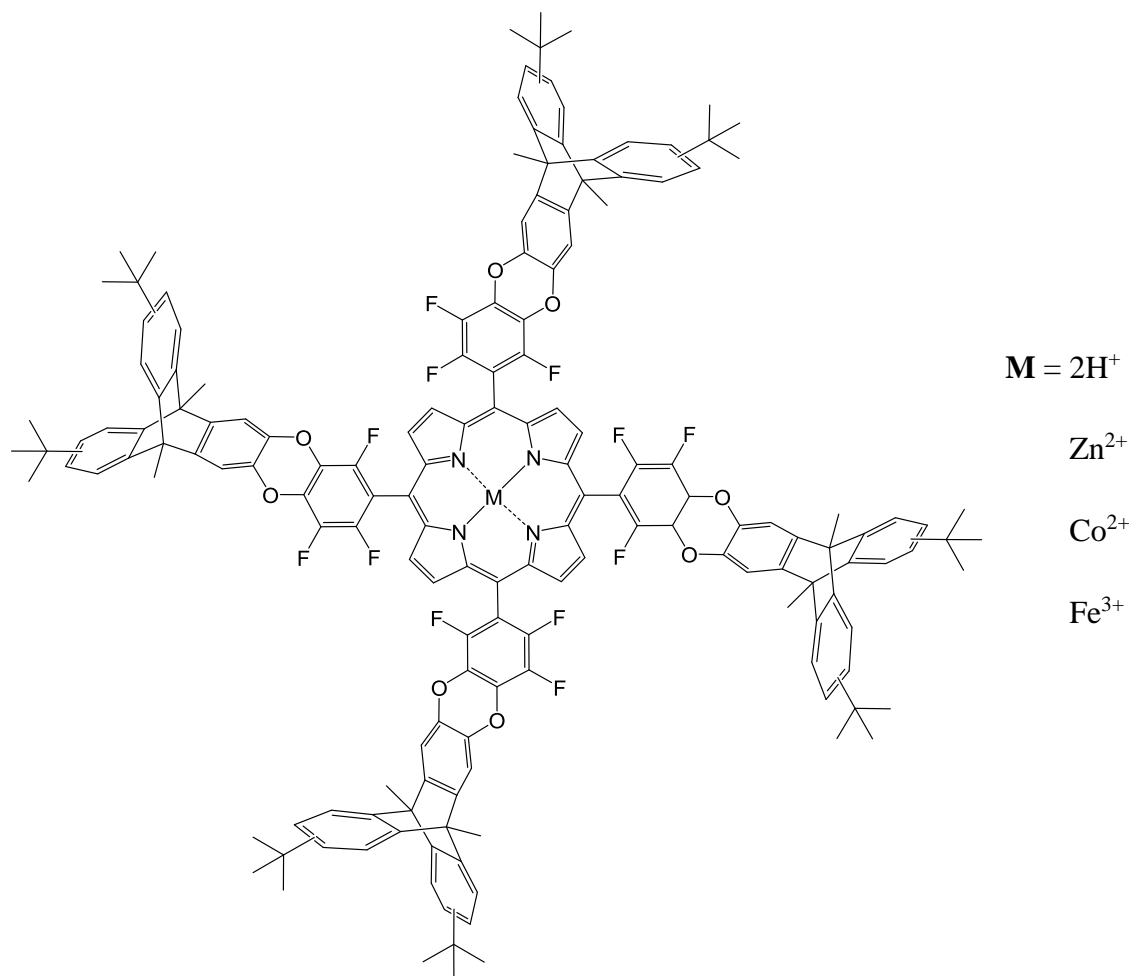
MPorph

5,10,15,20-Tetrakis(2,3,6-trifluoro-4,5-dioxytriptyceno(9,10-dimethyl)phenyl)porphyrin (H₂Porph1)

5,10,15,20-Tetrakis(2,3,4,5,6-pentafluorophenyl)porphyrin (0.088 g, 0.09 mmol), 2,3-dihydroxy-9,10-dimethyltriptycene (0.122 g, 0.39 mmol) and anhydrous potassium carbonate (0.32 g, 2.32 mmol) were stirred in anhydrous NMP (3.5 ml) under a nitrogen atmosphere at 100 °C for 18 hours. Upon cooling to room temperature, the mixture was poured into distilled water, filtered and dried. The crude product was further purified by stirring in methanol for a few hours and filtered to give **H₂Porph1** as a brown solid (0.15 g, 80 %). Mp > 300 °C; Elemental analysis (%) calcd. for C₁₃₂H₇₄N₄O₈F₁₂·2H₂O: C 75.21, H 3.73, N 2.66, F 10.81, found C 75.28, H 3.25, N 2.61, F 10.49; UV-vis (CHCl₃): λ_{max}, nm 418, 510, 544, 584, 634; IR (solid): ν, cm⁻¹ 2984, 2959, 1599, 1587, 1481, 1449, 1425, 1377, 1327, 1289, 1229, 1165, 1121, 1076, 1040, 1003, 920, 876, 829, 810, 783, 739, 633; ¹H NMR (250 MHz; CDCl₃): δ_H, ppm 8.96 (8H, s, ArH), 7.42 (16H, m, ArH), 7.21 (4H, s, ArH), 7.12 (20H, m, ArH), 2.48 (12H, s, CH₃), 2.41 (12H, s, CH₃), -2.93 (2H,

s, NH); ^{19}F NMR (282 MHz; CDCl_3): δ_{F} ppm -163.06 (4F, s, ArF), -140.32 (4F, s, ArF), -137.38 (4F, s, ArF); MS (MALDI-TOF): cluster centred at m/z 2090.1 (calcd. for $[\text{M}]^+$ 2071.5); BET surface area = $455 \text{ m}^2 \text{ g}^{-1}$; total pore volume = $0.90 \text{ cm}^3 \text{ g}^{-1}$ at $p/p^0 = 0.98$.

MPorph2



5,10,15,20-Tetrakis(2,3,6-trifluoro-4,5-dioxytrityceno(6,15-di-*tert*-butyl-9,10-dimethyl)phenyl)porphyrin ($\text{H}_2\text{Porph2}$)

5,10,15,20-Tetrakis(2,3,4,5,6-pentafluorophenyl)porphyrin (0.071 g, 0.07 mmol), 2,3-dihydroxy-6,15-di-*tert*-butyl-9,10-dimethyltritycene (0.133 g, 0.30 mmol) and anhydrous potassium carbonate (0.25 g, 1.8 mmol) were stirred in anhydrous NMP (3.5 ml) under a nitrogen atmosphere at $100 \text{ }^\circ\text{C}$ for 18 hours. Upon cooling to room temperature, the mixture was poured

into distilled water, filtered and dried. The crude product was further purified by stirring in methanol for a few hours and filtered to give **H₂Porph₂** as a brown solid (0.165 g, 92 %). Mp > 300 °C; Elemental analysis (%) calcd. for C₁₆₄H₁₃₈N₄O₈F₁₂·2H₂O: C 77.58, H 5.56, N 2.21, F 8.98, found C 77.23, H 4.94, N 1.89, F 8.28; UV-vis (CHCl₃): λ_{max}, nm 420, 508, 543, 585, 645; IR (solid): ν, cm⁻¹ 2984, 1491, 1474, 1452, 1425, 1325, 1306, 1231, 1167, 1078, 1042, 1005, 922, 883, 837, 775, 729, 646; ¹H NMR (250 MHz; CDCl₃): δ_H, ppm 8.95 (8H, s, ArH), 7.43 (8H, d, ³J_{HH} = 8.5 Hz, ArH), 7.35 (8H, m, ArH), 7.19 (4H, s, ArH), 7.11 (12H, m, ArH), 2.48 (12H, s, CH₃), 2.40 (12H, s, CH₃), 1.32 (72H, m, C(CH₃)₃), -2.93 (2H, s, NH); ¹⁹F NMR (282 MHz; CDCl₃): δ_F ppm -163.14 (4F, s, ArF), -140.42 (4F, s, ArF), -137.41 (4F, s, ArF); MS (MALDI-TOF): cluster centred at *m/z* 2520.1 (calcd. for [M]⁺ 2520.0); BET surface area = 531 m² g⁻¹; total pore volume = 0.97 cm³ g⁻¹ at *p/p*^o = 0.98.

5,10,15,20-Tetrakis(2,3,6-trifluoro-4,5-dioxytriptyceno(6,15-di-*tert*-butyl-9,10-dimethyl)phenyl)porphyrinatozinc (ZnPorph₂)

H₂Porph₂ (0.17 g, 0.07 mmol) and anhydrous zinc(II)acetate (0.26 g, 1.4 mmol) were heated in anhydrous NMP (3 ml) according to the general procedure (g). The crude product was further purified by stirring in methanol for a few hours and filtered to give **ZnPorph₂** as a red solid (0.15 g, 86 %). Mp > 300 °C; Elemental analysis (%) calcd. for C₁₆₄H₁₃₆N₄O₈F₁₂Zn·2H₂O: C 75.17, H 5.39, N 2.14, F 8.70, found C 74.75, H 4.95, N 2.16, F 8.37; UV-vis (CHCl₃): λ_{max}, nm 419, 544, 576; IR (solid): ν, cm⁻¹ 2965, 2955, 2361, 1597, 1472, 1454, 1414, 1377, 1364, 1325, 1306, 1231, 1167, 1117, 1072, 1055, 1005, 945, 883, 837, 806, 779, 729, 712, 648; ¹H NMR (250 MHz; C₇D₈): δ_H, ppm 9.16 (8H, s, ArH), 7.51 (8H, d, ³J_{HH} = 11.2 Hz, ArH), 7.21 (12H, m, ArH), 6.94 (4H, s, ArH), 6.87 (8H, m, ArH), 2.27 (12H, s, CH₃), 2.20 (12H, s, CH₃), 1.28 (72H, m, C(CH₃)₃); ¹⁹F NMR (282 MHz; C₇D₈): δ_F ppm -163.71 (4F, s, ArF), -140.80 (4F, s, ArF), -137.41 (4F, s, ArF); MS (MALDI-TOF): cluster centred at *m/z* 2584.9 (calcd. for [M]⁺ 2582.9); BET surface area = 595 m² g⁻¹; total pore volume = 0.99 cm³ g⁻¹ at *p/p*^o = 0.98.

5,10,15,20-Tetrakis(2,3,6-trifluoro-4,5-dioxytriptyceno(6,15-di-*tert*-butyl-9,10-dimethyl)phenyl)porphyrinatocobalt (CoPorph2)

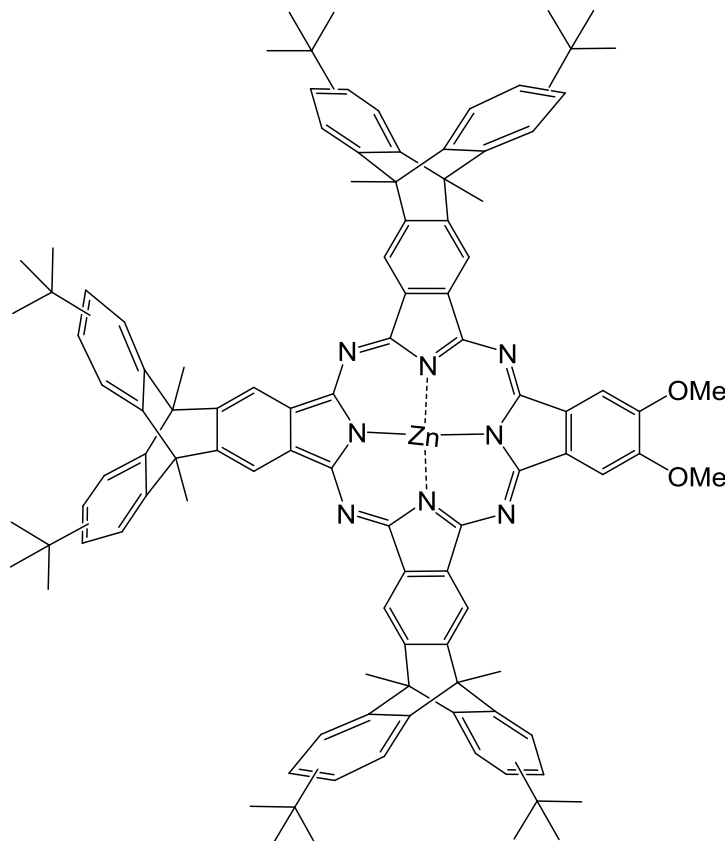
H₂Porph2 (0.17 g, 0.07 mmol) and anhydrous cobalt(II)acetate (0.25 g, 1.4 mmol) were heated in anhydrous NMP (3 ml) according to the general procedure (g). The crude product was further purified by stirring in methanol for a few hours and filtered to give **CoPorph2** as a red solid (0.12 g, 69 %). Mp > 300 °C; Elemental analysis (%) calcd. for C₁₆₄H₁₃₆N₄O₈F₁₂Co.2H₂O: C 75.36, H 5.40, N 2.14, F 8.72, found C 72.97, H 4.91, N 2.10, F 8.61; UV-vis (CHCl₃): λ_{max}, nm 410, 528, 560; IR (solid): ν, cm⁻¹ 2949, 2903, 1599, 1472, 1454, 1422, 1377, 1362, 1344, 1306, 1231, 1167, 1115, 1074, 1061, 1005, 947, 883, 837, 806, 781, 746, 729, 660, 646; MS (MALDI-TOF): cluster centred at *m/z* 2578.1 (calcd. for [M]⁺ 2577.0); BET surface area = 467 m² g⁻¹; total pore volume = 0.37 cm³ g⁻¹ at *p/p*^o = 0.98.

5,10,15,20-Tetrakis(2,3,6-trifluoro-4,5-dioxytriptyceno(6,15-di-*tert*-butyl-9,10-dimethyl)phenyl)porphyrinato iron (FePorph2)

H₂Porph2 (0.16 g, 0.06 mmol) and anhydrous iron(III)chloride (0.19 g, 1.2 mmol) were heated in anhydrous NMP (3 ml) according to the general procedure (g). The crude product was further purified by stirring in methanol for a few hours and filtered to give **FePorph2** as a black solid (0.10 g, 61 %). Mp > 300 °C; Elemental analysis (%) calcd. for C₁₆₄H₁₃₆N₄O₈F₁₂Fe: C 76.51, H 5.32, N 2.17, F 8.86, found C 73.54, H 4.90, N 2.17, F 8.72; UV-vis (CHCl₃): λ_{max}, nm 416, 504, 574, 636; IR (solid): ν, cm⁻¹ 2959, 1599, 1472, 1452, 1416, 1362, 1325, 1304, 1231, 1165, 1115, 1074, 1055, 1005, 945, 883, 835, 773, 745, 727, 716, 673, 658; MS (MALDI-TOF): cluster centred at *m/z* 2574.6 (calcd. for [M]⁺ 2574.0); BET surface area = 506 m² g⁻¹; total pore volume = 0.42 cm³ g⁻¹ at *p/p*^o = 0.98.

Unsymmetric phthalocyanines (3:1 isomers)

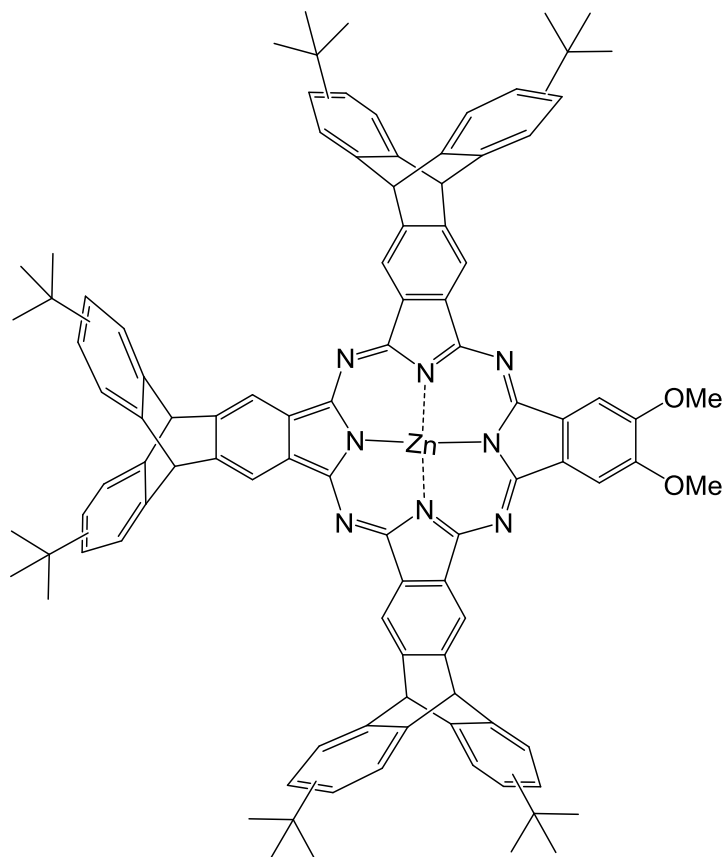
2,3-*o*-Benzenedimethoxy-7,8,12,13,17,18-tri(6,15-di-*tert*-butyl-9,10-dimethyltriptyceno) porphyrazinato zinc



A mixture of 2,3-dicyano-6,15-di-*tert*-butyl-9,10-dimethyltriptycene (1 g, 2.25 mmol), 4,5-dimethoxyphthalonitrile (0.06 g, 0.32 mmol) and zinc(II)acetate (0.41 g, 2.23 mmol) were stirred in anhydrous NMP according to the general procedure (h). Column chromatography on silica eluting with hexane:DCM (1:1) gave firstly a green fraction which was found to be the symmetric **ZnPz2** from MALDI-MS analysis. (Yield: 0.38 g, (37%); MS (MALDI-TOF): cluster centred at m/z 1841.5 (calcd. for $[M]^+$ 1842.0)). Further elution using hex:DCM:EtOAc (7:2:1) gave second fraction which was found to be the desired product **2,3-*o*-benzenedimethoxy-7,8,12,13,17,18-tri(6,15-di-*tert*-butyl-9,10-dimethyltriptyceno) porphyrazinato zinc** isolated as a green solid (0.07 g, 14 %). Mp > 300 °C; UV-vis (CHCl_3): λ_{max} , nm 680, 648, 614, 394, 344; IR (solid): ν , cm^{-1} 2944, 1738, 1603, 1539, 1456, 1395, 1375, 1362, 1269, 1229, 1217, 1144,

1101, 1082, 1063, 1038, 974, 887, 824, 748; $^1\text{H NMR}$ (400 MHz; CDCl_3): δ_{H} , ppm 8.62 (6H, s, ArH), 8.50 (2H, s, ArH), 7.51 (6H, br s, ArH), 7.40 (6H, br m, ArH), 7.08 (6H, br m, ArH), 4.05 (6H, br s, OCH_3), 2.85 (6H, br s, CH_3), 1.18 (54H, m, $\text{C}(\text{CH}_3)_3$); MS (MALDI-TOF): cluster centred at m/z 1585.8 (calcd. for $[\text{M}]^+$ 1586.8).

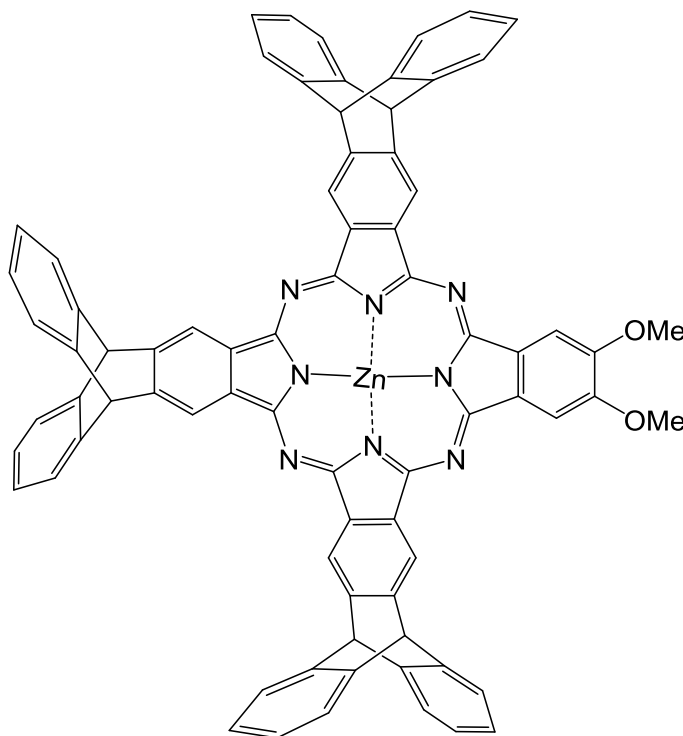
2,3-*o*-Benzenedimethoxy-7,8,12,13,17,18-tri(6,15-di-*tert*-butyltritypceno)porphyrinato zinc



A mixture of 2,3-dicyano-6,15-di-*tert*-butyltritypcene (1 g, 2.4 mmol), 4,5-dimethoxyphthalonitrile (0.065 g, 0.35 mmol) and zinc(II)acetate (0.44 g, 2.4 mmol) were stirred in anhydrous NMP (3.5 ml) according to the general procedure (h). Column chromatography on silica eluting with hexane:DCM:EtOAc (7:2:1) gave firstly a green fraction which was found to be the symmetric **ZnPz1** from MALDI-MS analysis. (Yield 0.40 g (38 %); MS (MALDI-TOF): cluster centred at m/z 1730.7 (calcd. for $[\text{M}]^+$ 1730.8)). Upon increasing the polarity of the eluent with DCM and EtOAc, the desired product **2,3-*o*-benzenedimethoxy-7,8,12,13,17,18-tri(6,15-**

di-tert-butyltritypceno)porphyrazinato zinc was isolated as a green solid (0.09 g, 17 %). Mp > 300 °C; UV-vis (CHCl₃): λ_{max} , nm 680, 648, 612, 384, 344; IR (solid): ν , cm⁻¹ 2959, 2953, 1772, 1734, 1713, 1607, 1479, 1464, 1395, 1362, 1325, 1277, 1263, 1207, 1123, 1088, 1061, 1024, 982, 932, 887, 837, 745; ¹H NMR (400 MHz; C₇D₈): δ_{H} , ppm 9.92 (6H, br s, ArH), 9.60 (2H, br s, ArH), 7.82 (6H, br s, ArH), 7.58 (6H, br m, ArH), 7.15 (6H, m, ArH), 6.10 (6H, br s, CH), 3.68 (6H, br s, OCH₃), 1.21 (54H, br s, C(CH₃)₃); MS (MALDI-TOF): clusters centred at m/z 1502.3 (calcd. for [M]⁺ 1502.7) and 3006.8 (calcd. for [M₂]⁺ 3005.3).

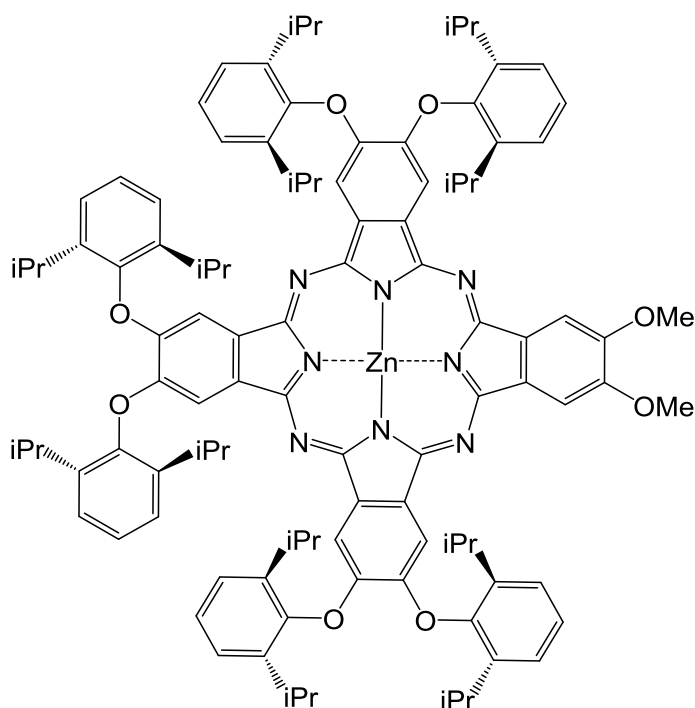
2,3-*o*-Benzenedimethoxy-7,8,12,13,17,18-tri(tritypceno)porphyrazinato zinc



A mixture of 2,3-dicyanotriptycene (1.27 g, 4.17 mmol), 4,5-dimethoxyphthalonitrile (0.11 g, 0.58 mmol) and zinc(II)acetate (0.77 g, 4.17 mmol) were stirred in anhydrous NMP (3.5 ml) according to the general procedure (h). Column chromatography on silica eluting with hexane:DCM:EtOAc (7:2:1) gave firstly a green fraction which was found to be the symmetric 2,3,7,8,12,13,17,18-octa-tritypceno zinc porphyrazine from MALDI-MS analysis. (Yield 0.45 g (34 %); MS (MALDI-TOF): cluster centred at m/z 1282.1 (calcd. for [M]⁺ 1281.3)). Upon

increasing the polarity of the eluent with DCM and EtOAc, the desired product **2,3-*o*-benzenedimethoxy-7,8,12,13,17,18-tri(triptyceno)porphyrazinato zinc** was isolated as a green solid (0.078 g, 11 %). Mp > 300 °C; UV-vis (CHCl₃): λ_{max}, nm 680, 612, 376, 344; IR (film): ν, cm⁻¹ 2960, 1636, 1490, 1458, 1396, 1346, 1275, 1134, 1084, 1060, 1023, 858, 794, 748; ¹H NMR (400 MHz; DMSO-*d*₆): δ_H, ppm 9.50 (6H, m, ArH), 8.90 (2H, s, ArH), 7.69 (12H, m, ArH), 7.11 (12H, br s, ArH), 6.35 (6H, m, CH), 4.38 (6H, s, OCH₃); MS (MALDI-TOF): cluster centred at *m/z* 1166.1 (calcd. for [M]⁺ 1166.6).

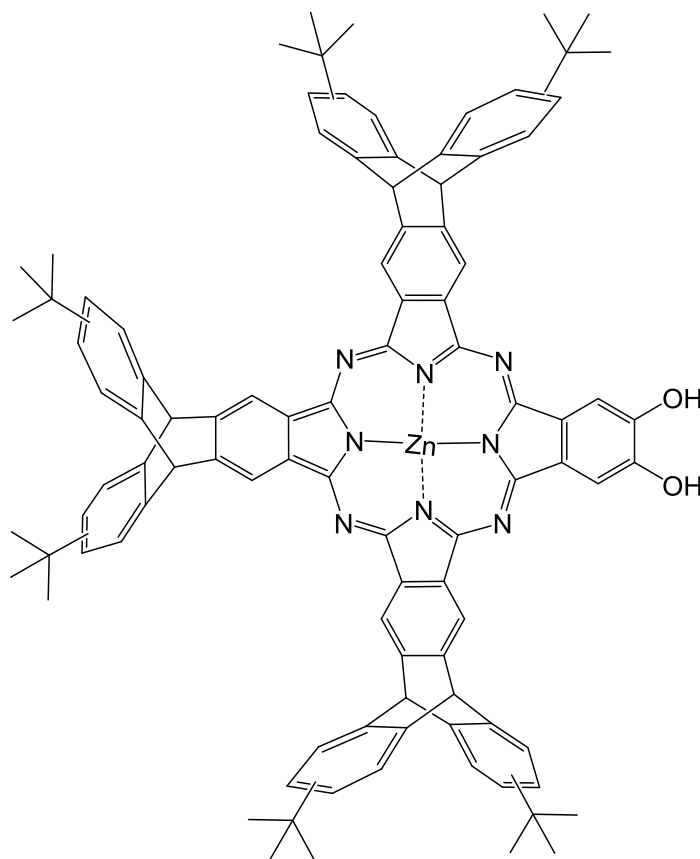
2,3-Dimethoxy-9,10,16,17,23,24-hexa(2',6'-di-*iso*-propylphenoxy)phthalocyaninato zinc



A mixture of 4,5-di(2,6-di-*iso*-propylphenoxy)phthalonitrile (3.45 g, 7.18 mmol), 4,5-dimethoxyphthalonitrile (0.19 g, 1.0 mmol) and zinc(II)acetate (1.3 g, 7.09 mmol) were stirred in anhydrous NMP (7 ml) according to the general procedure (h). Column chromatography on silica eluting with DCM:hexane (6:4) gave firstly a green fraction which was found to be the symmetric 2,3,9,10,16,17,23,24-octa(2',6'-di-*iso*-propylphenoxy)phthalocyaninato zinc from MALDI-MS analysis. (Yield 1.65 g (46 %); MS (MALDI-TOF): cluster centred at *m/z* 1987.1 (calcd. for [M]⁺ 1986.0)). Upon eluting with DCM and then DCM:MeOH (9:1), the desired

product **2,3-dimethoxy-9,10,16,17,23,24-hexa(2',6'-di-*iso*-propylphenoxy)phthalocyaninato zinc** was isolated as a green solid (0.2 g, 12 %). Mp > 300 °C; UV-vis (CHCl₃): λ_{max} , nm 682, 648, 614, 418, 342; IR (film): ν , cm⁻¹ 3070, 2963, 2869, 1610, 1493, 1460, 1399, 1345, 1329, 1270, 1185, 1095, 1026, 894, 854, 797, 775, 726; ¹H NMR (400 MHz; CDCl₃) δ_{H} , ppm 8.61 (2H, s, ArH), 8.40 (2H, s, ArH), 8.25 (2H, s, ArH), 8.22 (2H, s, ArH), 7.65 – 7.58 (4H, m, ArH), 7.51 (8H, m, ArH), 7.44 (6H, br s, ArH), 4.30 (6H, s, OCH₃), 3.52 (12H, sept, ³J_{HH} = 6.9 Hz, (CH₃)₂CH), 1.27 (72H, br s, (CH₃)₂CH); MS (MALDI-TOF): cluster centred at m/z 1694.0 (calcd. for [M]⁺ 1694.8).

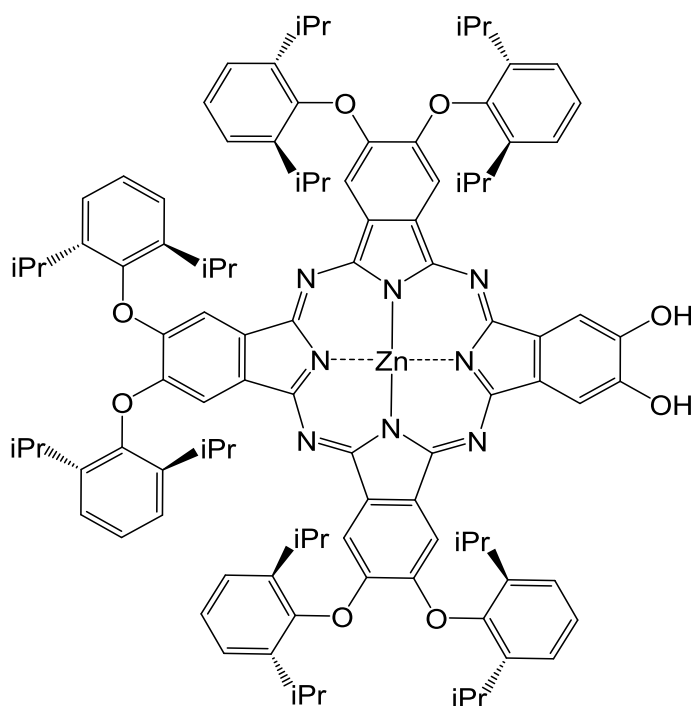
2,3-*o*-Benzenediol-7,8,12,13,17,18-tri(6,15-di-*tert*-butyltriptyceno)porphyrinato zinc



To a solution of 2,3-*o*-benzenedimethoxy-7,8,12,13,17,18-tri(6,15-di-*tert*-butyltriptyceno)porphyrinato zinc (0.3 g, 0.2 mmol) in DCM (30 ml) at 0 °C under a nitrogen atmosphere, BBr₃ (0.1 ml, 1.04 mmol) was added. The reaction mixture was then stirred for 6 h at RT and monitored by TLCs and MALDI. Upon completion, the reaction was quenched with

water and the product extracted with DCM. The organic extracts were combined, washed with sodium dithionite solution, dried over MgSO_4 and solvent evaporated. The obtained solid was stirred in a minimum amount of methanol and filtered to **2,3-*o*-benzenediol-7,8,12,13,17,18-tri(6,15-di-*tert*-butyltriptyceno)porphyrazinato zinc** as a green solid (0.27 g, 92 %). Mp > 300 °C; UV-vis (CHCl_3): λ_{max} , nm 721 (br), 380; IR (solid): ν , cm^{-1} 3399, 2951, 1709, 1605, 1481, 1460, 1412, 1362, 1346, 1310, 1263, 1202, 1167, 1098, 1076, 1020, 930, 887, 829, 793, 746; ^1H NMR (250 MHz; $\text{DMSO-}d_6$): δ_{H} , ppm 9.45 (6H, s, *ArH*), 9.02 (2H, br s, *ArH*), 7.33 – 7.70 (12H, br m, *ArH*), 7.01 (6H, br m, *ArH*), 6.12 (6H, br s, *CH*), 4.48 (6H, br s, *OCH}_3*), 1.20 (54H, s, $\text{C}(\text{CH}_3)_3$); MS (MALDI-TOF): cluster centred at m/z 1474.6 (calcd. for $[\text{M}]^+$ 1474.6).

2,3-Dihydroxy-9,10,16,17,23,24-hexa(2',6'-di-*iso*-propylphenoxy)phthalocyaninato zinc



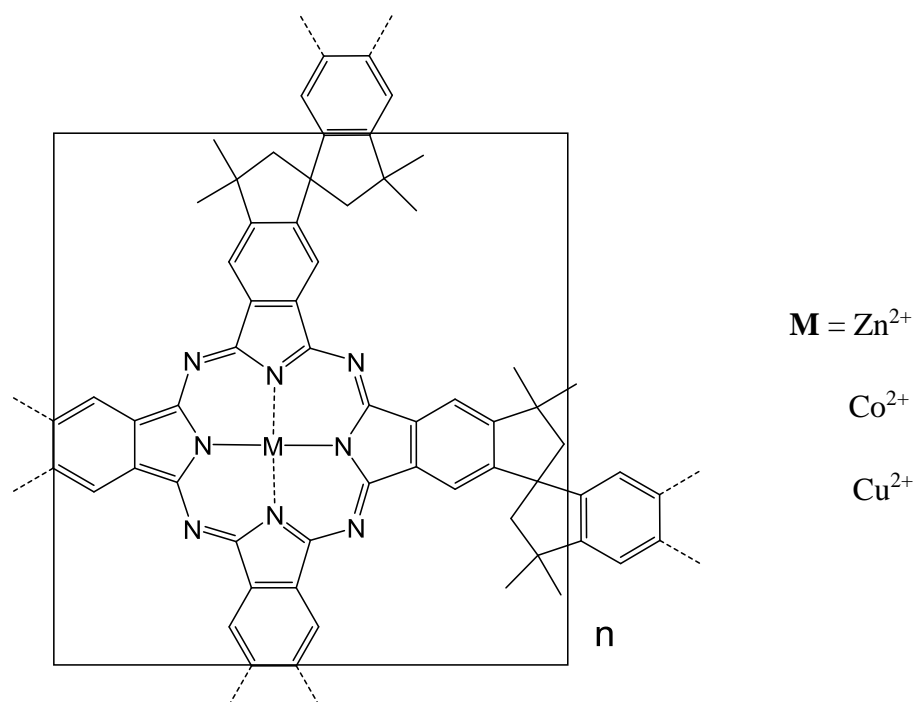
To a solution of 2,3-dimethoxy-9,10,16,17,23,24-hexa(2',6'-di-*iso*-propylphenoxy)phthalocyaninato zinc (0.17 g, 0.1 mmol) in DCM (20 ml) at 0 °C under a nitrogen atmosphere, BBr_3 (0.05 ml, 0.52 mmol) was added. The reaction mixture was then stirred for 8 h at RT and monitored by TLCs and MALDI. Upon completion, the reaction was quenched with water and the product extracted with DCM. The organic extracts were combined, washed with water, dried over MgSO_4 and solvent evaporated to give **2,3-dihydroxy-**

9,10,16,17,23,24-hexa(2',6'-di-*iso*-propylphenoxy)phthalocyaninato zinc as a green solid (0.15 g, 90 %). Mp > 300 °C; UV-vis (CHCl₃): λ_{max} , nm 700 (br), 386, 346; IR (solid): ν , cm⁻¹ 2961, 2868, 1607, 1439, 1397, 1325, 1258, 1246, 1177, 1157, 1088, 1072, 978, 963, 934, 870, 831, 791, 737; ¹H NMR (250 MHz; CDCl₃): δ_{H} , ppm 8.0 – 8.39 (8H, br m, ArH), 7.28 – 7.59 (18H, br m, ArH), 3.20 (12H, br m, (CH₃)₂CH), 1.19 (72H, br s, (CH₃)₂CH); MS (MALDI-TOF): cluster centred at m/z 1666.8 (calcd. for [M]⁺ 1666.8).

6.5 Synthesis of Pc and porphyrin based network polymers

Pc-based network polymers from the cyclotetramerisation of bis- and tris- phthalonitriles

SBI-MPc-Net-PIM (from tetraCN-SBI)



SBI-ZnPc-Net-PIM

5,5',6,6'-Tetracyano-3,3,3',3'-tetramethyl-1,1'-spirobisindane (0.7 g, 1.86 mmol) and anhydrous zinc(II)acetate (0.34 g, 1.86 mmol) were reacted in quinoline (3.5 ml) according to the general procedure (i). The solid was purified by refluxing in a range of solvents: THF, acetone and methanol over a few days and filtered off to give **SBI-ZnPc-Net-PIM** as a green powder (0.74 g, 97 %). UV-vis (DMF): λ_{max} , nm 682; IR (solid): ν , cm^{-1} 2953, 1728, 1641, 1601, 1443, 1395, 1362, 1335, 1306, 1275, 1233, 1196, 1107, 1072, 1020, 980, 895, 841, 762, 748, 689, 656; BET surface area = $577\ m^2\ g^{-1}$; total pore volume = $0.35\ cm^3\ g^{-1}$ at $p/p^0 = 0.98$; TGA (nitrogen): Initial weight loss due to thermal degradation commences at $\sim 454\ ^\circ C$.

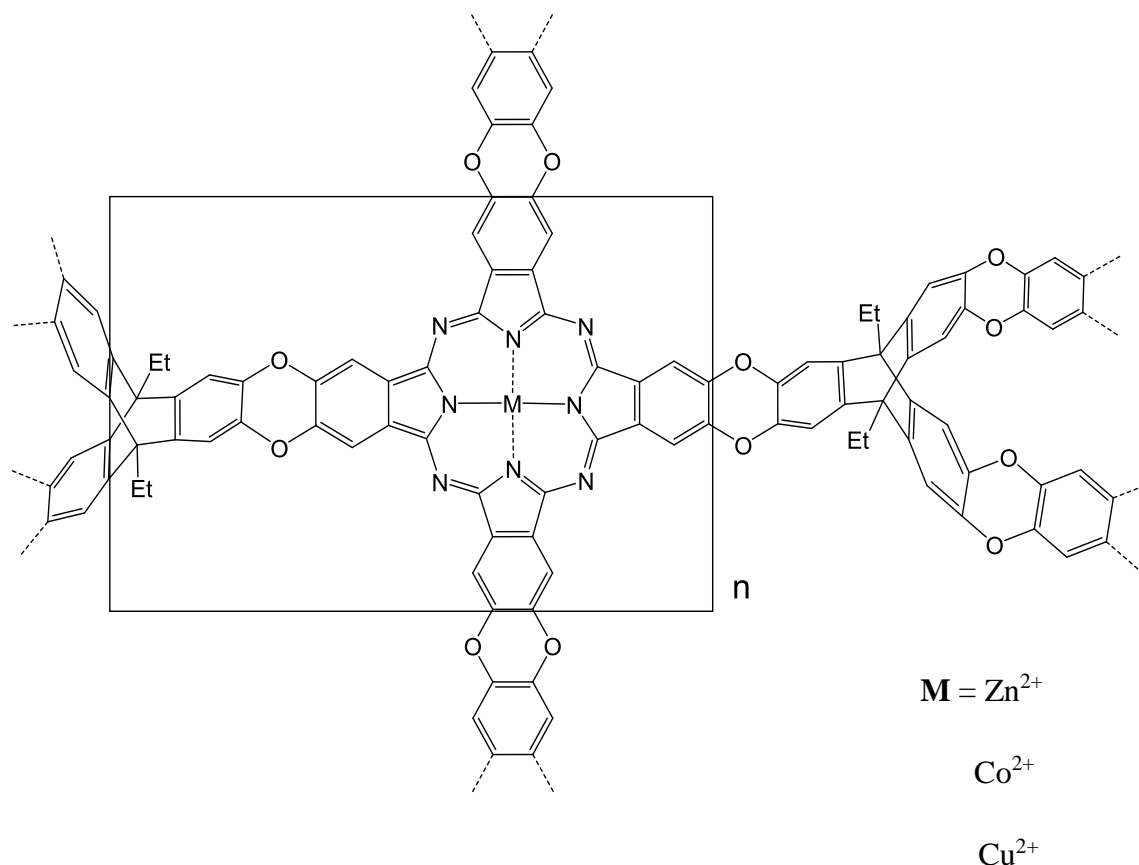
SBI-CoPc-Net-PIM

5,5',6,6'-Tetracyano-3,3,3',3'-tetramethyl-1,1'-spirobisindane (0.7 g, 1.86 mmol) and anhydrous cobalt(II)acetate (0.33 g, 1.86 mmol) were reacted in quinoline (3.5 ml) according to the general procedure (i). The solid was purified by refluxing in a range of solvents: THF, acetone and methanol over a few days and filtered off to give **SBI-CoPc-Net-PIM** as a green powder (0.73 g, 97 %). UV-vis (DMF): λ_{\max} , nm 676; IR (solid): ν , cm^{-1} 2955, 2859, 1767, 1726, 1710, 1593, 1441, 1410, 1364, 1310, 1279, 1235, 1132, 1078, 1030, 897, 758, 746, 681, 637; BET surface area = $377 \text{ m}^2 \text{ g}^{-1}$; total pore volume = $0.23 \text{ cm}^3 \text{ g}^{-1}$ at $p/p^o = 0.98$; TGA (nitrogen): Initial weight loss due to thermal degradation commences at $\sim 424 \text{ }^\circ\text{C}$.

SBI-CuPc-Net-PIM

5,5',6,6'-Tetracyano-3,3,3',3'-tetramethyl-1,1'-spirobisindane (0.61 g, 1.62 mmol) and anhydrous copper(II)acetate (0.30 g, 1.65 mmol) were reacted in quinoline (3.5 ml) according to the general procedure (i). The solid was purified by refluxing in a range of solvents: THF, acetone and methanol over a few days and filtered off to give **SBI-CuPc-Net-PIM** as a green powder (0.64 g, 97 %). UV-vis (DMF): λ_{\max} , nm 672; IR (solid): ν , cm^{-1} 2953, 1736, 1728, 1589, 1443, 1364, 1310, 1229, 1202, 1163, 1080, 999, 897, 829, 797, 760, 729, 696, 669, 619; BET surface area = $352 \text{ m}^2 \text{ g}^{-1}$; total pore volume = $0.28 \text{ cm}^3 \text{ g}^{-1}$ at $p/p^o = 0.98$; TGA (nitrogen): Initial weight loss due to thermal degradation commences at $\sim 428 \text{ }^\circ\text{C}$.

Hexa-oxy-diethyl-triptyceno-MPc-Net-PIM (from 2,3,6,7,14,15-tris(dioxinphthalonitrile)-9,10-diethyltriptycene)



Hexa-oxy-diethyl-triptyceno-ZnPc-Net-PIM

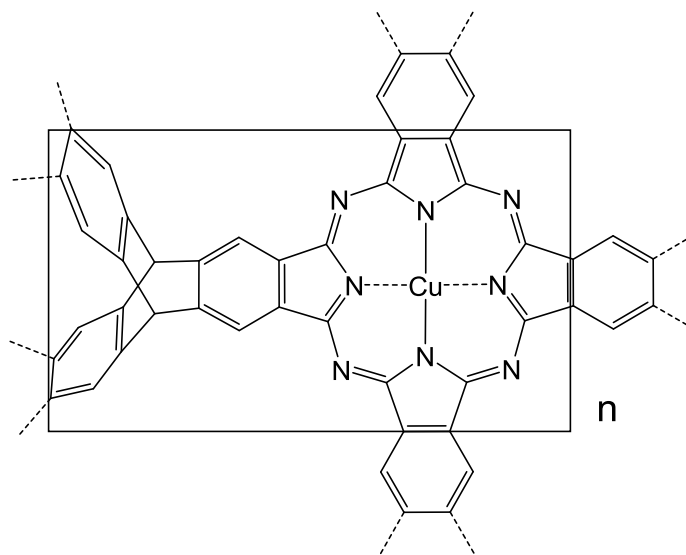
2,3,6,7,14,15-Tris(dioxinphthalonitrile)-9,10-diethyltriptycene (0.7 g, 0.90 mmol) and anhydrous zinc(II)acetate (0.17 g, 0.92 mmol) were reacted in quinoline (3.5 ml) according to the general procedure (i). The solid was purified by refluxing in a range of solvents: THF, acetone and methanol over a few days and filtered off to give **hexa-oxy-diethyl-triptyceno-ZnPc-Net-PIM** as a green powder (0.71 g, 96 %). UV-vis (1-chloronaphthalene): λ_{max} , nm 702; IR (solid): ν , cm^{-1} 1775, 1726, 1593, 1464, 1402, 1362, 1314, 1287, 1188, 1144, 1090, 1040, 986, 922, 885, 841, 818, 758, 746, 727, 692, 671, 640; BET surface area = $343\ m^2\ g^{-1}$; total pore volume = $0.51\ cm^3\ g^{-1}$ at $p/p^o = 0.98$; TGA (nitrogen): Initial weight loss due to thermal degradation commences at $\sim 350\ ^\circ C$.

Hexa-oxy-diethyl-triptyceno-CoPc-Net-PIM

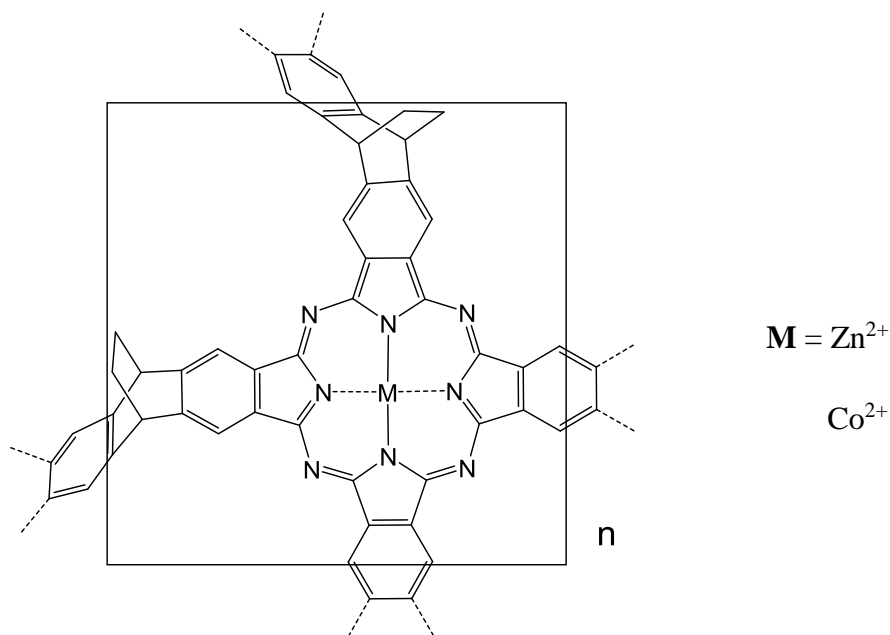
2,3,6,7,14,15-Tris(dioxinphthalonitrile)-9,10-diethyltriptycene (0.61 g, 0.78 mmol) and anhydrous cobalt(II)acetate (0.14 g, 0.79 mmol) were reacted in quinoline (3.5 ml) according to the general procedure (i). The solid was purified by refluxing in a range of solvents: THF, acetone and methanol over a few days and filtered off to give **hexa-oxy-diethyl-triptyceno-CoPc-Net-PIM** as a green powder (0.60 g, 94 %). UV-vis (1-chloronaphthalene): λ_{\max} , nm 686; IR (solid): ν , cm^{-1} 1775, 1740, 1591, 1466, 1412, 1360, 1316, 1289, 1184, 1146, 1096, 1051, 988, 926, 889, 847, 816, 781, 752, 704, 669; BET surface area = $88 \text{ m}^2 \text{ g}^{-1}$; total pore volume = $0.17 \text{ cm}^3 \text{ g}^{-1}$ at $p/p^o = 0.98$; TGA (nitrogen): Initial weight loss due to thermal degradation commences at $\sim 322 \text{ }^\circ\text{C}$.

Hexa-oxy-diethyl-triptyceno-CuPc-Net-PIM

2,3,6,7,14,15-Tris(dioxinphthalonitrile)-9,10-diethyltriptycene (0.45 g, 0.58 mmol) and anhydrous copper(II)acetate (0.11 g, 0.61 mmol) were reacted in quinoline (3.5 ml) according to the general procedure (i). The solid was purified by refluxing in a range of solvents: THF, acetone and methanol over a few days and filtered off to give **hexa-oxy-diethyl-triptyceno-CuPc-Net-PIM** as a green powder (0.47 g, 98 %). UV-vis (1-chloronaphthalene): λ_{\max} , nm 716; IR (solid): ν , cm^{-1} 1778, 1726, 1593, 1464, 1408, 1360, 1314, 1285, 1186, 1161, 1092, 1045, 986, 932, 883, 839, 752, 689, 637; BET surface area = $585 \text{ m}^2 \text{ g}^{-1}$; total pore volume = $0.81 \text{ cm}^3 \text{ g}^{-1}$ at $p/p^o = 0.98$; TGA (nitrogen): Initial weight loss due to thermal degradation commences at $\sim 337 \text{ }^\circ\text{C}$.

Triptyceno-CuPc-Net-PIM (from hexaBrTrip)

To a mixture of 2,3,6,7,14,15-hexabromotriptycene (2 g, 2.75 mmol) in anhydrous DMF (~ 25 ml) at 61 °C under a nitrogen atmosphere, copper cyanide (4.93 g, 55 mmol) was added and the mixture stirred under reflux for 72 hours. The solidified reaction mixture was then cooled to room temperature, poured into conc. ammonia, stirred for an hour and filtered. The solid was purified by refluxing in a range of solvents: THF, acetone and methanol over a few days and filtered off to give **triptyceno-CuPc-Net-PIM** as a bright green powder (1.2 g, 97 %). UV-vis (1-chloronaphthalene): λ_{max} , nm 732; IR (solid): ν , cm^{-1} 1761, 1715, 1586, 1559, 1503, 1454, 1398, 1354, 1321, 1244, 1152, 1092, 1017, 903, 746, 716, 646; BET surface area = $436 \text{ m}^2 \text{ g}^{-1}$; total pore volume = $0.25 \text{ cm}^3 \text{ g}^{-1}$ at $p/p^{\circ} = 0.98$; TGA (nitrogen): Initial weight loss due to thermal degradation commences at ~ 300 °C.

EA-MPc-Net-PIM (from tetraCN-EA)**EA-ZnPc-Net-PIM**

2,3,6,7-Tetracyano-9,10-dihydro-9,10-ethanoanthracene (0.7 g, 2.29 mmol) and anhydrous zinc(II)acetate (0.42 g, 2.29 mmol) were reacted in quinoline (3.5 ml) according to the general procedure (i). The solid was purified by refluxing in a range of solvents: THF, acetone and methanol over a few days and filtered off to give **EA-ZnPc-Net-PIM** as a green powder (0.76 g, 99 %). UV-vis (1-chloronaphthalene): λ_{max} , nm 724; IR (solid): ν , cm^{-1} 1713, 1537, 1452, 1393, 1366, 1316, 1256, 1161, 1140, 1084, 1007, 899, 883, 745, 638; BET surface area = $511\ m^2\ g^{-1}$; total pore volume = $0.26\ cm^3\ g^{-1}$ at $p/p^o = 0.98$; TGA (nitrogen): Initial weight loss due to thermal degradation commences at $\sim 285\ ^\circ C$.

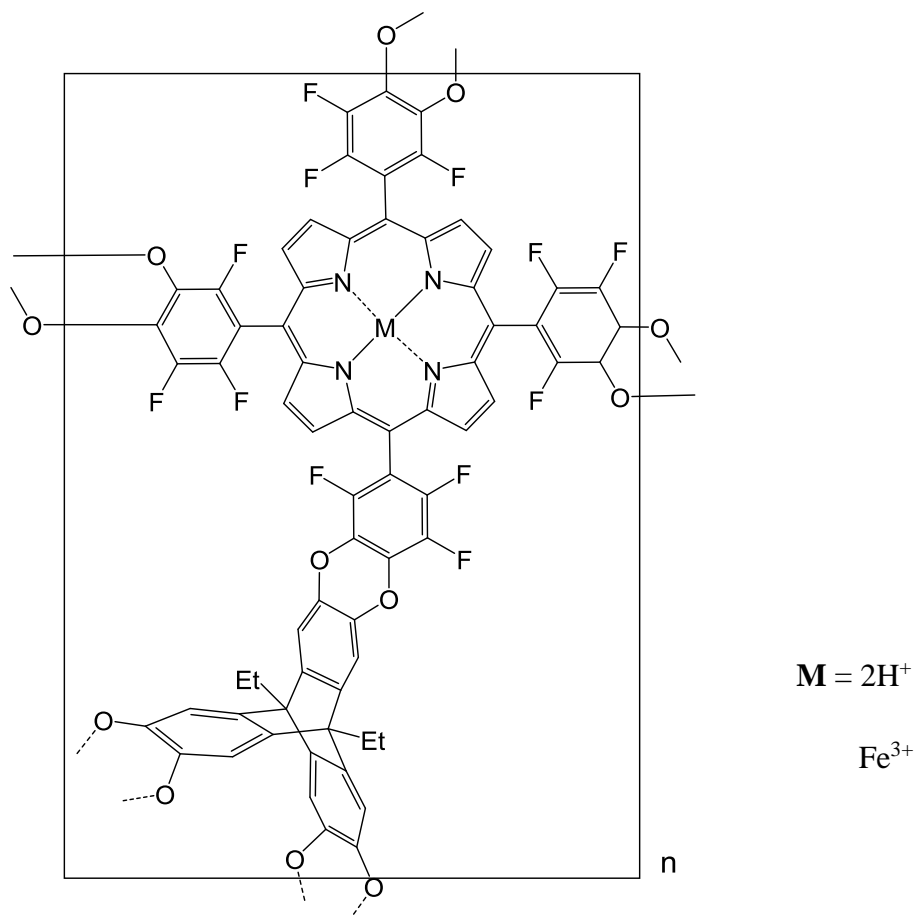
EA-CoPc-Net-PIM

2,3,6,7-Tetracyano-9,10-dihydro-9,10-ethanoanthracene (0.45 g, 1.47 mmol) and anhydrous cobalt(II)acetate (0.26 g, 1.47 mmol) were reacted in quinoline (3.5 ml) according to the general procedure (i). The solid was purified by refluxing in a range of solvents: THF, acetone and methanol over a few days and filtered off to give **EA-CoPc-Net-PIM** as a green powder (0.49 g, 99 %). UV-vis (1-chloronaphthalene): λ_{max} , nm 682; IR (solid): ν , cm^{-1} 2947, 1761, 1717, 1593,

1574, 1410, 1370, 1335, 1202, 1146, 1098, 909, 845, 750, 667; BET surface area = $462 \text{ m}^2 \text{ g}^{-1}$; total pore volume = $0.57 \text{ cm}^3 \text{ g}^{-1}$ at $p/p^o = 0.98$; TGA (nitrogen): Initial weight loss due to thermal degradation commences at $\sim 285 \text{ }^\circ\text{C}$.

Porph and Pc-based network polymers from fluorinated precursors

MPorph-Net-PIMs



H₂Porph-Net-PIM

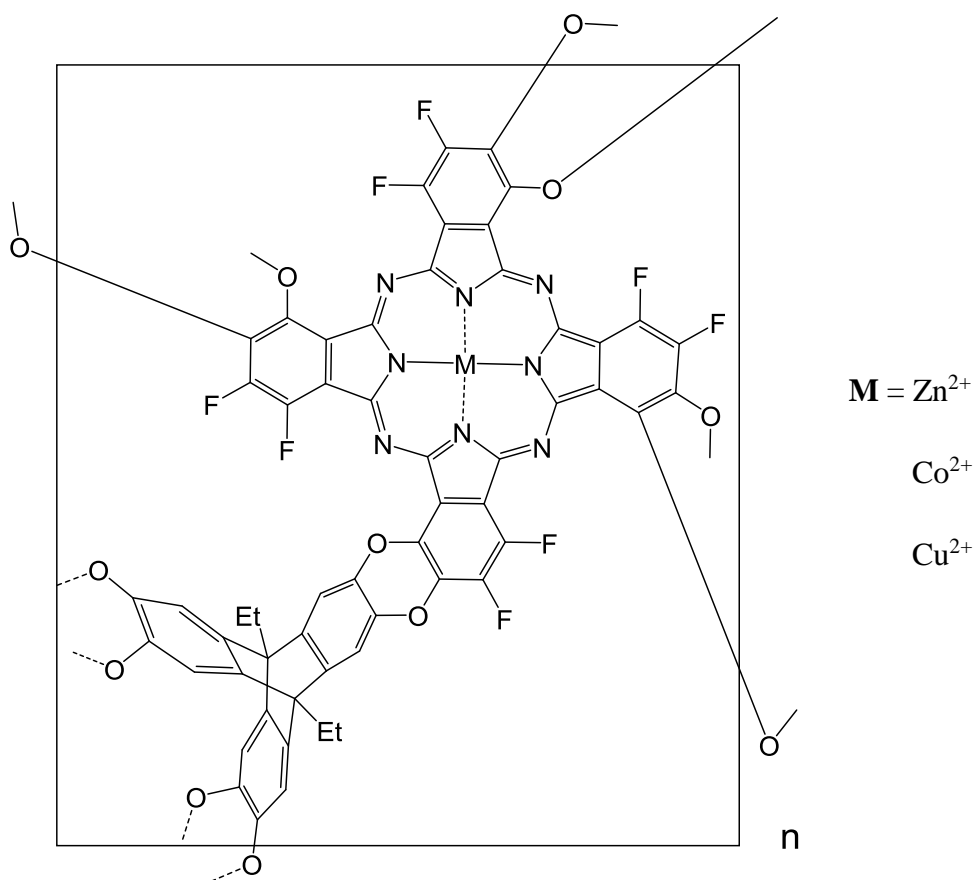
5,10,15,20-Tetrakis(2,3,4,5,6-pentafluorophenyl)porphyrin (0.11 g, 0.11 mmol), 2,3,6,7,14,15-hexahydroxy-9,10-diethyltriptycene (0.061 g, 0.15 mmol) and anhydrous potassium carbonate (0.17 g, 1.23 mmol) were stirred in anhydrous NMP (3.5 ml) under a nitrogen atmosphere at 180 °C. Within a few minutes, the reaction mixture turned solid. After ~ 18 hours, the reaction was cooled to room temperature, poured into distilled water, filtered and dried. The solid was purified by refluxing in a range of solvents: THF, acetone and methanol over a few days and filtered off to give **Tetra-triptyceno-H₂PorphNetPIM** as a purple solid (0.15 g, 98 %). Elemental analysis

(%) calcd. for $C_{76}H_{31}N_4O_8F_{12}$: C 67.30, H 2.33, N 4.13, F 16.81, found C 61.79, H 2.83, N 3.65, F 14.27; UV-vis (1-chloronaphthalene): λ_{max} , nm 412; IR (solid): ν , cm^{-1} 2959, 1738, 1643, 1589, 1454, 1395, 1373, 1343, 1277, 1233, 1202, 1126, 1042, 1003, 970, 920, 870, 856, 799, 773, 737, 714, 702, 667, 631; BET surface area = $1028\text{ m}^2\text{ g}^{-1}$; total pore volume = $0.57\text{ cm}^3\text{ g}^{-1}$ at $p/p^o = 0.98$; TGA (nitrogen): Initial weight loss due to thermal degradation commences at $\sim 330\text{ }^\circ\text{C}$.

FePorph-Net-PIM

Tetra-triptyceno- H_2 PorphNetPIM (0.197 g, 0.145 mmol) and anhydrous iron(III)chloride (0.47 g, 2.9 mmol) were stirred in anhydrous NMP (3.5 ml) at $140\text{ }^\circ\text{C}$ for 24 hrs. Upon cooling to room temperature, the mixture was poured into distilled water, filtered and dried. The solid was purified by refluxing in a range of solvents: THF, acetone and methanol over a few days and filtered off to give **Tetra-triptyceno-FePorphNetPIM** as a purple solid (0.183 g, 89 %). Elemental analysis (%) calcd. for $C_{76}H_{29}N_4O_8F_{12}Fe$: C 64.74, H 2.07, N 3.97, F 16.17, Fe 3.96, found C 56.91, H 2.10, N 4.12, F 17.36, Fe 2.86; UV-vis (1-chloronaphthalene): λ_{max} , nm 412; IR (solid): ν , cm^{-1} 1701, 1655, 1638, 1593, 1485, 1464, 1420, 1331, 1298, 1256, 1208, 1165, 1076, 1057, 1005, 976, 943, 870, 799, 772, 727, 710, 662, 642; BET surface area = $867\text{ m}^2\text{ g}^{-1}$; total pore volume = $0.46\text{ cm}^3\text{ g}^{-1}$ at $p/p^o = 0.98$; TGA (nitrogen): Initial weight loss due to thermal degradation commences at $\sim 317\text{ }^\circ\text{C}$.

OctaF-Trip-MPc-NetPIMs



OctaF-Trip-ZnPc-NetPIM

Zinc(II) 1,2,3,4,8,9,10,11,15,16,17,18,22,23,24,25-hexadecafluoro-29*H*,31*H* phthalocyanine (0.15 g, 0.17 mmol), 2,3,6,7,14,15-hexahydroxy-9,10-diethyltriptycene (0.094 g, 0.23 mmol) and anhydrous potassium carbonate (0.28 g, 2.04 mmol) were reacted in anhydrous NMP (3.5 ml) according to the general procedure (j). The solid was purified by refluxing in a range of solvents: THF, acetone and methanol over a few days and filtered off to give **Tetra-trip-octa-fluoroZnPcNetPIM** as a black solid (0.21 g, 97 %). Elemental analysis (%) calcd. for $C_{64}H_{21}N_8O_8F_8Zn$: C 61.60, H 1.70, N 8.98, F 12.18, found C 56.67, H 3.07, N 8.46, F 6.22; UV-vis (1-chloronaphthalene): λ_{max} , nm 686; IR (solid): ν , cm^{-1} 2979, 1730, 1439, 1358, 1223, 1211, 1139, 1041, 975, 869, 798, 720, 635; BET surface area = $482\ m^2\ g^{-1}$; total pore volume = $0.25\ cm^3\ g^{-1}$ at $p/p^o = 0.98$; TGA (nitrogen): Initial weight loss due to thermal degradation commences at $\sim 329\ ^\circ C$.

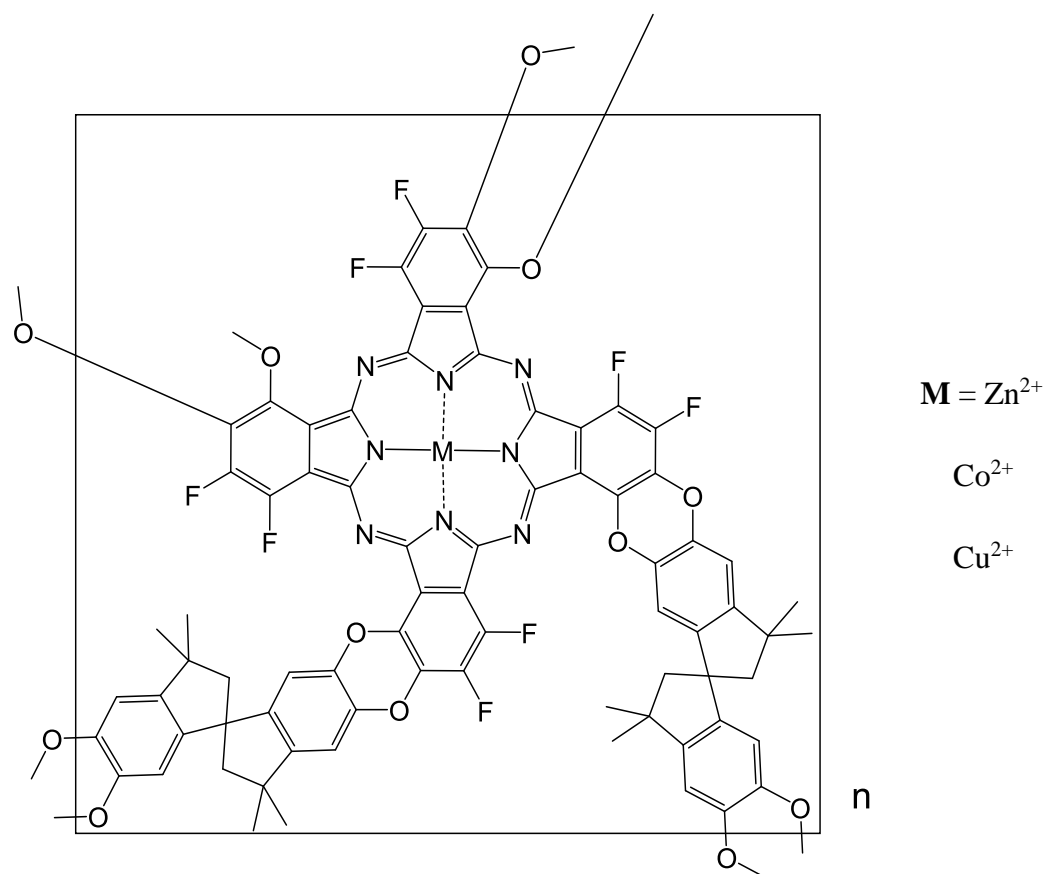
OctaF-Trip-CoPc-NetPIM

Cobalt(II) 1,2,3,4,8,9,10,11,15,16,17,18,22,23,24,25-hexadecafluoro-29*H*,31*H* phthalocyanine (0.15 g, 0.17 mmol), 2,3,6,7,14,15-hexahydroxy-9,10-diethyltriptycene (0.094 g, 0.23 mmol) and anhydrous potassium carbonate (0.28 g, 2.04 mmol) were reacted in anhydrous NMP (3.5 ml) according to the general procedure (j). The solid was purified by refluxing in a range of solvents: THF, acetone and methanol over a few days and filtered off to give **Tetra-trip-octa-fluoroCoPcNetPIM** as a green solid (0.21 g, 98 %). Elemental analysis (%) calcd. for C₆₄H₂₁N₈O₈F₈Co: C 61.91, H 1.70, N 9.02, F 12.24, found C 53.92, H 2.97, N 7.83, F 9.68; UV-vis (1-chloronaphthalene): λ_{max} , nm 652; IR (solid): ν , cm⁻¹ 2978, 1710, 1584, 1468, 1454, 1370, 1310, 1263, 1211, 1148, 1071, 968, 880, 843, 758, 689, 662, 625; BET surface area = 565 m² g⁻¹; total pore volume = 0.37 cm³ g⁻¹ at $p/p^{\circ} = 0.98$; TGA (nitrogen): Initial weight loss due to thermal degradation commences at ~ 300 °C.

OctaF-Trip-CuPc-NetPIM

Copper(II) 1,2,3,4,8,9,10,11,15,16,17,18,22,23,24,25-hexadecafluoro-29*H*,31*H* phthalocyanine (0.144 g, 0.167 mmol), 2,3,6,7,14,15-hexahydroxy-9,10-diethyltriptycene (0.09 g, 0.22 mmol) and anhydrous potassium carbonate (0.28 g, 2.0 mmol) were reacted in anhydrous NMP (3.5 ml) according to the general procedure (j). The solid was purified by refluxing in a range of solvents: THF, acetone and methanol over a few days and filtered off to give **Tetra-trip-octa-fluoroCuPcNetPIM** as a black solid (0.20 g, 98 %). Elemental analysis (%) calcd. for C₆₄H₂₁N₈O₈F₈Cu: C 61.72, H 1.70, N 8.99, F 12.20, found C 57.22, H 3.22, N 7.49, F 7.37; UV-vis (1-chloronaphthalene): λ_{max} , nm 686; IR (solid): ν , cm⁻¹ 2858, 1728, 1661, 1580, 1454, 1397, 1300, 1262, 1204, 1140, 1044, 980, 870, 797, 746, 719, 677, 635; BET surface area = 485 m² g⁻¹; total pore volume = 0.33 cm³ g⁻¹ at $p/p^{\circ} = 0.98$; TGA (nitrogen): Initial weight loss due to thermal degradation commences at ~ 313 °C.

OctaF-SBI-MPc-NetPIMs



OctaF-SBI-ZnPc-NetPIM

Zinc(II) 1,2,3,4,8,9,10,11,15,16,17,18,22,23,24,25-hexadecafluoro-29*H*,31*H* phthalocyanine (0.133 g, 0.15 mmol), 5,5',6,6'-tetrahydroxy-3,3,3',3'-tetramethyl-1,1'-spirobisindane (0.105 g, 0.31 mmol) and anhydrous potassium carbonate (0.25 g, 1.8 mmol) were reacted in anhydrous NMP (3.5 ml) according to the general procedure (j). The solid was purified by refluxing in a range of solvents: THF, acetone and methanol over a few days and filtered off to give **Tetra-SBI-octa-fluoroZnPcNetPIM** as a green-black solid (0.20 g, 94 %). Elemental analysis (%) calcd. for $C_{74}H_{40}N_8O_8F_8Zn$: C 64.10, H 2.91, N 8.08, F 10.96, found C 61.89, H 3.29, N 7.83, F 5.75; UV-vis (1-chloronaphthalene): λ_{max} , nm 664; IR (solid): ν , cm^{-1} 2873, 1723, 1614, 1456, 1418, 1366, 1304, 1296, 1248, 1209, 1175, 1121, 1105, 1057, 963, 941, 870, 746, 633; BET surface area = $636\text{ m}^2\text{ g}^{-1}$; total pore volume = $0.36\text{ cm}^3\text{ g}^{-1}$ at $p/p^o = 0.98$; TGA (nitrogen): Initial weight loss due to thermal degradation commences at $\sim 347\text{ }^\circ\text{C}$.

OctaF-SBI-CoPc-NetPIM

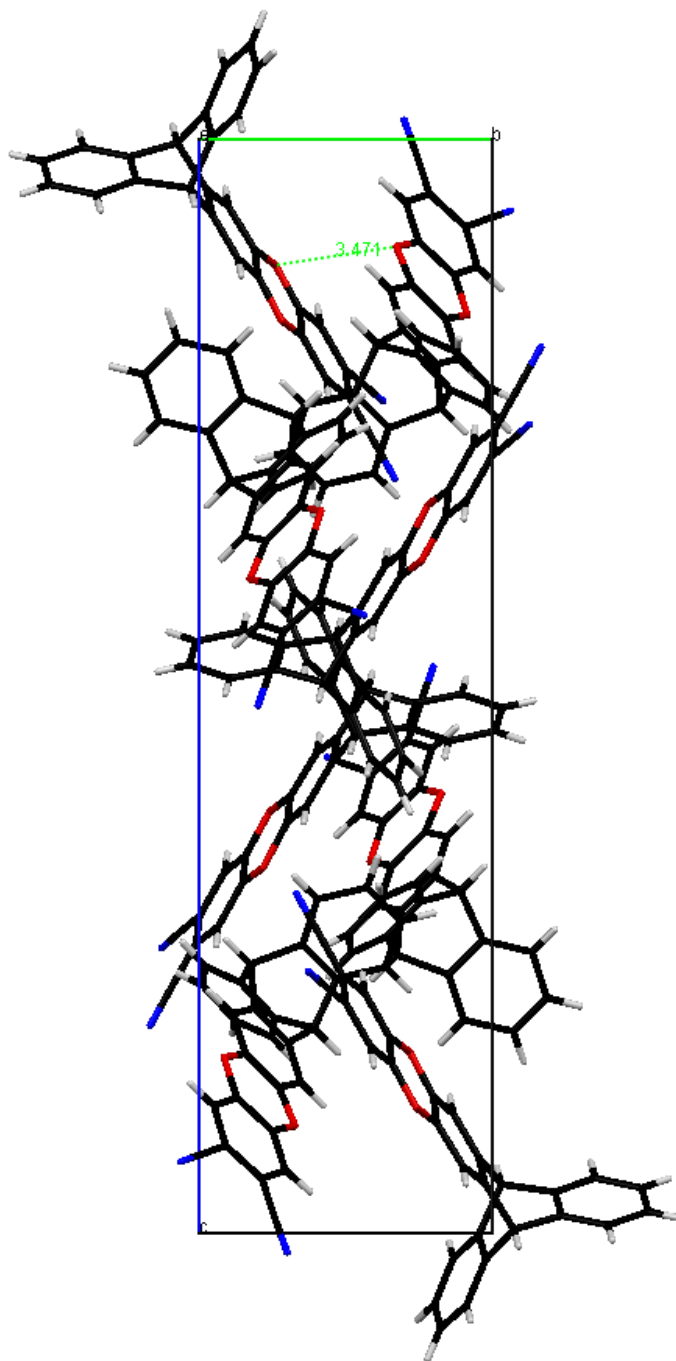
Cobalt(II) 1,2,3,4,8,9,10,11,15,16,17,18,22,23,24,25-hexadecafluoro-29*H*,31*H* phthalocyanine (0.13 g, 0.15 mmol), 5,5',6,6'-tetrahydroxy-3,3,3',3'-tetramethyl-1,1'-spirobisindane (0.103 g, 0.30 mmol) and anhydrous potassium carbonate (0.25 g, 1.8 mmol) were reacted in anhydrous NMP (3.5 ml) according to the general procedure (j). The solid was purified by refluxing in a range of solvents: THF, acetone and methanol over a few days and filtered off to give **Tetra-SBI-octa-fluoroCoPcNetPIM** as a green-black solid (0.191 g, 91 %). Elemental analysis (%) calcd. for C₇₄H₄₀N₈O₈F₈Co: C 64.40, H 2.92, N 8.12, F 11.01, found C 58.74, H 3.44, N 6.93, F 4.94; UV-vis (1-chloronaphthalene): λ_{max} , nm 682; IR (solid): ν , cm⁻¹ 2951, 1713, 1587, 1472, 1437, 1362, 1312, 1256, 1207, 1136, 1113, 1061, 1032, 963, 874, 752, 692; BET surface area = 524 m² g⁻¹; total pore volume = 0.32 cm³ g⁻¹ at $p/p^o = 0.98$; TGA (nitrogen): Initial weight loss due to thermal degradation commences at ~ 330 °C.

OctaF-SBI-CuPc-NetPIM

Copper(II) 1,2,3,4,8,9,10,11,15,16,17,18,22,23,24,25-hexadecafluoro-29*H*,31*H* phthalocyanine (0.089 g, 0.103 mmol), 5,5',6,6'-tetrahydroxy-3,3,3',3'-tetramethyl-1,1'-spirobisindane (0.07 g, 0.21 mmol) and anhydrous potassium carbonate (0.17 g, 1.23 mmol) were reacted in anhydrous NMP (3.5 ml) according to the general procedure (j). The solid was purified by refluxing in a range of solvents: THF, acetone and methanol over a few days and filtered off to give **Tetra-SBI-octa-fluoroCuPcNetPIM** as a green-black solid (0.14 g, 98 %). Elemental analysis (%) calcd. for C₇₄H₄₀N₈O₈F₈Cu: C 64.19, H 2.91, N 8.09, F 10.98, found C 61.19, H 3.29, N 6.92, F 3.52; UV-vis (1-chloronaphthalene): λ_{max} , nm 686; IR (solid): ν , cm⁻¹ 1749, 1618, 1580, 1462, 1435, 1310, 1294, 1252, 1134, 1055, 970, 870, 826, 791, 727, 702, 683, 648; BET surface area = 680 m² g⁻¹; total pore volume = 0.45 cm³ g⁻¹ at $p/p^o = 0.98$; TGA (nitrogen): Initial weight loss due to thermal degradation commences at ~ 376 °C.

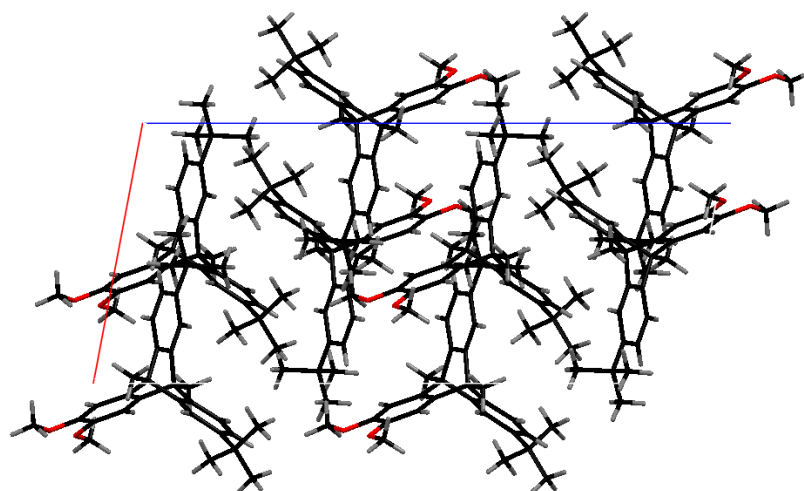
Appendix 2: Solid state crystal structure parameters and packing diagrams

A 2.1: Packing along the a-axis for 2,3-dioxin-phthalonitrile-triptycene. Crystals were prepared from slow evaporation of a THF solution. Solvent molecules are removed for clarity.



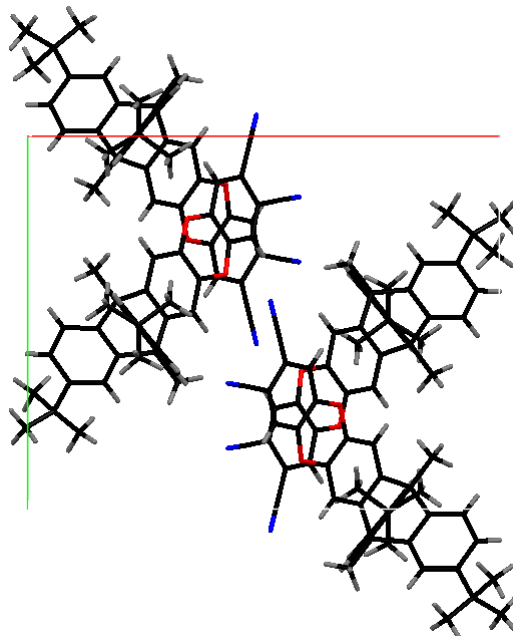
Formula	$C_{59.50} H_{52.50} N_{3.50} O_{3.50}$
Molecular weight	872.55
Wavelength (Å)	0.71073
Temperature (K)	293(2)
Crystal system	monoclinic
Space group	$P 2_1/c$
Unit cell dimensions	
a	19.884(5) Å
b	8.044(5) Å
c	30.274(5) Å
α	90.000(5) °
β	96.255(5) °
γ	90.000(5) °
Volume (Å ³)	4813(3)
Z	4
Density (calculated)	1.204
F(0 0 0)	1848
Absorption coefficient	0.075 mm ⁻¹
Range for data collection	1.03 – 27.56°
All reflections collected	29851
Independent reflections	10447
Observed reflections	8142
Goodness-of-fit	1.399
Final R indices [$I > 2\sigma(I)$]	R1 = 0.0823, wR2 = 0.2821
R indices (all data)	R1 = 0.1014 , wR2 = 0.3252

A 2.2: Packing along the b-axis for 2,3-dimethoxy-9,10-dimethyl-6,15-di-*tert*-butyltritycene. Crystals were prepared from slow diffusion of MeOH into a $CHCl_3$ solution.



Formula	C ₃₂ H ₃₈ O ₂
Molecular weight	454.28
Wavelength (Å)	0.71073
Temperature (K)	150(2)
Crystal system	Monoclinic
Space group	C2/c
Unit cell dimensions	
a	11.2766(2) Å
b	18.5541(6) Å
c	25.0651(6) Å
α	90.00 °
β	100.732(2) °
γ	90.00 °
Volume (Å ³)	5152.6(2)
Z	8
Density (calculated)	1.172
F(0 0 0)	1968
Crystal size	0.35 x 0.15 x 0.10 mm ³
Absorption coefficient	0.071 mm ⁻¹
Range for data collection	3.01 – 27.49°
All reflections collected	9955
Independent reflections	5846
Observed reflections	4359
Goodness-of-fit	1.023
Final R indices [I > 2σ(I)]	R1 = 0.0631, wR2 = 0.1426
R indices (all data)	R1 = 0.0897, wR2 = 0.1596

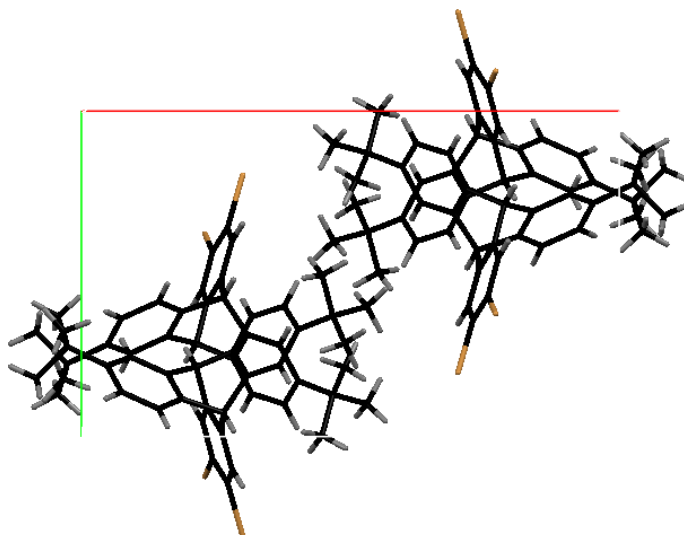
A 2.3: Packing along the c-axis for 2,3-dioxin-phthalonitrile-9,10-dimethyl-6,15-di-*tert*-butyltritycene (**Pn4**). Crystals were prepared from slow diffusion of MeOH into a CHCl₃ solution. It seems that the introduction of bulkier group onto the periphery of the Pn does not seem to avoid the aggregation and dimers are still formed.



Formula	C ₃₈ H ₃₄ N ₂ O ₂
Molecular weight	550.67
Wavelength (Å)	1.54180
Temperature (K)	293(2)
Crystal system	Monoclinic
Space group	P 2 ₁ /c
Unit cell dimensions	
a	18.9292(4) Å
b	14.6433(2) Å
c	11.1365(2) Å
α	90.00 °
β	101.540(2) °
γ	90.00 °
Volume (Å ³)	3024.48(9)
Z	4
Density (calculated)	1.209
F(0 0 0)	1168
Crystal size	0.12 x 0.10 x 0.04 mm ³
Absorption coefficient	0.581 mm ⁻¹
Range for data collection	3.85 – 73.41°

All reflections collected	11743
Independent reflections	5896
Observed reflections	4547
Goodness-of-fit	1.033
Final R indices [$I > 2\sigma(I)$]	R1 = 0.0496, wR2 = 0.1316
R indices (all data)	R1 = 0.0656, wR2 = 0.1457

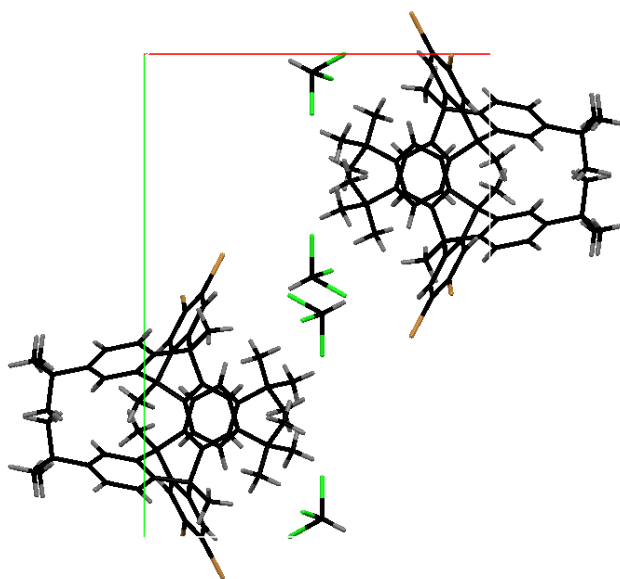
A 2.4: Packing along the c-axis for 2,3-dibromo-6,15-di-*tert*-butyltritycene.



Formula	C ₂₈ H ₂₈ Br ₂
Molecular weight	524.32
Wavelength (Å)	1.54184
Temperature (K)	296(2)
Crystal system	Monoclinic
Space group	P 2 ₁ /c
Unit cell dimensions	
a	18.6134(10) Å
b	11.1479(5) Å
c	12.0010(5) Å
α	90.00 °
β	98.439(5) °
γ	90.00 °
Volume (Å ³)	2463.2(2)
Z	4
Density (calculated)	1.414
F(0 0 0)	1064
Crystal size	0.37 x 0.25 x 0.06 mm ³

Absorption coefficient	4.244
Range for data collection	4.64-75.47°
All reflections collected	18135
Independent reflections	4897
Observed reflections	3943
Goodness-of-fit	1.085
Final R indices [$I > 2\sigma(I)$]	R1 = 0.0530, wR2 = 0.1511
R indices (all data)	R1 = 0.0632, wR2 = 0.1676

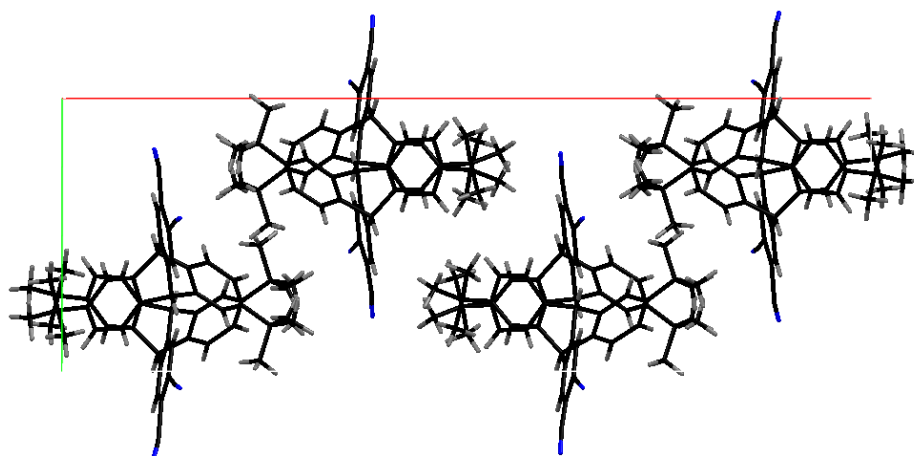
A 2.5: Packing along the c-axis for 2,3-dibromo-6,15-di-*tert*-butyl-9,10-dimethyltritycene. Crystals were prepared from slow diffusion of MeOH into a CHCl₃ solution. CHCl₃ molecules are also visible.



Formula	C ₃₁ H ₃₃ Br ₂ Cl ₃
Molecular weight	671.74
Wavelength (Å)	1.54184
Temperature (K)	150(2)
Crystal system	Monoclinic
Space group	P 2 ₁ /c
Unit cell dimensions	
a	14.5821(3) Å
b	20.1342(3) Å
c	10.3225(2) Å
α	90.00°
β	100.426(2)°
γ	90.00°
Volume (Å ³)	2980.64(10)

Z	4
Density (calculated)	1.497
F(0 0 0)	1360
Crystal size	0.38 x 0.30 x 0.17 mm ³
Absorption coefficient	6.056
Range for data collection	3.08 - 73.54°
All reflections collected	11838
Independent reflections	5825
Observed reflections	5391
Goodness-of-fit	1.048
Final R indices [I > 2σ(I)]	R1 = 0.0494, wR2 = 0.1289
R indices (all data)	R1 = 0.0527, wR2 = 0.1327

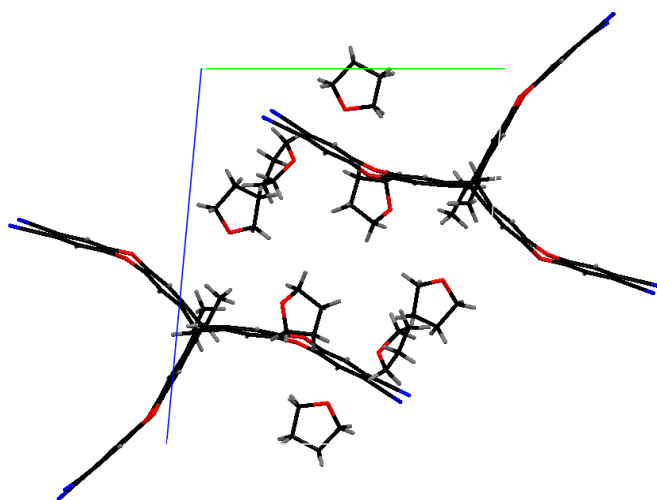
A 2.6: Packing along the *c*-axis for 2,3-dicyano-6,15-di-*tert*-butyltritycene. Crystals were prepared from slow diffusion of MeOH into a CHCl₃ solution.



Formula	C ₃₀ H ₂₈ N ₂
Molecular weight	416.54
Wavelength (Å)	1.54180
Temperature (K)	150(2)
Crystal system	Monoclinic
Space group	P 2 ₁ /c
Unit cell dimensions	
a	34.815(3) Å
b	11.7189(6) Å
c	11.5941(12) Å
α	90.030(6)°
β	90.070(8)°
γ	90.046(5)°

Volume (Å ³)	4730.3(7)
Z	8
Density (calculated)	1.170
F(0 0 0)	1776
Absorption coefficient	0.518 mm ⁻¹
Range for data collection	3.77 - 73.35°
All reflections collected	19096
Independent reflections	8582
Observed reflections	4197
Goodness-of-fit	1.090
Final R indices [I > 2σ(I)]	R1 = 0.1348, wR2 = 0.3396
R indices (all data)	R1 = 0.2109, wR2 = 0.3997

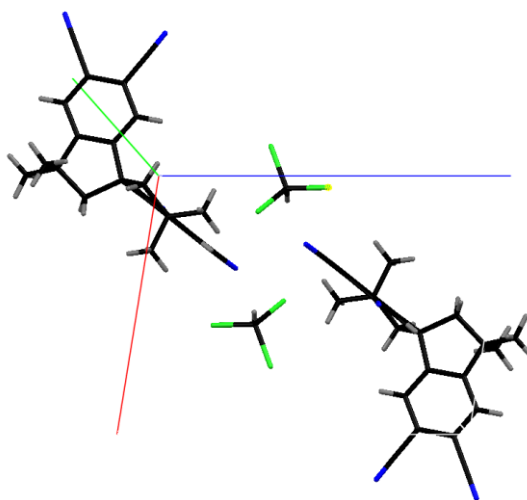
A 2.7: Packing along the a-axis for TrisPn triptycene. Crystals were obtained by slow evaporation of a THF solution. Solvent molecules are also visible.



Formula	C ₆₈ H ₆₂ N ₆ O ₁₁
Molecular weight	1139.24
Wavelength (Å)	1.54180
Temperature (K)	150(2)
Crystal system	Triclinic
Space group	P-1
Unit cell dimensions	
a	10.7268(4) Å
b	15.3620(6) Å
c	18.6391(7) Å
α	93.123(3) °
β	97.338(3) °

γ	105.212(4) °
Volume (Å ³)	2927.10(19)
Z	2
Density (calculated)	1.293
F(0 0 0)	1200
Crystal size	0.19 x 0.17 x 0.04 mm ³
Absorption coefficient	0.720 mm ⁻¹
Range for data collection	3.66 – 73.45°
All reflections collected	20779
Independent reflections	11410
Observed reflections	7964
Goodness-of-fit	1.029
Final R indices [I > 2σ(I)]	R1 = 0.0704, wR2 = 0.1943
R indices (all data)	R1 = 0.1006, wR2 = 0.2247

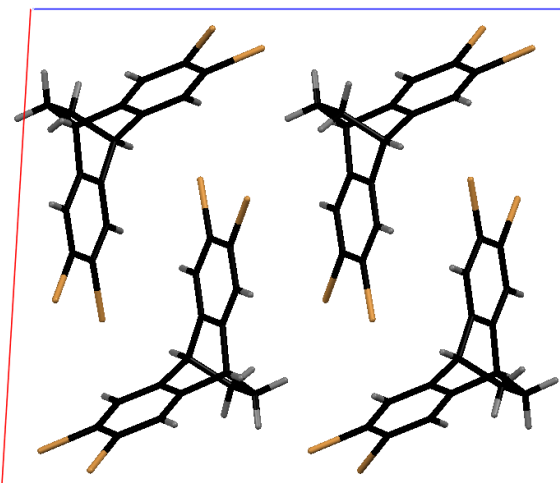
A 2.8: Packing along the b-axis for tetracyanospirobisindane. Crystals were obtained from slow diffusion of MeOH into a CHCl₃ solution. CHCl₃ molecules are also visible.



Formula	C ₂₆ H ₂₁ Cl ₃ N ₄
Molecular weight	495.82
Wavelength (Å)	0.71073
Temperature (K)	293(2)
Crystal system	Triclinic
Space group	P-1
Unit cell dimensions	
a	10.0893(5) Å
b	10.3879(4) Å

c	13.5531(6) Å
α	108.661(4) °
β	99.168(4) °
γ	107.874(4) °
Volume (Å ³)	1227.47(9)
Z	2
Density (calculated)	1.342
F(0 0 0)	512
Crystal size	0.28 x 0.19 x 0.10 mm ³
Absorption coefficient	0.395 mm ⁻¹
Range for data collection	2.84 - 29.67°
All reflections collected	11281
Independent reflections	5755
Observed reflections	4600
Goodness-of-fit	1.029
Final R indices [I > 2 σ (I)]	R1 = 0.0497, wR2 = 0.1059
R indices (all data)	R1 = 0.0649, wR2 = 0.1169

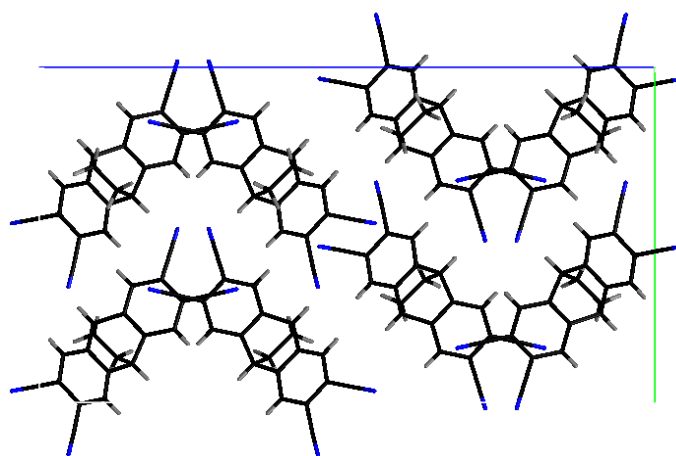
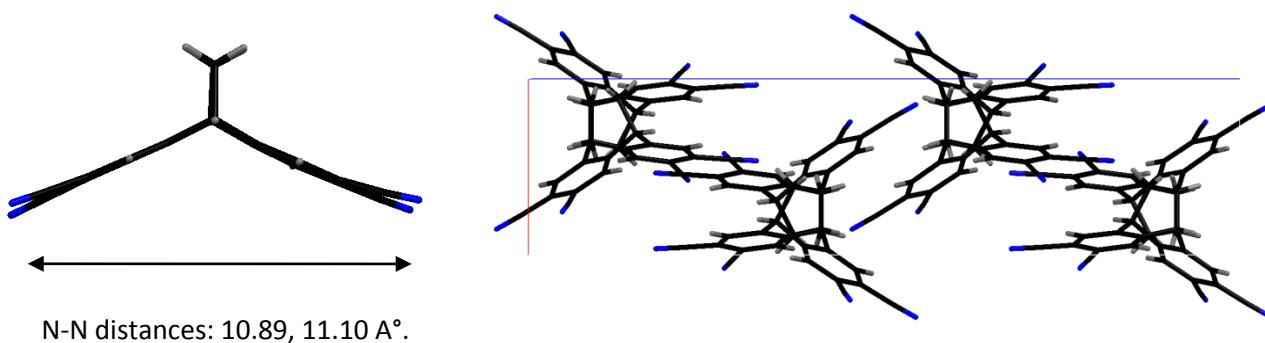
A 2.9: Packing along the b-axis for tetrabromoethanoanthracene. Crystals were obtained from slow diffusion of MeOH into a CHCl₃ solution.



Formula	C ₁₆ H ₁₀ Br ₄
Molecular weight	521.88
Wavelength (Å)	1.54184
Temperature (K)	150(2)
Crystal system	Monoclinic
Space group	P 2 ₁ /c
Unit cell dimensions	
a	14.5275(3)

b	6.55070(10)
c	16.2667(4)
α	90
β	93.456(2)
γ	90
Volume (\AA^3)	1545.21
Z	4
Density (calculated)	2.243
F(0 0 0)	984
Crystal size	0.179 x 0.089 x 0.076 mm ³
Absorption coefficient	12.592
Range for data collection	3.047 – 74.095°
All reflections collected	5940
Independent reflections	3042
Observed reflections	2801
Goodness-of-fit	1.079
Final R indices [$I > 2\sigma(I)$]	R1 = 0.0365, wR2 = 0.0955
R indices (all data)	R1 = 0.0396, wR2 = 0.0981

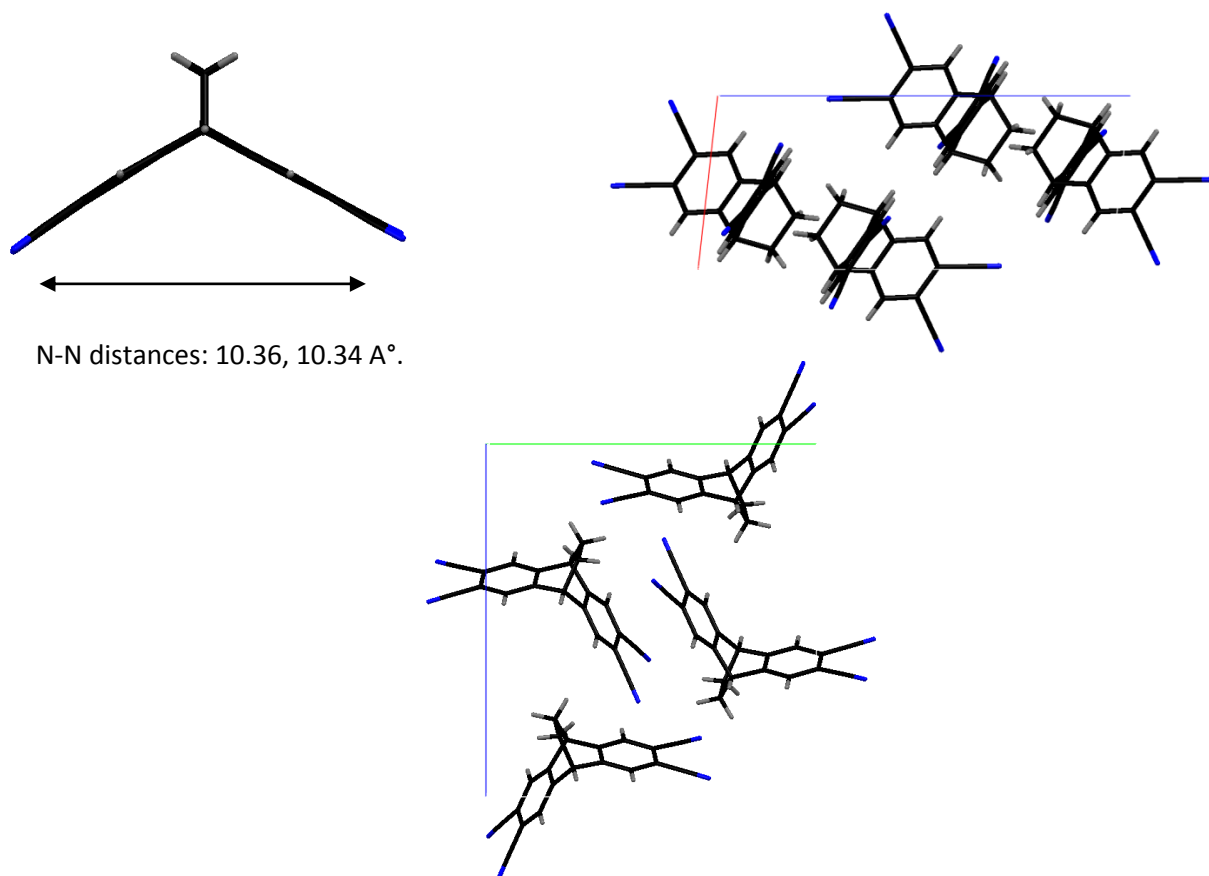
A 2.10: Crystal structure (top left) and packing along the b-axis (top right) and along the a-axis (centre) for the first polymorph of tetracyanoethanoanthracene (Orthorhombic, *Pbca*). Crystals were obtained by slow evaporation of a CHCl_3 solution.



Formula	$\text{C}_{20}\text{H}_{10}\text{N}_4$
Molecular weight	306.32
Wavelength (Å)	1.54184
Temperature (K)	293(2)
Crystal system	orthorhombic
Space group	<i>Pbca</i>
Unit cell dimensions	
a	6.9455(2)
b	15.5407(4)
c	28.3868(8)
α	90
β	90

γ	90
Volume (\AA^3)	3064.01(15)
Z	8
Density (calculated)	1.328
F(0 0 0)	1264
Crystal size	0.284 x 0.193 x 0.131 mm ³
Absorption coefficient	0.652
Range for data collection	3.114 – 73.987°
All reflections collected	10557
Independent reflections	3065
Observed reflections	2584
Goodness-of-fit	1.095
Final R indices [$I > 2\sigma(I)$]	R1 = 0.0523, wR2 = 0.1289
R indices (all data)	R1 = 0.0641, wR2 = 0.1365

A 2.11: Crystal structure (top left) and packing along the b-axis (top right) and along the a-axis (centre) for the second polymorph of tetracyanoethanoanthracene (Monoclinic, $P2_1/n$). Crystals were obtained by slow evaporation of a CHCl_3 solution.



Formula	C ₂₀ H ₁₀ N ₄
Molecular weight	306.32
Wavelength (Å)	1.54184
Temperature (K)	150(2)
Crystal system	Monoclinic
Space group	P2 ₁ /n
Unit cell dimensions	
a	6.6157(5)
b	14.5927(8)
c	15.6830(10)
α	90
β	96.449(7)
γ	90
Volume (Å ³)	1504.47(17)
Z	4
Density (calculated)	1.352
F(0 0 0)	632
Crystal size	0.116 x 0.123 x 0.196 mm ³
Absorption coefficient	0.664
Range for data collection	4.150 – 73.847 °
All reflections collected	5666
Independent reflections	2917
Observed reflections	1998
Goodness-of-fit	1.029
Final R indices [I > 2σ(I)]	R1 = 0.0615, wR2 = 0.1639
R indices (all data)	R1 = 0.0885, wR2 = 0.1905

Bibliography

- [1] McKeown, N. B. *Phthalocyanine Materials: Structure, Synthesis and Function*, 1998.
- [2] de Diesbach, H.; von der Weid, E. *Helv. Chim. Acta* **1927**, *10*, 886-888.
- [3] Braun, A.; Tcherniac, J. *Ber. Dtsch. Chem. Ges.* **1907**, *40*, 2709-2709.
- [4] Gregory, P. J. *Porphyrins Phthalocyanines* **2000**, *4*, 432-432.
- [5] Gregory, P. J. *Porphyrins Phthalocyanines* **1999**, *3*, 468-476.
- [6] Linstead, R. P. *J. Chem. Soc.* **1934**, 1016-1017.
- [7] Byrne, G. T.; Linstead, R. P.; Lowe, A. R. *J. Chem. Soc.* **1934**, 1017-1022.
- [8] Linstead, R. P.; Lowe, A. R. *J. Chem. Soc.* **1934**, 1022-1022.
- [9] Dent, C. E.; Linstead, R. P. *J. Chem. Soc.* **1934**, 1027-1031.
- [10] Linstead, R. P.; Lowe, A. R. *J. Chem. Soc.* **1934**, 1031-1033.
- [11] Dent, C. E.; Linstead, R. P.; Lowe, A. R. *J. Chem. Soc.* **1934**, 1033-1039.
- [12] Tomoda, H.; Saito, S.; Ogawa, S.; Shiraiishi, S. *Chem. Lett.* **1980**, *9*, 1277-1280.
- [13] Kobayashi, N.; Lever, A. B. P. *J. Am. Chem. Soc.* **1987**, *109*, 7433-7441.
- [14] McKeown, N. B.; Chambrier, I.; Cook, M. J. *J. Chem. Soc., Perkin Trans. 1* **1990**, 1169-1177.
- [15] Snow, A. W.; Jarvis, N. L. *J. Am. Chem. Soc.* **1984**, *106*, 4706-4711.
- [16] Lowery, M. K.; Starshak, A. J.; Esposito, J. N.; Krueger, P. C.; Kenney, M. E. *Inorg. Chem.* **1965**, *4*, 128-128.
- [17] Sommerauer, M.; Rager, C.; Hanack, M. *J. Am. Chem. Soc.* **1996**, *118*, 10085-10093.
- [18] Ungurenasu, C. *Synthesis* **1999**, *1999*, 1729-1730.
- [19] Silver, J.; Lukes, P. J.; Hey, P. K.; O'Connor, J. M. *Polyhedron* **1989**, *8*, 1631-1635.
- [20] Thompson, J. A.; Murata, K.; Miller, D. C.; Stanton, J. L.; Broderick, W. E.; Hoffman, B. M.; Ibers, J. A. *Inorg. Chem.* **1993**, *32*, 3546-3553.
- [21] McKeown, N. B.; Makhseed, S.; Msayib, K. J.; Ooi, L.-L.; Helliwell, M.; Warren, J. E. *Angew. Chem. Int. Ed.* **2005**, *44*, 7546-7549.
- [22] Rosenmund, K. W.; Struck, E. *Ber. Dtsch. Chem. Ges. (A and B Ser.)* **1919**, *52*, 1749-1756.
- [23] v. Braun, J.; Manz, G. *Justus Liebigs Ann. Chem.* **1931**, *488*, 111-126.
- [24] Duro, J. A.; de la Torre, G.; Barberá, J.; Serrano, J. L.; Torres, T. *Chem. Mater.* **1996**, *8*, 1061-1066.
- [25] Kempa, A.; Dobrowolski, J. *Can. J. Chem.* **1988**, *66*, 2553-2555.
- [26] Shaabani, A. *J. Chem. Res., Synop.* **1998**, 672-673.
- [27] Weber, J. H.; Busch, D. H. *Inorg. Chem.* **1965**, *4*, 469-471.
- [28] Nemykin, V. N.; Lukyanets, E. A. *ARKIVOC* **2010**, 136-208.
- [29] Kim, K. N.; Choi, C. S.; Kay, K.-Y. *Tetrahedron Lett.* **2005**, *46*, 6791-6795.
- [30] Brewis, M.; Clarkson, G. J.; Goddard, V.; Helliwell, M.; Holder, A. M.; McKeown, N. *Angew. Chem. Int. Ed.* **1998**, *37*, 1092-1094.
- [31] Makhseed, S.; Ibrahim, F.; Samuel, J.; Helliwell, M.; Warren, J. E.; Bezzu, C. G.; McKeown, N. B. *Chem. Eur. J.* **2008**, *14*, 4810-4815.
- [32] Kostka, M.; Zimcik, P.; Miletin, M.; Klemra, P.; Kopecky, K.; Musil, Z. *J. Photochem. Photobiol., A: Chem.* **2006**, *178*, 16-25.
- [33] Zimcik, P.; Novakova, V.; Kopecky, K.; Miletin, M.; Uslu Kobak, R. Z.; Svandrlikova, E.; Váchová, L.; Lang, K. *Inorg. Chem.* **2012**, *51*, 4215-4223.
- [34] Zefirov, T. V. D. a. L. G. T. a. N. S. *Russ. Chem. Rev.* **2013**, *82*, 865-865.

- [35] Sastre, A.; Torres, T.; Díaz-García, M. A.; Agulló-López, F.; Dhenaut, C.; Brasselet, S.; Ledoux, I.; Zyss, J. *J. Am. Chem. Soc.* **1996**, *118*, 2746-2747.
- [36] Marks, T. J.; Stojakovic, D. R. *J. Am. Chem. Soc.* **1978**, *100*, 1695-1705.
- [37] Emmelius, M.; Pawlowski, G.; Vollmann, H. W. *Angew. Chem. Int. Ed. Engl.* **1989**, *28*, 1445-1471.
- [38] Mustroph, H.; Stollenwerk, M.; Bressau, V. *Angew. Chem. Int. Ed.* **2006**, *45*, 2016-2035.
- [39] Bao, Z.; Lovinger, A. J.; Brown, J. *J. Am. Chem. Soc.* **1998**, *120*, 207-208.
- [40] Anthopoulos, T. D.; Shafai, T. S. *Appl. Phys. Lett.* **2003**, *82*, 1628-1630.
- [41] Chaidogiannos, G.; Petraki, F.; Glezos, N.; Kennou, S.; Nešpůrek, S. *Appl. Phys. A* **2009**, *96*, 763-767.
- [42] K. Nazeeruddin, M.; Humphry-Baker, R.; Gratzel, M.; A. Murrer, B. *Chem. Commun.* **1998**, 719-720.
- [43] Panda, D. K.; Goodson, F. S.; Ray, S.; Saha, S. *Chem. Commun.* **2014**, *50*, 5358-5360.
- [44] Ragoussi, M.-E.; Ince, M.; Torres, T. *Eur. J. Org. Chem.* **2013**, *2013*, 6475-6489.
- [45] Allen, C. M.; Sharman, W. M.; Van Lier, J. E. *J. Porphyrins Phthalocyanines* **2001**, *5*, 161-169.
- [46] Ogura, S.-i.; Tabata, K.; Fukushima, K.; Kamachi, T.; Okura, I. *J. Porphyrins Phthalocyanines* **2006**, *10*, 1116-1124.
- [47] Guillaud, G.; Simon, J.; Germain, J. P. *Coord. Chem. Rev.* **1998**, *178-180*, 1433-1484.
- [48] Brunet, J.; Pauly, A.; Mazet, L.; Germain, J. P.; Bouvet, M.; Malezieux, B. *Thin Solid Films* **2005**, *490*, 28-35.
- [49] Meunier, B.; Sorokin, A. *Acc. Chem. Res.* **1997**, *30*, 470-476.
- [50] Abe, T.; Taira, N.; Tanno, Y.; Kikuchi, Y.; Nagai, K. *Chem. Commun.* **2014**, *50*, 1950-1952.
- [51] de la Torre, G.; Claessens, C. G.; Torres, T. *Chem. Commun.* **2007**, 2000-2015.
- [52] Li, X.; He, X.; Chen, Y.; Fan, X.; Zeng, Q. *J. Mol. Struct.* **2011**, *1002*, 145-150.
- [53] Ray, A.; Santhosh, K.; Bhattacharya, S. *Spectrochim. Acta., Part A* **2011**, *78*, 1364-1375.
- [54] McKeown, N. B. *J. Mater. Chem.* **2000**, *10*, 1979-1995.
- [55] Bilgin, A.; Mendi, A.; Yildiz, U. *Polymer* **2006**, *47*, 8462-8473.
- [56] Konarev, D. V.; Zorina, L. V.; Ishikawa, M.; Khasanov, S. S.; Otsuka, A.; Yamochi, H.; Saito, G.; Lyubovskaya, R. N. *Cryst. Growth Des.* **2013**, *13*, 4930-4939.
- [57] Palewska, K.; Sworakowski, J.; Lipiński, J. *Opt. Mater.* **2012**, *34*, 1717-1724.
- [58] Contakes, S. M.; Beatty, S. T.; Dailey, K. K.; Rauchfuss, T. B.; Fenske, D. *Organometallics* **2000**, *19*, 4767-4774.
- [59] Hassan, B. M.; Li, H.; McKeown, N. B. *J. Mater. Chem.* **2000**, *10*, 39-45.
- [60] Brewis, M.; Clarkson, G. J.; Helliwell, M.; Holder, A. M.; McKeown, N. B. *Chem. Eur. J.* **2000**, *6*, 4630-4636.
- [61] Anthony, J. E. *Chem. Rev.* **2006**, *106*, 5028-5048.
- [62] Bottari, G.; de la Torre, G.; Guldi, D. M.; Torres, T. *Chem. Rev.* **2010**, *110*, 6768-6816.
- [63] Dong, H.; Zhu, H.; Meng, Q.; Gong, X.; Hu, W. *Chem. Soc. Rev.* **2012**, *41*, 1754-1808.
- [64] Imahori, H.; Umeyama, T.; Kurotobi, K.; Takano, Y. *Chem. Commun.* **2012**, *48*, 4032-4045.
- [65] Lu, Z.; Zhan, C.; Yu, X.; He, W.; Jia, H.; Chen, L.; Tang, A.; Huang, J.; Yao, J. *J. Mater. Chem.* **2012**, *22*, 23492-23496.
- [66] Cheng, Y.-J.; Cao, F.-Y.; Lin, W.-C.; Chen, C.-H.; Hsieh, C.-H. *Chem. Mater.* **2011**, *23*, 1512-1518.

- [67] Rouquerol, J.; Avnir, D.; Fairbridge, C. W.; Everett, D. H.; Haynes, J. M.; Pernicone, N.; Ramsay, J. D. F.; Sing, K. S. W.; Unger, K. K. *Pure Appl. Chem.* **1994**, *66*, 1739-1758.
- [68] Sing, K. S. W. *Pure Appl. Chem.* **1985**, *57*, 603-619.
- [69] Langmuir, I. *J. Am. Chem. Soc.* **1916**, *38*, 2221-2295.
- [70] Brunauer, S.; Emmett, P. H.; Teller, E. *J. Am. Chem. Soc.* **1938**, *60*, 309-319.
- [71] Carmody, O.; Frost, R.; Xi, Y.; Kokot, S. *Surf. Sci.* **2007**, *601*, 2066-2076.
- [72] Jiao, Y.; Stillinger, F. H.; Torquato, S. *Phys. Rev. E* **2009**, *79*, 41309-41309.
- [73] Jiao, Y.; Stillinger, F. H.; Torquato, S. *Phys. Rev. Lett.* **2008**, *100*, 245504-245504.
- [74] McKeown, N. B.; Budd, P. M. *Macromolecules* **2010**, *43*, 5163-5176.
- [75] Ilinitch, O. M.; Fenelonov, V. B.; Lapkin, A. A.; Okkel, L. G.; Terskikh, V. V.; Zamaraev, K. I. *Microporous Mesoporous Mater.* **1999**, *31*, 97-110.
- [76] Dunitz, J. D.; Filippini, G.; Gavezzotti, A. *Tetrahedron* **2000**, *56*, 6595-6601.
- [77] Budd, P. M.; Elabas, E. S.; Ghanem, B. S.; Makhseed, S.; McKeown, N. B.; Msayib, K. J.; Tattershall, C. E.; Wang, D. *Adv. Mater.* **2004**, *16*, 456-459.
- [78] Adymkanov, S. V.; Yampol'skii, Y. P.; Polyakov, A. M.; Budd, P. M.; Reynolds, K. J.; McKeown, N. B.; Msayib, K. J. *Polym. Sci. Ser. A* **2008**, *50*, 444-450.
- [79] Vandezande, P.; Gevers, L. E. M.; Vankelecom, I. F. J. *Chem. Soc. Rev.* **2008**, *37*, 365-405.
- [80] Robeson, L. M. *J. Membr. Sci.* **2008**, *320*, 390-400.
- [81] Ahn, J.; Chung, W.-J.; Pinnau, I.; Song, J.; Du, N.; Robertson, G. P.; Guiver, M. D. *J. Membr. Sci.* **2010**, *346*, 280-287.
- [82] Maffei, A. V.; Budd, P. M.; McKeown, N. B. *Langmuir* **2006**, *22*, 4225-4229.
- [83] Wood, C. D.; Tan, B.; Trewin, A.; Su, F.; Rosseinsky, M. J.; Bradshaw, D.; Sun, Y.; Zhou, L.; Cooper, A. I. *Adv. Mater.* **2008**, *20*, 1916-1921.
- [84] Germain, J.; Frechet, J. M. J.; Svec, F. *J. Mater. Chem.* **2007**, *17*, 4989-4997.
- [85] Rakow, N. A.; Wendland, M. S.; Trend, J. E.; Poirier, R. J.; Paolucci, D. M.; Maki, S. P.; Lyons, C. S.; Swierczek, M. J. *Langmuir* **2010**, *26*, 3767-3770.
- [86] Makhseed, S.; Al-Kharafi, F.; Samuel, J.; Ateya, B. *Catal. Commun.* **2009**, *10*, 1284-1287.
- [87] Budd, P. M.; Ghanem, B.; Msayib, K.; McKeown, N. B.; Tattershall, C. *J. Mater. Chem.* **2003**, *13*, 2721-2726.
- [88] Hasell, T.; Wood, C. D.; Clowes, R.; Jones, J. T. A.; Khimyak, Y. Z.; Adams, D. J.; Cooper, A. I. *Chem. Mater.* **2009**, *22*, 557-564.
- [89] McKeown, N. B.; Ghanem, B.; Msayib, K. J.; Budd, P. M.; Tattershall, C. E.; Mahmood, K.; Tan, S.; Book, D.; Langmi, H. W.; Walton, A. *Angew. Chem.* **2006**, *118*, 1836-1839.
- [90] Vile, J.; Carta, M.; Bezzu, C. G.; McKeown, N. B. *Polym. Chem.* **2011**, *2*, 2257-2260.
- [91] Ghanem, B. S.; Msayib, K. J.; McKeown, N. B.; Harris, K. D. M.; Pan, Z.; Budd, P. M.; Butler, A.; Selbie, J.; Book, D.; Walton, A. *Chem. Commun.* **2007**, 67-69.
- [92] McKeown, N. B.; Budd, P. M.; Msayib, K. J.; Ghanem, B. S.; Kingston, H. J.; Tattershall, C. E.; Makhseed, S.; Reynolds, K. J.; Fritsch, D. *Chem. Eur. J.* **2005**, *11*, 2610-2620.
- [93] Wöhrle, D.; Schulte, B. *Die Makromolekulare Chemie* **1988**, *189*, 1229-1238.
- [94] McKeown, N. B.; Makhseed, S.; Budd, P. M. *Chem. Commun.* **2002**, 2780-2781.
- [95] Lindsey, J. S.; Schreiman, I. C.; Hsu, H. C.; Kearney, P. C.; Marguerettaz, A. M. *J. Org. Chem.* **1987**, *52*, 827-836.
- [96] McKeown, N. B.; Hanif, S.; Msayib, K.; Tattershall, C. E.; Budd, P. M. *Chem. Commun.* **2002**, 2782-2783.

- [97] Battioni, P.; Brigaud, O.; Desvaux, H.; Mansuy, D.; Traylor, T. G. *Tetrahedron Lett.* **1991**, *32*, 2893-2896.
- [98] Mackintosh, H. J.; Budd, P. M.; McKeown, N. B. *J. Mater. Chem.* **2008**, *18*, 573-578.
- [99] Azerraf, C.; Grossman, O.; Gelman, D. *J. Organomet. Chem.* **2007**, *692*, 761-767.
- [100] Zhang, C.; Chen, C.-F. *J. Org. Chem.* **2007**, *72*, 9339-9341.
- [101] Zhu, X.-Z.; Chen, C.-F. *J. Am. Chem. Soc.* **2005**, *127*, 13158-13159.
- [102] Peng, X.-X.; Lu, H.-Y.; Han, T.; Chen, C.-F. *Org. Lett.* **2007**, *9*, 895-898.
- [103] Xue, M.; Chen, C.-F. *Chem. Commun.* **2008**, 6128-6130.
- [104] Long, T. M.; Swager, T. M. *J. Mater. Chem.* **2002**, *12*, 3407-3412.
- [105] Soldatov, D. V. *J. Chem. Crystallogr.* **2006**, *36*, 747-768.
- [106] Chong, J. H.; MacLachlan, M. J. *Inorg. Chem.* **2006**, *45*, 1442-1444.
- [107] Wen, M.; Munakata, M.; Li, Y.-Z.; Suenaga, Y.; Kuroda-Sowa, T.; Maekawa, M.; Anahata, M. *Polyhedron* **2007**, *26*, 2455-2460.
- [108] Zhang, Q.; Li, S.; Li, W.; Zhang, S. *Polymer* **2007**, *48*, 6246-6253.
- [109] Akutsu, F.; Saito, G.; Miyamoto, M.; Kasashima, Y.; Inoki, M.; Naruchi, K. *Macromol. Chem. Phys.* **1996**, *197*, 2239-2245.
- [110] Long, T. M.; Swager, T. M. *Adv. Mater.* **2001**, *13*, 601-604.
- [111] Hilton, C. L.; Jamison, C. R.; Zane, H. K.; King, B. T. *J. Org. Chem.* **2008**, *74*, 405-407.
- [112] Venugopalan, P.; Bürgi, H.-B.; Frank, N. L.; Baldridge, K. K.; Siegel, J. S. *Tetrahedron Lett.* **1995**, *36*, 2419-2422.
- [113] Hart, H. *Pure Appl. Chem.* **1993**, *65*, 27-34.
- [114] Swager, T. M. *Acc. Chem. Res.* **2008**, *41*, 1181-1189.
- [115] Chong, J. H.; MacLachlan, M. J. *J. Org. Chem.* **2007**, *72*, 8683-8690.
- [116] Chong, J. H.; Ardakani, S. J.; Smith, K. J.; MacLachlan, M. J. *Chem. Eur. J.* **2009**, *15*, 11824-11828.
- [117] Ghanem, B. S.; Hashem, M.; Harris, K. D. M.; Msayib, K. J.; Xu, M.; Budd, P. M.; Chaukura, N.; Book, D.; Tedds, S.; Walton, A.; McKeown, N. B. *Macromolecules* **2010**, *43*, 5287-5294.
- [118] Hashem, M.; Grazia Bezzu, C.; Kariuki, B. M.; McKeown, N. B. *Polym. Chem.* **2011**, *2*, 2190-2192.
- [119] Koh, K.; Wong-Foy, A. G.; Matzger, A. J. *J. Am. Chem. Soc.* **2009**, *131*, 4184-4185.
- [120] Budd, P. M.; Ghanem, B. S.; Makhseed, S.; McKeown, N. B.; Msayib, K. J.; Tattershall, C. E. *Chem. Commun.* **2004**, 230-231.
- [121] Ogasawara, S.; Kato, S. *J. Am. Chem. Soc.* **2010**, *132*, 4608-4613.
- [122] Du, N.; Robertson, G. P.; Song, J.; Pinnau, I.; Guiver, M. D. *Macromolecules* **2009**, *42*, 6038-6043.
- [123] Du, N.; Robertson, G. P.; Pinnau, I.; Thomas, S.; Guiver, M. D. *Macromol. Rapid Commun.* **2009**, *30*, 584-588.
- [124] Wang, Y.; McKeown, N. B.; Msayib, K. J.; Turnbull, G. A.; Samuel, I. D. W. *Sensors* **2011**, *11*, 2478-2487.
- [125] Tanabe, K. K.; Cohen, S. M. *Angew. Chem. Int. Ed.* **2009**, *48*, 7424-7427.
- [126] Li, J.-R.; Kuppler, R. J.; Zhou, H.-C. *Chem. Soc. Rev.* **2009**, *38*, 1477-1504.
- [127] Rosi, N. L.; Eckert, J.; Eddaoudi, M.; Vodak, D. T.; Kim, J.; O'Keeffe, M.; Yaghi, O. M. *Science* **2003**, *300*, 1127-1129.
- [128] Chen, B.; Xiang, S.; Qian, G. *Acc. Chem. Res.* **2010**, *43*, 1115-1124.
- [129] Li, H.; Eddaoudi, M.; O'Keeffe, M.; Yaghi, O. M. *Nature* **1999**, *402*, 276-279.

- [130] Kepert, C.; Rosseinsky, M. *Chem. Commun.* **1999**, 375-376.
- [131] Yaghi, O. M.; Li, H.; Davis, C.; Richardson, D.; Groy, T. L. *Acc. Chem. Res.* **1998**, *31*, 474-484.
- [132] Eddaoudi, M.; Kim, J.; Rosi, N.; Vodak, D.; Wachter, J.; O'Keeffe, M.; Yaghi, O. M. *Science* **2002**, *295*, 469-472.
- [133] Côté, A. P.; Benin, A. I.; Ockwig, N. W.; O'Keeffe, M.; Matzger, A. J.; Yaghi, O. M. *Science* **2005**, *310*, 1166-1170.
- [134] El-Kaderi, H. M.; Hunt, J. R.; Mendoza-Cortés, J. L.; Côté, A. P.; Taylor, R. E.; O'Keeffe, M.; Yaghi, O. M. *Science* **2007**, *316*, 268-272.
- [135] Spitler, E. L.; Dichtel, W. R. *Nat. Chem.* **2010**, *2*, 672-677.
- [136] Liang, J.; Shimizu, G. K. H. *Inorg. Chem.* **2007**, *46*, 10449-10451.
- [137] Thallapally, P. K.; McGrail, B. P.; Atwood, J. L.; Gaeta, C.; Tedesco, C.; Neri, P. *Chem. Mater.* **2007**, *19*, 3355-3357.
- [138] Tant, J.; Geerts, Y. H.; Lehmann, M.; De Cupere, V.; Zucchi, G.; Laursen, B. W.; Bjørnholm, T.; Lemaire, V.; Marcq, V.; Burquel, A.; Hennebicq, E.; Gardebien, F.; Viville, P.; Beljonne, D.; Lazzaroni, R.; Cornil, J. *J. Phys. Chem. B.* **2005**, *109*, 20315-20323.
- [139] McKeown, N. B. *J. Mater. Chem.* **2010**, *20*, 10588-10597.
- [140] Bezzu, C. G.; Helliwell, M.; Warren, J. E.; Allan, D. R.; McKeown, N. B. *Science* **2010**, *327*, 1627-1630.
- [141] Holst, J. R.; Trewin, A.; Cooper, A. I. *Nat. Chem.* **2010**, *2*, 915-920.
- [142] Jelfs, K. E.; Wu, X.; Schmidtman, M.; Jones, J. T. A.; Warren, J. E.; Adams, D. J.; Cooper, A. I. *Angew. Chem. Int. Ed.* **2011**, *50*, 10653-10656.
- [143] Granzhan, A.; Riis-Johannessen, T.; Scopelliti, R.; Severin, K. *Angew. Chem. Int. Ed.* **2010**, *49*, 5515-5518.
- [144] Zhang, G.; Presly, O.; White, F.; Oppel, I. M.; Mastalerz, M. *Angew. Chem. Int. Ed.* **2014**, *53*, 1516-1520.
- [145] Abbott, L. J.; McDermott, A. G.; Del Regno, A.; Taylor, R. G. D.; Bezzu, C. G.; Msayib, K. J.; McKeown, N. B.; Siperstein, F. R.; Runt, J.; Colina, C. M. *J. Phys. Chem. B.* **2012**, *117*, 355-364.
- [146] Taylor, R. G. D.; Carta, M.; Bezzu, C. G.; Walker, J.; Msayib, K. J.; Kariuki, B. M.; McKeown, N. B. *Org. Lett.* **2014**, *16*, 1848-1851.
- [147] Tian, J.; Thallapally, P. K.; Dalgarno, S. J.; McGrail, P. B.; Atwood, J. L. *Angew. Chem. Int. Ed.* **2009**, *48*, 5492-5495.
- [148] Kohl, B.; Rominger, F.; Mastalerz, M. *Org. Lett.* **2014**, *16*, 704-707.
- [149] Dogru, M.; Handloser, M.; Auras, F.; Kunz, T.; Medina, D.; Hartschuh, A.; Knochel, P.; Bein, T. *Angew. Chem. Int. Ed.* **2013**, *52*, 2920-2924.
- [150] Brutschy, M.; Schneider, M. W.; Mastalerz, M.; Waldvogel, S. R. *Adv. Mater.* **2012**, *24*, 6049-6052.
- [151] Dodsworth, E. S.; Lever, A. B. P.; Seymour, P.; Leznoff, C. C. *J. Phys. Chem.* **1985**, *89*, 5698-5705.
- [152] Mizuguchi, J.; Matsumoto, S. *J. Phys. Chem. A.* **1999**, *103*, 614-616.
- [153] Ethirajan, M.; Chen, Y.; Joshi, P.; Pandey, R. K. *Chem. Soc. Rev.* **2011**, *40*, 340-362.
- [154] Brewis, M.; Hassan, B. M.; Li, H.; Makhseed, S.; McKeown, N. B.; Thompson, N. *J. Porphyrins Phthalocyanines* **2000**, *4*, 460-464.
- [155] Makhseed, S.; McKeown, N. B.; Msayib, K.; Bumajdad, A. *J. Mater. Chem.* **2005**, *15*, 1865-1870.

- [156] Shatsskaya T. A., G. M. G., Skvarchenko V. R., Lukyanets E. A., *Zh. Obshch. Khim.* **1986**, *56*, 392-397.
- [157] Piechocki, C.; Simon, J.; Skoulios, A.; Guillon, D.; Weber, P. *J. Am. Chem. Soc.* **1982**, *104*, 5245-5247.
- [158] Parton, R. F.; Vankelecom, I. F. J.; Casselman, M. J. A.; Bezoukhanova, C. P.; Uytterhoeven, J. B.; Jacobs, P. A. *Nature* **1994**, *370*, 541-544.
- [159] Long, T. M.; Swager, T. M. *J. Am. Chem. Soc.* **2002**, *124*, 3826-3827.
- [160] Tsui, N. T.; Paraskos, A. J.; Torun, L.; Swager, T. M.; Thomas, E. L. *Macromolecules* **2006**, *39*, 3350-3358.
- [161] Bezzu, C. G.; Helliwell, M.; Kariuki, B. M.; McKeown, N. B. *J. Porphyrins Phthalocyanines* **2011**, *15*, 686-690.
- [162] De Vries, J. G.; Kellogg, R. M. *J. Org. Chem.* **1980**, *45*, 4126-4129.
- [163] Wöhrle, D.; Eskes, M.; Shigehara, K.; Yamada, A. *Synthesis* **1993**, *1993*, 194-196.
- [164] Gong, K.; Zhu, X.; Zhao, R.; Xiong, S.; Mao, L.; Chen, C. *Anal. Chem.* **2005**, *77*, 8158-8165.
- [165] Fu, P. P.; Harvey, R. G. *J. Org. Chem.* **1977**, *42*, 2407-2410.
- [166] Brasca, R.; Kneeteman, M. N.; Mancini, P. M. E.; Fabian, W. M. F. *J. Mol. Struct.* **2012**, *1010*, 158-168.
- [167] Yagodkin, E.; Douglas, C. J. *Tetrahedron Lett.* **2010**, *51*, 3037-3040.
- [168] Organ, M. G.; Abdel-Hadi, M.; Avola, S.; Hadei, N.; Nasielski, J.; O'Brien, C. J.; Valente, C. *Chem. Eur. J.* **2007**, *13*, 150-157.
- [169] Tamao, K.; Sumitani, K.; Kumada, M. *J. Am. Chem. Soc.* **1972**, *94*, 4374-4376.
- [170] Ishikawa, N.; Ohno, O.; Kaizu, Y.; Kobayashi, H. *J. Phys. Chem.* **1992**, *96*, 8832-8839.
- [171] Kleinwächter, J.; Hanack, M. *J. Am. Chem. Soc.* **1997**, *119*, 10684-10695.
- [172] de la Escosura, A.; Martínez-Díaz, M. V.; Thordarson, P.; Rowan, A. E.; Nolte, R. J. M.; Torres, T. *J. Am. Chem. Soc.* **2003**, *125*, 12300-12308.
- [173] Selyutin, G. E.; Podrugina, T. A.; Gal'pern, M. G.; Luk'yanets, E. A. *Chem. Heterocycl. Compd.* **1995**, *31*, 146-149.
- [174] Harriman, A. *J. Chem. Soc., Faraday Trans. 1* **1980**, *76*, 1978-1985.
- [175] Harriman, A. *J. Chem. Soc., Faraday Trans. 1* **1981**, *77*, 369-377.
- [176] Harriman, A. *J. Chem. Soc., Faraday Trans. 2* **1981**, *77*, 1281-1291.
- [177] Iehl, J.; Vartanian, M.; Holler, M.; Nierengarten, J.-F.; Delavaux-Nicot, B.; Strub, J.-M.; Van Dorsselaer, A.; Wu, Y.; Mohanraj, J.; Yoosaf, K.; Armaroli, N. *J. Mater. Chem.* **2011**, *21*, 1562-1573.
- [178] Leznoff, C. C.; Sosa-Sanchez, J. L. *Chem. Commun.* **2004**, 338-339.
- [179] Bhardwaj, N.; Andraos, J.; Leznoff, C. C. *Can. J. Chem.* **2002**, *80*, 141-147.
- [180] Lee, C.-H.; Filler, R.; Lee, J.; Li, J.; Mandal, B. K. *Renewable Energy* **2010**, *35*, 1592-1595.
- [181] Shklyae, Y. V.; Nifontov, Y. V. *Russ. Chem. Bull.* **2002**, *51*, 844-849.
- [182] Carta, M.; Malpass-Evans, R.; Croad, M.; Rogan, Y.; Jansen, J. C.; Bernardo, P.; Bazzarelli, F.; McKeown, N. B. *Science* **2013**, *339*, 303-307.
- [183] Hoffman, A. *J. Am. Chem. Soc.* **1929**, *51*, 2542-2547.
- [184] Barclay, L. R. C.; Chapman, R. A. *Can. J. Chem.* **1964**, *42*, 25-35.
- [185] Dong, G.; Li, H.; Chen, V. *J. Mater. Chem. A* **2013**, *1*, 4610-4630.
- [186] Stoll, S.; Schweiger, A. *J. Magn. Reson.* **2006**, *178*, 42-55.

- [187] Wang, J.; Wan, W.; Jiang, H.; Gao, Y.; Jiang, X.; Lin, H.; Zhao, W.; Hao, J. *Org. Lett.* **2010**, *12*, 3874-3877.
- [188] Metz, J.; Schneider, O.; Hanack, M. *Inorg. Chem.* **1984**, *23*, 1065-1071.
- [189] Hart, H.; Bashir-Hashemi, A.; Luo, J.; Meador, M. A. *Tetrahedron* **1986**, *42*, 1641-1654.
- [190] Lee, C.-H.; Guo, J.; Chen, L. X.; Mandal, B. K. *J. Org. Chem.* **2008**, *73*, 8219-8227.

